10 December 2004

Science

Vol. 306 No. 5703
Pages 1845–1984 $10

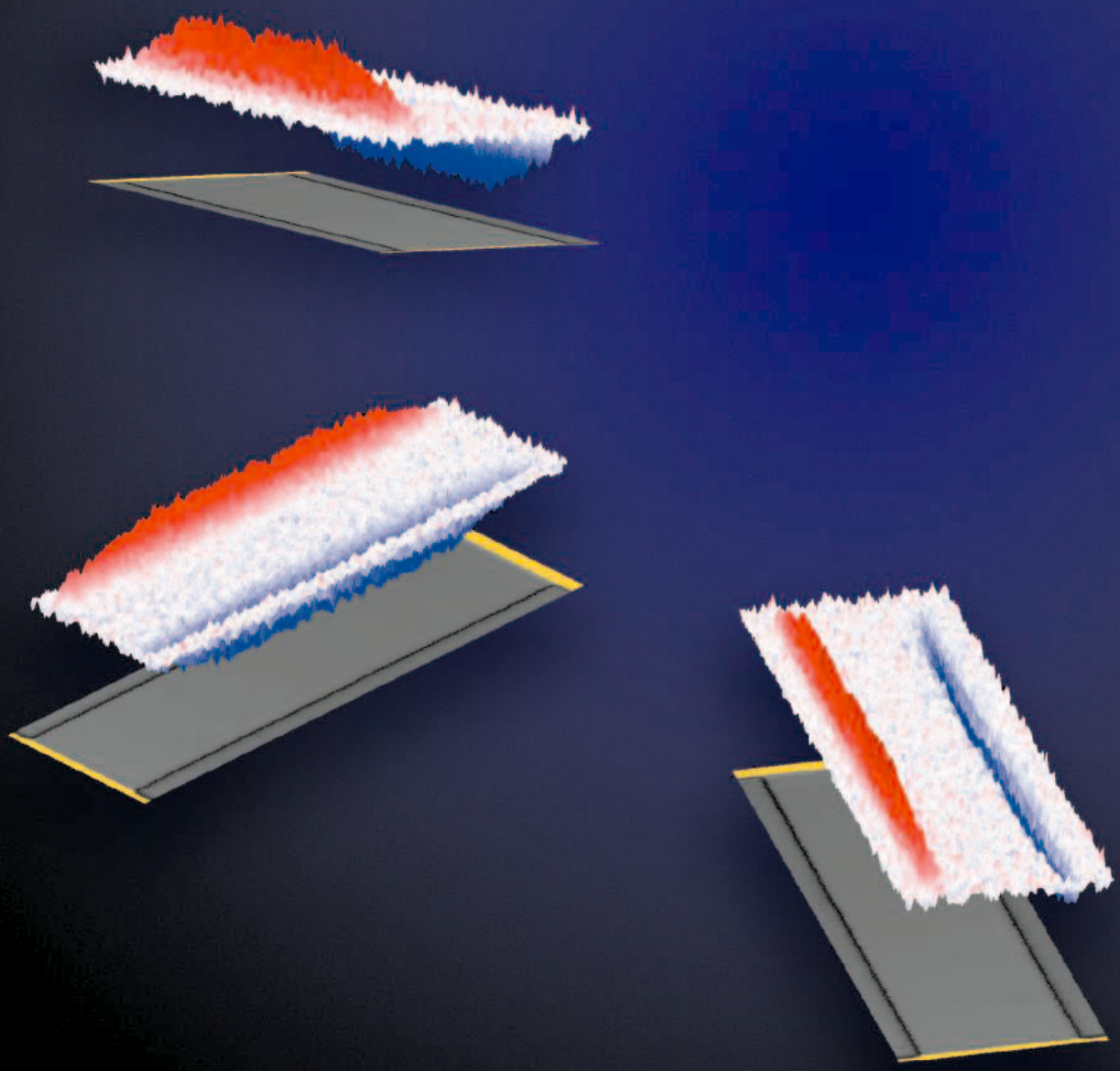

AAAS

Science

Volume 306
10 December 2004
Number 5703

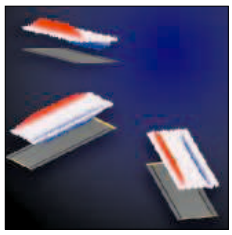

COVER An optical reflectivity image of a semiconductor wire (lower layer) and a digitally filtered image of the spin polarization (upper layer) in three different perspectives. When an electrical current passes through a nonmagnetic semiconductor, the spin Hall effect gives rise to a spin current—a combination of currents of spin-up electrons (red hill) and spin-down electrons (blue valley) in opposite directions—without application of a magnetic field. See page 1910. [Image: Y. K. Kato and D. D. Awschalom]

DEPARTMENTS

1880

NEWS OF THE WEEK

1894

NEWS FOCUS

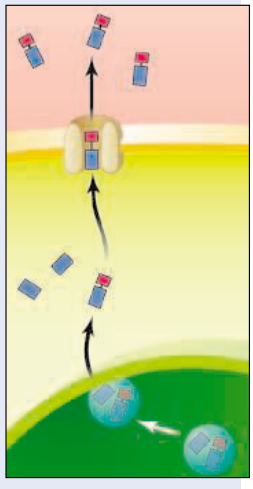

1897, 1930, & 1934

LETTERS

BOOKS *ET AL.*

POLICY FORUM

PERSPECTIVES

REVIEW

Contents continued

SCIENCE EXPRESS www.sciencexpress.org

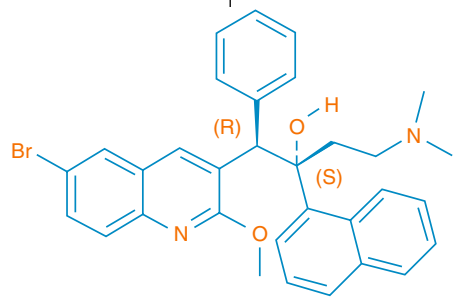

BREVIA

RESEARCH ARTICLE

REPORTS

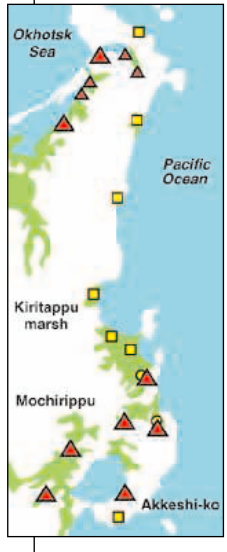

1918

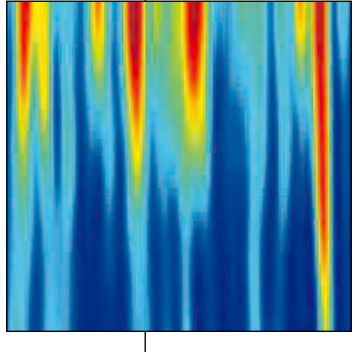

1925

Contents continued

REPORTS CONTINUED

1937

1899 & 1960

AAAS
ADVANCING SCIENCE, SERVING SOCIETY

SCIENCE (ISSN 0036-8075) is published weekly on Friday, except the last week in December, by the American Association for the Advancement of Science, 1200 New York Avenue, NW, Washington, DC 20005. Periodicals Mail postage (publication No. 484460) paid at Washington, DC, and additional mailing offices.

Domestic individual membership and subscription (51 issues): $130 ($74 allocated to subscription). Domestic institutional subscription (51 issues): $500; Foreign postage extra: Mexico, Caribbean (surface mail) $55; other countries (air assist delivery) $85. First class, airmail, student, and emeritus rates on request. Canadian rates with GST available upon request, GST #1254 88122. Publications Mail Agreement Number 1069624. **Printed in the U.S.A.**

Change of address: allow 4 weeks, giving old and new addresses and 8-digit account number. **Postmaster:** Send change of address to *Science*, P.O. Box 1811, Danbury, CT 06813–1811. **Single copy sales:** $10.00 per issue prepaid includes surface postage; bulk rates on request. **Authorization to photocopy** material for internal or personal use under circumstances not falling within the fair use provisions of the Copyright Act is granted by AAAS to libraries and other users registered with the Copyright Clearance Center (CCC) Transactional Reporting Service, provided that $15.00 per article is paid directly to CCC, 222 Rosewood Drive, Danvers, MA 01923. The identification code for *Science* is 0036-8075/83 $15.00. *Science* is indexed in the *Reader's Guide to Periodical Literature* and in several specialized indexes.

Contents continued ▶

At Bristol-Myers Squibb, our mission is clear. To discover and develop innovative treatments for the world's most serious diseases, such as cancer, AIDS and mental illness. To erase their devastating effects. And someday, to wipe them off the face of the earth. The employees of Bristol-Myers Squibb around the globe are united in our dedication and commitment to extend and enhance human life.

Bristol-Myers Squibb Company

Hope, Triumph, and the Miracle of Medicine

Science
www.scienceonline.org

sciencenow www.sciencenow.org Daily News Coverage

An Ancient Vintage
9000-year-old Chinese recipe for wine contained rice, fruit, and honey.

High-Altitude Hovering
Big wings help Andean hummingbirds aloft in thin air.

Toxic Sperm Blocker
Enzyme that creates hydrogen peroxide ensures that only one sperm hits the mark.

Biomechanist Siân Lawson.

science's next wave www.nextwave.org Career Resources for Young Scientists

UK: A Scientist Goes to the Movies *S. Lawson*
A biomechanist applies her expertise in medical biometrics to movies like "Troy" and "King Arthur."

US: Academic Scientists at Work—The Job Talk *J. Boss and S. Eckert*
How do you give a job talk that will appeal to a diverse audience?

US: Transitions from Physics to Biology *The GrantDoctor*
Here's one theoretical particle physicist who wants to be a biologist when he grows up.

MiSciNet: Believing Is Achieving *E. Francisco*
The first tribally enrolled Native American astronaut advises students on how to pursue science and engineering careers.

UK: Christmas Wrap-Up *The CareerDoctor*
The CareerDoctor offers new morsels of advice, just in time for the holidays.

science's sage ke www.sageke.org Science of Aging Knowledge Environment

Review: Poly(ADP-Ribosyl)ation, PARP, and Aging *S. Beneke and A. Bürkle*
PARP enzymes serve to protect the genome.

News Focus: Young at Brain *M. Leslie*
Long-lived mice pump out extra neurons.

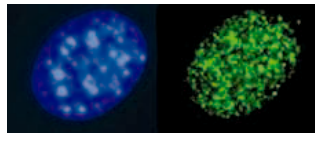

DNA damage stimulates poly(ADP-ribosyl)ation.

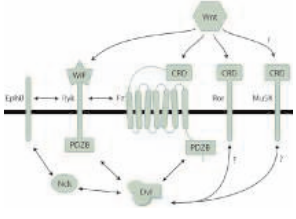

Noncanonical Wnt signaling.

science's stke www.stke.org Signal Transduction Knowledge Environment

Perspective: Ryk—Another Heretical Wnt Receptor Defies the Canon *B. N. R. Cheyette*
Wnt signaling through Ryk-containing receptors may proceed through canonical and noncanonical pathways.

Comment: Role of ERK in Neuronal Survival and Death *L. Colucci-D'Amato, C. Perrone-Capano, U. di Porzio*
Researchers comment on a recent STKE Perspective.

Comment: RAC4 Is a Pseudogene *J. Colicelli*
New information relates to the STKE Review "Human RAS Superfamily Proteins and Related GTPases."

Separate individual or institutional subscriptions to these products may be required for full-text access.

Fluent in any language.

Introducing EndNote 8

EndNote is the industry standard for creating, managing, and publishing bibliographies. And with EndNote 8, your options have increased dramatically.

- *Unicode support for any language*
- *Unlimited library size*
- *New reference types and fields*
- *Enhanced support for electronic sources*
- *Perfectly formatted bibliographies for more than 1,100 publication styles*

See why millions of researchers, students, librarians, professors and writers worldwide use EndNote to search online databases, organize references, images and PDF files, and create bibliographies instantly. It's easy to use, easy to learn, saves you from retyping references, and now provides unlimited capacity. There simply is no better way to manage bibliographies.

Download your Free demo or buy online today at www.endnote.com.

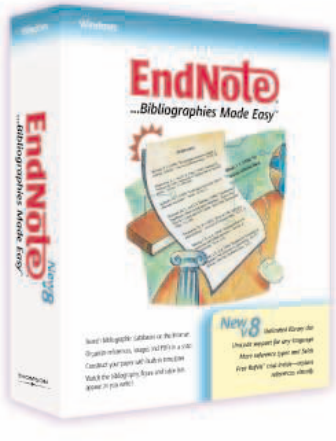

"I've used EndNote since version 1, and find it to be an indispensable component of my academic toolbox. EndNote makes it easier for me to do my job well. I would not want to be without it."
—Barry J. Fishman,
School of Education,
The University of Michigan

THOMSON™

Sales: 800-722-1227 • 760-438-5526 • Fax: 760-438-5573
info@isiresearchsoft.com • www.endnote.com

edited by Stella Hurtley and Phil Szuromi

Semiconductors in a Spin

A current flow through a conductor in a magnetic field leads to a measurable voltage in the transverse direction (the Hall effect). Recent theoretical work has predicted the existence of an analogous effect for the spin in semiconductors, the spin Hall effect. **Kato *et al.*** (p. 1910, published online 11 November 2004; see the 12 November news story by **Service**, the cover, and the Perspective by **Bauer**) present experimental data confirming the accumulation of net spin on opposite sides of a GaAs sample. The ability to create and detect a spin current in a nonmagnetic material, without the need for an external magnetic field, may lead to applications in spin electronics.

Brainy and Agile Birds

Anecdotal evidence and human folklore have always ascribed a comparatively high level of intelligence to corvids—crows, rooks, jays, and ravens—and recent experiments on their cognitive abilities have begun to put this reputation on a factual basis. **Emery and Clayton** (p. 1903) review field studies and experimental studies which show that for a number of tasks that involve higher cognitive functions, corvids' abilities rival or excel those of apes. Corvids are amazingly skilled in three areas: Tool manufacture and use; mental time travel; and social cognition. In another area of convergent evolution, that of flight, our understanding of insect flight was greatly improved almost a decade ago with the discovery of leading-edge vortices on their wings. Technical difficulties of monitoring air flow around wing surfaces of flying birds to look for similar effects have now been overcome by using water instead of air as the moving fluid. Using models of wings of the common swift in a water tunnel, **Videler *et al.*** (p. 1960; see the Perspective by **Müller and Lentink**) show that leading-edge vortices can also generate lift for birds. In birds, the lift generated appears to be important for aerobatic prowess, rather than simply keeping airborne.

Large Shallow Quakes

An estuary along the eastern coast of Japan shows evidence for multiple episodes of uplift during the past few hundred thousand years, but the cause of this uplift is poorly understood. **Sawai *et al.*** (p. 1918) found a tsunami deposit closely followed by a series of uplifted mudflats that formed in the 17th century. The large size of the tsunami along with the large amount of uplift indicate that a large magnitude, shallow earthquake occurred along the subducting plate boundary. The uplift was probably produced by transient creep along the subduction zone or mantle relaxation for tens of years after the event.

Oscillatory Superconductivity

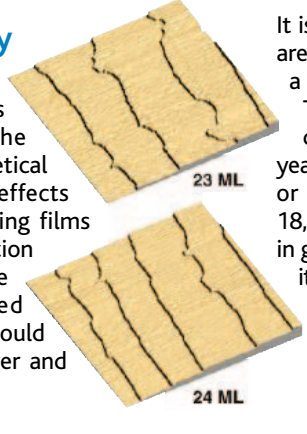

When the thickness of films approach several monolayers, quantum size effects may result from the confinement of the electrons in the vertical direction. Theoretical work has predicted that quantum size effects should also appear in thin superconducting films as a well-defined oscillation of the transition temperature T_c. **Guo *et al.*** (p. 1915; see the Perspective by **Chiang**) produced uniform thin Pb films whose thickness could be controlled to within a single monolayer and observed the predicted oscillations in T_c.

Recombination and Diversity

DNA recombination may represent the driving force for sex in eukaryotes and a major source of adaptation and diversification in bacteria. The role of recombination in the third branch of life, Archaea, has not been clear. **Papke *et al.*** (p. 1928) analyze a population of haloarchaea in solar salterns near Alicante, Spain. The association of gene alleles is essentially arbitrary, which suggests that the saltern populations are likely to be recombining their DNA freely with each other. The high level of "linkage equilibrium" measured for haloarchaea is similar to levels seen in sexual eukaryotic populations.

Which Way Out for *Plasmodium* Proteins?

In mammals, malaria parasites live within red blood cells and decorate the host cell surface with immune evasive variant antigens encoded by the *var* genes. Erythrocytes lack a secretory machinery, and so the parasite must create one. **Hiller *et al.*** (p. 1934) and **Marti *et al.*** (p. 1930) now define motifs that route proteins into the red cell cytoplasm (see the Perspective by **Przyborski and Lanzer**). Without these signals, or if critical residues are mutated, the proteins are trapped within the parasitophorous vacuole.

Genetic Blueprint of the Silkworm

It is easy to see the differences between moths and flies, but what are the differences at the genetic level? **Xia *et al.*** (p. 1937) present a draft genome sequence for the silkworm moth, *Bombyx mori*. This lepidopteran diverged from the previously sequenced dipteran insects (fruit fly and mosquito) more than 280 million years ago. Domains can now be identified that are unique to insects or unique to the silkworm. The silkworm genome (more than 18,000 genes) is larger than that of *Drosophila* because of increases in gene number and size. As more sequence information is analyzed, it will be possible to correlate the dramatic morphological diversity that is seen among the insects with gene diversity.

Learning from Experience in Parkinson's Disease

Learning from experience means that positive feedback or reward is used to reinforce behaviors, and negative feedback is used to avoid such behavior. Dopaminergic pathways are thought to

CONTINUED ON PAGE 1859

CREDITS (TOP TO BOTTOM): EMERY AND CLAYTON; GUO *ET AL.*

Now see beneath the surface of living cells.

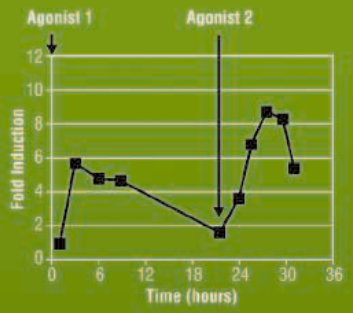

Real-time, kinetic measurement of sequential agonist induction from live cells.

The new Promega EnduRen™ Live Cell Substrate lets you catch everything going on in the cell as it happens. Reveal a wide range of intracellular activity without disturbing your cells. Perform *Renilla* luciferase-based kinetic reporter gene analysis, multiplexed assays (e.g. reporter and cell viability) and BRET analysis with unparalleled ease. To learn more about how you can capture your cell's behavior in action, visit **www.promega.com/enduren**

PROMEGA CORPORATION • www.promega.com

Promega

contribute to both kinds of feedback. **Frank *et al.*** (p. 1940, published online 4 November 2004) previously formulated a computational model which predicted that the loss of dopamine in patients with Parkinson's disease should make it more difficult for them to learn from positive reinforcement but, counterintuitively, easier to learn from negative feedback. Conversely, patients on medication that increases dopamine levels should display the opposite pattern of learning efficiency. Testing patients on two kinds of cognitive tasks, on and off medication, confirmed these predictions and may provide an explanation for the sometimes puzzling effects on learning during treatment of patients with Parkinson's disease .

Organic Aerosols Overstay

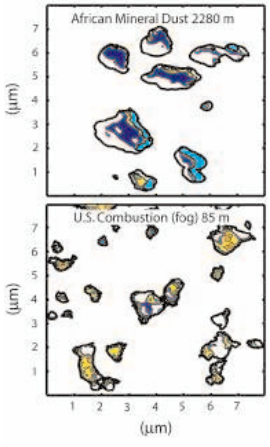

Aerosols affect climate by their influence on how much solar radiation is reflected into space or absorbed in the atmosphere. The effects occur both directly as well as indirectly (by modifying cloud distributions and properties). The effects of chemical reactions on the properties of aerosols have been difficult to characterize. **Maria *et al.*** (p. 1921) calculated the oxidation rates of the organic molecules in carbonaceous aerosols, which comprise a large fraction of the total atmospheric aerosol burden. They measured which organic functional groups occur in individual particles and combined those data with insights into the microphysical processes that direct particle growth. With this method, they conclude that conversion rates are a factor of 3 lower than those typically used in climate models, thus leading to longer aerosol lifetimes and changes in their overall effects on cooling and warming.

Cocaine Signals Never Disappoint

The temporal difference reinforcement learning (TDRL) model provides a computational framework for describing how future rewards are valued, how current choices are made, and how differences between what is received and what is expected are fed back into updated calculations of future rewards. In TDRL, the difference signal between receipt and expectation is carried by neurons that use the transmitter dopamine. **Redish** (p. 1944; see the Perspective by **Ahmed**) applies this model and develops an explanation, in neural computational terms, for some aspects of behavior in the context of addictive substances. The key point is that cocaine induces, via pharmacologic pathways, a dopamine signal that does not accurately reflect or respond to the difference in actual and expected reward; cocaine is always valued as being more rewarding than originally thought.

Controlling Ovulation

In the mammalian ovary, oocytes are maintained in meiotic arrest until the female ovulation cycle directs meiosis to resume just prior to ovulation. A G_s-linked receptor in the mouse oocyte membrane acts as a regulator of the transition between meiotic prophase and metaphase. **Mehlmann *et al.*** (p. 1947) now identify GPR3 as the oocyte receptor required for the maintenance of prophase arrest.

Estrogen Receptors Act in Atherosclerosis

Men experience a more rapid progression of atherosclerosis, but the basis for this gender difference has not been clear. The prostacyclin PGI_2 prevents many processes associated with the formation of atherosclerotic lesions, and the atheroprotective effect of estrogen in women may be via stimulation of PGI_2 production. **Egan *et al.*** (p. 1954, published online 18 November 2004; see the 19 November news story by **Couzin**) now show in a mouse model of atherosclerosis that estrogen acts through the estrogen receptor subtype to generate PGI_2 through cyclooxygenase 2 (COX-2). Female mice lacking a receptor for PGI_2 developed atherosclerosis as rapidly as male mice and had poor response to estrogen therapy. This mechanism may be important in assessing the effects of hormone replacement therapy and selective COX-2 inhibitors.

CREDIT: MARIA *ET AL.*

Looking for a career that defies the law of gravity?

Then talk to someone who knows science.

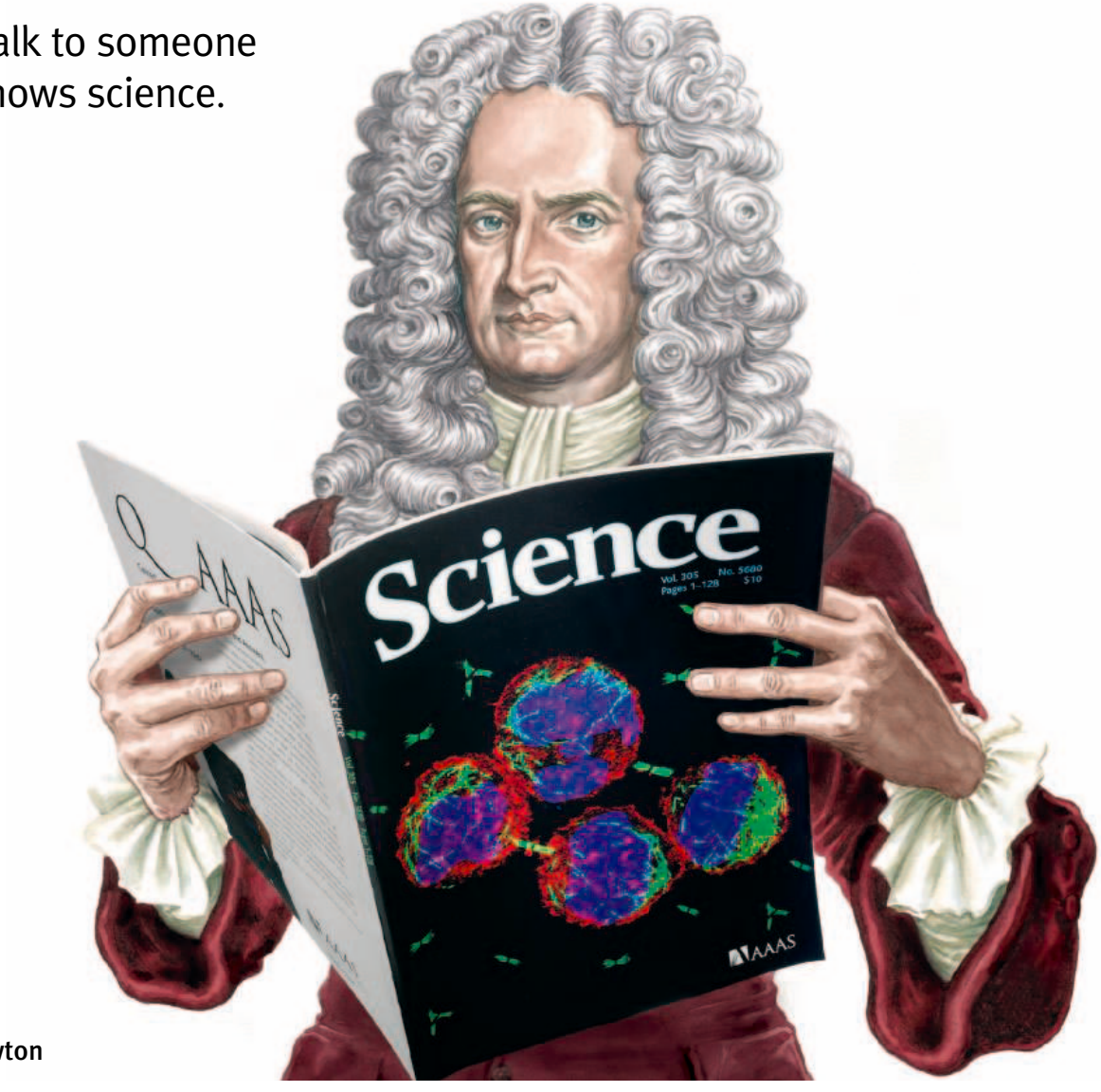

Isaac Newton
1642–1727

If you want to head upward in the world of science, it's essential you don't leave your career to chance. At ScienceCareers.org we know science. We are committed to helping you find the right job, and to delivering the advice you need. Our knowledge is firmly founded on the expertise of *Science*, the premier scientific journal, and the long experience of AAAS in advancing science around the world. So if you want your career to bear fruit, trust the specialist in science. Go to ScienceCareers.org

ScienceCareers.org
We know science AAAS

Extremist Tendencies

There is a Chinese proverb, 过犹不及, "Going too far is as bad as not going far enough," which aptly describes the visa situation enforced by the current U.S. administration, especially with regard to scientific exchange.

An increasing number of Chinese scientists and students are encountering delays and refusals when applying for visas to go to the United States. Most of them are bona fide students who intend to study in the United States or scientists who plan to participate in scientific conferences or collaborations with U.S. colleagues. It is now very costly with respect to both time and money to go through the visa application process. The result is lost opportunities to present new research at important international conferences or to participate in scientific collaborations. This situation even affects some of the most prominent scientists in China, such as the vice president of the Chinese Academy of Sciences (CAS) and the director of the Shanghai Institutes of Biological Sciences, CAS.

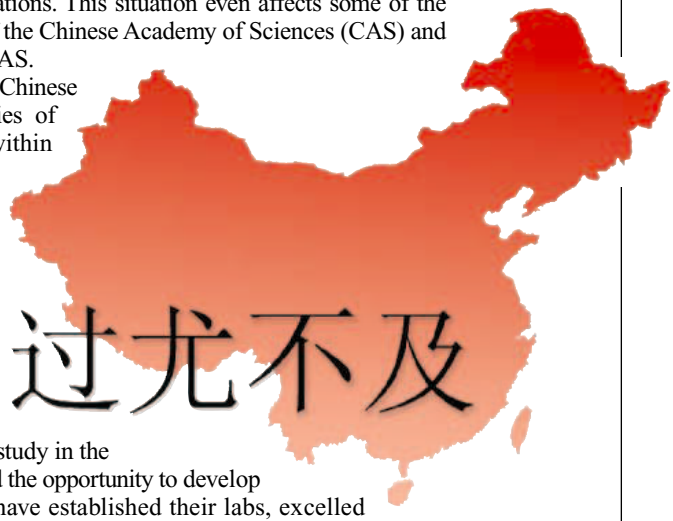

For this Editorial, we sent a simple e-mail survey to about 400 Chinese professors and graduate students at CAS and the Universities of Peking, Fudan, Yunnan, and Wuhan. We received 76 replies within 2 weeks. 71% of respondents said that they would avoid going to the United States; 91% are seriously rethinking their collaborations with U.S. scientists and intend to work with scientists in countries where obtaining a visa is not a problem; and 95% believe that the visa situation is damaging to Sino-U.S. scientific exchange. Both authors have had outstanding graduate students who abandoned plans to go to the United States after experiencing tremendous frustration with the visa process, taking up postdoctoral positions in Europe or Canada instead.

China produces a lot of talent simply because of the size of its population. Tens of thousands of Chinese students have gone to study in the United States, attracted by the excellent scientific environment and the opportunity to develop a successful career. Many remain in the United States; they have established their labs, excelled in their research, and most of them maintain extensive connections with the scientific community in China. On the other hand, an increasing number of Chinese students trained in the United States have returned to China to start their own labs, and most of them maintain extensive connections with the U.S. scientific community. As of 17 September 2004, 53% of the research papers published in *Science* and *Nature* this year that are from Chinese laboratories are coauthored with American scientists. This degree of Sino-U.S. collaboration is important for both Chinese and U.S. science, but it is being damaged by the current problems with the U.S. visa process. Scientists in other countries are also experiencing similar frustrations in obtaining U.S. visas.

Fencing the United States off from the rest of the world is a backward step. Communication, exchange, and international collaboration are essential for high-quality scientific research. One reason why the United States maintains preeminence in scientific research is that it attracts talent from, and keeps a close connection with, scientific institutions all over the world. Ironically, overreaction to terrorism to the degree that every aspect of normal life is disrupted is exactly the result the terrorists aimed to achieve. We sincerely hope that unnecessary barriers between U.S. and international scientific communities can be removed and that healthy collaboration and exchange can be encouraged. This is in the interest of every country, including the United States.

Ya-Ping Zhang and Shigang He

Ya-Ping Zhang is vice director of the Kunming Institute of Zoology, Chinese Academy of Sciences (CAS), and a professor at Yunnan University, Kunming, China. Shigang He is a professor at the Institute of Biophysics, CAS, Beijing, China.

10.1126/science.1107002

edited by Gilbert Chin

APPLIED PHYSICS

Tracking a Trap

The movement of molecular motors along nucleic acids can be detected by imaging the fluorescence of single molecules or by following the movement of attached beads in optical traps. Both methods have resolution limits of 1 to 2 nm. For optical trapping, noise from Brownian motion can be decreased by time averaging, but the other source of noise, instrumental drift, cannot; and methods such as interferometry and back-focal plane detection have been used to combat this noise. Nugent-Glandorf and Perkins have developed a differential back-focal plane detection method that reduces instrument noise. They used two diode lasers, with wavelengths of 785 and 850 nm, to follow the motion of two 200-nm polystyrene beads stuck to the same glass coverslip; they also mechanically stabilized each beam to improve pointing stability. Both bead positions drifted several nanometers in 1 min, but the differential position drifted only 0.5 nm, and the resolution was better than 0.1 nm on the millisecond time scale. They could also follow apparent motion of 0.4-nm steps (equivalent to a one-base step along the DNA helix) by stepping one beam while leaving the other in place. — PDS

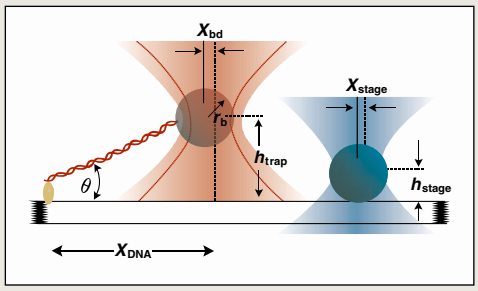

Measuring stage motion in an optical trapping microscope removes mechanical drift.

Opt. Lett. **29**, 2611 (2004).

CELL BIOLOGY

Metalloprotease, Migration, and Mitosis

The cell division cycle is controlled by the interplay of phosphorylation pathways and regulated proteolysis. McHugh *et al*. describe a new player involved in promoting mitotic progression—a metalloprotease they call invadolysin. Mutant *Drosophila* larvae lacking invadolysin display defects in nuclear and mitotic spindle morphology, and in addition exhibit abnormalities in the directed migration of germ cells. Invadolysin appears to act as a protease that degrades nuclear lamin proteins, whose disassembly is a key event at the beginning of mitosis. Generally, invadolysin is found localized in the cytoplasm in structures resembling invadopodia, which are found in invasive tumor cells munching their way through extracellular matrix. In migrating macrophages, invadolysin is concentrated at the leading edge, where it likely facilitates cell migration. — SMH

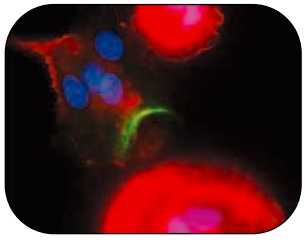

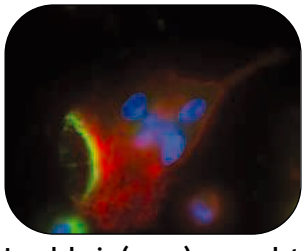

Invadolysin (green) accumulates at the leading edge of migrating macrophages (actin, red; DNA, blue).

J. Cell Biol. **167**, 673 (2004).

IMMUNOLOGY

How to Be a Good Host

In the middle of the past century, the Australian government took advantage of the species specificity of myxoma virus to control the spread of European wild rabbits, by then considered a pest. Although other poxviruses display specificity to varying degrees, it is not clear what influences host/virus compatibility.

Wang *et al*. observed that myxoma virus infection of primary mouse embryo fibroblasts, which are nonpermissive for replication of this virus, activated the kinase Erk1/2. In the presence of an Erk1/2 inhibitor or in cells with impaired Erk1/2 expression, viral replication increased, suggesting that this kinase normally represses this virus. Erk1/2 is linked with interferon regulatory factor 3, which in turn induces expression of type I interferons (IFNs). The possibility that these cytokines maintain the nonpermissive state induced by Erk1/2 activation is supported by the fact that cells unable to produce IFNs or the IFN-dependent transcription factor STAT-1 became susceptible to myxoma infection. Furthermore, STAT-1–deficient mice succumbed to inocula of the virus that had no effect on wild-type animals, raising the possibility that similar cellular mechanisms may govern species specificity of other poxviruses. — SJS

Nature Immunol. **5**, 1266 (2004).

MICROBIOLOGY

Same Genes, Distinct Lifestyles

The continuing efforts and accomplishments of genome sequencers have furnished the raw material for mapping networks of molecular interactions and pathway regulation. Winfield and Groisman use both this new kind of systems analysis and some tried-and-true molecular microbiology to show how homologous parts can evolve and be assembled in distinct ways.

In the *Salmonella enterica* PmrA/PmrB two-component system, PmrB senses high (0.1 mM) Fe and phosphorylates PmrA, which then activates transcription of genes that mediate resistance to the antibiotic polymixin; low (10 μM) Mg is sensed by the PhoP/PhoQ system, which generates PmrD, which then stimulates PmrA. In comparison, *Escherichia coli* carries homologs (amino acid identity 84 to 93%) of four of these proteins and of PmrD (55%) and can detect both low Mg and high Fe, but these pathways do not interact because PmrD does not talk to PmrA. Substituting the *S. enterica* version of *pmrD* restores communication and also the feedback inhibition of PmrA on *pmrD* transcription. Why does this matter? The *S. enterica* regulatory network involving PmrA supports virulence in mice, survival in soil, and colonization of chicken macrophages, and thus enables this bacterium to occupy a broader range of niches. — GJC

Proc. Natl. Acad. Sci. U.S.A. **101**, 17162 (2004).

CREDITS: (TOP) NUGEUT-GLANDORF AND PERKINS, *OPT. LETT.* **29**, 2611 (2004); (BOTTOM) MCHUGH *ET AL.*, *J. CELL. BIOL.* **167**, 673 (2004)

PALEOCLIMATE

Drier Tropics, Wetter Poles

Earth's climate was noticeably warm during the Late Cretaceous, a time when dinosaurs and plants were found at polar latitudes. Climate models with enhanced greenhouse gases—notably CO_2 and water vapor—and increased poleward ocean circulation have not been able to simulate fully the high polar temperatures of that period. One possibility is that much more moisture generated by evaporation in the tropics may have been transported poleward than what occurs today. This process effectively transfers heat from the tropics to the poles, because evaporation consumes considerable heat whereas precipitation releases it. Ufnar *et al.* calculate the changes in precipitation and evaporation that could account for the anomalously warm climate and reproduce stable isotope data reflecting rainfall at that time. The data imply that, compared to today, the greenhouse climates of that time dried (decrease in precipitation minus evaporation) latitudes below 40° dramatically and increased precipitation at higher latitudes, resulting in a two- to threefold increase in latent heat tranport toward the poles. — BH

Geology **32**, 1049 (2004).

CHEMISTRY

Polymerizing Peas in a Pod

When materials are introduced into the narrow interior of a carbon nanotube, the confinement can alter their properties; for example, by stabilizing crystal forms that are unstable in the bulk. Britz *et al.* show that confinement can also affect the reactivity of fullerene epoxide ($C_{60}O$) molecules that are lined up inside single-walled carbon nanotubes like peas in a pod, in a fashion similar to what has already been observed for fullerene (C_{60}). When the $C_{60}O$-containing nanotubes are heated for three days at 260°C, the $C_{60}O$ molecules form linear $(C_{60}O)_n$ chains connected via C–O–C bonds. In contrast, when heated under bulk conditions, $C_{60}O$ forms a tangled, branched, three-dimensional polymer. — JFU

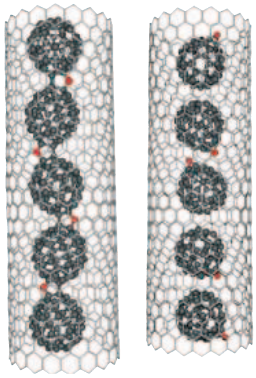

Forming a linear polymer (left) of $C_{60}O$ (oxygen, red).

Chem. Commun. 10.1039/b414247k (2005).

CREDITS: BRITZ *ET AL. CHEM COMMUN.* 10.1039/B414247K (2005).

HIGHLIGHTED IN *SCIENCE*'S SIGNAL TRANSDUCTION KNOWLEDGE ENVIRONMENT

Science's stke www.stke.org

Better Learning Without Channels

Nolan *et al.* conclude that a single type of ion channel can play different roles in learning and memory from their studies of mice lacking the HCN1 protein, a subunit of a channel that accounts for hyperpolarization-activated inward currents. HCN1-knockout mice exhibit motor learning deficits, but mice lacking HCN1 in forebrain neurons actually performed better than wild-type animals on a spatial memory task. Loss of the channel also enhanced long-term memory of how to perform the task. In the CA1 region of the hippocampus, enhanced low-frequency oscillations in neuronal activity were detected in the knockout animals. The pyramidal cells in this region integrate inputs that come from the entorhinal cortex (the perforant pathway) with those from the Schaffer collateral pathway. HCN1 channels are more abundant in the distal dendrites where perforant pathway inputs are localized, and loss of HCN1 preferentially enhanced postsynaptic responses to a single input from the perforant pathway. Similarly long-term potentiation was enhanced at these perforant path synapses. The authors propose that learning may be suppressed by HCN1 channels because they inhibit postsynaptic changes at distal dendrites that would otherwise result in synaptic plasticity. The loss of HCN1 changes the way in which pyramidal cells integrate incoming signals, enhancing responses to low-frequency waveforms and favoring responses to the distal rather than proximal dendrites. This may be particularly important for spatial learning and memory because CA1 pyramidal neurons are thought to compare sensory input from the perforant pathway with stored information from the CA3 region. — LBR

Cell **119**, 719 (2004).

WHERE SCIENCE IS A

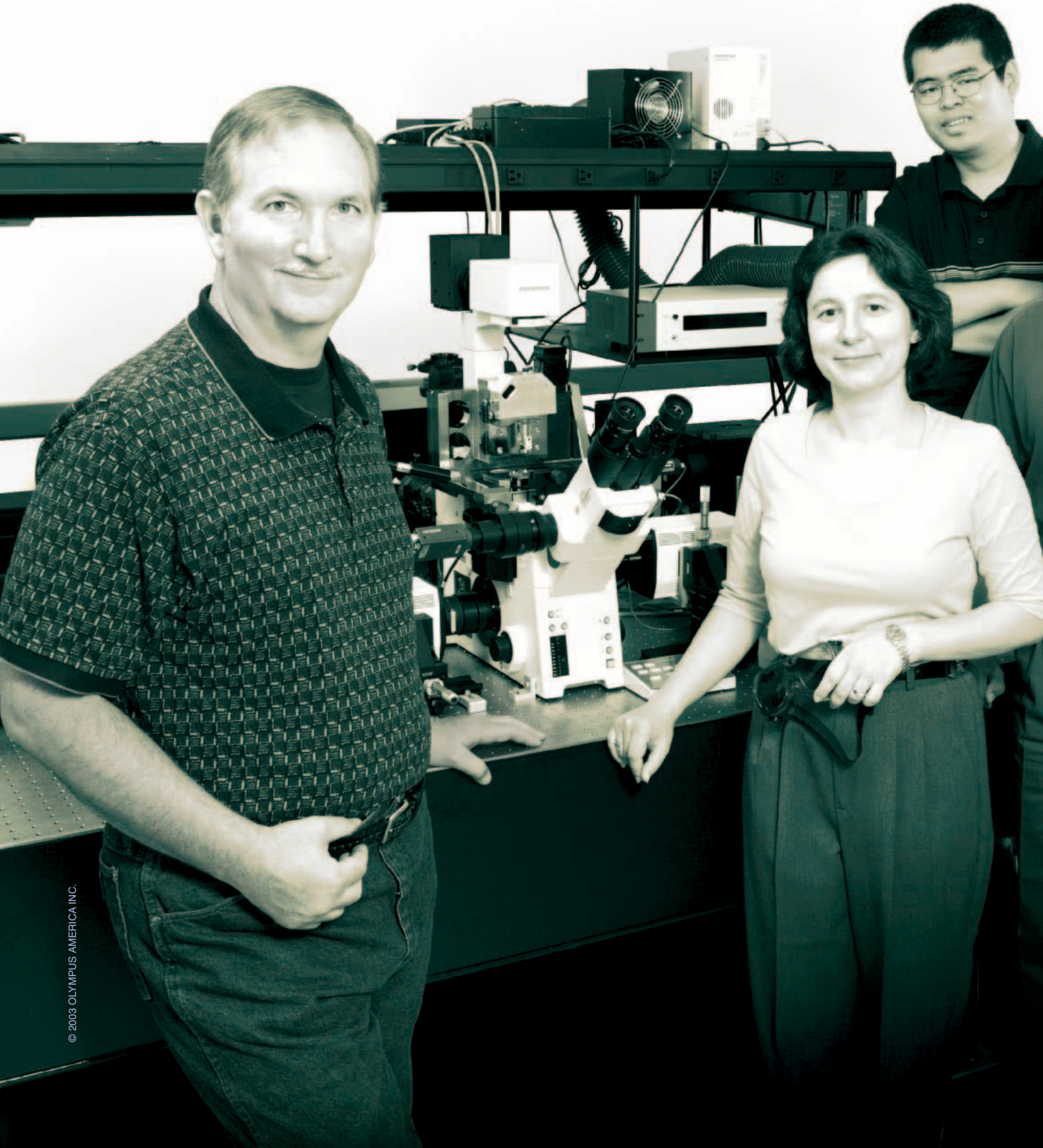

CONTACT SPORT.

They don't just sit around and wait for stuff to happen at Gerry Meininger's lab. As pioneers in vascular biology using atomic force microscopy, they poke cells; prod them; make them squirm. To discover how they react to external forces. "I grew up in Michigan wanting to be a car guy," says Meininger."When I ran into biology, I realized the body is like a machine. You've got to reverse engineer to figure out how it works."

His team is hand picked - - and from around the world. Luke Sun is well pleased to be a small star in a large universe. "I make little steps every day. I hope this will help others make larger steps." Luis A. Martinez-Lemus has a three-word mantra - - prevent, treat, improve - - as he studies the degenerative effects of hypertension and how they might be reversed. Andreea Trache is the high-concept engineer - - orchestrating the union of atomic force and fluorescence microscopy to help the lab accomplish its objectives. Dr. Meininger is both leader and mentor.
"When will they leave to answer their own calling?" we asked.
"When they're ripe," he said.

(From L to R)
Gerald A. Meininger, Ph.D. - Director;

Andreea Trache, Ph.D./Physics-Optics;

Luke Sun, Ph.D./Bioengineering;

Luis A. Martinez-Lemus, D.V.M., Ph.D./Avian Physiology

Division of Vascular Biology
Cardiovascular Research Institute
Texas A&M University

IX81 MOTORIZED INVERTED MICROSCOPE.

Olympus's most advanced motorized inverted microscope is the cornerstone of the Meininger lab's unique "NanoFluor" system which features the capabilities of both Atomic Force (AFM) and fluorescence microscopes.

Through the use of elegant techniques such as fluorescence, TIRFM, FRET and IRM (Interference Reflection Microscopy), they are gaining a detailed knowledge of the minute structures of muscle cells in the vascular wall and how these cells may change as stress is applied.

The IX81 is totally motorized from the built-in focus drive all the way to the filter wheels. Nine access ports allow you to keep dedicated cameras and lasers in place and still keep plenty of ports available for new devices.

The V-shaped light path makes laser setup and adjustment easy and fast.

Critical to the selection of the IX81 was the 3i software which controls the microscope for FRET analysis. But at the core, it is the capability, versatility and flexibility that make the IX81 the ideal microscope to satisfy the most demanding research applications.

OLYMPUS MICROSCOPES. ROCKET SCIENCE™.

Find out more: www.olympusamerica.com/microscopes or: 800-455-8236

OLYMPUS®
Your Vision, Our Future

www.sciencemag.org

Science

1200 New York Avenue, NW
Washington, DC 20005
Editorial: 202-326-6550, FAX 202-289-7562
News: 202-326-6500, FAX 202-371-9227

Bateman House, 82-88 Hills Road
Cambridge, UK CB2 1LQ
+44 (0) 1223 326500, FAX +44 (0) 1223 326501

Subscription Services For change of address, missing issues, new orders and renewals, and payment questions: 800-731-4939 or 202-326-6417, FAX 202-842-1065. Mailing addresses: AAAS, P.O. Box 1811, Danbury, CT 06813 or AAAS Member Services, 1200 New York Avenue, NW, Washington, DC 20005

Institutional Site Liscences please call 202-326-6755 for any questions or information

Reprints Ordering/Billing/Status 800-635-7171; Corrections 202-326-6501

Permissions 202-326-7074, FAX 202-682-0816

Member Benefits Bookstore: AAAS/Barnes&Noble.com bookstore www.aaas.org/bn; Car purchase discount: Subaru VIP Program 202-326-6417; Credit Card: MBNA 800-847-7378; Car Rentals: Hertz 800-654-2200 CDP#343457, Dollar 800-800-4000 #AA1115; AAAS Travels: Betchart Expeditions 800-252-4910; Life Insurance: Seabury & Smith 800-424-9883; Other Benefits: AAAS Member Services 202-326-6417 or www.aaasmember.org.

science_editors@aaas.org (for general editorial queries)
science_letters@aaas.org (for queries about letters)
science_reviews@aaas.org (for returning manuscript reviews)
science_bookrevs@aas.org (for book review queries)

Published by the American Association for the Advancement of Science (AAAS), *Science* serves its readers as a forum for the presentation and discussion of important issues related to the advancement of science, including the presentation of minority or conflicting points of view, rather than by publishing only material on which a consensus has been reached. Accordingly, all articles published in *Science*—including editorials, news and comment, and book reviews—are signed and reflect the individual views of the authors and not official points of view adopted by the AAAS or the institutions with which the authors are affiliated.

AAAS was founded in 1848 and incorporated in 1874. Its mission is to advance science and innovation throughout the world for the benefit of all people. The goals of the association are to: foster communication among scientists, engineers and the public; enhance international cooperation in science and its applications; promote the responsible conduct and use of science and technology; foster education in science and technology for everyone; enhance the science and technology workforce and infrastructure; increase public understanding and appreciation of science and technology; and strengthen support for the science and technology enterprise.

Information for Contributors

See pages 102 and 103 of the 2 January 2004 issue or access www.sciencemag.org/feature/contribinfo/home.shtml

EDITOR-IN-CHIEF **Donald Kennedy**
EXECUTIVE EDITOR **Monica M. Bradford**
DEPUTY EDITORS **R. Brooks Hanson, Katrina L. Kelner**
NEWS EDITOR **Colin Norman**

Editorial supervisory senior editors Barbara Jasny, Phillip D. Szuromi; senior editor/perspectives Orla Smith; senior editors Gilbert J. Chin, Pamela J. Hines, Paula A. Kiberstis (Boston), Beverly A. Purnell, L. Bryan Ray, Guy Riddihough (Manila), Linda R. Rowan, David Voss; associate editors Lisa D. Chong, Marc S. Lavine, H. Jesse Smith, Valda Vinson, Jake S. Yeston; online editor Stewart Wills; associate online editor Tara S. Marathe; book review editor Sherman J. Suter; associate letters editor Etta Kavanagh; information specialist Janet Kegg; editorial manager Cara Tate; senior copy editors Jeffrey E. Cook, Harry Jach, Barbara P. Ordway; copy editors Cynthia Howe, Sabrah M. n'haRaven, Jennifer Sills, Trista Wagoner, Alexis Wynne; editorial coordinators Carolyn Kyle, Beverly Shields; publication assistants Chris Filiatreau, Joi S. Granger, Jeffrey Hearn, Scott Miller, Jerry Richardson, Tunisia L. Riley, Brian White, Anita Wynn; editorial assistants Ramatoulaye Diop, E. Annie Hall, Lisa Johnson, Patricia M. Moore, Jamie M. Wilson; executive assistant Sylvia S. Kihara; administrative support Patricia F. Fisher

News senior correspondents Jean Marx; deputy news editors Robert Coontz, Jeffrey Mervis, Leslie Roberts, John Travis; contributing editors Elizabeth Culotta, Polly Shulman; news writers Yudhijit Bhattacharjee, Jennifer Couzin, Constance Holden, Jocelyn Kaiser, Richard A. Kerr, Andrew Lawler (New England), Gregory Miller, Elizabeth Pennisi, Charles Seife, Robert F. Service (Pacific NW), Erik Stokstad; David Grimm (intern); contributing correspondents Marcia Barinaga (Berkeley, CA), Barry A. Cipra, Adrian Cho, Jon Cohen (San Diego, CA), Daniel Ferber, Ann Gibbons, Robert Irion, Mitch Leslie (NetWatch), Charles C. Mann, Evelyn Strauss, Gary Taubes, Ingrid Wickelgren; copy editors Linda B. Felaco, Rachel Curran, Sean Richardson; administrative support Scherraine Mack, Fannie Groom bureaus: Berkeley, CA: 510-652-0302, FAX 510-652-1867, New England: 207-549-7755, San Diego, CA: 760-942-3252, FAX 760-942-4979, Pacific Northwest: 503-963-1940

Production director James Landry; senior manager Wendy K. Shank; assistant manager Rebecca Doshi; senior specialists Vicki J. Jorgensen, Jessica K. Moshell, Amanda K. Skelton; specialist Jay R. Covert

Preflight director David M. Tompkins; manager Marcus Spiegler

Art director Joshua Moglia; associate art director Kelly Buckheit; illustrator Katharine Sutliff; senior art associates Holly Bishop, Laura Creveling, Preston Huey, Julie White; associate Nayomi Kevitiyagala; photo researcher Leslie Blizard

***Science* International**

Europe (science@science-int.co.uk) editorial: international managing editor Andrew M. Sugden; senior editor/perspectives Julia Fahrenkamp-Uppenbrink; senior editors Caroline Ash, Stella M. Hurtley, Ian S. Osborne, Peter Stern; associate editor Stephen J. Simpson; editorial support Cheryl Sharp, Emma Westgate; administrative support Janet Clements, Phil Marlow, Jill White; news: international news editor Eliot Marshall deputy news editor Daniel Clery; correspondent Gretchen Vogel (Berlin: +49 (0) 30 2809 3902, FAX +49 (0) 30 2809 8365); contributing correspondents Michael Balter (Paris), Martin Enserink (Amsterdam and Paris); intern Fiona Proffitt

Asia Japan Office: Asca Corporation, Eiko Ishioka, Fusako Tamura, 1-8-13, Hirano-cho, Chuo-ku, Osaka-shi, Osaka, 541-0046 Japan; +81 (0) 6 6202 6272, FAX +81 (0) 6 6202 6271; asca@os.gulf.or.jp japan news bureau: Dennis Normile (contributing correspondent, +81 (0) 3 3391 0630, FAX 81 (0) 3 5936 3531; dnormile@gol.com); china representative Hao Xin, + 86 (0) 10 6307 4439 or 6307 3676, FAX +86 (0) 10 6307 4358; haoxin@earthlink.net; south asia Pallava Bagla (contributing correspondent +91 (0) 11 2271 2896; pbagla@vsnl.com); central asia Richard Stone (+7 3272 6413 35, rstone@aas.org)

EXECUTIVE PUBLISHER **Alan I. Leshner**
PUBLISHER **Beth Rosner**

Fulfillment & Membership Services (membership@aaas.org) director Marlene Zendell; fulfillment systems: manager Waylon Butler; member services: manager Michael Lung; senior specialist Pat Butler; specialist Laurie Baker, Tamara Alfson; representative Karena Smith; marketing associate Deborah Stromberg

Business Operations and Administration director Deborah Rivera-Wienhold; business manager Randy Yi; senior financial analysts Lisa Donovan, Jason Hendricks; analyst Jessica Tierney; rights and permissions: administrator Emilie David; associate Elizabeth Sandler; marketing: director John Meyers; membership marketing manager Darryl Walter; marketing associates Karen Nedbal, Julianne Wielga; recruitment marketing manager Allison Pritchard; associates Mary Ellen Crowley, Amanda Donathen, Catherine Featherston; director of international marketing and recruitment advertising Deborah Harris; international marketing manager Wendy Sturley; marketing/member services executive: Linda Rusk; japan sales and marketing manager Jason Hannaford; site license sales: director Tom Ryan; sales and customer service Mehan Dossani, Catherine Holland, Adam Banner, Yaniv Snir; electronic media: internet production manager Lizabeth Harman; assistant production manager Wendy Stengel; senior production associates Carla Cathey, Sheila Mackall, Lisa Stanford; production associate Nichele Johnston; lead applications developer Carl Saffell

Product Advertising (science_advertising@aaas.org); midwest Rick Bongiovanni: 330-405-7080, FAX 330-405-7081 • west coast/w. canada B. Neil Boylan (Associate Director): 650-964-2266, FAX 650-964-2267 • east coast/e. canada Christopher Breslin: 443-512-0330, FAX 443-512-0331 • uk/scandinavia/france/italy/belgium/netherlands Andrew Davies (Associate Director): +44 (0)1782 750111, FAX +44 (0) 1782 751999 • germany/switzerland/austria Tracey Peers (Associate Director): +44 (0) 1782 752530, FAX +44 (0) 1782 752531 japan Mashy Yoshikawa: +81 (0) 33235 5961, FAX +81 (0) 33235 5852 israel Jessica Nachlas +9723 5449123 • traffic manager Carol Maddox; sales coordinator Deiandra Simms

Classified Advertising (advertise@sciencecareers.org); u.s.: sales director Gabrielle Boguslawski: 718-491-1607, FAX 202-289-6742; internet sales manager Beth Dwyer: 202-326-6534; inside sales manager Daryl Anderson: 202-326-6543; west coast/midwest Kristine von Zedlitz: 415-956-2531; east coast Jill Downing: 631-580-2445; line ad sales Emnet Tesfaye: 202-326-6740; senior sales coordinator Erika Bryant; sales coordinators Rohan Edmonson, Caroline Gallina, Christopher Normile, Joyce Scott, Shirley Young; international: sales manager Tracy Holmes: +44 (0) 1223 326525, FAX +44 (0) 1223 326532; sales Emilie Stott; sales assistant Claire Griffiths; japan: Jason Hannaford: +81 (0) 52 777 9777, FAX +81 (0) 52 777 9781; production: manager Jennifer Rankin; assistant manager Deborah Tompkins; associate Amy Hardcastle; senior trafficking associate Christine Hall; senior publications assistant Robert Buck; publications assistant Natasha Pinol

AAAS Board of Directors retiring president, chair Mary Ellen Avery; president Shirley Ann Jackson; president-elect Gilbert S. Omenn; treasurer David E. Shaw; chief executive officer Alan I. Leshner; board Rosina M. Bierbaum; John E. Burris; John E. Dowling; Karen A. Holbrook; Richard A. Meserve; Norine E. Noonan; Peter J. Stang; Kathryn D. Sullivan; Lydia Villa-Komaroff

AAAS
ADVANCING SCIENCE, SERVING SOCIETY

Q What's the best way to send SEAAASON'S GREETINGS?

A Give a AAAS membership with 51 issues of *Science*.

Remember friends, family or colleagues with a gift that lasts all year. Your gift of annual membership in AAAS helps us to support human rights, promote a sound science policy, improve science education, and advance science around the world. It also gives the recipient 51 issues of *Science* to help him or her stay up-to-date with the latest scientific advances and groundbreaking research. Not to mention online access to *Science* archives, career and grant information, exclusive discounts, and more. Order today at **www.promo.aaas.org/hgift9**

Science
AAAS

Special offer rates	Student	Prof./Postdoc
US	US$ 75.00	US$ 99.00
Canada	US$ 139.10	US$ 164.78
Mexico/Caribbean	US$ 130.00	US$ 154.00
All other countries	US$ 160.00	US$ 184.00

Gift givers will receive a limited edition AAAS shirt.

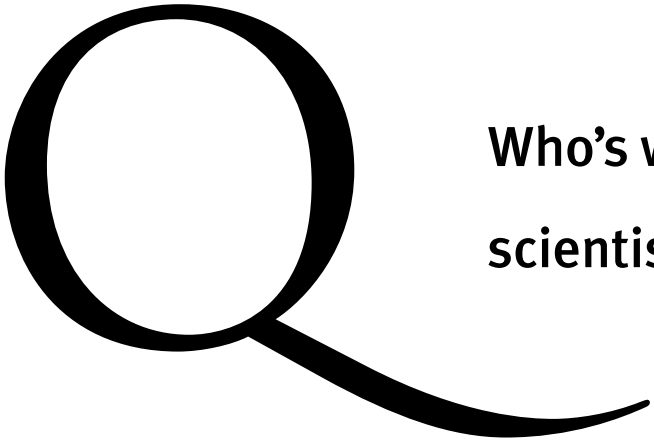

Who's working for tomorrow's scientists today?

"I read my *Science* with my kids. Theodore and Lillian enjoy the pictures of animals, people and planets as I browse through the magazine. It's a fun way for us all to learn more about science."

AAAS member Mark Petersen, post-doctoral researcher for the Climate, Ocean, and Sea Ice Modeling Group, Los Alamos National Laboratory, New Mexico

AAAS

Mark, Theodore and Lillian Petersen

AAAS is committed to advancing science and giving a voice to scientists around the world. We work to improve science education, promote a sound science policy, and support human rights.

Helping our members stay abreast of their field is a key priority for AAAS. One way we do this is through *Science*, which features all the latest breakthroughs and groundbreaking research, and keeps scientists connected wherever they happen to be. Members like Mark find it essential reading.

To join the international family of science, go to www.aaas.org/join

AAAS

ADVANCING SCIENCE, SERVING SOCIETY

www.aaas.org/join

Innovative Filtration Technology

DNA Clean & Concentrator

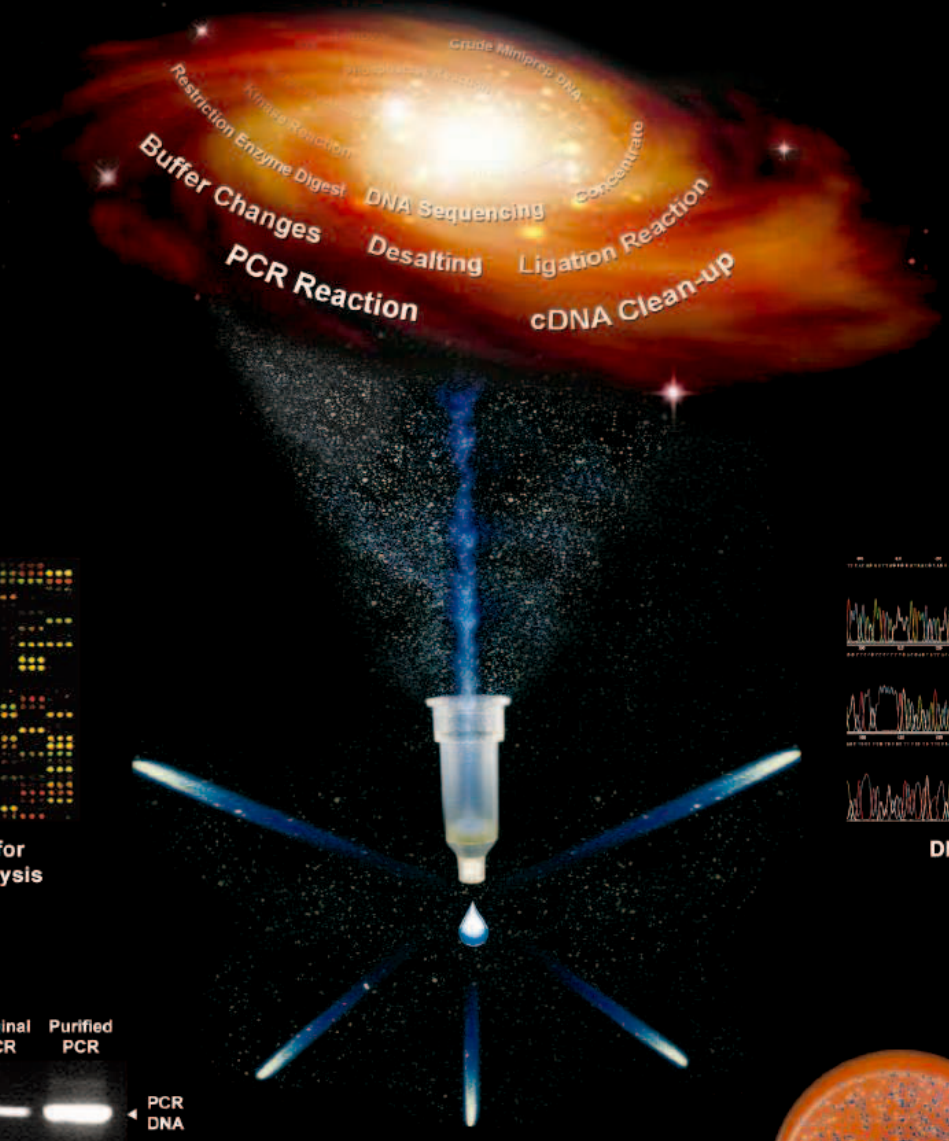

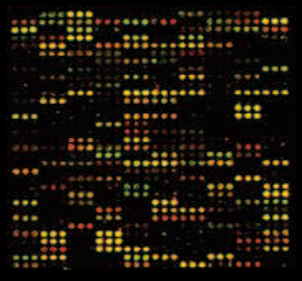

Dye Removal for Microarray Analysis

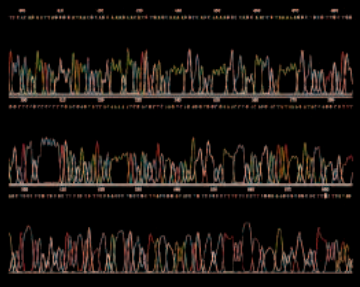

DNA Sequencing

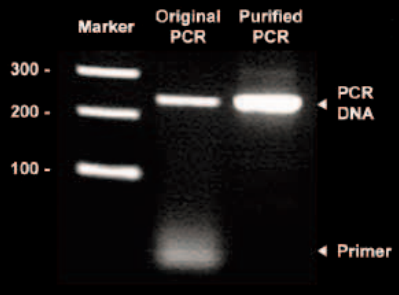

PCR Reaction Clean-Up

Cloning
Ligation
Restriction Digest
RNA Transcription &
All Molecular Biology Applications

E. coli Electroporation

Clean and concentrate your DNA into

6 µl in 2 minutes with 0 µl wash residue contamination

DNA Clean & Concentrator™ (DCC) has been used by thousands of scientists from all major universities and research institutions for years. **DCC** is used for clean-up and concentration of DNA from a variety of sources: PCR reaction, cDNA clean-up, dye removal for microarray analysis, DNA clean-up for sequencing, DNA clean-up for RNA transcription, and among other uses.

Contact us or visit www.zymoresearch.com to request your ***FREE KIT***

ZYMO RESEARCH
The Beauty of Science is to Make Things Simple

Tel: 888-882-9682 • Fax: 714-288-9643 • www.zymoresearch.com • info@zymoresearch.com

NetWatch

edited by Mitch Leslie

IMAGES

Parasite Portfolio

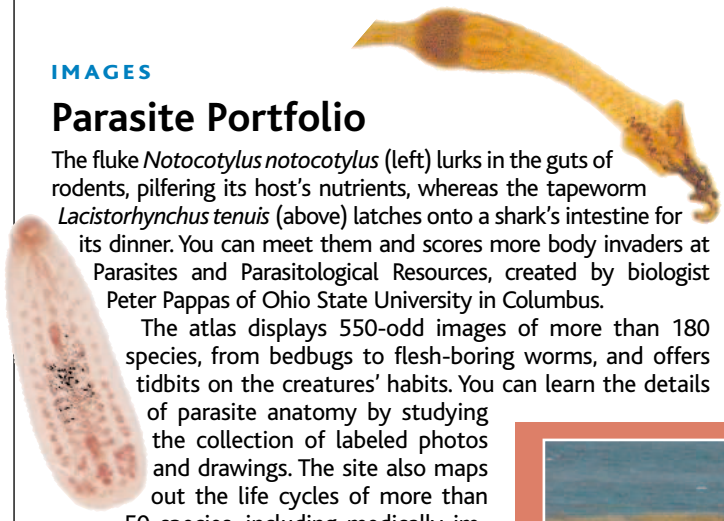

The fluke *Notocotylus notocotylus* (left) lurks in the guts of rodents, pilfering its host's nutrients, whereas the tapeworm *Lacistorhynchus tenuis* (above) latches onto a shark's intestine for its dinner. You can meet them and scores more body invaders at Parasites and Parasitological Resources, created by biologist Peter Pappas of Ohio State University in Columbus.

The atlas displays 550-odd images of more than 180 species, from bedbugs to flesh-boring worms, and offers tidbits on the creatures' habits. You can learn the details of parasite anatomy by studying the collection of labeled photos and drawings. The site also maps out the life cycles of more than 50 species, including medically important parasites such as the protozoan that causes African sleeping sickness and ecologically intriguing examples such as *Notocotylus*.

www.biosci.ohio-state.edu/~parasite/home.html

COMMUNITY SITE

The Sweet Science

Dieters are shunning carbohydrates, but scientists are hungry for information about these molecules. They help the immune system discriminate friend from foe, are an ingredient in the goo that surrounds and supports cells, and may play a role in aging and diseases such as cancer.

The Japanese site Glycoforum, sponsored by the Seikagaku Corp. and the Mizutani Foundation for Glycoscience, is a gathering place for researchers with a taste for carbohydrate biology. Four main sections post short articles, written by academic experts in Japan and other countries, on topics from the evolution of the sugars in milk to the importance of carbohydrate-adorned receptors for flu susceptibility. One focus of the site is hyaluronan, a molecule prevalent in the gel around cells. You can learn about its effects on ovulation and development and read about how the cell's carbohydrate milieu can encourage the spread of cancer. Malignant cells exude more hyaluronan, which in turn alters the cell's internal skeleton and membrane to promote movement. The site also features a calendar of upcoming meetings and links to proceedings from past conferences.

www.glycoforum.gr.jp

NET NEWS

Einstein for the Masses

Readers flummoxed by Einstein's special theory of relativity might soon get help, thanks to an Internet challenge. To mark the 100th anniversary of Einstein's achievement, the Italian company Pirelli, which runs an annual Web site contest, is offering a prize for the best 5-minute multimedia presentation that makes special relativity intelligible to a general audience. Entries are due by 15 March 2005, and the winner, to be announced next summer, will pocket €25,000 (about $30,000). Get more details here:

www.pirelliaward.com/einstein.html

RESOURCES

Portents of Change in the Arctic ...

Polar bears could vanish by the end of the century, warned a scientific report on Arctic climate change last month. Higher temperatures are reducing sea ice, which the animals need to stalk seals. Shrinking sea ice is one of many signs of northern warming in recent decades, as you can see at Arctic Change, a new site from the U.S. National Oceanic and Atmospheric Administration.

Aimed at decision-makers and the general public, the site provides historical perspective on more than 20 climate change indicators, from wildlife behavior to river outflow, that mostly reflect rising Arctic temperatures. The number of months that northern residents can travel on ice roads has fallen from more than six in the early 1970s to fewer than four today, for example. Not all species have suffered from these changes, however: Populations of walleye pollock, a fish that prefers open water, have spiked in the Bering Sea as the ice wanes. The site's brief backgrounders offer plenty of links to reports and more detailed data.

www.arctic.noaa.gov/detect

EXHIBITS

... and an Antarctic Anniversary

The New York Times.

BYRD SAFELY FLIES TO SOUTH POLE AND BACK, LOOKING OVER 'ALMOST LIMITLESS PLATEAU'; DROPS FOOD, LIGHTENS SHIP ON PERILOUS TRIP

FIRST MESSAGE EVER SENT FROM THE SOUTH POLE

They cleared the 3300-meter Polar Plateau only after ditching their emergency provisions, and on 29 November 1929, U.S. aviator Richard E. Byrd and his crew became the first explorers to fly over the South Pole. A new site from the U.S. National Science Foundation honors the 75th anniversary of the event by reviewing Byrd's impact on Antarctic aviation. You can play a video that includes footage from the famous flight and tag along as modern pilots retrace Byrd's route.

www.nsf.gov/od/lpa/events/byrd

Send site suggestions to netwatch@aaas.org. Archive: www.sciencemag.org/netwatch

CREDITS (TOP TO BOTTOM): PETER PAPPAS/OHIO STATE UNIVERSITY; GENE AUGUSTINE/U.S. AIR FORCE; NATIONAL SCIENCE FOUNDATION

This Week

PAGE 1875
Pollution in the Arctic

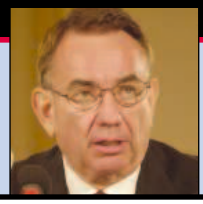

1876
Thompson bows out

MEDICINE

New TB Drug Promises Shorter, Simpler Treatment

A chief reason that tuberculosis persists as a global killer—and is on the rise in parts of the world—is that existing antibiotics require up to 9 months of daily use, making it difficult for people to complete the treatment. Those who miss doses, in turn, fuel the emergence of drug-resistant strains of the mycobacterium that causes the illness. Yet the only new TB drugs to become available during the past 4 decades have been variations of the existing ones. Now researchers at Johnson & Johnson (J&J) in Belgium have discovered a compound that may dramatically reduce the amount of time it takes to cure the disease and that also appears to work against multidrug-resistant strains of *Mycobacterium tuberculosis*. "It's extraordinarily promising," says TB researcher and clinician Jacques Grosset of Johns Hopkins University in Baltimore.

Directly observed. TB clinics, like this one in India, monitor drug taking to ensure that patients complete the long course.

As a team led by J&J's Koen Andries reports online 9 December in *Science* Express (www.sciencemag.org/cgi/content/abstract/1106753), extensive studies in the test tube and mice have shown that the compound, dubbed R207910, is more potent than existing drugs, stays in the body longer, and works by a novel mechanism that makes it broadly effective. Experiments in a small number of uninfected humans and toxicology studies in rats and dogs so far suggest that the compound is safe. "It's like a dream come true," says Andries, a microbiologist. "If you would make a wish list of the assets that an ideal TB compound would have," he says, this would be it.

Like the rest of the pharmaceutical industry, J&J has little financial incentive to develop treatments for TB, a disease that mainly afflicts the poor. But while screening for a new broad-spectrum antibiotic, J&J researchers stumbled upon the finding that a class of compounds called diarylquinolines worked against *M. smegmatis*, a cousin of TB. Chemical tinkering led them to the even more potent R207910. To date, the company has bankrolled development of the drug.

TB DRUG PIPELINE

Sponsors	Drug	Development Stage
Johnson & Johnson	Diarylquinoline, R207910	Early clinical trials
Bayer	* Moxifloxacin	Early clinical trials
European Commission, WHO	* Gatifloxacin	Early clinical trials
Chiron, TB Alliance	Nitroimidazole, PA-824	Preclinical
Lupin	Pyrrole, LL-3858	Preclinical
Procter & Gamble	Nonfluorinated quinolone	Preclinical
Sequella	Ethambutol analog	Preclinical

*Already approved for other indications.

Andries's group has joined with outside research teams to conduct many of the experiments described in the current report. In particular, researchers in France provided a critical mouse model for TB, which led to the finding that the compound lasted unusually long in the rodent, suggesting that it might kill *M. tuberculosis* with fewer doses. The French researchers added the drug to the most popular triple combination now used—rifampin, isoniazid, and pyrazinamide—and found that it achieved the same bactericidal effects in half the time. Various combinations with two of the existing drugs also showed significant benefits.

As expected, resistance to R207910 developed when given to mice as a monotherapy, but the mouse data have convinced leading TB researchers that swapping the drug for one of the three in the current cocktail would delay development of resistant strains and would vastly shorten treatment. "This is quite frankly an astonishing set of results," says Denis Mitchison of St. George's Hospital Medical School in London. "They've managed with some of the combinations to get complete sterilization of organs within 2 months rather than 4. That's never been done before."

Mitchison (who consulted with J&J about the results) and several other researchers were particularly intrigued by the drug's novel mechanism of action. After sequencing the genomes of strains of *M. tuberculosis* and *M. smegmatis* that were resistant to R207910, Andries and his colleagues compared the results to the DNA from susceptible strains. The genetic mutations they discovered in the resistant strains all pointed to a gene that codes for an enzyme that makes ATP, which provides energy for cells. "Nobody before has identified that as a drug target for TB," says William Jacobs of the Albert Einstein School of Medicine in New York City.

Mel Spigelman of the Global Alliance for TB Drug Development, a nonprofit organization based in New York City that partners with industry and academics to accelerate R&D of faster-acting compounds, says R207910 is one of several novel agents now entering or nearing human trials (see chart). "There is a revolution in the development of drugs for TB," says Spigelman. Although R207910 has moved further than other novel drugs in the development pipeline, Spigelman predicts that several of the drugs will prove their worth in human tests. He imagines a day when combining the drugs now under development offers a therapy that cures the disease in as little as 1 week. He stresses, however, that the challenge is not simply developing new drugs but delivering them at an affordable price—a key mission of the alliance, which may work with J&J in the future.

J&J's Andries says the company understands that most of the 8 million people who suffer from TB each year cannot afford expensive new drugs. "What drives us most is the medical need for such compounds," says Andries, who adds that the lower rate of financial return could be offset by "goodwill toward the company." The drug will soon enter into trials in people who have active TB cases. Many promising drugs of course fail in human tests, notes Andries, but if all goes well, he says the compound could be on the market in 5 years.

—JON COHEN

CREDITS: TB ALLIANCE; MALCOM LINTON

1878
Controlling a cursor by brain waves

1880
The costly locust campaign

1884
Flushing the Colorado

DEPARTMENT OF ENERGY

Outlook for Cold Fusion Is Still Chilly

A Department of Energy (DOE) review of "cold fusion" has generated some heat but very little light on the controversial subject.

Since 1989, when Martin Fleischmann and Stanley Pons announced that a small hunk of palladium metal had apparently induced deuterium atoms to fuse at room temperature, a small cadre of cold-fusion enthusiasts has doggedly kept on the trail of endless energy. So when DOE decided in March to conduct a review of cold-fusion research, the move raised eyebrows among mainstream scientists who have long since abandoned the quest. "They asked me to serve on it, but I resolutely refused," says William Happer, a plasma physicist at Princeton University and a harsh critic of cold-fusion research. That attitude didn't surprise those proponents of cold fusion who had pushed DOE to take another look. "I was told going into this that we would be facing an extremely skeptical and pretty hostile crowd of reviewers," says Peter Hagelstein, a cold-fusion researcher at the Massachusetts Institute of Technology.

The outcome appears to reinforce the views of both sides, although it's hard to tell because the reviewers didn't meet to hammer out a consensus. Instead, DOE simply compiled a written summary of the reviewers' individual comments. All told, DOE asked 18 reviewers—nine by mail in July, and nine others who attended a 1-day meeting in August—to study a summary of the field prepared by Hagelstein and others as well as published results and to evaluate the evidence for nuclear reactions in matter at low energies to determine whether it's worthwhile to continue studying the phenomenon.

Several reviewers were indeed extremely critical of the research, saying that many of the experiments were poorly conducted, had results that were inconsistent with each other, and often weren't reproducible. One skeptical reviewer went further, opining that "[cold fusion] workers are true believers, and so there is no experiment that can make them quit."

At the same time, about one-third of the reviewers, however, were receptive to claims of cold fusion. "There is strong evidence of nuclear reactions in palladium," one wrote. Said another: "Further work that would add to the understanding of [low-energy nuclear reactions] is warranted and should be funded by U.S. funding agencies."

DOE's position on cold fusion hasn't changed as a result of the review, says James Decker, deputy director of the Office of Science. "We never closed the door to good proposals," he says, adding that the real value of the study was to "bring people up to date" on the issue. Hagelstein says that his side has also accomplished its goals. "In the end, the reviewers said that a study should be funded if a proposal is strong. You can't ask for much more than that."

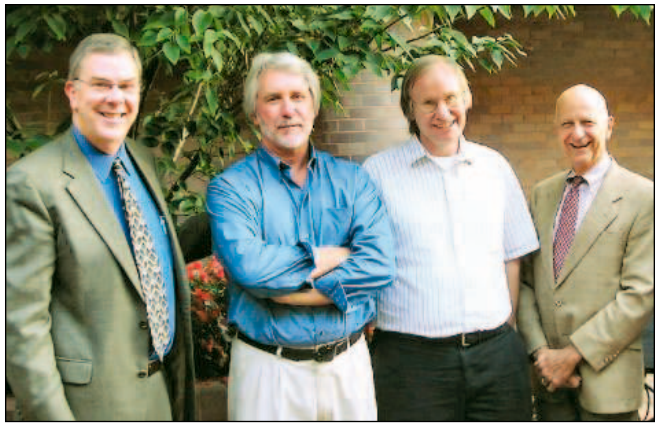

To coldly go. MIT's Peter Hagelstein (second from right) and three colleagues pushed DOE to reexamine cold fusion.

—CHARLES SEIFE

U.S. RESEARCH POLICY

NSF Blocked From Funding Smithsonian Scientists

Congress has squashed a move by the National Science Foundation (NSF) to allow all Smithsonian Institution (SI) scientists to compete for NSF funds. The decision represents a victory for Senator Kit Bond (R–MO), who chairs the spending panel that sets NSF's budget, over his counterparts in the House, who had pushed for the change.

NSF's current policy allows so-called Smithsonian trust scientists—those whose salaries come from a pot created by the institution's benefactor, James Smithson—to be treated like any other eligible NSF applicant. Most of the Smithsonian's 187 trust scientists work for its astrophysical observatory in Cambridge, Massachusetts, which relies on grants from NASA and other sources.

But the vast majority of museum curators are paid from the institution's annual federal appropriation and are therefore ineligible for NSF grants. Last spring the National Science Board (NSB), NSF's oversight body, embraced equal treatment for all 431 SI scientists, despite concern that it might open the door to researchers in other federal settings to plead for similar treatment (*Science*, 2 April, p. 26).

Bond, however, saw the proposed expansion as double dipping. So last month he inserted language into the massive 2005 spending bill (*Science*, 3 December, p. 1662) passed by both the House and Senate ordering NSF to maintain the status quo. "Senator Bond felt very strongly about this matter," says a House aide, "and conference reports are about compromises."

"The board shares Senator Bond's concerns for setting no precedent that would allow scientists at federal research agencies or federally funded research centers to become eligible to apply for NSF grants," says NSB Chair Warren Washington about the congressional diktat. As a result, Washington says NSF has called off talks with the Smithsonian on any changes to its grants policy. The language, he notes, also reminds NSF program managers to be fair to trust employees submitting grant proposals.

—JEFFREY MERVIS

catch the wave

2005/06 NEB catalog & technical reference is now available.

catalog highlights:

- 15 new Restriction Enzymes (not to mention 225 old favorites)
- Antarctic Phosphatase – the only commercially available phosphatase that is 100% heat inactivated in 5 minutes at 65°C; it's a better enzyme than SAP
- ShortCut siRNA Mixes – highly potent siRNA mixes that can be used at low (1-20 nM) concentration
- TransPass Transfection Reagents for siRNA and DNA
- Peptide-Carrier Kit – ligate your peptide of interest to a carrier protein for detection on Western blots or peptide arrays
- Updated Reference Appendix
- Environmental Theme – the impact of non-governmental organizations (NGOs) on the well-being of our planet

www.neb.com

The new NEB website complements our catalog and features access to an extensive library of product technical literature as well as computer tools such as Enzyme Finder and NEBcutter. The improved interface provides greater functionality when ordering products online, including customer-specific pricing, order history and shipment tracking.


1975/76


1978


1979

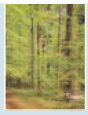
1980/81

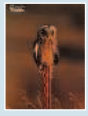
1981/82


1982/83


1983/84


1985/86


1986/87


1988/89


1990/91


1992

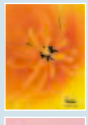
1993/94


1995


1996/97


1998/99


2000/01


2002/03

www.neb.com

New England Biolabs Inc.
32 Tozer Road • Beverly • MA 01915 USA • 1-800-NEB-LABS • Tel. (978) 927-5054 • Fax (978) 921-1350 • info@neb.com
Canada: Tel. (800) 387-1095 • info@ca.neb.com **Germany:** Tel. 0800/246 5227 • info@de.neb.com
UK: Tel. (0800) 318486 • info@uk.neb.com **China:** Tel. 010-82378266 • beijing@neb-china.com
For a complete list of international offices, please visit www.neb.com.

NEW ENGLAND BioLabs® Inc.
the leader in enzyme technology

PERSISTENT TOXIC SUBSTANCES

Study Finds Heavy Contamination Across Vast Russian Arctic

The first comprehensive look at persistent toxic substances (PTS) across the Russian Arctic reinforces what studies in other Arctic nations have revealed: that indigenous peoples in this northern swath of the world are inordinately exposed to pesticides, industrial compounds, and heavy metals, with uncertain health effects. Due to northward flows in rivers, oceans, and atmospheric currents, persistent toxins released elsewhere, along with some local contaminants, have accumulated heavily in many areas of the Arctic, where frigid temperatures retard their dispersal and degradation.

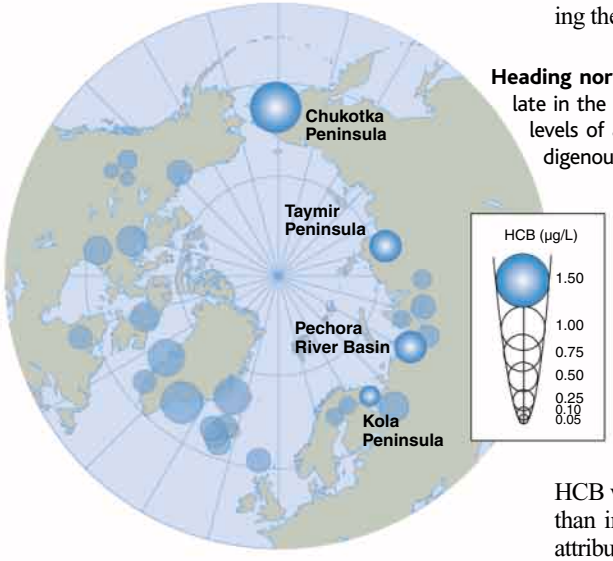

Heading north. Persistent toxic compounds accumulate in the Russian Arctic; a new study finds elevated levels of an insecticide (HCH) in breast milk of indigenous people in the Chukotka region.

Conducted by the Arctic Monitoring and Assessment Program (AMAP), the environmental research arm of the eight-nation Arctic Council, the 4-year, $2.8 million study sampled pollutant levels in the four major regions of the Russian Arctic. The researchers found that breast milk and maternal and umbilical cord blood samples contained moderate to extremely high levels of a variety of chemicals: hexachlorobenzene (HCB), hexachlorocyclohexane (HCH), dioxins, DDT, PCBs, oxychlordane, toxaphene, mirex, mercury, cadmium, lead, and brominated flame retardants. "The mean concentration for PTS across the Russian Arctic is comparable to what's been found in Canada and Greenland," says the study's human health research coordinator Valery Chashchin of the Northwest Public Health Research Centre in St. Petersburg.

The highest human contamination levels were found in the Chukotka region on the eastern coast of the Russian Arctic, where indigenous people eat large quantities of marine mammals and fish, which can be heavily contaminated both with local and long-range pollutants. Researchers found that about 5% of the population, mostly males, have some of the highest PCB contamination levels—10,000 nanograms per gram of blood lipid—ever seen, says Éric Dewailly of the Centre for Inuit Health and Changing Environments at the National Institute of Public Health of Québec. The Chukotka region, Chashchin notes, "is a wasteland where millions of tons of chemicals were imported during the Soviet era and never cleaned up."

The body burdens of some compounds—brominated flame retardants, dioxins, and furans—were actually lower in Chukotka than in the Canadian Arctic and Greenland, probably, says Chashchin, because the region is more isolated from sources of these substances in Europe and North America. But breast milk concentrations of the insecticide HCH and the fungicide HCB were 30 and 5 times higher, respectively, than in Arctic Canada, says Chashchin, who attributes these levels to historical use of these chemicals in indigenous people's homes.

Preliminary evidence, from comparisons of contamination data with information reported in health interviews, suggests that exposure to some persistent toxics (PCBs, HCH, DDT, lead, cadmium, and mercury) may be linked to reproductive effects such as stillbirths, birth defects, low birth weight, and spontaneous abortions. AMAP also noted an apparent association between reduced numbers of male births and increases in Arctic maternal blood concentrations of both lead and some types of PCBs.

A similar and more significant association was reported 20 years after a 1976 dioxin accident in Seveso, Italy, but this is the first time a link between Arctic levels and gender skewing has been reported, although the association is weak. "We are surprised and a little worried," says a member of the study's Steering Committee, Jon Øyvind Odland of the Institute of Community Medicine at the University of Tromsø in Norway. Chashchin, Odland, and others call for further investigation of the human health effects evidence, a recommendation Inuit researchers support.

–PAUL WEBSTER

Paul Webster is a science writer in Toronto, Canada.

CREDIT: ARCTIC MONITORING AND ASSESSMENT PROGRAM

ScienceScope

IOM to Probe Disease Math

Following allegations that government scientists last spring hyped the risks of dying from obesity, experts plan to meet at the Institute of Medicine (IOM) in Washington, D.C., on 13 to 14 December to consider the best methodology to calculate risks associated with common disorders.

The workshop, paid for by the U.S. Centers for Disease Control and Prevention (CDC), comes on the heels of a fight within the agency over an article co-signed by CDC's chief Julie Gerberding and published in the *Journal of the American Medical Association* (*JAMA*) in March. Some CDC scientists charged that the paper's estimate that 400,000 U.S. residents died from obesity in 2000—nearly the number of tobacco-related deaths—was grossly exaggerated (*Science*, 7 May, p. 804).

CDC held an inquiry into the charges that the numbers were inflated but has not disclosed the results. Meanwhile, CDC spokesperson Karen Hunter confirms news reports that the agency has "submitted an erratum" to *JAMA* and plans to release the details of its new obesity toll when it is published.

–ELIOT MARSHALL

GM Rice Bid Still Cooking

BEIJING—The status of several proposals to commercialize genetically modified (GM) rice in China remains uncertain after a closed-door meeting last week of a Chinese biosafety committee.

"No application has been approved or rejected so far," says Fang Xiangdong, director of the agricultural ministry's GM biosafety office, who says the 58-member panel is preparing a report on its deliberations (*Science*, 26 November, p. 1458). But Zhu Zhen, a biotechnologist at the Institute of Genetics and Developmental Biology of the Chinese Academy of Sciences in Beijing, suggests that the panel may reject his application for an insect-resistant rice line, one of four under review. Some observers are more optimistic about a variety resistant to bacterial blight.

Ronald Cantrell, director general of the International Rice Research Institute in Los Baños, the Philippines, is also troubled by the uncertainty, noting that previously there had been "encouraging signs [of acceptance] from the committee and other interested groups." If China does delay the introduction of GM rice, a blight-resistant GM rice variety now undergoing field trials in the Philippines could be the first in the world to win approval.

–DENNIS NORMILE AND XIONG LEI

UNDERGRADUATE EDUCATION

Tweaks to High-Tech Visas Revive NSF Scholarships

A popular federal scholarship program for low-income and disadvantaged undergraduates that was scheduled to end this year has won a reprieve, thanks to reforms in the process that allows foreign workers to hold high-tech U.S. jobs.

The National Science Foundation (NSF) began the Computer Science, Engineering, and Mathematics Scholarships (CSEMS) program in 1999 after Congress imposed an application fee for skilled worker visas (H-1Bs), tripled the maximum number, and channeled a portion of the revenue to NSF (*Science*, 7 April 2000, p. 40). The authority to collect that $1000 fee expired in 2003, however, leading NSF to make what would have been its last round of CSEMS earlier this year.

But now the program is ready for a comeback, thanks to a provision in the recently passed omnibus spending bill for 2005 that not only reinstates the H-1B fee but also raises it to $1500. The same legislation increases NSF's share of the fee from 22% to 30% and raises the overall cap from 65,000 to 85,000. Under the new rules, NSF could reap as much as $38.3 million a year.

That won't happen until 2006, however, because this year's applications generated no revenue. (The 65,000 quota for 2005 was filled on 1 October, the first day of the fiscal year.) NSF's Duncan McBride says the agency likely won't hold a competition until next fall and will make its first round of new awards in the summer of 2006.

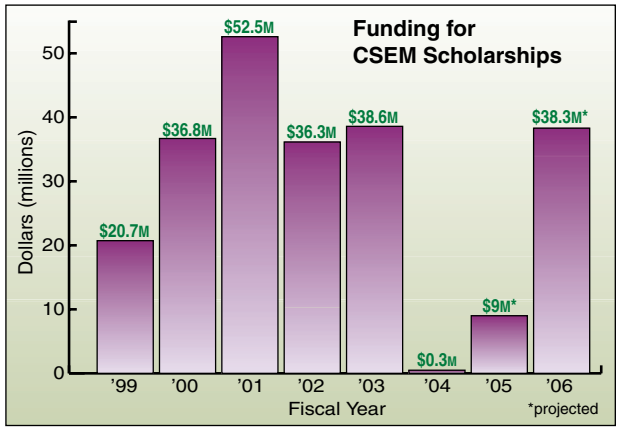

Going back up. Congress gives new life to NSF scholarship program.

The pool of eligible institutions—those that normally qualify for NSF grants—remains the same under the new program, with community colleges receiving about 40% of the awards. But there are a few new twists. The maximum amount of the 2-year scholarship will triple, to $10,000 a year, and the areas of study that can be supported will be expanded to include more fields in which job demand is high, McBride says. "Some universities have had trouble recruiting students because of that ceiling," he says about increasing the size of the scholarship. He also welcomes the move to expand the program "into more high-tech disciplines such as biotechnology."

The continuation of the program is "fantastic news," says Scott Wolpert, associate dean in the College of Computer, Mathematical, and Physical Sciences at the University of Maryland, College Park, which has enrolled 60 scholarship students under a previous grant. The program helps students from low-income, minority backgrounds "break the downward spiral of high student debt leading to part-time employment, which leads to an increased risk of not graduating," he says.

—YUDHIJIT BHATTACHARJEE

U.S. SCIENCE POLICY

Tommy Thompson Leaves a Mixed Legacy

Department of Health and Human Services (HHS) Secretary Tommy Thompson announced his resignation last week after a tenure marked by the post-9/11 anthrax scare, the completion of a doubling of the budget of the National Institutes of Health (NIH), a much-criticized policy on stem cell research, and a controversy over politics and science. His successor will face issues from drug safety to a flat NIH budget.

At a press conference, the former Wisconsin governor, 63, spoke with typical candor, saying that as he leaves HHS, his top worries are pandemic influenza and the safety of the food supply: "I, for the life of me, cannot understand why the terrorists have not" tampered with it yet, he said. His comments prompted President George W. Bush to declare the next day that the government is working to protect Americans from such terrorist threats. Thompson defended the Food and Drug Administration (FDA), which recently came under fire when safety problems arose with drugs already on the market, but he expressed support for an independent office to review drug safety data.

Bowing out. Thompson joins the Cabinet exodus.

The secretary listed HHS's role in the president's $15 billion international HIV/AIDS program and his foreign travels as among his top accomplishments, along with promoting healthy lifestyles. He said his next job, likely in the private sector, would keep him involved in "medical diplomacy."

In addition to the doubling of NIH funding, Thompson has also overseen a huge expansion of biodefense research and preparedness and implementation of the president's policy of restricting funding for stem cell research to a few approved lines. On the latter topic, Thompson insisted that the policy "is working," and that the problem is not a lack of new cell lines but rather too few scientists involved and trained to use them. He reflected on a controversy over industry consulting by NIH scientists, praising NIH Director Elias Zerhouni for working toward a policy that is not too restrictive, because "we want the best researchers and scientists" at NIH.

Thompson's legacy includes actions that have upset scientists within and outside HHS. His office has questioned candidates for advisory committees about their political views, for example, and ordered the removal of information on condoms from the HHS Web site as part of a move to promote abstinence-only sex education. "Secretary Thompson has to bear responsibility for these developments," says Representative Henry Waxman (D–CA), who claims to have documented political interference with science in the Bush Administration. Thompson's office has also clamped down on NIH management and limited travel to foreign meetings, irking NIH scientists accustomed to independence.

Rumored successors to Thompson include Medicare chief and former FDA commissioner Mark McClellan, a physician and economist. Thompson plans to stay until 4 February or until a successor is confirmed.

—JOCELYN KAISER

CREDITS (TOP TO BOTTOM): NSF; CHRISTOPHER SMITH

MATH AND SCIENCE EDUCATION

Hong Kong, Finland Students Top High School Test of Applied Skills

Fifteen-year-olds in Hong Kong, Finland, and Korea excel in applying the science and math concepts they've learned, whereas U.S. students trail their peers in much of the industrial world. That's one lesson from the latest results of a 41-nation test that goes beyond the usual assessment of what students know.

The Program for International Student Assessment (PISA) is part of an ongoing effort to compare the educational performance of students around the world. PISA, which covers science, math, and reading literacy, complements a set of tests called the Trends in International Mathematics and Science Study (TIMSS), which measures fourth- and eighth-graders' knowledge of specific concepts, such as geometrical formulas and chemical principles. PISA takes the premise a step further by measuring how students apply the sum of this education to new problems. "We're not asking whether students can read," says Thomas Romberg, a math educator at the University of Wisconsin, Madison, who helped design a version of the PISA exam administered in 2000 that focused primarily on reading literacy but included science and math questions. "We're seeing whether they can understand a book they've never seen before."

Math Ranking for Selected Nations

Country	Score
Hong Kong, China	550
Finland	544
Korea	542
Netherlands	538
Japan	534
Canada	532
Switzerland	527
Australia	524
Czech Republic	516
Denmark	514
France	511
Germany	503
Ireland	503
Poland	490
Spain	485
United States	483
Russian Federation	468
Italy	466
Greece	445
Mexico	385
Indonesia	360

CREDIT: PISA/OECD

The 2003 test, the results of which were presented this week, emphasized math comprehension, whereas the 2006 test will emphasize science. The 3-year cycle will repeat in 2009. The test is coordinated by the Organisation for Economic Co-operation and Development (OECD) in Paris. Results from the latest TIMSS survey will appear next week.

The 2003 PISA test was taken by 270,000 students in 41 countries. Students had 2 hours to complete the exam, which consisted of twice as many open-ended or short answer questions as the TIMSS test. A sample math question asks students to figure out how much money they lose by exchanging their South African rands for Singapore dollars given fluctuating exchange rates. In the science section, students must decide whether scientific research can be used to determine the amount of chlorofluorocarbons in the atmosphere.

Hong Kong students placed first in math in the 2003 test, and Finland held the top spot in science. The ranking of individual countries changed little between 2000 and 2003, although Poland, Germany, and the Czech Republic did significantly better the second time around. Wealthier countries tended to place higher on the PISA charts, although students in Korea, with a national income 30% below the OECD average, placed third in math and fourth in science. U.S. students stood 24th in math and 23rd in science, similar to their relevant rankings in 2000.

"What these results say is that a student in Finland will have an easier time using his math and science knowledge to make sense of an unfamiliar situation than will a student from the U.S.," says Romberg. Larry Suter, deputy director of the Division of Research, Evaluation, and Communication at the National Science Foundation, says he was surprised that Canadian students did so much better than their U.S. counterparts, given the similar socioeconomic profiles of the two countries. "This study is going to force us to think about what we teach in our schools," he says.

As for PISA's impact on U.S. science and math education, Suter also believes that state assessments should be reevaluated to gauge the application of knowledge, not just retention, as a marker of student progress. U.S. high schools need to pay particular attention to practical knowledge, agrees Eugene Hickok, the U.S. deputy secretary of education: "In the international context, we have some mountains to climb." –DAVID GRIMM

ScienceScope

Stem Cell Alternatives

Interest appears to be growing in technologies that can circumvent the destruction of human embryos for stem cell research. At last week's meeting of the President's Council on Bioethics, Columbia University researchers Donald Landry and Howard Zucker suggested using cells from embryos in fertility clinics that have stopped dividing—a procedure they compared to taking organs from brain-dead people. And council member William Hurlbut, a physician at Stanford University, elaborated on an approach he first floated in 2002, "altered nuclear transfer," in which genes essential for development of an embryo have been inactivated.

Some panelists were enthusiastic, and council chair Leon Kass suggested that such techniques might lead a way through the "political impasse" over cloning. Although the council's actions have not always pleased scientists, stem cell researcher Gerald Schatten of the University of Pittsburgh says "I'm especially encouraged" by the latest meeting because it shows that the council is serious about finding a solution that satisfies all sides. –CONSTANCE HOLDEN

Vaccine Pledge Sparks Protest

Two prominent malaria experts have criticized a U.K. government pledge to purchase a promising malaria vaccine, a trial of which was described this fall in *The Lancet* (*Science*, 22 October, p. 587). Robert Snow of the Kenyan Medical Research Institute in Nairobi and Nicholas White of Mahidol University in Bangkok say the government could save many more lives by paying for existing weapons against malaria.

In a 24 November speech, Treasury chief Gordon Brown said the U.K. government would stimulate production of new vaccines for developing countries by guaranteeing manufacturers a market; he singled out the GlaxoSmithKline (GSK) malaria vaccine as "a revolution in our time." But Snow and White told Brown in a 3 December letter that "this good intention is misguided. ... We fear you have been advised poorly." The duo points out that the vaccine, which would cost $10 to $20 a shot when it becomes available, is only partially effective and needs further study; insecticide-impregnated bed nets and a new group of drugs based on artemisinin can save lives right away at lower cost, they say.

"I think it's a bit of a false debate," says Melinda Moree of the Malaria Vaccine Initiative, which supported the new vaccine. "It's not either this or that—it's both."

–MARTIN ENSERINK

NEUROPROSTHETICS

Brain-Computer Interface Adds a New Dimension

This fall, surgeons implanted 100 electrodes into the brain of a 25-year-old quadriplegic man and connected them to a computer that enables him to check his e-mail and choose a television channel with his thoughts alone. And monkeys with similarly implanted electrodes have used brain signals to move cursors or robotic arms in two dimensions (*Science*, 24 January 2003, p. 496). Now, in a groundbreaking development, two neuroscientists from the Wadsworth Center, part of the New York State Department of Health in Albany, have shown that similar feats may be possible without the dangers of inserting electrodes into the brain. This week, in the online *Proceedings of the National Academy of Sciences*, Wadsworth's Jonathan Wolpaw and Dennis McFarland demonstrate a brain-computer interface (BCI) that can translate externally detected brain signals into both horizontal and vertical movement of a computer cursor.

"It's earthshattering that we may be able to reconnect the brain to a paralyzed limb or a robotic arm without surgery," says computer scientist Melody Moore, who directs the Brain Lab at Georgia State University in Atlanta. "This disproves something people have been saying for a long time."

Two-dimensional cursor control, Moore says, could be used to operate a wheelchair, a chess-playing robot, or a computer mouse, for example. Once you have the second dimension, she notes, "the third dimension is within reach." And that could enable full movement of a limb.

Such a possibility seemed remote when Wolpaw, McFarland, and their colleagues described their first BCI in a journal in 1991. That system enabled a person to move a cursor on a screen up or down some indeterminate amount by raising or lowering the amplitude of electrical brain currents called mu or beta rhythms. By imagining actions such as running, floating, or moving one arm or the other, the subjects could influence these currents, which are generated by a brain area involved in sensation and movement. The researchers recorded the brain-wave changes using a detector called an electroencephalogram (EEG). It was a crude yes-no device, and skeptics doubted that this sort of BCI, which sums input from millions of neurons, would get much further.

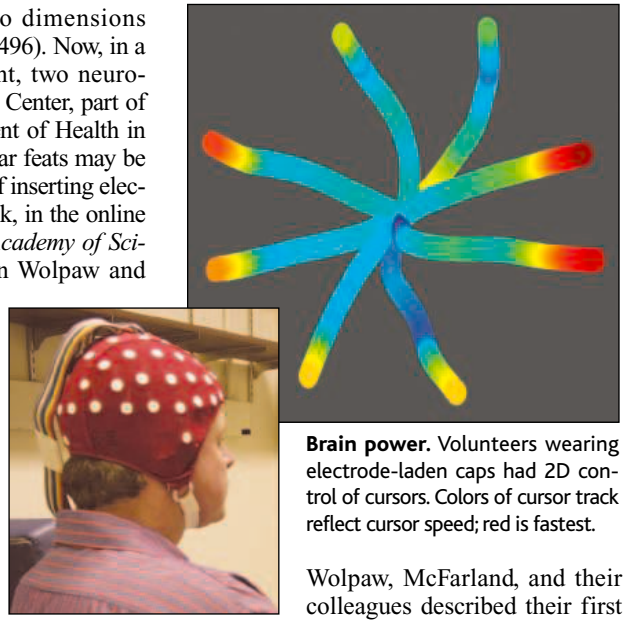

Brain power. Volunteers wearing electrode-laden caps had 2D control of cursors. Colors of cursor track reflect cursor speed; red is fastest.

In the following years, the Wadsworth group improved this one-dimensional BCI, enabling subjects to nudge a cursor a precise distance to land on one of four icons. Then, early last year, they translated that progress into two dimensions. One critical advance was a learning algorithm: The software program translating brain signals into cursor movement optimizes a user's performance by adjusting its parameters based on the trials a user has completed so far.

Putting the BCI to the test, Wolpaw and McFarland asked four volunteers—two of them with spinal cord injuries—to don caps speckled with 64 recording electrodes and to use whatever kind of imagery they could to push a cursor from the center of a computer screen to a target in any of eight possible locations on the periphery. As the volunteers did the task, a computer translated their brain's mu and beta rhythms into horizontal and vertical cursor movements.

After dozens of short practice sessions spread out over weeks, the two volunteers with spinal cord injuries could hit the tar- ▶

NATIONAL INSTITUTES OF HEALTH

Report Seeks Stability for Behavioral Sciences

Basic behavioral and social scientists want the National Institutes of Health (NIH) to pay more attention to their field. But a report calling for a "secure and stable home" for their research received a tepid reception last week from NIH Director Elias Zerhouni, and a tightening budget may limit what NIH could do even if it wanted to help.

The report comes from a 14-member panel led by University of Chicago sociologist Linda Waite, which was asked to assess NIH's current portfolio in these areas. It tallied $936 million in basic social and behavioral and another $1.75 billion in clinical research in NIH's 2003 budget of $26.4 billion. This research is vulnerable, however, says the panel, because it is housed mostly at institutes focused on specific diseases or life stages. One major source, the National Institute of Mental Health, has recently stopped funding some of those grants to support more translational work (*Science*, 22 October, p. 602).

The panel proposed a solution: secure funding and a stable home at an existing institute. The top candidate is the National Institute of General Medical Sciences (NIGMS), NIH's basic research institute, followed by the aging or child health institutes. The report notes that Congress has repeatedly encouraged NIGMS to enlarge its current $13 million portfolio. The report does not suggest that grants be transferred to this home institute, however, a strategy NIH followed in creating the National Institute for Biomedical Imaging and Bioengineering in 2000. The panel also recommends a bigger role for NIH's director-level Office of Behavioral and Social Sciences Research, which now coordinates and promotes these research areas across institutes.

Members of the NIH's director's advisory committee, which requested the study, agreed during a meeting last week that basic behavioral research is valuable. But there were questions about the panel's "structural" recommendations. Zerhouni, for instance, said he was not "clear" on whether the group was asking for a larger pot of money or a shift in existing resources now devoted to behavioral research. The former would require NIH "to scale something back" elsewhere, he noted.

NIGMS is "willing to support more" behavioral research such as genetics studies, says institute chief Jeremy Berg, but areas such as the social sciences would not be a natural fit. And finding new funding would be a tall order, Berg adds. Alan Kraut, executive director of the American Psychological Society, agrees: "This is going to come down to a budget issue." —JOCELYN KAISER

CREDITS: J. WOLPAW AND D. MCFARLAND/WADSWORTH CENTER; (INSET) MICHAEL WREN/WADSWORTH CENTER

get about 90% of the time within the 10-second time limit. (The others did so 70% to 80% of the time, perhaps because they were less motivated.) The best subject hit the target in an average of 2 seconds and with 92% accuracy—results comparable to the best achieved by monkeys operating implanted BCIs. Three of the volunteers went on to hit targets in eight additional places on the screen with similar speed and accuracy. "It did not throw them off to go to a new location," Wolpaw says.

He and his colleagues are now working on adding a brain-wave switch that could enable a person to grasp or release an object using a robot arm or to click on icons on a computer screen after moving a cursor to them. But supporters of the implanted electrode strategy still question how flexible noninvasive BCIs can be. Brown University's John Donoghue, for example, says that complex movements requiring many dimensions of control may require devices like the 100-electrode array he and his colleagues at the firm Cyberkinetics in Foxborough, Massachusetts, are starting to implant in people. Such systems "engage the actual neural substrate intended for use in the lost voluntary movements," as opposed to more diffuse EEG patterns, he says.

Yet the risks of neurosurgery, which include infection and brain damage, may make implanted sensing devices a hard sell for many patients. "There's a lot you can do with signals from the scalp," says Wolpaw.

–INGRID WICKELGREN

U.S. AGRICULTURAL RESEARCH

Report, Lawmaker Promote an Independent Institute

Funding for agricultural and food research has traditionally been a dry patch compared to the well-watered scientific fields supported by the National Science Foundation (NSF) or the National Institutes of Health (NIH). Now its supporters are hoping that a recent report from a blue-ribbon panel will lead to a bumper crop of basic agricultural research. But first they have to figure out where to plant the seeds.

In 2002, on orders from Congress, the U.S. Department of Agriculture (USDA) asked a group of eminent scientists to ponder a national institute of food and agricultural science. This summer the panel, led by Chancellor Emeritus William Danforth of Washington University in St. Louis, Missouri, concluded that the greatest need was for an institute that would award extramural, peer-reviewed grants for basic research.* "We felt a whole new culture has to be created that is more similar to NSF and NIH," says Danforth.

Last month Senator Kit Bond (R–MO), who chairs the panel that sets NSF's budget, took Danforth at his word. He introduced a bill (S.3009) that would place the institute within NSF's biology directorate but give it an unusual degree of independence and its own advisory council. Although the bill has expired, Bond has said he acted quickly to stimulate discussion. And ag lobbyists are thrilled: "We've gotten to the starting line," says R. Thomas Van Arsdall, executive director of the National Coalition for Food and Agricultural Research, an advocacy group based in Savoy, Illinois.

The task force found that basic research has been shortchanged. More than 90% of USDA's $2.4 billion research budget is not awarded by peer review. Instead, funds are distributed directly to land-grant universities and spent on intramural, mainly applied, activities through the Agricultural Research Service. Even the $180 million a year awarded competitively through the National Research Initiative (NRI) has its drawbacks: USDA grants are smaller and shorter than those of NSF or NIH and come from a much smaller pot (see chart). The task force recommended that the proposed new institute have an annual budget of $1 billion after 5 years. In addition, the number of grants should be doubled, to 1000, and their size boosted by 187%, to $225,000 per year.

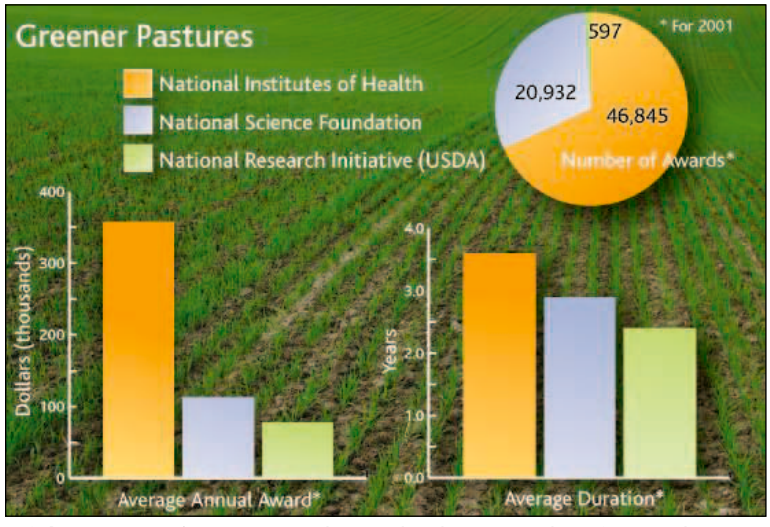

Left hungry. USDA's peer-reviewed research pales next to that of NSF and NIH.

Lobbyists say that they aren't worried about confusion over whether the new institute should be part of USDA or NSF. "Focus on the broader message: We need to boost federal support for basic research in the agricultural sciences," says Howard Gobstein, vice president for governmental affairs at Michigan State University in East Lansing, who also works on behalf of the National Association of State Universities and Land-Grant Colleges, to which MSU belongs.

Advocates say that housing the new institute within NSF offers many advantages. "You could be sure that first-rate research would be done," Danforth says. However, NSF officials worry that it could lead to similar demands from other interests, such as transportation or energy, traditionally outside NSF's purview. That would squeeze a budget that shrunk by $107 million this year and may erode further in 2006. Supporters have a quick answer: An agricultural institute, they say, could be a rallying cry for the foundation to seek a bigger budget.

USDA prefers another approach. It says that boosting the NRI budget, which will grow by 10% in 2005, would be a logical way to strengthen basic research in food and agriculture. The agency has already increased average grant size by 80% since 2001.

Bond is expected to reintroduce his bill, with some changes, after the new Congress convenes next month. Lobbyists are hoping for a companion bill in the House of Representatives, and Representative Bill Goodlatte (R–VA), chair of the House Committee on Agriculture, tops their list of desired sponsors. A spokesperson for the committee says that members will meet with Danforth in the coming weeks but declined to speculate on any possible legislation. David Goldston, staff director for the House Science Committee, says the panel, which has jurisdiction over NSF but not USDA, would welcome a discussion of how best to achieve the aims of the USDA report.

–ERIK STOKSTAD

With reporting by Jeffrey Mervis.

CREDIT: USDA TASK FORCE REPORT

*www.ars.usda.gov/SP2UserFiles/Place/00000000/NATIONAL.doc

Can the War on Locusts Be Won?

"They shall cover the surface of the land, so that no one will be able to see the land. They shall devour the last remnant left you after the hail, and they shall devour every tree of yours that grows in the field."

Exodus 10:5

SEBT BOUNAAMANE, MOROCCO—So this is what Moses was talking about. On a beautiful November morning, it's clear even from afar that something's terribly wrong with the trees around this tiny village. They are covered with a pinkish-red gloss, as if their leaves were changing color—except these argan trees are evergreens. As you get closer, the hue becomes a wriggling mass; a giant cap of insects on every tree, devouring the tiny leaves. Get closer still, and you'll hear a soft drizzle: the steady stream of locust droppings falling to the ground.

But Morocco has locust-fighting weapons far beyond anything that ancient Egyptians could imagine. Later that morning, two yellow aircraft swoop down across the nearby Anti-Atlas mountain range, releasing a fine mist as they start skimming the land. Soon, the faintly soapy smell of pesticides fills the air. When entomologist Abdelghani Bouaichi jumps in his Land Rover to drive back to the National Centre for Locust Control in Ait Melloul, he's satisfied. Within 8 hours, most of these locusts will be dead.

Hungry. Desert locusts—which are pink until they have fully matured—are descending on Morocco by the billions.

Africa is once again fighting a battle against the desert locust, *Schistocerca gregaria*, and this winter, southern Morocco is Ground Zero. Vast waves of locusts are entering the country—as well as parts of neighboring Algeria—from Mauritania and Senegal. Dozens of planes make their deadly trips every morning; if they can manage to kill enough locusts, perhaps the emergency won't develop into a full-blown plague.

Perhaps. Even after 50 years of experience, fighting locusts is still more an art than a science. Nobody is quite sure how to prevent locust plagues or squash them once they're under way, nor is it clear how effective the thousands of liters of pesticides drizzling on the red earth are. Environmentally friendlier alternatives are in development, but questions linger about their efficacy as well. Compounding the problem, there aren't nearly enough locust researchers in this obscure field to tackle the questions—nor enough locusts. Plagues often occur many years apart, leaving researchers short of experimental material in the interim.

Progress is also hamstrung by long-running doubts about whether locusts really warrant all this trouble and expense. Locust-stricken countries claim huge economic costs, but some scientists argue that, overall, the toll is not that bad—certainly not compared to that of other pests and droughts. "They just have that reputation," says Philip Symmons, a retired veteran of the locust wars who lives in France. "It's all because of Exodus."

Ounce of prevention

The latest emergency is the most serious since a vast 3-year plague ended in 1989, after locust swarms had visited more than 30 countries from West Africa to India and donors had spent more then $300 million in emergency aid to kill them, in addition to a similar sum spent by the affected countries themselves. It's not nearly as bad this time—at least not yet. The U.N.'s Food and Agriculture Organization (FAO) in Rome, which coordinates the battle, classifies it as an "upsurge" rather than a plague, because it's affecting only one major breeding area, West and northwest Africa. A few swarms have ventured farther out—one staged a stunning photo op in front of Cairo's pyramids—but so far, these are exceptions of less concern.

Still, the situation is bad enough—especially because it wasn't supposed to happen. Since the last plague, FAO and many countries have prided themselves on their ability to prevent crises of this magnitude. Most of the time desert locusts are solitary insects; only after heavy rainfall and an increase in vegetation do they sometimes undergo a spectacular transformation that leads them to band together (see sidebar). Small swarms merge, and merge again, until they're gigantic. Nip 'em in the bud is the philosophy; then you won't have to pull out all the stops later.

To do the nipping, countries at risk have set up early-warning systems: local teams that search for early infestations in the desert—"outbreaks" in locust parlance—and kill them. They are helped by FAO's locust forecasts, which pinpoint potential trouble spots on the basis of past locust sightings, the weather, and satellite data about vegetation growth.

It's easier said than done, however. The area where outbreaks can originate is vast (see map on p. 1882); most of it is extremely rugged, inaccessible, and virtually uninhabited. Some of it is war-torn. Survey teams have gotten lost, and some have perished. Complacency is always a danger—it's hard to stay focused on a threat you haven't encountered for years—and vehicles and other equipment are often in short supply. Corruption and political favoritism occasionally stand in the way as well. "Sometimes you meet a national head of locust control who doesn't know the first thing about locusts," says Arnold van Huis, a locust expert at Wageningen Agricultural University in the Netherlands.

Several specific problems conspired to

CREDITS: M. ENSERINK

An Insect's Extreme Makeover

Schistocerca gregaria, the desert locust, is a dull-looking, shy insect that tends to stay put, avoid other locusts, fly by night, and never cause trouble. And then there's the desert locust, *Schistocerca gregaria*, a conspicuous yellow-and-black—or bright pink when not fully mature—thrill seeker that bands together in swarms of billions that cross vast distances in broad daylight and devour tons of vegetation in their path.

So striking is the difference between the desert locust's "solitary" and "gregarious" phases that it wasn't until 1921 that Russian entomologist Boris Uvarov realized they were the same species. And only recently have scientists begun to piece together a detailed picture of how the insect switches from one phase to the other. University of Oxford entomologist Stephen Simpson, the uncontested leader in this small field, hopes that this understanding may eventually help prevent plagues. "The phase change is the defining feature of locust biology," he says, "and also the main problem."

The makeover is the locust's answer to harsh life in the desert, Simpson explains. Most of the time, the sparse vegetation can sustain only small numbers of desert locusts, and they do best by staying out of one another's way. After intense rain, however, plant life explodes and locust numbers skyrocket; when the inevitable drought sets in, the insects find themselves coalescing in high numbers around shrinking food supplies. This increased density is what triggers the shift from solitary to gregarious—presumably because, once they run out of food, the insects need to migrate and, like many species, they seek safety in numbers.

Different animals. Locusts' appearance and behavior change dramatically when they go from the solitary (left) to the gregarious phase (right).

Researchers have long known that the locust's behavior is the first thing to change. A solitary locust becomes more attracted to its mates and more active after spending just 4 hours in a crowded cage, for instance. The spectacular morphological transformation, on the other hand, can take several generations to complete. (When densities drop—for instance, when enough members of a swarm die—the process reverses.)

Researchers have long wondered what tips off the locusts to the crowded environment: a visual, olfactory, or tactile cue. To find out, Simpson and his colleagues tested combinations of three stimuli: exposing solitary insects to air samples that had passed over a group of locusts, to the sight of 10 of them behind a glass wall, or to a tactile stimulus caused by being jostled by small paper balls. The tactile stimulus was by far the most potent trigger. Later, the group discovered that touching the insects' beefy thighs—which contain many so-called mechanoreceptors—in particular resulted in gregarization. The bottom line, according to Simpson: Locusts become social animals once their legs start bumping together.

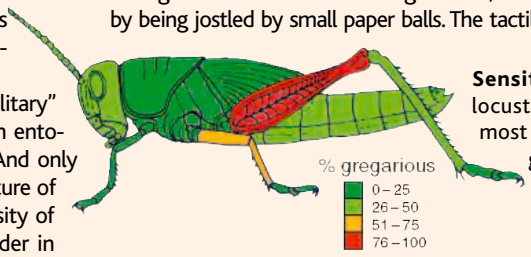

Sensitive legs. Touching the locust's upper hind leg is the most effective trigger of gregarization.

Since then, Simpson's group, in collaboration with Malcolm Burrows and Thomas Matheson of the University of Cambridge, has delved into the physiology of the shift, discovering, for instance, that they could induce the change by electrical stimulation of a particular leg nerve. They have also shown that the central nervous systems of solitary and gregarious locusts have marked differences in the levels of 11 neurotransmitters. In this week's online early edition of the *Proceedings of the National Academy of Sciences*, Le Kang of the Beijing Genomics Institute in China and his colleagues take the search to the genetic level, although for another species, the migratory locust. Comparing solitary and gregarious larvae, they found differences in the expression levels of 532 genes.

Eventually, such studies could lead to the development of compounds that block or reverse gregarization. But entomologist Arnold van Huis of Wageningen Agricultural University in the Netherlands is skeptical that this would ever become a practical tool; you'd still have to find the right populations in the vast desert and spray them, he notes—precisely the problem with current, pesticide-based control.

But other findings could have a more immediate impact. Simpson and his collaborators have also discovered that it's not just the number of locusts and the amount of vegetation that determines whether a population flips from solitary to gregarious; it's also the vegetation's "patchiness." A clump of 10 plants close together might trigger gregarization, but 10 plants far apart may not. Locust forecasting models use satellite data to gauge the amount of vegetation, Simpson notes—but they should also take into account how patchy it is. Locust forecaster Keith Cressman of the United Nations Food and Agriculture Organization says he's "very interested" in finding out if this can help refine his forecasts. **–M.E.**

bring about the current upsurge, says Clive Elliott, head of FAO's locust program. There was quite a bit of rain throughout the summer of 2003 in the Sahel, triggering serious locust outbreaks in Mauritania, Mali, and Niger that overwhelmed those countries' control systems. Then a few days of extreme rainfall in October provided perfect breeding conditions for the next 6 months. FAO pleaded for $9 million in emergency funds in February, but rich countries were slow to react; the money didn't start flowing in earnest until searing pictures of ravaged crops made news this summer. But by that time, the locusts had already been through a winter and spring breeding season in North Africa and another one in the summer in the Sahel. (FAO now says it needs $100 million and maybe more.)

Some experts question whether the ounce-of-prevention strategy could have worked, even with plenty of resources. The first congregations of desert locusts are so small, and the area in which they can occur so vast, that—unless hundreds of planes and entire armies are dispatched—it's futile to try to find them all, Symmons says. Rather than clinging to the idea of prevention, he says, countries should focus their fight on the later stages, when big swarms make easy targets.

Elliott disagrees. Upsurge prevention can and does work if it's done well, he says. At the same time the swarms first appeared in West Africa last year, they also surfaced in Sudan and soon crossed the Red Sea to Saudi Arabia, the traditional springboard for India and Pakistan. But that outbreak was effectively dealt with. Elliott credits the Emergency Prevention System (EMPRES) for locusts and other pests, a multinational program set up by FAO that aims to build the capacity necessary for early intervention. The plan is to expand EMPRES to West Africa.

CREDITS (TOP TO BOTTOM): *PNAS* **98**, 7 (2001); GREG SWORD

Gone with the wind

The heavy use of pesticides is another issue of continuing debate. Since October 2003, some 110,000 square kilometers of land have been sprayed, FAO says, which corresponds to more than about 11 million liters of pesticides, most of it organophosphates. The risks to humans can be mitigated: In Morocco, for instance, planes are ordered to avoid villages, and control workers regularly have their blood checked for increased levels of the compounds. But there's pressure to reduce their use, especially from the donor countries. Already, thousands of tons of leftover pesticides from previous campaigns have been abandoned across Africa, often with their packaging decaying; few Western countries are eager to add to that sinister stock.

Research on alternatives is occurring "at a glacial pace," says Allan Showler, a former EMPRES head who now works at a U.S. Department of Agriculture lab in Weslaco, Texas. Field testing is particularly difficult because outbreaks are so rare—and when they do happen, the first priority is squashing them. Still, FAO is encouraging new studies. This summer, for instance, two field trials were conducted on 400-hectare plots—one in Niger, the other in Mauritania—with a much-touted safer alternative, a toxin produced by the fungus *Metarhizium anisopliae*, which is marketed under the name Green Muscle. The trials had several logistical problems—in Mauritania, the products' formulation had a "yogurtlike consistency" that made spraying difficult, and the results were inconclusive, Elliot says: "It certainly didn't work like a dream." FAO is hoping to do a bigger trial next year. Other promising candidates include a relatively new insecticide called fipronil and a class of hormones called insect growth regulators, but they, too, have yet to prove their mettle.

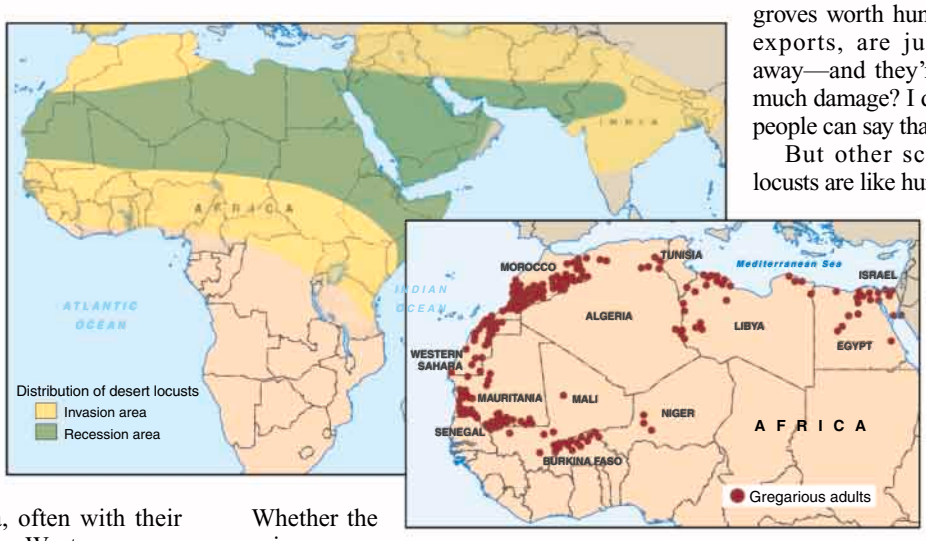

Well traveled. During upsurges and plagues, locusts can invade countries far beyond their usual habitat, called the recession area (top). Swarms currently concentrate in West and Northwest Africa (bottom).

Whether the spraying operations can end an outbreak—or even alter its course significantly—is also still an open question. FAO locust forecaster Keith Cressman says there's a good chance they can; if Algeria and Morocco keep up the fight for the next 3 or 4 months—and there isn't too much rain in winter and spring—they may kill enough locusts to end the upsurge. He finds hope in the fact that, during their migration from the Sahel to North Africa, many swarms are becoming trapped by the cold just south of the Atlas mountains. That makes them sitting ducks.

But others doubt that human intervention alone can do the job. When the last plague was finally over in 1989, some credited the costly control campaigns, but others thanked strong winds in October and November 1988 that blew some locusts all the way to the Caribbean—and billions of others to their deaths in the Atlantic. (That wasn't the first time this happened: Once the pharaoh repented, Exodus 10 reports, "the Lord changed the wind into a very strong west wind, which lifted the locusts and drove them into the Red Sea.")

War of attrition. Abdelghani Bouaichi of the National Centre for Locust Control shows how Morocco defends itself against locusts. (Inset) A ravaged young olive tree.

Counting the cost

Beneath the questions on the best control strategy, there's another unresolved issue: Is it all worth it? Standing in a field in Morocco, surrounded by millions of insects, Bouaichi says he can hardly believe anybody doubts the urgency of the fight. Earlier that morning, he had reassured anxious villagers that the planes would arrive soon to save their olive and date trees. The Sous valley, which has citrus groves worth hundreds of millions in exports, are just 100 kilometers away—and they're at risk, too. "Not much damage? I don't understand how people can say that," he says.

But other scientists argue that locusts are like hurricanes: The damage is devastating on a local scale but limited at the national level. In a 1990 report about the 1980s plague, for instance, the U.S. Congress's Office of Technology Assessment called the rationale for intervention "shaky." When locust expert Stephan Krall and his colleagues at the German aid agency GTZ tried to assess the damage from the same plague, "we really didn't find all that much," he says. Stories about the astronomical appetites of locust swarms—based on the well-known factoid that the insects can devour their body weight in vegetation every day—need to be taken with a grain of salt, Krall asserts. Besides, Van Huis notes, locusts are primarily desert creatures that often dine on the natural vegetation.

Many are skeptical about recent claims that half of Mauritania's crops were lost last summer. Countries are well aware that nothing opens donors' wallets faster than a big disaster, Cressman says. But there are more than economic costs to consider. Although the value of cash crops may be relatively easy to establish, how do you measure the loss of a harvest for a subsistence farmer? What about the social costs, such as the drift to cities that can follow a bad harvest?

Besides, the alternatives to control are either not feasible in poor countries or politically unpalatable. Food aid for stricken subsistence farmers is an unpopular idea, and some form of insurance—which is how developed nations would deal with the problem—simply isn't available in Africa. And no government can be seen as sitting on its hands when locusts strike. Says Bouaichi: "Imagine there was a locust plague in Britain or France and the government did nothing." So the battle continues.

–MARTIN ENSERINK

CREDITS: (TOP, LEFT TO RIGHT) ADAPTED FROM *RADCLIFFE'S IPM WORLD TEXTBOOK*/UNIVERSITY OF MINNESOTA; ADAPTED FROM FAO; (BOTTOM) M. ENSERINK

NIH Launches Controversial Long-Term Study of 100,000 U.S. Kids

Although funding is not guaranteed for the $2.7 billion National Children's Study, planners have settled on an innovative sampling strategy and are seeking proposals

Congress, advocacy groups, and researchers want to know more about how the environment—defined as everything from physical to social factors—influences a child's development and health. Could chemical pollutants, for example, be contributing to childhood diseases such as autism? To find out, federal scientists and other experts have wrangled over the design of a hugely ambitious $2.7 billion study that would follow the health of 100,000 U.S. children from before birth to age 21.

Now, after 4 years of planning, the National Institute of Child Health and Human Development (NICHD) has released a draft study blueprint* and is seeking proposals for contracts to run pilot centers. But questions loom about the methodology of the project, which would begin enrolling pregnant women and their newborns in 2007. Planners want to screen for subjects by contacting, in effect, a random sample of U.S. households in selected areas—standard procedure for the census but an untested approach for a long-term medical study.

Researchers who helped plan the National Children's Study (NCS) admit that this sampling strategy carries risks, from making it hard to get clinical samples to eroding support from researchers outside the selected areas. "It's extremely ambitious," says epidemiologist David Savitz of the University of North Carolina, Chapel Hill, who chaired a sampling design panel. "Whether it's gone from extremely ambitious to impractical, only time will tell." Another question is whether Congress will pony up the money for the study, which would cost about $70 million to $200 million a year starting in 2006.

Four years ago, Congress called for a longitudinal study of environmental influences on children's health, modeled on projects such as the famous heart study conducted in Framingham, Massachusetts (*Science*, 11 July 2003, p. 162). Hundreds of outside researchers and four agencies have narrowed scores of possible hypotheses to about 30. The current list includes whether pesticide exposures can alter cognitive development, whether violent TV shows and video games raise a child's risk of gun injury, and whether underweight newborns are more prone to obesity as teens. The study will collect environmental data in unprecedented detail, supporters say, including data on exposures to infections, stress, and pollutants even before some parents conceive.

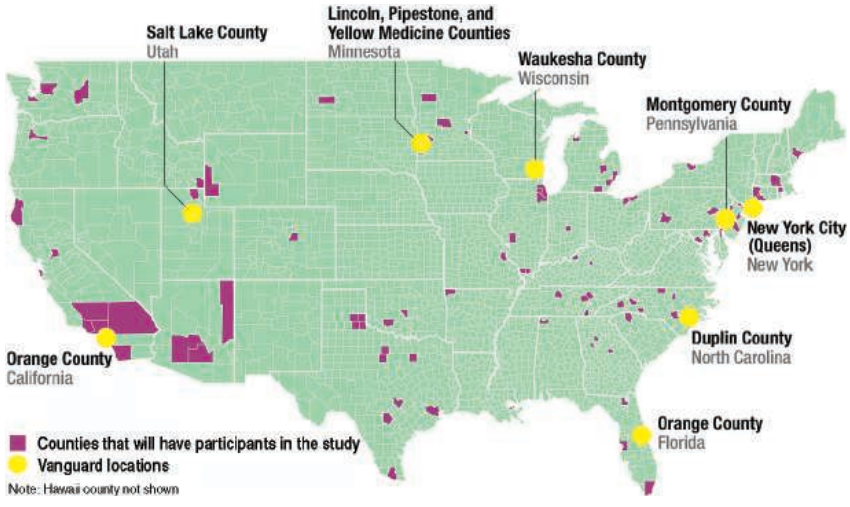

CREDIT: NATIONAL CHILDREN'S STUDY

Luck of the draw. The new children's study will recruit mothers and newborns in a sample of 96 locations statistically chosen to represent U.S. population diversity.

One contentious issue has been how to recruit subjects—through academic medical centers, or by selecting a probability-based sample representing America's ethnic, social, and geographical diversity. Social scientists prefer the latter so the study's results will reflect the entire population. After planners agreed with that goal last summer, federal statisticians crunched demographic and birth data, and then last month NCS unveiled 96 study sites scattered across the country, from rural Minnesota to Queens, New York (see map). Eight were picked as possible sites for initial "vanguard" centers. They will likely screen for couples planning to have a child by calling or knocking on doors of randomly chosen households.

Although any institution can apply for a center in its quadrant of the country, organizers acknowledge it may be impractical for, say, a Boston team to lead rather than collaborate with a center in New York City. NIH does not usually solicit proposals for fixed locations. "This is very much top-down," which may not please some researchers, says epidemiologist Grace Lemasters of the University of Cincinnati in Ohio, who is on the NCS advisory committee. Although she's disappointed that no sites fell closer to Cincinnati, Lemasters says she supports the study's sampling approach. "It almost has to be that way" so the results will reflect all of America, she says.

Also unusual is that subjects won't be chosen through their medical care provider. That makes it more likely that many will move or drop out: "Retention is going to be a huge issue," says Savitz. Another challenge will be the logistics of collecting biological samples, such as placentas and cord blood, from the hospital in which the mother happens to deliver. And if a family has no regular doctor, "we'll have to figure out how to deal with that," says NICHD epidemiologist Mark Klebanoff. To help fill gaps, the centers will also recruit some subjects through prenatal care providers.

Aware of these uncertainties, NICHD considers the three to eight "vanguard" centers to be pilots that will help refine the study plan released last month, says NCS director Peter Scheidt. (The study has $12 million for contracts in 2005, enough to launch these centers, which will recruit 250 newborns a year for 5 years.) The vanguard centers will later serve as models for other centers, Scheidt says. Eventually, NICHD hopes to fund up to 50 centers that cover all 96 locations.

Future funding is the big unknown. Although congressional appropriators recently expressed support for the study, they did not allocate an extra $15 million in 2005 that advocates hoped for. (A long list of advocacy groups supports the study, from the American Chemistry Council to the American Academy of Pediatrics.) Backers are hoping that the selection of vanguard centers will build support in Congress by putting the study on the radar screens of local representatives.

—JOCELYN KAISER

*www.nationalchildrensstudy.gov

The Grand (Canyon) Experiment

Last month, researchers learning from a previous failure once again flooded the Colorado River in an ambitious attempt to rebuild eroded shoreline in the Grand Canyon

LEES FERRY, ARIZONA—Some researchers chase tornadoes. Ted Melis rides waves. Big, river ones. But on the eve of the ride of a lifetime, the geomorphologist with the U.S. Geological Survey (USGS) in Flagstaff, Arizona is miserable. Situated on the banks of the Colorado River, Melis is struggling to keep sensitive electronic equipment dry as a cold downpour spills out of the dark, gray sky. He's fashioned a blue tarp into a makeshift tent covering the front half of his 11-meter motorized raft, but it's sagging precariously from the buildup of water.

Melis's wet, chilled fingers work in slow motion, packing away instruments. Colleagues at a nearby second raft stow food and supplies, including spare outboard motors, insurance against breakdowns. For the next several days, Melis and his fellow rafters will collect samples and monitor the river's behavior as rushing waters push and pull sand and silt along its long and winding course. "You have to carry all your equipment and be self-sustaining," explains Jeffrey Cross, director of the National Park Service's (NPS's) Grand Canyon Science Center in Arizona. "Once you launch, you have to go the whole 240 miles."

Last month, floating by native American ruins and spectacular scenery, Melis, Cross, and a dozen other researchers and journalists headed down the Colorado. Their journey marked the beginning of an audacious, 18-month experiment in which scientists and conservationists will test whether a giant wave of water let loose down the river can restore sandbars in the Grand Canyon, one of Earth's great wonders and a popular tourist destination for more than a century.

The stakes are high. For 40 years, the canyon's bars and beaches have been eroding, taking away critical habitat for riverside life and robbing human visitors of comfortable campsites. Yet playing with the Colorado's flow out of Glen Canyon Dam, about 25 kilometers upstream from where Melis and Cross set in, is no small matter: It's the source of hydropower for about 170 utility companies, reservations, and municipalities, and it contributes to the water supply of three states downstream. And if Melis and his colleagues see no improvement in the Colorado's shorelines, it will be the second time in a decade that this multimillion-dollar experiment has failed. That may leave land managers with no choice but to consider even more costly measures, such as shipping in sediment, for rebuilding the river's real estate.

What a rush. This November, a dam release (above) may restore the majestic Grand Canyon riverscape (top).

A damming problem?

In theory, the Grand Canyon's problem and the solution to it are straightforward. Glen Canyon Dam, completed in 1963, restricted the Colorado's natural flow, disturbing the balance of sand deposition and erosion. A flood of extra water released from the dam should carry sediment to the degraded areas. The restored sand and gravel bars should in turn restore nursery grounds for an endangered fish, the humpback chub. As an added bonus, wind whipping up newly settled sand would blow over and rebury native American ruins and other vulnerable archaeological sites exposed by erosion.

Historically, however, any flood was "bad." Water was viewed as a resource that should be corralled and harnessed. In the mid-20th century, the U.S. government began constructing dams to tame the Colorado and other rivers feeding it. Among the more majestic was Glen Canyon Dam, at 216 meters tall. Behind it, Lake Powell holds about 34 trillion liters. At the bottom of the dam, eight turbines generate enough electricity to satisfy, for the moment, the West's need for power at the peak consumption times.

Today, the flow from the once-mighty Colorado River is highly regulated. By law, in 2005, 10 billion cubic meters of water must pass through the dam to ensure that downriver states are adequately supplied with water. To maximize power output, the dam operators usually allow about 283 cubic meters per second (cms) of water to pour through the turbines during the day and reduce that flow to as little as 145 cms at night, creating artificial "tides" along the river's 386-kilometer run from Lake Powell to Lake Mead. Because those turbines pull water from the lake bottom, the released water is relatively cold and sediment-free compared to the Colorado's free-flowing days.

Faced with these unnatural conditions over the past 40 years, native fish disappeared, non-native fish thrived, and sandbars washed away. Few thought much about mitigating these detrimental effects until the Grand Canyon Protection Act of 1992 charged the dam and the canyon's caretakers to do something about these problems. Four years later, the Bureau of Reclamation, working with USGS and NPS, took action with the first deliberate flooding of the canyon. The bureau sent 1274 cms of water through Glen Canyon Dam's four bypass tubes for a week (*Science*, 19 April 1996, p. 344). As predicted, the newly surging river—its waters the color of cocoa—picked up sediment from the river bottom. Initially, the scientists were ecstatic as sandbars downstream expanded. But over the course of the weeklong experiment, the water turned clear—a sign that the flood had scoured all sand and silt—and it proceeded

CREDITS (TOP TO BOTTOM): E. PENNISI; JOSH BIGGS

Sediment seeker. USGS's Ted Melis kept to a tight schedule to catch the Colorado flood's sands.

to slurp up the just-laid sediment from bars and beaches. "What we learned is that that sediment is moved out early," says Charles Groat, director of USGS.

From a policy perspective, the outcome was disappointing, but from Melis's point of view, the $4.5 million experiment taught the scientists an important lesson: They had overestimated how much silt and sand had built up in the riverbed. So they hatched a new plan. Timing, they realized, was of the essence.

The key would be to release water from the dam after heavy rains had flushed lots of sediment from the Paria River—a large tributary 25 kilometers downstream from the Glen Canyon Dam—into the Grand Canyon. Also, the researchers planned to shorten the time they would release the highest flows, limiting them to 60 hours instead of the 90 hours done in 1996. And after the large releases, they would hold the flow for a few days at a relatively small 227 cms, to let the sand settle and to see the results of the flood.

It would be a delicate balance. They needed to wait for the sand pile from the Paria and, to a lesser extent, other tributaries to accumulate, but if they waited too long, it would wash away. Likewise, the flush from the dam needed to last just long enough to scoop up and redeposit the sediment but not so long that the water ran a deficit and carried it away again. Melis compares the sediment loading to a financial accounting scheme—and he wants to make sure the river stays in the black.

In 2002, after much political debate, the management group overseeing scientific projects in Glen and Grand canyons gave the plan a tenuous nod (see sidebar). Yet it took 2 years to move ahead. A prolonged drought took hold of the region, and runoff was scarce. "There was the will, but we were waiting for significant sediment," says Melis.

Then, from September to early November, tropical storms swept through, flushing a million tons of sediment down the Paria and into the Colorado River. On 21 November, at 7 a.m., dam operators opened two 240-centimeter-diameter discharge tubes, each carrying 107 cms. Water shot out and crashed into the river, sending spray tens of meters into the air. Three hours later, two other discharge tubes were opened as well. Including the water exiting the dam through turbines, the flow eventually topped 1161 cms, four times the usual daytime high.

Riding the waves

The surge reached Lees Ferry and Melis less than a day later. By that time, "the river [was] lousy with scientists," says Groat. About 50 researchers, some who in the weeks before had determined the baseline conditions needed for a postflood comparison, were busy with 20 projects. Airborne researchers had used remote sensing to get a precise accounting of the shape of the riverbed. Aerial photographs and light detection and ranging equipment had also documented the size and shape of 150 sandbars.

Back on the river, Melis set out early on

A Cowboy Lawyer Goes Down the River

Bennett Raley looked a little out of place on a river raft as he rode down the Colorado 2 weeks ago to observe an experimental flood as it took place. Once a rodeo competitor, he protected his face from breaking waves with a cowboy hat instead of a raincoat hood. In lieu of rain pants, he wore oilcloth slacks, further reinforcing the cowboy look. But Raley certainly belonged on the raft: While a Republican political appointee as assistant secretary for water and science at the U.S. Department of the Interior (DOI), he was instrumental in preventing the Grand Canyon flood project from being scuttled by discord among the six federal and state agencies, seven states, two environmental groups, six Indian tribes, and two utility companies that had a stake in the effort.

Early in his time at DOI, Raley was skeptical of the project. He worried that it was aimed at altering Glen Canyon Dam's power production and represented "advocacy" science. He had a change of heart, however, when he took a raft trip on the Colorado with the researchers involved. "I think he saw the passion of the scientists, of the boatman, and of the community," says Jeffrey Cross, director of the National Park Service's Grand Canyon Science Center. Raley agrees: "That trip was instrumental in persuading me there was a basis for trusting the scientists." Soon after that trip, he recommended to the secretary of the interior to give the flood project a green light.

River rider. Washington insider Bennett Raley helped keep the Grand Canyon flood on course.

In August, however, the Glen Canyon Dam Adaptive Management Group, which had approved the project in 2002, took a second look at the plan and voted it down. "No one expected that," says Raley. He rode into the fray, and after a soul-searching conference call with various representatives from the group, everyone came back on board and the flood was on again.

A final hurdle appeared in November. For the dam release to do any good, there needed to be enough sediment-laden runoff from the Paria, a key tributary downstream from the dam. Despite rains in September and October, it was not clear whether the amount of sand and silt at the Paria's mouth was what the approved plan called for. "We were still in the gray zone," Raley recalls. Still, he opted to let the release proceed, and by the day of the flood, subsequent storms brought in those missing tons, confirming that his decision was the right one. "We might have had a different outcome," he says, "had there not been that trust." **–E.P.**

CREDITS: (TOP) E. PENNISI; (BOTTOM, LEFT AND RIGHT) JOSH BIGGS

22 November to observe the fate of the sediment swirling around at the front of the wave. His arsenal was a combination of tried-and-true instruments and high-tech devices. An isokinetic point sampler built in 1961 with parts stripped from a B-29 bomber sampled the river at fixed depths, yielding hundreds of packets of water and sediment that would be analyzed on shore. Meanwhile, a sleek, $30,000 device provided details about grain size and concentration, sampling the water once per second and providing data in real time on particles as small as 3 mm.

Immediately after leaving Lees Ferry, "we didn't see any evidence of high sand concentrations" in the main river, says Melis. Instead, the researchers saw the preexisting sand in a large eddy being stirred up—a disturbing observation given that the goal was to put more sand into these quiet spots and not pull it out. But 1.5 kilometers later, "the whole river was brown with sand," he notes, and on target for building bars. The researchers expect that this color transition also signaled a change in the size of the grains in the flow, a shift that may be crucial to the experiment's success, as it takes just the right mix of sediments to make stable sandbars and beaches. "It's like Nature's way of mixing concrete," Melis explains. As in concrete, the mix of grain sizes determines the properties of a sandbar. "We hope to find a wider range of sand and silt grain sizes in these bars" than in 1996, says Melis.

By late afternoon on that first day on the river, Melis's boat passed colleagues who had set up a field lab behind a rock pile. Computer in hand, satellite dish mounted on a nearby rock, and laser-emitting and -receiving monitor by his side, USGS hydrologist Scott Wright measured the amount of sediment as well as the distribution of grain size in the water passing by. His was one of several stationary "labs" that complemented Melis's mobile one.

On the opposite bank, Mark Schmeeckle, a river mechanics expert from Arizona State University in Tempe, was tracking water speed using an acoustic Doppler device that bounced sound waves off sand in the water columns. Changes in the frequency of the returning sound waves translated into water speed. "A surprise is how fast the bottom is moving," notes Neil Ganju, a USGS hydrologist based in Sacramento, California, who was doing similar tests 50 kilometers away. The flood was apparently moving more sand, more quickly than expected.

Saving snails

Schmeeckle shared his field site with biologists who viewed the dam release with trepidation because the rising waters threatened an endangered snail. The 10-cm Kanab amber-snail lives primarily in a natural spring called Vasey's Paradise that is about 18 kilometers downstream from Lees Ferry. The snail thrives on a native plant, monkey flower, which grows close to the water's edge. The flood therefore put as many as 7000 snails in jeopardy. In 1996, conservationists rescued many of the snails by taking them temporarily to higher ground, but that wasn't enough, says Clay Nelson, a biologist with the Arizona Game and Fish Department. "The habitat was inundated and scoured away," he says. This time Nelson and his colleagues took even more radical action. In advance of the approaching flood, they dug up a 35-square-meter swath of monkey flowers and the surrounding soil and moved them on palettes 10 meters above water level. "It's a heroic effort," says NPS's Cross.

When Melis came upon these snail savers, they were waiting out the flood in a makeshift kitchen and sitting area protected by two tarps, one held up by a river oar. They expected to be there another week, missing Thanksgiving at home. "Once the water recedes, we can put [the snails] back in place," Nelson explains.

Another 50 kilometers downstream, Bill Parsons, a biologist with the Arizona Game and Fish Department, and his colleagues kept tabs on another endangered species, the humpback chub. It is one of the canyon's four remaining native fish species, although estimates suggest that fewer than 4000 are left here. Typically, the chub hatch in gravel bars in a tributary called the Little Colorado. Then young fish wash down into warm, shallow pools that form behind sandbars, eventually making their way into the river.

The Glen Canyon Dam has made life difficult for the chub. There are fewer warm pools and more dangers once the fish leave these protected areas. When they hit the Colorado, now colder because water is released from the bottom of the dam, growth slows, leaving them vulnerable to trout, which thrive at the lower temperatures. Moreover, the clear water—sediments settle in Lake Powell—helps the trout visually track prey. Parsons and his colleagues hope the flood-induced turbidity will benefit the chub and that new sandbars will mean more backwater refuges. One worry: The flood may push the chub downriver, away from their normal environs. Still, floods used to be a way of life for this species—unlike the trout, which are not native to the canyon.

Even if the river builds its shoreline and sandbars back up, and the chub and snails do well, the ecosystem will never be the same as in decades past. "It's not a natural ecosystem," Cross explains. "It's a managed ecosystem." The sediment provided by the Paria, for example, is less than a tenth of what the dam-free Colorado carried. And this bolus includes more fine sand than in earlier days. Nonetheless, "we have to manage with the tools we have left," says Nick Melcher, a hydrologist at the USGS in Tucson. Indeed, the Grand Canyon's caretakers may have to perform controlled releases from Glen Canyon Dam every few years, just to make up for the erosion that occurs during the time in between. "If we build a whole lot of sediment on the banks, it will not stay there forever," says Pam Hyde of the Grand Canyon Wildlands Council in Flagstaff. "[This flood] will not solve the problem once and for all."

—ELIZABETH PENNISI

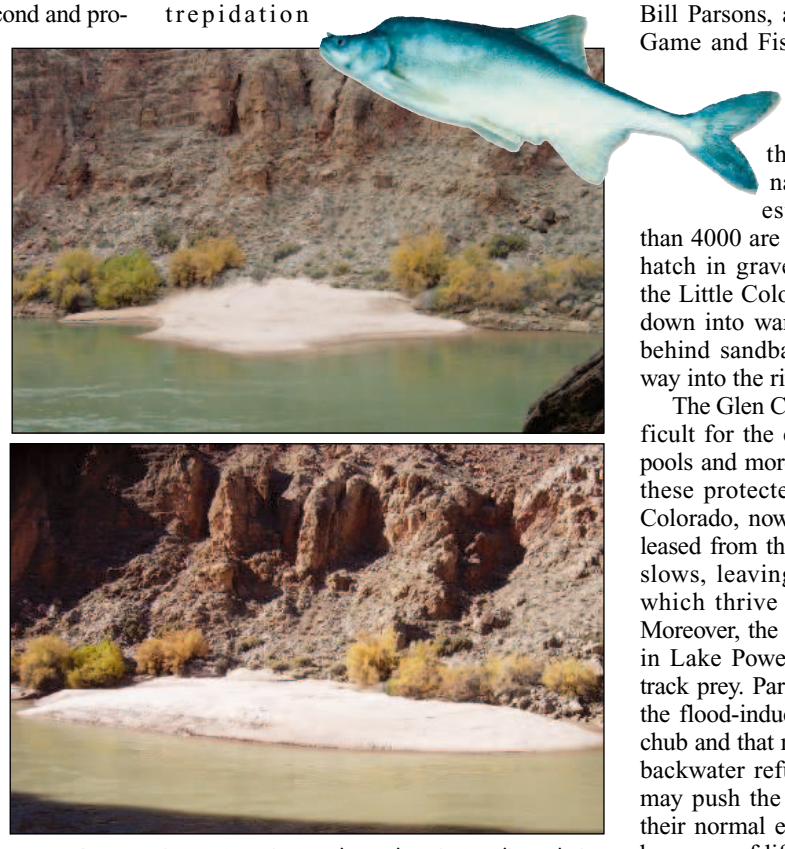

Bigger, better. Photos from before (upper) and after (lower) the flood show how it pumped up sandbars, changes that should benefit an endangered fish called the humpback chub (top).

CREDITS: MARK SCHMEECKLE; (INSET) U.S. FISH & WILDLIFE SERVICE

Tracking the Dirty Byproducts of A World Trying to Stay Clean

Stain protectors and other perfluorinated chemicals are part of our lives—and they are having a growing effect on the environment

They keep ketchup out of the carpet, sauce off your shirt, and fat inside the fast food wrapper. But although fluorinated stain protectors may be a boon in the home and on the run, the almost indestructible byproducts of these chemicals are fouling the planet. Amid growing concerns about the byproducts' ubiquitous presence and possible toxicity, scientists are trying to answer an even more fundamental question: How does a class of chemicals that isn't manufactured in large quantities and that can't travel far become so pervasive?

Fluorinated stain protectors consist of fluorinated surfactants chemically bound to polymers. The fluorinated surfactants work because their strong and rigid carbon-fluoride backbones act like tiny bristles to keep dirt, water, and grease off fabrics, carpets, and paper. Most surfactants don't travel in the environment. But their volatile precursors, fluorotelomer alcohols, travel and degrade into a class of chemicals, perfluorocarboxylates, that is extremely persistent. After a half-century of increasing use, the perfluorocarboxylates are showing up at growing levels in seals and polar bears roaming the Arctic as well as dolphins patrolling the mid-Atlantic.

Over the past 2 years, a team led by University of Toronto chemist Scott Mabury has published dozens of papers identifying these various chemicals in the air and in animals. They've also explained how the volatile precursors, which can be surfactants themselves, can travel thousands of miles in the atmosphere and then be transformed by reaction with oxygen into perfluorocarboxylates. Last month one of Mabury's students, chemist Craig Butt, reported that perfluorocarboxylate concentrations are doubling in Arctic animals every 4 to 10 years (see map).

Drawing on Mabury's work, Canada this summer banned for at least 2 years the production and importation of three polyfluorinated stain protectors that degrade into the long-chain carboxylates Butt is finding in seals. The ban, a first by any government, was triggered by a request from chemical manufacturers to scale up production of the trio of chemicals. John Arseneau, director general of Environment Canada's risk-assessment directorate in Ottawa, concedes that the ban is a "preventative" step that could be lifted or altered. But despite the uncertainty, he says, the government decided "it was time to take action."

Canada is not alone. In the United States, the Environmental Protection Agency is investigating one perfluorinated carboxylate breakdown product and manufacturing aid, perfluorooctanoic acid. PFOA is pervasive in human blood, and there is laboratory evidence of developmental and maternal toxicities in mice at higher levels. In 2000, 3M Corp. voluntarily stopped making Scotchgard, its stain repellent, because a breakdown product, perfluorooctanoic sulfonate, was ubiquitous and accumulating in animals.

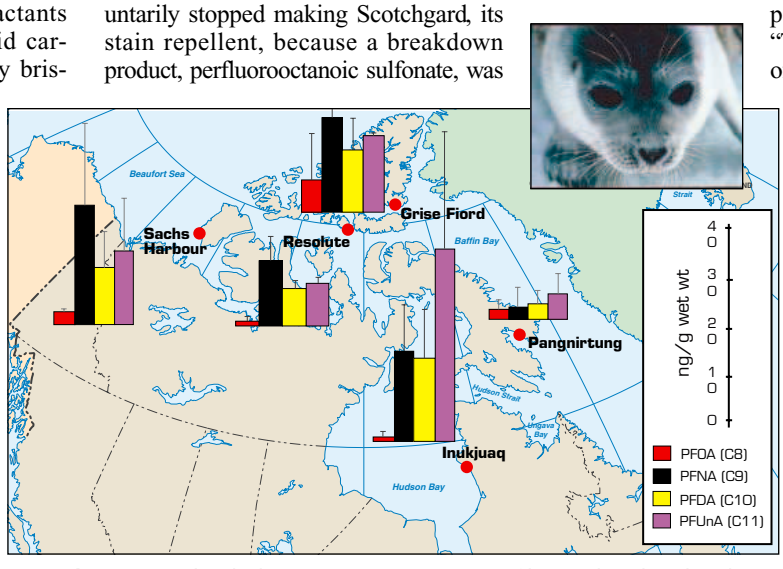

Stained. Arctic ringed seals show varying concentrations of longer chain-length carboxylates, byproducts of industrial stain protectors in carpets and food wrappers.

Mabury has developed a theory to explain both the diffusion and transport of volatile fluorotelomer alcohols: the chemicals used to make fluorosurfactants that sometimes serve as stain protectors themselves. The alcohols, he says, can be released into the air during surfactant manufacturing or the application of stain protectors. Domestic releases also occur. Once they escape, they get blown aloft and dispersed before breaking down to the indestructible perfluorocarboxylic acids found in arctic animals.

Mabury has identified two sources for telomer alcohols in the home. The industrial application process can leave a residue of telomer alcohols that is not bound to the polymer. This residue, says Mabury, is likely to move out of the product and into the air, although the timing and rate of volatilization is not clear. When telomer alcohols are the fluorosurfactant, they can be released if the bond between the surfactant and the polymer breaks through use or abrasion.

A growing number of scientists accept Mabury's theory. "Mabury's group has described a compelling pathway that potentially explains the presence of long-chain carboxylates in remote environments," says chemist Jennifer Field of Oregon State University in Corvallis. Field recently detected perfluorinated breakdown products in domestic waste water, strengthening the argument for home products as a source.

DuPont chemist Robert Buck also thinks the theory offers a viable explanation for how the carboxylates are transported such long distances. But he says it doesn't preclude other sources. Perfluorocarboxylates have been used in a variety of industrial applications, he notes: "This puzzle still has a lot of missing pieces."

Although Mabury agrees that more research is needed, he doubts that other sources are large enough to account for his group's Arctic observations. "Perfluorocarboxylates are not volatile, so they can't travel," he says. "And it seems unlikely that they would be used in the remote regions of the Arctic."

Mabury is no foe of stain protectors, and he opposes the blanket ban that some environmentalists are demanding. "Perfluorinated stain protectors are amazing materials. It would be a waste to abandon them," he says.

Instead, he and others would like to see companies find ways to reduce their products' impact on the environment. 3M is now selling a reformulated Scotchgard with a shorter carbon-fluorine chain length that doesn't accumulate in animals, for example. But if companies don't act quickly, he warns, government regulators could demand substitutes whose impact on the environment is unknown—and potentially worse than the current crop of fluorinated stain protectors.

–REBECCA RENNER

Rebecca Renner is a freelance writer in Williamsport, Pennsylvania.

CREDITS: ADAPTED FROM MAP BY BUTT, MUIR AND MABURY; (INSET) LEW CONSIGLIERI/NOAA

Random Samples

Edited by Constance Holden

Brits and Bikes

The British value bicycles more than vaccinations, computers, or electricity, according to a poll run by *The Times* newspaper last month. Aided by some ballot stuffing, the Rover Safety Bicycle, which with its rear-wheel drive and other modifications turned bikes into a practical mode of transport after being introduced in 1885 by John Kemp Starley, was voted the greatest British invention of the past 250 years, garnering almost two-thirds of the votes cast.

In *The Times*' Internet poll, electricity (Michael Faraday) came in a poor second with 20%, followed by vaccination (Edward Jenner) at 9% and the computer (Charles Babbage) and the World Wide Web (Tim Berners-Lee) at 7%. The electric light (Joseph Swan, who came up with a bulb the same year as Thomas Edison) won in the runner-up category (3%). The poll was aimed at counteracting cynicism and boredom over science and technology, says Lindsay Sharp, director of the U.K.'s Science Museum in London and one of the competition judges. But it was turned into a testimonial for two-wheelers, says Sharp, by a "cabal" of cyclists who bombarded *The Times*' Web site.

Inventor riding his Safety Bicycle.

Fish Consciousness

Citing recent research on the surprising intelligence and sensitivity of fish, the animal-rights group People for the Ethical Treatment of Animals (PETA) has launched a new Fish Empathy Project. "Fish are smart and suffer a great deal," says project manager Karin Robertson.

PETA relies in particular on recent research by biologist Culum Brown of the University of Edinburgh, U.K., who has followed individual fish over time and suggests that they have distinguishable and stable personalities with traits such as boldness and risk taking. Brown also claims to have demonstrated that hatchery-reared fish released to the wild can learn "life skills" from "trainer fish."

The group also cites animal-welfare scientist Donald Broom of the University of Oxford, U.K., who argues that the fish's system for sensing and relaying pain to the brain "overlaps significantly" with that of mammals. The issue of whether fish feel pain is still highly controversial, though. Neuroscientist James Rose of the University of Wyoming in Laramie says fish lack the complex brain structures—namely the neocortex—necessary to experience pain as mammals do.

PETA eventually hopes to push the fishing industry toward more humane practices. For now, the campaign is geared toward raising public awareness.

The Lying Brain

Although it's easy for psychopaths and well-trained spies to cheat the lie detector, many scientists believe it may be possible to nab liars by going straight to the source of mendacity: the brain.

A recent study by radiologist Scott Faro of Temple University in Philadelphia, Pennsylvania, has furnished some new evidence. In Chicago last week at the meeting of the Radiological Society of North America, Faro reported on an experiment in which six subjects fired blank bullets from a toy gun while five others acted as "innocent" controls. The researchers then quizzed the "guilty" and "innocent" subjects while their brains were scanned using functional magnetic resonance imaging. The shooters were instructed to lie.

The scans revealed that lying and truth-telling activate decidedly different areas of the brain. And lying generated more overall activity, firing up regions associated with emotions as well as those involved in the inhibition of responses, Faro's team found.

Although the sample size was small, the study will be useful because the experimenters also collected physiological data, such as heart rate and blood pressure, used in traditional polygraph tests, notes Stanford University neuroscientist John Gabrieli. The comparison between brain imaging and physiological data could help advance the art of lie detecting, he says.

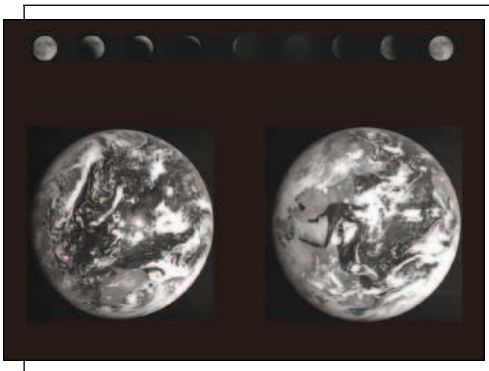

Eclipse Close-Up

At left is "the first family portrait of Earth and moon taken during a lunar eclipse," according to the European Space Agency's chief scientist, Bernard H. Foing. The composite photo was taken by cameras on the SMART 1 (Small Missions for Advanced Research in Technology) spacecraft over a 6-hour period on 28 October. It shows views of Earth from 300,000 kilometers and views from 660,000 kilometers of the moon passing through Earth's shadow. Foing says no other lunar mission has captured this spectacle because they all were in such a hurry to reach the moon. Propelled by a novel solar-powered engine that generates and ejects ions for thrust, SMART 1 took 13 months to reach lunar orbit.

CREDITS (TOP TO BOTTOM): SCIENCE AND SOCIETY PICTURE LIBRARY; PHOTOS.COM; ESA/SMART-1/SPACE-X

Edited by Yudhijit Bhattacharjee

A Shrine to Natural History

When Korean ophthalmologist Rhee Ki-seok was looking for a home for his lifetime collection of fossils and other artifacts, he was dismayed to find that the country had only two natural history museums. So he decided to build one of his own.

The result is a 6800-square-meter museum in the beautiful Gyerong mountains west of Daejeon, which opened to the public this fall. Among its exhibits are a 600-year-old Korean mummy, an ancient mammoth, and a *Brachiosaurus* skeleton excavated in Montana by a dig that Rhee financed (www.krnamu.or.kr).

A veteran of the Korean war, Rhee made a fortune as one of the first ophthalmologists to start a practice in his province and by opening a health sciences college in 1977. He spent $43 million on the museum, acquiring artifacts beyond his personal collection and hiring professors as consultants. Not only did the project receive no help from the government, the 83-year-old Rhee says he had to fight with officials in the nearby city of Daejeon to put up road signs to the museum.

But the outcome has been rewarding: With hundreds of visitors flowing in every day, the museum has already improved "cultural life" in the region, says Rhee. And he hopes it will inspire more Korean students to take up science.

AWARDS

Descartes winners. A pan-European team of life scientists and a transatlantic team of physicists are the joint winners of this year's Descartes Prize from the European Union.

Molecular biologist Howy Jacobs (left in picture) of the University of Tampere, Finland, and his colleagues win half of the $1.33 million prize for elucidating the role of mitochondrial DNA in degenerative diseases and aging. The other half goes to a group led by Anders Karlsson (right, above) of the Royal Institute of Technology in Stockholm, Sweden, for developing telecommunication systems based on quantum cryptography.

Five people will share $330,000 as winners of an inaugural prize for science communication. The honorees are French film producer Vincent Lamy, Hungarian biochemist Péter Csermely, British broadcaster David Attenborough, German biophysicist Wolfgang M. Heckl, and Belgian metallurgist Ignaas Verpoest.

Psychology prize. Memory researcher Elizabeth Loftus has won the $200,000 Grawemeyer Award for Psychology from the University of Louisville in Kentucky. A professor at the University of California, Irvine, Loftus receives the honor for her research on false recollections, which has influenced the way courts and law enforcement agencies view eyewitness testimonies.

MONEY MATTERS

Bedside to bench. Germany's Helmholtz Association has announced a program to help young researchers restart careers put on hold to raise families. Starting next year, the association will fund 29 "reentry" positions for Ph.D. students and postdoctoral scholars across its 15 research centers, which cover fields from space science to cancer research. The program is intended for both men and women, says program coordinator Christian Cobbers, who hopes to take a hiatus from his own career in administration once his first child is born next spring.

Got any tips for this page? E-mail people@aaas.org

HONORS

One with nature. The Australian government last week named a section of the Great Barrier Reef after U.S. marine biologist Nancy Foster, who died in 2000 after a 23-year career at the National Oceanic and Atmospheric Administration. The honor is in recognition of Foster's lifelong efforts to conserve coastal aquatic life, both as a researcher and an administrator.

CREDITS (TOP TO BOTTOM): (PHOTO AND INSET) MARK RUSSELL; DG RESEARCH; NOAA; UNIV. OF LOUISVILLE

LETTERS

Letters to the Editor

Letters (~300 words) discuss material published in *Science* in the previous 6 months or issues of general interest. They can be submitted through the Web (www.submit2science.org) or by regular mail (1200 New York Ave., NW, Washington, DC 20005, USA). Letters are not acknowledged upon receipt, nor are authors generally consulted before publication. Whether published in full or in part, letters are subject to editing for clarity and space.

Microbicides: Anti-HIV Efficacy and Ethics

IN THEIR POLICY FORUM "REGULATORY challenges in microbicide development" (25 June, p. 1911), P. M. Coplan *et al.* discuss the Food and Drug Administration's (FDA's) concern that use of HIV transmission—inhibiting microbicides in the future could decrease condom use and result in an increase in HIV transmission. Coplan *et al.* question this concern on the basis of a mathematical modeling study by Foss *et al.* indicating that a partially efficacious microbicide could undermine the benefit only in settings where condoms are used in more than 70% of coital acts (*1*). This "threshold" has also been quoted in various microbicide meetings; however, the validity of this view depends on intrinsic assumptions of microbicide efficacy and use.

We wish to stress that condom abandonment in favor of microbicides could only be a problem if the efficacies of the introduced microbicides are substantially less than the efficacy of condoms. If microbicide efficacy is similar to condom efficacy, then replacement of one protection option (condoms) by another protection option (microbicides) will not increase HIV transmission rates. Thus, the central focus of discussions should be on the efficacy of microbicides.

> **"Is it not unethical to authorize a study that recruits more than 800 women as volunteers to a study arm that cannot be expected to yield scientifically useful information?"**
>
> –STEIN AND ZUSSER

Current condom usage is generally much less than the level that would yield a negative outcome if condoms were abandoned in favor of reasonably efficacious microbicides [especially in the developing world, where only approximately 1% of sexually active women report condom use in the past month (*2*)]. We support the point made by Coplan *et al.* that the FDA concerns are unwarranted, especially in resource-constrained countries. We emphasize, however, that discussion of any threshold condom usage should be qualified by the appropriate assumptions, and, more importantly, the discussion should address the efficacy of microbicides.

DAVID P. WILSON AND SALLY M. BLOWER
Department of Biomathematics and UCLA AIDS Institute, School of Medicine, University of California at Los Angeles, Los Angeles, CA 90024, USA.

References
1. A. Foss *et al.*, *AIDS* **17**, 1227 (2003).
2. Rwandan Office National de la Population, *Demographic and Health Survey 2000* (Macro International, Calverton, MD, 2001).

WE WOULD LIKE TO ADD SOME COMMENTS TO the excellent and long-overdue Policy Forum "Regulating challenges in microbicide development" by P. M. Coplan *et al.* (25 June, p. 1911). The U.S. National Institutes of Health is at present sponsoring a large microbicide trial. In addition to the necessary putative microbicides being tested and the placebo, this trial has an open arm, namely, "condom only" or "no gel." NIH has been severely criticized both in print (*1*) and at open hearings (*2*) for taking this step. In controlled trials, the double-blinding rule aims to ensure that differences between intervention and control arms are inapparent to both subjects and researchers. Any "open arm" violates this rule and threatens the integrity of the findings; in unmeasurable ways, it may modify both the administration of treatment and the response of subjects to that treatment. Moreover, adding an arm with numbers (already very large) to equal those of either the treatment under test or the placebo cannot but entail more effort, time, and costs in executing a trial. The figure in Coplan *et al.*'s Policy Forum clearly illustrates that imperviousness to criticism on this point results in tragic delay. Delay is unacceptable in a world that needs a microbicide and needs it with great urgency.

Also, we pose a question for consideration by institutional review boards and ethicists: Is it not unethical to authorize a study that recruits more than 800 women as volunteers to a study arm that cannot be expected to yield scientifically useful information?

ZENA STEIN AND MERVYN SUSSER
Gertrude H. Sergievsky Center, Columbia University, 630 West 168 Street, New York, NY 10032, USA.

References
1. Z. Stein, L. Myer, M. Susser, *Epidemiology* **14**, 80 (2003).
2. Division of Antiviral Drug Products, Center for Drug Evaluation and Research, Food and Drug Administration, memo for Antiviral Drugs Advisory Committee, 20 August 2003 (available at www.fda.gov/ohrms/dockets/ac/03/briefing/3970B1_01_FDA%20Briefing%20Document.pdf.

Response

WE AGREE WITH THE LETTERS BY WILSON AND Blower and Stein and Susser and thank them for their comments. Concerns that the benefits of an effective microbicide to prevent HIV infection could be decreased by reduced male condom use have little relevance in countries where male condom use is infrequent. As Wilson and Blower indicate, the benefits of a microbicide that is equally efficacious as condoms could not be decreased by less frequent condom use. In many countries, the greatest risk factor for women becoming infected with HIV is marriage (*1*). Married women often cannot insist that their husbands use condoms. Thus, even a partially effective microbicide would provide women with a valuable means to protect themselves from HIV infection.

> **"We must seriously consider not only the relevance but the ethics of insisting that microbicide ... trials show statistically significant benefits against an unblinded 'no gel' arm when thousands of women are being infected with HIV daily."**
>
> –COPLAN ET AL.

The FDA has stated that vaginal microbicide programs that demonstrate safety and efficacy in protecting against HIV infection in placebo-controlled, randomized trials may not receive licensure approval unless the randomized trials demonstrate significantly greater efficacy than both a placebo-controlled blinded arm and an unblinded "condom only" or "no gel" arm (*2*). We must seriously consider not only the relevance but the ethics of insisting that microbicide pivotal efficacy trials show statistically significant benefits against an unblinded "no gel" arm, when thousands of women are being infected with HIV daily.

PAUL M. COPLAN, MARK MITCHNIK, ZEDA F. ROSENBERG
International Partnership for Microbicides, 1010 Wayne Avenue, Suite 510, Silver Spring, MD 20910, USA.

References
1. UNAIDS, Report on the Global AIDS Epidemic, 2004.
2. Division of Antiviral Drug Products, Center for Drug Evaluation and Research, Food and Drug Administration, memo for Antiviral Drugs Advisory Committee, 20 August 2003 (available at www.fda.gov/ohrms/dockets/ac/03/briefing/3970B1_01_FDA%20Briefing%20Document.pdf).

Qs & AAAs

www.sciencedigital.org/subscribe

For just US$130, you can join AAAS TODAY and start receiving *Science* Digital Edition immediately!

Neglect of Women in Science

TO STANFORD NEUROSCIENTIST BEN BARRES, and all others who are "outraged" by the gender imbalance but "actually think it's more a matter of neglect than of sexism" ("Male sweep of new award raises questions of bias," J. Mervis, News of the Week, 22 Oct., p. 595), I would like to politely point out that neglect of women in science is sexism. A female/male 4/60 ratio of reviewers seems a little low. How about 32/32 next time? Or even 60/4?

VERA RUBIN

Department of Terrestrial Magnetism, Carnegie Institution of Washington, 5241 Broad Branch Road NW, Washington, DC 20015, USA.

Null Model Trumps Accusations of Bias

THE NATIONAL INSTITUTES OF HEALTH HAVE been accused of gender bias on the basis of having awarded all nine of their Director Pioneer Awards for innovative research to men ("Male sweep of new award raises questions of bias," J. Mervis, News of the Week, 22 Oct., p. 595). However, those scientists and scientific organizations making these accusations do not seem to be applying the same rigor to their accusations that they do to their own research. Eighty percent of the award applicants were male. If the review process were completely gender-blind and there were no gender differences in the quality of proposals, the possibility that all nine awardees would be male is 13%. Presumably, those accusing NIH of gender bias do not reject null models in their own research with comparable P values. Why should they be so quick to reject it here? It is likely that historical gender bias throughout the scientific community is partly responsible for the low proportion of award applications by women. However, the data do not justify accusations of gender bias against NIH in this case.

MARK A. DAVIS

Department of Biology, Macalester College, 1600 Grand Avenue, St. Paul, MN 55105, USA.

Nuclear Material Loopholes

READERS OF *SCIENCE* SHOULD BE GRATEFUL TO L. Palmer and G. Milhollin for describing Brazil's intention to operate a new uranium enrichment plant, and the proliferation concerns this action arouses ("Brazil's nuclear puzzle," Policy Forum, 22 Oct., p. 617). If apprehension about global warming causes an expansion of nuclear power deployment during the next half century (*1*), it is vital to limit the spread of dangerous fuel cycle activities—enrichment and reprocessing—that can lead to nuclear weapons.

Palmer and Milhollin suggest that if Brazil cooperates with International Atomic Energy Agency (IAEA) inspections and presumably accepts the "additional protocol" for challenge inspections, Brazil will be a "good nuclear citizen," and the United States and the rest of the world should accept Brazil's enrichment activity.

We disagree. As we (*2*), and others, have argued, the proper policy is to avoid all new enrichment and reprocessing activity in non–nuclear weapons states and for nuclear supplier states to provide recipient states with internationally assured enrichment and spent fuel disposal services at attractive prices. This would begin with a "stay-put" period of 10 to 15 years, after which nations could reevaluate in light of nuclear power and nonproliferation developments.

We should not adopt a policy toward Brazil that we are unwilling to accept for Iran and North Korea. The latter have brought to a head the shortcomings of the Nuclear Nonproliferation Treaty (NPT) implementation regime—these states employ the regime to move to the brink of a weapons capability within the treaty framework. Closing NPT loopholes needs urgent attention, and Brazil will jeapordize the possibilities for successful resolution if they move forward with their uranium enrichment plant. The argument that Brazil is not seeking a weapons capability has not always been true, and IAEA inspections are not an adequate safeguard against states that are seeking nuclear capability, such as Iran and North Korea. IAEA inspections are not sufficient for controlling the spread of nuclear weapons capability, and the United States will not be successful with a policy based on a chosen few—the United States and other nuclear weapons states—deciding which other nations can safely develop fuel cycle activities and which cannot. The United States should vigorously oppose the Brazilian enrichment plant and offer Brazil concrete incentives to abandon this dangerous course of action. Brazil faces a choice of being a spoiler in modernizing the NPT implementation regime or of being a leader in accomplishing that important end.

JOHN DEUTCH[1] AND ERNEST MONIZ[2]

[1]Department of Chemistry, [2]Department of Physics, Massachusetts Institute of Technology, Cambridge, MA 02139, USA. E-mail: jmd@mit.edu, ejmoniz@mit.edu

References

1. *The Future of Nuclear Power–An Interdisciplinary MIT Study* (Massachusetts Institute of Technology, Cambridge, MA, 2003) (available at http://web.mit.edu/nuclearpower/).
2. J. Deutch, A. Kanter, E. Moniz, D. Ponoman, *SURVIVAL*, in press.

Fishery Management and Culling

IN THEIR RECENT POLICY FORUM "Ecosystem-based fishery management" (16 July, p. 346), E. K. Pikitch *et al*. review ecosystem-based fishery management (EBFM) as it is currently conceived. However, the conceptual boundaries of EBFM are being challenged. In May 2004, the Norwegian Parliament voted for a new policy regarding marine mammals, based on a white paper from the Royal Norwegian Ministry of Fisheries (*1*). The "central topic" of this paper is "the establishment of an ecosystem-based management regime for marine mammals in areas under Norwegian jurisdiction" (*1*). The policy includes proposals to increase hunt quotas for minke whales, "substantially" increase catches of harp seals, and "regulate population growth in coastal seals to reduce damage to the fisheries." The policy also identifies the need to "introduce a set of general principles to be used as a basis for marine mammal management in Norway, and seek to achieve the widest possible international support for them." The policy includes almost no mention of management approaches that constitute EBFM as described elsewhere (e.g., by Pikitch *et al.*). The two views of EBFM overlap with regard to monitoring by-catch of marine mammals and protecting endangered species (blue and bowhead whales).

The principle embodied in the new Norwegian policy is to reduce marine mammal populations, or prevent population increases, in the hopes of increased fisheries production. This is culling (*2*). International acceptance that culling predators is a primary component of EBFM will be a retrograde step in marine environmental management.

PETER J. CORKERON*

Norwegian Institute of Marine Research, Pb 6404, N-9294, Tromsø, Norway. E-mail: petercorkeron 2000@yahoo.com.au

*The opinions expressed are the author's and are not the official position of the Institute of Marine Research.

References

1. *Norsk sjøpattedyrpolitikk* [Stortingsmelding 27 (2003–04), available at http://odin.dep.no/filarkiv/207622/STM0304027-TS.pdf]. English quotations are from a translation of the white paper's summary chapter (available at http://odin.dep.no/filarkiv/202967/marine_mammal_summary_final.pdf.).
2. P. Yodzis, *Trends Ecol. Evol.* **16**, 78 (2001).

Response

IN OUR OPINION, CULLING IS NOT "A PRIMARY component" of ecosystem-based fishery management (EBFM).

The key point of our Policy Forum is that EBFM reverses the order of management priorities so that the objective of sustaining ecosystem structure and function supersedes the objective of maximizing fisheries yields. Achieving this might involve selectively harvesting and protecting different parts of the ecosystem at different times—for example, protecting depleted populations and habitats, harvesting target populations with an intensity related to their recent productivity, and targeted removal of invasive species or species greatly favored by anthropogenic activities such as fishing and pollution. Therefore, EBFM does not preclude culling to achieve the objective of healthy ecosystems, provided that it would not cause harm to the structure and function of the ecosystem and would be undertaken in an adaptive, precautionary manner. On the other hand, our interpretation of EBFM is not supportive of large reductions in the natural levels of native populations or ecosystem elements to enhance fisheries yields or with intentionally depleting predators to help compensate for fishery overharvesting of prey species. Furthermore, because marine ecosystems are highly complex, variable, and difficult to predict, attempts to manipulate the ecosystem to enhance commercial fishery yield might not produce the intended consequence and may further degrade the ecosystem.

We believe EBFM is a new, better and all-encompassing way to manage marine fisheries, and it would be unhelpful if the debate were to be overshadowed by a tangential issue such as culling.

ELLEN K. PIKITCH,[1] CHRISTINE SANTORA,[1] ELIZABETH BABCOCK,[2] ANDREW BAKUN,[3] RAMON BONFIL,[4] DAVID CONOVER,[5] PAUL DAYTON,[6] PHAEDRA DOUKAKIS,[1] DAVID FLUHARTY,[7] BURR HENEMAN,[8] ED HOUDE,[9] PAT LIVINGSTON,[10] MARC MANGEL,[11] MURDOCH MCALLISTER,[12] JOHN POPE,[13] KEITH SAINSBURY[14]

[1]Pew Institute for Ocean Science, Rosenstiel School of Marine and Atmospheric Science (RSMAS), University of Miami, 126 East 56th Street, New York, NY 10022, USA. [2]Pew Institute for Ocean Science, RSMAS, University of Miami, 4600 Rickenbacker Causeway, Miami, FL 33149–1098, USA. [3]RSMAS, University of Miami, Miami, FL 33149–1098, USA. [4]Wildlife Conservation Society, 2300 Southern Boulevard, Bronx, NY 10460, USA. [5]Marine Sciences Research Center, Stony Brook University, Stony Brook, NY 11794–5000, USA. [6]Scripps Institution of Oceanography, La Jolla, CA 92093–0227, USA. [7]School of Marine Affairs, University of Washington, Seattle, WA 98105, USA. [8]Commonweal Ocean Policy Program, Bolinas, CA 94924, USA. [9]University of Maryland Center for Environmental Science, Chesapeake Biological Laboratory, Solomons, MD 20688, USA. [10]Alaska Fisheries Science Center, Seattle, WA 98115, USA. [11]Department of Applied Mathematics and Statistics, Jack Baskin School of Engineering, University of California, Santa Cruz, CA 95064, USA. [12]Department of Environmental Science and Technology, Imperial College, Royal School of Mines Building, Prince Consort Road, London SW7 2BP, UK. [13]National Research Council (Europe) Ltd., Norfolk NR34 OBT, UK. [14]Division of Marine Research, CSIRO, Hobart, Tasmania 7001, Australia.

CORRECTIONS AND CLARIFICATIONS:

Perspectives: The Godfrey Perspective in the 3 December issue (p. 1687) was incorrectly marked as having been enhanced. The Kargel Perspective (p. 1689) was in fact enhanced.

Special Issue on Genes in Action: "Solving gene expression" by B. R. Jasny and L. Roberts (22 Oct., p. 629). In the second paragraph, Elaine Alarid's name was mistakenly spelled as Alaric.

MATHEMATICS

Parallel Worlds

Fernando Q. Gouvêa

The discovery of non-Euclidean geometry surely counts as one of the crucial turnings in the history of human thought. It was a slow turn, begun in the early 1830s and only really completed at the dawn of the 20th century. In the process, it caused a transformation in how scientists and philosophers thought about mathematics, about the space surrounding us, and about the relation between the two. *János Bolyai, Non-Euclidean Geometry, and the Nature of Space* gives us a rich account of what happened and how.

János Bolyai, Non-Euclidean Geometry, and the Nature of Space
by Jeremy J. Gray

MIT Press, Cambridge, MA, 2004. 224 pp. Paper, $20, £12.95. ISBN 0-262-57174-9. Burndy Library Publications.

The story begins, as many mathematical stories do, with Euclid's magisterial compendium of Greek mathematics, *The Elements*. Euclid based his account of geometry on five assumptions that he seems to have regarded as self-evident properties of space. Four of these assumptions are fairly simple, but the fifth, known as the "parallel postulate," is quite complicated. Many of Euclid's readers over the centuries have wondered whether it really needed to be that complicated. Even Euclid seems to have felt that there was something unusual about this postulate, as he carefully avoided using it until it became absolutely necessary.

Dissatisfaction with the parallel postulate led many mathematicians to attempt to prove it on the basis of the other four postulates or to find some simpler fact that could be reasonably described as a "self-evident" truth about the space in which we live and from which the parallel postulate could be deduced. Everyone shared the assumptions that Euclidean geometry provided a true description of actual space and that what was missing was simply a full understanding of how the parallel postulate fit into the picture.

In the early 19th century, János Bolyai and Nikolai Ivanovich Lobachevskii both started to investigate the problem. Independently, each looked carefully at what sort of geometry would result if one did not assume the parallel postulate. (Bolyai called this a "geometry of absolute space.") They concluded that a geometry in which the parallel postulate did not hold true—a non-Euclidean geometry—was in fact possible and free from contradictions. Both published their work in obscure places, making it difficult for their achievements to be absorbed by the mathematics community. But slowly it dawned on mathematicians that a true intellectual revolution had occurred.

If geometry does not have to be Euclidean, then in what sense is it a description of the actual space in which we live? Was it that our space is truly Euclidean, and these new geometries were purely imaginary worlds? Or could it be that one of these other geometries actually described our space better? The latter was possible because being non-Euclidean turned out to be a large-scale characteristic: space could "look Euclidean" on a small scale even if it was non-Euclidean overall. Such questions led mathematicians to back away from any claim that their geometries (now in the plural) described actual space. Instead, they came to view their work as simply describing possible geometries—and so to the idea that mathematics at best provides models of what reality might be like rather than somehow accessing reality directly. Deciding which of the possible models came closest to describing our actual physical space became a question for physicists.

The reviewer is in the Department of Mathematics, Colby College, Mayflower Hill 5830, Waterville, ME 04901. E-mail: fqgouvea@colby.edu

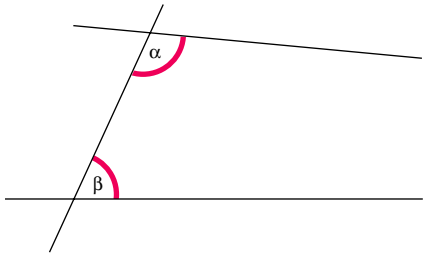

Parallel postulate. "That, if a straight line falling on two straight lines makes the interior angles on the same side less than two right angles [that is, $\alpha + \beta < 180°$], the two straight lines, if produced indefinitely, meet on that side on which are the angles less than two right angles."

János Bolyai, Non-Euclidean Geometry, and the Nature of Space is the first in a new series of books published by the Burndy Library at MIT's Dibner Institute for the History of Science and Technology. The series is intended to make available to a wide audience the resources contained in the library. Accordingly, the volume reproduces in facsimile two items from the library's collection: Bolyai's original Latin publication (which was published in 1832 as an appendix to a much longer mathematical work by his father) and the 1896 English translation by George B. Halsted (an American mathematician whose writings did much to popularize the new geometry). These are preceded by a long "preface" by Jeremy Gray (a mathematician and historian of mathematics, at the Open University)—which is in fact a very full account of the story of the parallel postulate, the discovery of non-Euclidean geometry, and the impact of these ideas from

BROWSINGS

M. C. Escher. Visions of Symmetry. 2nd ed. *Doris Schattschneider.* Abrams, New York, 2004. 384 pp. $29.95, C$45. ISBN 0-8109-4308-5.

Escher's periodic tilings have made the artist a favorite of mathematicians and scientists. In her classic 1990 book, Schattschneider analyzed his art and notebooks to explain how Escher created his colorful, puzzlelike regular divisions of the plane—such as *No. 42* (1941). This new edition adds a short survey of reflections of his work in mathematics, computer graphics, the Internet, and contemporary art.

the mid-19th to the early 20th centuries.

Gray's preface is a delight. He tells us of various purported "proofs" of the parallel postulate, of Kant's controversial argument that Euclidean geometry provided an example of synthetic a priori knowledge, and much more. Having set up the context, he turns to Bolyai's own work and attempts to guide the reader through the contents of the papers reproduced later in the book. This shifts the discussion from overview to detailed mathematics; nonmathematicians are likely to find this section difficult. Should they persist, however, they will reach Gray's fascinating account of the reception of non-Euclidean geometry by mathematicians, physicists, philosophers, and even artists, which does not make serious mathematical demands on the reader.

Any author who attempts to reach an audience that includes specialists and nonspecialists alike—as the preface specifies that books in the Burndy Library series should—is faced with difficult decisions. Though Gray often speaks successfully to both kinds of reader, the results are not uniform; at times, the reader will need a little bit of patience when dealing with material meant for others. Those who make that effort will find that they have acquired a much deeper understanding of the "non-Euclidean revolution" and its far-reaching consequences.

DOI: 10.1126/science.1105298

MATHEMATICS

Circumferential Curiosities

Eli Maor

The past 15 years have seen a surge in interest among the general public in popular books on mathematics. In particular, the six most famous numbers in mathematics—zero, π, *e* (the base of natural logarithms, approximately 2.7183), phi (the "golden ratio," about 0.6180), *i* (the "imaginary unit," the square root of negative one), and gamma (also known as Euler's constant, about 0.5772)—have each been covered in at least one such book. That these numbers have entered the realm of popular science is reflected in the subtitles of some of these books: "the World's Most Astonishing Number" (*1*), "The Biography of a Dangerous Idea" (*2*), and now *π: A Biography of the World's Most Mysterious Number*, by Alfred Posamentier and Ingmar Lehmann.

π
A Biography of the World's Most Mysterious Number
by Alfred S. Posamentier and Ingmar Lehmann
Prometheus, Amherst, NY, 2004. 324 pp. $26. ISBN 1-59102-200-2.

The reviewer is in the Department of Mathematics and Statistics, Loyola University, 6525 North Sheridan Road, Chicago, IL 60626, USA. E-mail: emaor@math.luc.edu

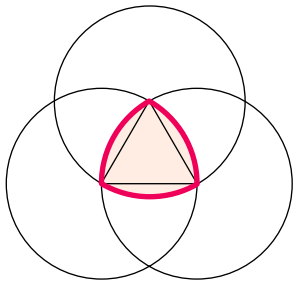

Reuleaux triangle. The constant width of the closed curve equals the radius of the circles used to construct it.

Any new popular book on π must inevitably be judged against the standard set by the first of the line of these biographies: Petr Beckmann's *A History of* π (*3*), which has gone through several editions since it first appeared in 1970. The two books are about the same length as far as the text goes, and they target the same audience—the layperson with an interest in the history of science and mathematics. But here the similarities end. Whereas Beckmann's account is all history, Posamentier and Lehmann (mathematicians and mathematics educators at the City University of New York and Humboldt University, Berlin, respectively) write mostly about curiosities associated with π; only one chapter is exclusively history.

Some of these curiosities can be mind-boggling. My favorite is an exotic curve known as the Reuleaux triangle, named after its discoverer, the 19th-century German engineer Franz Reuleaux. Its construction is so simple that one wonders why no one before him had come up with the idea (see the figure). What makes this curve a close relative of the circle is the fact that it has a constant width—a diameter of sorts: no matter how one measures it, the distance *d* between two opposite points is always the same. But that's not all. A straightforward calculation shows that the circumference of the curve is equal to πd—exactly as with the circle. (However, the familiar formula for the area of a circle, $\pi(d/2)^2$, does not work for this curve.) And lest one think that this is just an interesting curiosity, the Reuleaux curve was put to practical use in Felix Wankel's internal combustion engine, invented in 1957, which powered the 1964 Mazda. Posamentier and Lehmann effectively and engagingly describe the properties of this unusual curve.

Other curiosities, however, are elevated to a status they hardly deserve. For example, the authors devote a full 20 pages to a trivial "paradox" that could have been described in half a page. Imagine a rope tightly wound around Earth's equator. Now imagine a second rope, 1 meter longer than the first and floating in space above the equator. At what height will the second rope be hanging above the ground? The answer, just under 16 centimeters, is simply a consequence of the formula for the circumference of a circle. Let *R* be Earth's radius and *C* its circumference (both measured in meters). We have $C = 2\pi R$ and $C + 1 = 2\pi(R + h)$, where *h* is the required height. Subtracting the first equation from the second, we get $2\pi h = 1$, so $h = {}^1/_{2\pi} \sim 0.159$ meters. The surprise is that the answer does not depend on Earth's radius; only the difference between the two radii matters. A surprise it is, but to elevate this to the status of a sensational paradox is, I think, a bit excessive.

The book's many curiosities include the value of π to one hundred thousand decimal places, taking up 28 pages. (The current world's record is 1.24 trillion places, a bit too long to be printed in a book of reasonable size.) And one will find the world record for memorizing the digits of π: over 42,000 digits, a feat achieved by Hiroyuki Goto in nine hours of reciting.

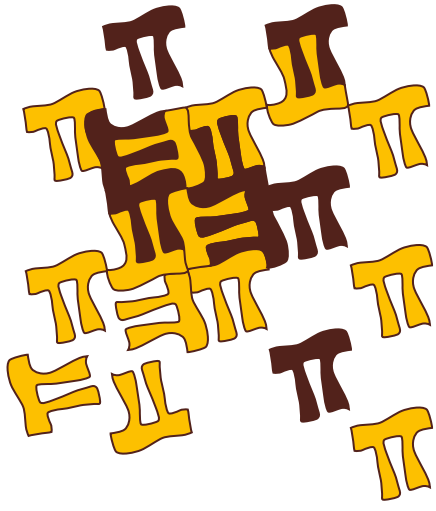

I enjoyed reading the book, if not for any new deep mathematical insights, then at least for its many applications, curiosities, and anecdotes. My enjoyment was tempered, however, by the presence of more than just a few typos, including erroneous formulas (which can be rather frustrating if one tries to work through them). Hopefully, a future edition will undergo a more thorough editing, so as to make this a truly pleasurable account.

References and Notes

1. M. Livio, *The Golden Ratio: The Story of Phi, the World's Most Astonishing Number* (Broadway, New York, 2002); reviewed by E. Maor, *Science* **299**, 1016 (2003).
2. C. Seife, *Zero: The Biography of a Dangerous Idea* (Viking, New York, 2000).
3. P. Beckmann, *A History of π* (Golem, Boulder, CO, 1970).

DOI: 10.1126/science.1106082

CREDITS: (TOP) ADAPTED FROM *π*; (BOTTOM) COURTESY JOSEPH TEETERS

INFORMATION ACCESS

NIH Public Access Policy

Elias A. Zerhouni

A new National Institutes of Health public access draft policy is raising a tremendous amount of interest in the scientific, patient, and publishing communities. I would like to clarify what the proposed policy is, describe its rationale, and explain why the NIH thinks this is a reasonable, balanced policy that will serve all interests.

As recently outlined (*1*, *2*) the draft policy requests, but does not require or mandate, that NIH-funded investigators submit electronically to the NIH the final, peer-reviewed author's copy of their manuscript (unless the publisher agrees to replace it with the final published copy). The author's copy will be embargoed from release by NIH for 6 months after the publisher's date of publication, providing at minimum a 6-month delay between final peer review and public availability in the National Library of Medicine's (NLM) PubMed Central (PMC) (*3*).

Some are concerned that grantees or smaller or not-for-profit publishers will be harmed. This is why NIH elected to leave the decision to submit the author's copy to PMC in the hands of the investigators and their publishers. We believe that this aspect, combined with the 6-month window, will preserve the critical role of journals and publishers in peer review, editing, and scientific quality control.

We believe a stable, permanent archive of peer-reviewed, NIH-funded research publications will help NIH better meet its mission and will augment the ability of scientists to exchange information more effectively. This archive, searchable with modern information technology tools, will enable NIH to manage more efficiently and to understand better its research portfolio, to monitor its scientific productivity, and to help set research priorities. It will also help us to create an end-to-end, paperless grants-management process.

NLM and its predecessors have been responsible for building and maintaining medical literature archives for more than 150 years. NLM pioneered electronic database retrieval in the 1960s. Congress assigned to the NLM the responsibility to acquire, organize, disseminate, and preserve biomedical information for the benefit of public health. However, the proposed policy does not mandate that PMC will be the sole repository of NIH-funded published research. In fact, NIH welcomes multiple archiving approaches.

The Internet is used increasingly to search for health-related information. For example, about 93 million Americans searched for at least 1 of 16 health topics online within the past year (*4*). In a 2003 survey, 58% of Internet users said they brought information obtained from the Internet to their doctor's office (*5*). Now, research information is largely available only to scientists, clinicians, patients, and educators through personal subscriptions or at academic and hospital libraries. It is important for NIH to provide the public access to an electronic archive of the findings resulting from publicly funded research.

NIH supports the current publishing process by encouraging publication of NIH-supported original research in scientific journals. NIH already provides an estimated $30 million annually in direct costs for page charges and other publication costs (*6*). In addition, NIH provides funds, through indirect costs, to grantee institutions for library journal subscriptions and electronic site licenses.

NIH highly values traditional routes of research information dissemination through peer-reviewed journals. Peer review is a hallmark of quality and is vital for validating accuracy and interpretation. Publication in peer-reviewed journals is a major factor in determining professional standing and in making hiring, promotion, and tenure decisions. We also value the communities of research created by scientific organizations and the journals they publish.

NIH support is involved in approximately 65,000 articles per year. Using 2003 data, NLM estimates that publications resulting annually from NIH-funded research represent about 10% of the articles in the nearly 5000 journals indexed by PubMed. NIH-funded articles account for more than half of the total published articles for only 1% of these journals (*7*). It is unlikely that scientists and libraries would use the proposed public access policy to gain access to the scientific literature in lieu of their journal subscriptions, because if they did, they would be able to access only a fraction of a journal's content. In addition, there are many other components of journals, such as science news, industry information, literature reviews, job announcements, and other products that bring value to the reader. These will not be a part of the NIH archive.

The proposed NIH policy will not affect the ability of NIH-funded investigators and journals to copyright works. Investigators may assign these rights to journals in accordance with current practice, and copyright holders may continue to enforce their rights as before. A member of the public viewing or downloading a copyrighted document from PMC is subject to the same rights and restrictions as when copying an article from the library. In addition, PMC includes a notice alerting the public to the rights of copyright holders and will continue to post this notice as part of any NIH public access system.

Some have expressed concern that archiving NIH-funded manuscripts in PMC will incur huge costs. In fact, by building on an existing information technology infrastructure housed at the NLM, the NIH public access policy can be exceptionally cost-effective. Our estimates of $2 to $4 million per year (*7*) reflect incremental costs from creating a Web site for the manuscripts and for XML tagging them into PubMed Central's archival format. Implementation of the proposed policy may result in certain efficiencies for our grantees, the majority of whom currently submit paper copies of their published articles for end-of-year reporting and for renewal competition.

NIH has received over 6000 comments on its proposed policy. We plan to make these available in a public reading room. Currently, the NIH Web site (www.nih.gov/about/publicaccess/index.htm) contains answers to frequently asked questions about the public access draft policy. Because our proposed policy is timely and flexible, NIH is confident that it will not only advance science, but also be advantageous to scientists, to publishers, and to the public.

The author is director, National Institutes of Health, Bethesda, MD 20892, USA.

References and Notes

1. "Enhanced public access to NIH research information" (Notice NOT-OD-04-064, NIH Guide to Grants and Contracts, 3 September 2004).
2. *Fed. Regist.* **69** (180), 56074 (17 September 2004).
3. See www.pubmedcentral.nih.gov/.
4. Internet Health Resources, Pew Internet and American Life Project, Washington, DC, 2003; available at www.pewinternet.org/pdfs/PIP_Health_Report_July_2003.pdf
5. Cybercitizen Health 3.0 Survey, Table 10 (Manhattan Research, New York, 2003); available for purchase at www.manhattanresearch.com.
6. The estimated $30 million is a conservative figure based on amounts spent on page charges and other publication costs on a sample of R01 grant application budgets, scaled up to provide an estimate of direct costs paid on all research grants.
7. Details are in the supporting online material.

10.1126/science.1106929

Supporting Online Material

www.sciencemag.org/cgi/content/full/306/5703/1895

Q

Working conditions making your performance a bit scary?

Face it. You're good at what you do. And you deserve to work in the kind of environment that helps you succeed. So, look around you. Is the balance between science and survival tipping in your favor? If not, get yourself and your career back on solid ground with a visit to ScienceCareers.org.

With a few mouse clicks you'll find:

- hundreds of job postings
- employer profiles
- a resume/CV database
- an e-mail job alert service

With ScienceCareers.org the number of opportunities is almost scary. And that's the kind of fear you can handle.

A

Science @ CAREERS

www.ScienceCareers.org

Science AAAS

PARASITOLOGY

The Malarial Secretome

Jude Przyborski and Michael Lanzer

Malaria, caused by the *Plasmodium* protozoan parasite, kills more than 1 million children in Africa alone each year. New interventions are needed to relieve the burden that malaria places on public health and economic development, particularly in Africa, which bears the brunt of the disease. Malarial parasites not only have a complex life cycle alternating between a vertebrate and invertebrate host, but also are capable of developing within highly specialized red blood cells—a challenge met by only a few intracellular pathogens. In this issue, two papers by Marti *et al*. (*1*) on page 1930 and Hiller *et al*. (*2*) on page 1934 provide fascinating insight into how *Plasmodium falciparum*, the most virulent human malarial parasite, remodels the host red blood cell to ensure its own survival.

P. falciparum replicates in a parasitophorous vacuole within human erythrocytes. The evolutionary decision to inhabit terminally differentiated denucleated host cells places the parasite in a difficult situation. It severs itself from the external nutrient supply essential for growth and reproduction, and renders itself vulnerable to clearance by the spleen of the host organism, which removes senescent and infected erythrocytes from the circulation. To circumvent these problems, the parasite modifies the host cell by exporting its own proteins into the cytoplasm and plasma membrane of the erythrocyte, establishing immune evasion mechanisms and creating new permeation pathways for nutrient uptake. To transfer proteins across the parasitophorous vacuolar membrane (PVM) and then through the erythrocyte cytoplasm, the parasite establishes a protein-trafficking system beyond the bounds of its own plasma membrane. The erythrocyte lacks a secretory apparatus and so cannot contribute.

Many *P. falciparum* proteins exported into the erythrocyte contain functional amino-terminal signal sequences, which garner them entry into the parasite's secretory pathway, resulting in their secretion into the parasitophorous vacuole. To translocate these proteins across the PVM, additional signals are required. Previous studies located such signals ~60 amino acids after the signal sequence (*3*, *4*). By closely examining this region, both Marti *et al*. (*1*) and Hiller *et al*. (*2*) independently identified a unique conserved motif (see the figure). By replacing key amino acids in this motif, they confirmed its functional role in translocation of parasite proteins across the PVM.

Although the discovery of a host cell–targeting (HCT) signal answers a long-standing question in malaria research, the greater importance of this finding is that it enables a search for other parasite proteins that are exported into the erythrocyte (the parasite secretome). Screening *P. falciparum* sequence databases, Marti *et al*. and Hiller *et al*. identified a surprisingly large number of proteins (250 to 350) containing the HCT signal. Many of these belong to the previously described Rifin/Stevor superfamily implicated in antigenic variation (*5*). However, another 150 proteins are unknown, and most of them are unique to *P. falciparum*. Among the annotated (characterized) proteins are phosphatases, serine-threonine kinases, a putative ABC transporter, and proteins with chaperone domains. Remodeling of the infected erythrocyte appears to be more extensive and to involve more parasite proteins than previously thought. The HCT signal is also present in proteins exclusively synthesized in the liver, gametocyte, and invasive stages of the parasite. Apparently, the parasite uses the HCT signal in different host cell settings and early in host cell invasion. Notably absent from the output are a number of known exported proteins, including COPII proteins, Exp1, and Sbp1. How these proteins are targeted to the host cell remains unclear; perhaps alternative pathways are involved.

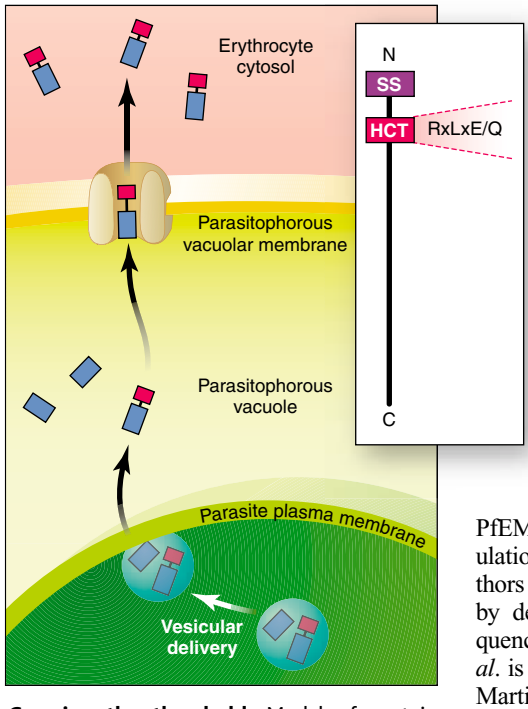

Crossing the threshold. Model of protein translocation across the parasitophorous vacuolar membrane of a *P. falciparum*–infected erythrocyte. Parasite proteins in transport vesicles are delivered to the parasitophorous vacuole. Here, they are recognized on the basis of their HCT signal by a putative translocon and are released into the erythrocyte cytosol. (**Inset**) The structure of a typical exported parasite protein. SS, cleavable signal sequence (purple); HCT, host cell–targeting signal (red). RxLxE/Q is the core HCT signal.

A special case in terms of its HCT signal is PfEMP1, a family of immunovariant adhesins exported to the surface of infected erythrocytes and implicated in the pathophysiology of cerebral and placental malaria (*6*). PfEMP1 did not appear in the initial screen for a conserved HCT signal, and only when PfEMP1 variants were separately analyzed could conserved trafficking motifs be recognized. Unexpectedly, Hiller *et al*. and Marti *et al*. report different sequences. Is it possible that PfEMP1 has two independent HCT signals? The data would suggest so. Genes that encode PfEMP1 are not readily amenable to manipulation because of their large size. The authors therefore created PfEMP1 minigenes by deleting large parts of the coding sequence. But the motif identified by Hiller *et al*. is absent in the minigene investigated by Marti *et al*., and vice versa (fig. S1). Two independent HCT signals in a protein that rapidly undergoes genetic variation may ensure that at least one retains its function.

The identification of a HCT signal in *P. falciparum* inspired Hiller *et al*. and Marti *et al*. to search for this signal in other malarial parasites, and indeed they found it. Apparently, the HCT signal and the machinery recognizing it evolved early in the genus *Plasmodium*. That the HCT signal remains conserved among plasmodial

The authors are in the Department of Parasitology, Universitätsklinikum Heidelberg, Im Neuenheimer Feld 324, 69120 Heidelberg, Germany. E-mail: michael_lanzer@med.uni-heidelberg.de

species after millions of years of divergent evolution (*7*) testifies to its importance in parasite survival. Perhaps the HCT signal is also conserved in other intraerythrocytic protozoan parasites. From an evolutionary standpoint, it is intriguing that the vast majority of proteins targeted to the host cell are encoded in the subtelomeric domains of chromosomes. Because these domains are dynamic (*8*), they are ideally suited to harboring genes involved in host-parasite interactions, allowing adaptation to a particular host.

The next step is to isolate factors interacting with the HCT signal and to investigate their contribution to the transport process. A simple model would be a translocon, which selectively recognizes proteins and transports them across the PVM (see the figure). Such a model is easy to imagine for the transport of soluble proteins, but is difficult to reconcile with the transport of transmembrane proteins. However, it seems that PfEMP1, at least, travels in a soluble form through the parasite's secretory system and only enters a membrane-bound state after translocation across the PVM (*9*). Much remains to be done to elucidate protein-sorting mechanisms in *Plasmodium*, but it is increasingly clear that lessons can be learned from this fascinating parasite, distinct from its starring role as an agent of human disease and misery.

References

1. M. Marti, R. T. Good, M. Rug, E. Knuepfer, A. F. Cowman, *Science* **306**, 1930 (2004).
2. N. L. Hiller *et al.*, *Science* **306**, 1934 (2004).
3. M. E. Wickham *et al.*, *EMBO J.* **20**, 5636 (2001).
4. C. Lopez-Estrano *et al.*, *Proc. Natl. Acad. Sci. U.S.A.* **100**, 12402 (2003).
5. Q. Cheng *et al.*, *Mol. Biochem. Parasitol.* **97**, 161 (1998).
6. L. H. Miller *et al.*, *Nature* **415**, 673 (2002).
7. A. A. Escalante, F. J. Ayala, *Proc. Natl. Acad. Sci. U.S.A.* **92**, 5793 (1995).
8. L. H. Freitas-Junior *et al.*, *Nature* **407**, 1018 (2000).
9. J. Papakrivos *et al.*, *Mol. Microbiol.*, in press.

Supporting Online Material

www.sciencemag.org/cgi/content/full/306/5703/1897/DC1
Fig. S1

10.1126/science.1107072

APPLIED PHYSICS

Mesmerizing Semiconductors

Gerrit E. W. Bauer

Since the Renaissance, physicians have used ferromagnets as a therapeutic tool, believing in the beneficial effects of their mysterious stray magnetic fields. Franz Anton Mesmer (*1*) discovered that he could magnetize ("mesmerize") his patients even without using magnets. Recently, Kato *et al*. have performed a similar feat: They have magnetized nonmagnetic semiconductors without ferromagnets (*2*, *3*). On page 1910 of this issue (*4*), they report that this magnetization can flow. The observations confirm earlier predictions (*5*–*9*). They do not require a completely new type of magnetism, but many details remain mysterious.

The electron has a charge and a magnetic moment, the spin. In a few materials (such as iron, cobalt, and nickel), the spins align below a certain temperature to create a macroscopic magnetic moment. Such ferromagnets are used, for example, in information storage devices. The young field of spintronics aims to also employ the electron spin in semiconductor-based microelectronic devices. Unfortunately, semiconductors resist direct injection of spins through ferromagnetic contacts.

Theoreticians proposed possible alternative routes. It was predicted, for example, that in some nonmagnetic conductors, an electric current would excite a magnetization (*10*). The magic ingredient is the relativistic interaction between the spin and the motion of the electron (spin-orbit coupling). Electrons moving in a magnetic field experience an electric field. Similarly, electrons moving in an electric field experience a magnetic field. This internal magnetic field tends to align the spins, but they precess like a top, maintaining a constant projection along the direction of the magnetic field (see the figure, left panel). As electrons scatter at defects and impurities, the magnetic field fluctuates. On average, only those spins accumulate that are aligned normal to the electric current. In piezoelectric materials such as III-V semiconductors, the electric field can be generated by a built-in strain (*2*–*4*). The theory is complicated, but sometimes reduces to the simple picture sketched above (*11*, *12*).

In their recent studies, Kato *et al.* (*2*, *3*) realized these theoretical ideas. The authors monitored the spin accumulation with a noninvasive optical spectroscopy technique that can resolve, both spatially and temporally, the spins that are aligned with the probing light beam. They investigated thin GaAs and InGaAs films that are lightly doped to maximize the lifetime of the spins. In (*2*), the authors confirmed the existence of the internal magnetic field in strained GaAs by observing the precession of an optically injected spin accumulation. In (*3*), they detected the current-induced spin accumulation in strained InGaAs.

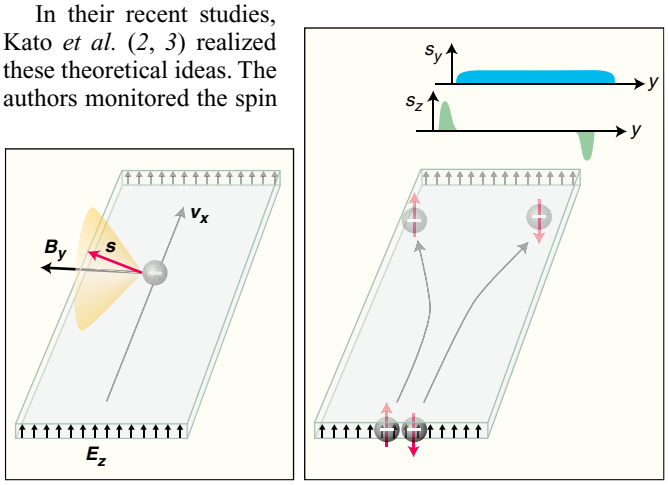

Spins at the edge. (**Left**) Electrons moving with velocity v_x in an electric field E_z experience a spin-orbit coupling that causes a top-spin precession (yellow cone), with constant projection on the internal magnetic field $\boldsymbol{B}_y = \boldsymbol{v}_x \times \boldsymbol{E}_z$ (black). (**Right**) The spin Hall current is caused by the separation of up and down spins due to the spin-orbit interaction. Kato *et al.* (*4*) report that the *z*-component of the spin accumulation (s_z, green) peaks at the edges as a result of the spin Hall current. They previously showed that the *y*-component of the spin accumulation (s_y, blue) is constant across the sample (*3*).

The observed magnetization is believed to differ fundamentally from the one that is injected into metals by ferromagnetic contacts. It is, for example, not accompanied by a spin current (*13*)—that is, a net flow of spin angular momentum—in the field direction.

The flow of information encoded by spins is, however, an essential ingredient of spintronics applications. The prediction of the spin Hall effect—that is, a net flow of spin momentum normal to the driving current (see the figure, right panel)—has therefore attracted a lot of attention. An "extrinsic" spin Hall effect can occur when impurities with strong spin-orbit interaction deflect the up and down spin electrons to opposite edges of the sample (*5*–*7*). More recently, two groups predicted "intrinsic" spin Hall effects for semiconductors that do not require impurities. Sinova *et al.* (*8*) examined finely layered structures, in which carriers are lo-

The author is at the Kavli Institute of NanoScience, Delft University of Technology, Delft, Netherlands. E-mail: g.e.w.bauer@tnw.tudelft.nl

calized at the interfaces between semiconductors but are free to move in lateral directions (the two-dimensional electron gas). Murakami *et al*. (*9*) considered empty states (holes) in the valence band. The latter system is more complicated, but its phenomenology fits the simple picture sketched above.

In the present work (*4*), Kato *et al*. focus on the spin accumulation in thin films of doped GaAs and strained and doped InGaAs layers in the presence of an electric current. They observe a component of the spin accumulation that is normal to the film and strongly localized at the edges (see the figure, right panel). The data provide strong evidence for the existence of the spin Hall effect. The spin Hall current is blocked at the edges, where the spins accumulate. The same impurities that create the spin Hall current dissipate the spin accumulation that diffuses back into the film (*7*), on a length scale that can be estimated by inspecting the image of the spin accumulation (*4*).

The results for the two semiconductors are very different, highlighting the importance of differences in band structure and strain field. The direct proof for an internal field in the strained InGaAs film makes this material a candidate for the intrinsic spin Hall effect. Nevertheless, Kato *et al*. suggest that it is extrinsic, because the effect is small and no dependence on crystal direction is observed. Hence, in the present samples, the intrinsic Hall effect appears to be suppressed by the the scattering from impurities and defects.

The experiments reported by Kato *et al* (*2*–*4*) provide an unprecedented glimpse into a new magnetic effect, but many open questions remain. For instance, there is no consensus among theoreticians about the resilience of the intrinsic spin Hall effect to defect scattering (*14*), and some voice doubts about the concept of a spin current in the presence of spin-orbit interactions.

It should be very interesting to repeat the present experiments on hole-doped samples with a larger internal magnetic field. Such experiments may confirm the observation of the intrinsic spin Hall effect in the two-dimensional hole gas (*15*) or test theories that predict a more robust effect in the valence band (*16*). Another big challenge also remains: To fulfill the promises of spintronics, scientists must transform the novel spin accumulation and spin currents into voltage differences and charge currents in micro- or nanoelectronic circuits.

References

1. V. Buranelli, *The Wizard from Vienna* (Coward, McCann and Geoghegan, New York, 1975).
2. Y. Kato *et al*., *Nature* **427**, 50 (2004).
3. Y. K. Kato, R. C. Myers, A. C. Gossard, D. D. Awschalom, *Phys. Rev. Lett.* **93**, 176601 (2004).
4. Y. K. Kato, R. C. Myers, A. C. Gossard, D. D. Awschalom, *Science* **306**, 1910 (2004); published online 11 November 2004 (10.1126/science.1105514).
5. M. I. Dyakonov, V. I. Perel, *JETP Lett. USSR* **13**, 467 (1971).
6. J. E. Hirsch, *Phys. Rev. Lett.* **83**, 1834 (1999).
7. S. Zhang, *Phys. Rev. Lett.* **85**, 393 (2000).
8. J. Sinova *et al*., *Phys. Rev. Lett.* **92**, 126603 (2004).
9. S. Murakami, N. Nagaosa, S.-C. Zhang, *Science* **301**, 1348 (2004).
10. L. S. Levitov, Yu.V. Nazarov, G. M. Éliashberg, *Sov. Phys. JETP* **61**, 133 (1985).
11. Yu. A. Bychkov, E. I. Rashba, *JETP Lett.* **39**, 78 (1984).
12. B. A. Bernevig, S.-C. Zhang, http://arxiv.org/abs/cond-mat/0408442.
13. J. Inoue, G. E. W. Bauer, L. W. Molenkamp, *Phys. Rev. B* **67**, 033104 (2003).
14. J. Inoue, G. E. W. Bauer, L. W. Molenkamp, *Phys. Rev. B* **70**, 041303 (2004).
15. J. Wunderlich, B. Kaestner, J. Sinova, T. Jungwirth, http://arxiv.org/abs/cond-mat/0410295.
16. S. Murakami, *Phys. Rev. B* **69**, 241202 (2004).

10.1126/science.1106931

PHYSIOLOGY

Turning on a Dime

Ulrike K. Müller and David Lentink

Scientists may think that insects are the masters of unconventional lift (*1*–*4*), but it seems that birds have caught on to the same trick, using it to outsmart their insect prey. On page 1960 of this issue, Videler *et al*. (*5*) report how swifts—agile aerial hunters that catch insects on the wing—produce unconventional lift: They use their wings to generate a so-called leading-edge vortex. Biologists first caught on to this vortex in 1996 when trying to explain how insects fly (*1*). Since then, this vortex has been observed again and again in flying insects (*2*–*4*). The new study reveals that a bird's wing also can generate this type of vortex (*5*).

Enhanced online at www.sciencemag.org/cgi/content/full/306/5703/1899

A leading-edge vortex forms on the top of a wing when the angle between the wing and the oncoming air flow is large. The flow then separates from the wing at the leading edge and rolls up into a vortex. To form a leading-edge vortex at lower angles of attack, some wings have a sharp rather than blunt leading edge. To exploit this vortex, the flying animal needs to keep the vortex close to its wing. Insects and swifts have found different solutions to this problem. To stabilize the vortex, flying insects beat their wings rapidly (*1*), whereas gliding swifts sweep their wings backward (*5*). The leading-edge vortex spirals out toward the tip of the wing, adopting the shape of a tornado. Like a tornado, the air pressure in the core of the vortex is low, sucking the wing upward and sometimes forward (during flapping).

Swifts have scythe-shaped wings that consist of a long curved hand-wing, which is attached to the body by a short arm-wing. The hand-wing is composed of primary feathers, which form a sharp and swept-back leading edge. Both features help to generate and stabilize a leading-edge vortex. Videler *et al*. cast a model of a single swift wing in fast gliding posture and recorded the flow fields around the wing in a water tunnel using digital particle image velocimetry. (Flow patterns in water are the same as in air as long as the same Reynolds number is used.) They observed that a vortex forms on top of the wing close behind the wing's leading edge. This leading-edge vortex is robust against changes in flow speed and angle of attack—observations that agree well with those of other biologists studying the leading-edge vortices of insects. However, surprisingly, the swift wing produces such a vortex at angles of attack as small as 5°, compared with 25° to 45° typical for insects (*6*, *7*).

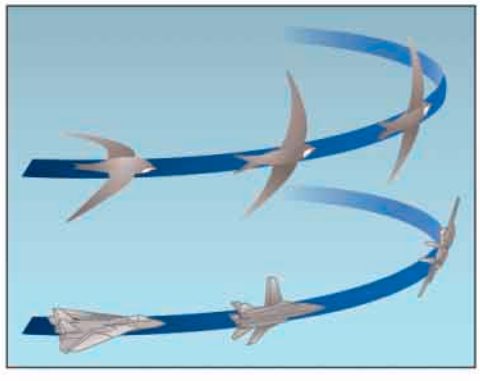

On the wing. Swifts are aerial hunters, catching flying insects on the wing. To outmaneuver their agile prey, swifts are able to fly fast and to make very tight turns. To maximize flight speed as well as maneuverability, evolution and aeronautic engineering converged on the same solution—variable wing sweep. Swifts (**top**) and the Tomcat jet fighter (**bottom**) keep their wings swept back to reach high flight speeds. To execute tight turns, both flyers reduce their wing sweep.

The achievements of aerospace engineers have inspired biologists to study the aerodynamics of flying animals. Engineers first discovered the extraordinary amount of lift that leading-edge vortices produce when they solved the problem of how to land supersonic fighter jets and passenger aircraft like the Concorde. Swept-back wings not

The authors are in the Department of Experimental Zoology, Wageningen University, the Netherlands. E-mail: ulrike.muller@wur.nl

only make supersonic flight possible, but also generate stable leading-edge vortices at high angles of attack. The resulting extra lift enables delta-wing aircraft to land safely despite their small wings, which are much smaller than those of conventional aircraft.

The swept wing of a swift generates a stable leading-edge vortex. Yet the exact role of this vortex in the swift's flight performance can only be inferred from observations of their flight. Swifts in flight turn on a dime while catching insects, a spectacular aerobatic display. Anybody observing swifts circling in a yard will notice that the birds hold their wings swept back during fast flight and swiftly change the wing sweep to execute tight turns (see the figure). Aerospace engineers converged on the same solution for their military aircraft, which have to perform optimally both during supersonic and subsonic flight (*8*). Pilots of fighter jets such as the F-14 Tomcat and the Tornado can choose between different wing sweeps for maximal dogfight and cruise performance (see the figure).

The gliding flight of storks inspired the first airplane designs of Otto Lilienthal in the late 19th century. The benevolent flight characteristics of these slow and stately gliders invested airplane pioneers with the confidence to take to the skies. Swifts are radically different gliders from storks: They are nimble and fast. These attributes require the ability not only to generate large aerodynamic forces from unsteady lift mechanisms, but also to exercise exquisite control over these forces. The next challenge for Videler and his team is to elucidate how swifts use their variable wing sweep to gain direct control over leading-edge vortices in order to increase their flight performance. In the future, the swift's flight control might inspire a new generation of engineers to develop morphing microrobotic vehicles that can fly with the agility, efficiency, and short take-off and landing capabilities of insects and birds.

References

1. C. P. Ellington *et al.*, *Nature* **384**, 626 (1996).
2. M. H. Dickinson *et al.*, *Science* **284**, 1954 (1999).
3. R. B. Srygley, A. L. R. Thomas, *Nature* **420**, 660 (2004).
4. F. O. Lehmann, *Naturwissenschaften* **91**, 101 (2004).
5. J. J. Videler *et al.*, *Science* **306**, 1960 (2004).
6. J. R. Usherwood, C. P. Ellington, *J. Exp. Biol.* **205**, 1547 (2002).
7. S. P. Sane, M. H. Dickinson, *J. Exp. Biol.* **204**, 2607 (2001).
8. E. C. Polhamus, T. A. Toll, *NASA TM* 83121 (1981).

10.1126/science.1107070

PHYSICS

Superconductivity in Thin Films

Tai-Chang Chiang

Since the 1960s (*1*), researchers have explored the possibility that the superconducting properties of thin films may be superior to, or at least different from, those of bulk materials. Guo *et al.* now demonstrate on page 1915 of this issue (*2*) that film thickness can indeed affect superconducting behavior. Their data show convincingly that the superconducting transition temperature (T_c) of thin lead films oscillates with film thickness.

As the thickness of a film is reduced to the nanometer scale, the film's surface and interface confine the motions of the electrons, leading to the formation of discrete electronic states known as quantum well states (*3*). This quantum size effect changes the overall electronic structure of the film. At small thicknesses, physical properties are thus expected to vary, often dramatically, with thickness.

Recent experimental studies have demonstrated such variations with film thickness for properties such as the electronic density of states, electron-phonon coupling, surface energy, and thermal stability (*4*–*8*). The variations are expected to follow a damped oscillatory curve that is superimposed on a $\pm N^{-\gamma}$ baseline (where N is the number of atomic layers in the film and the exponent γ is often close to 1).

The superconducting transition temperature for a metal such as lead depends on the density of states and on electron-phonon coupling. It should thus also vary with film thickness. Early work generally showed a reduction in T_c for small film thicknesses, in qualitative agreement with a $N^{-\gamma}$ dependence. However, in most cases, structural defects were probably the main reason for the reduction (*9*).

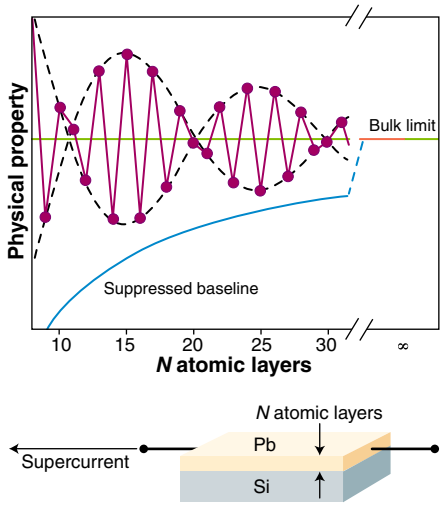

Quantum oscillations in thin films. (**Top**) Schematic variations in physical properties (including the superconducting transition temperature T_c) of lead films as a function of atomic layers (N) in the film, assuming a flat baseline (green). The dashed curves are envelope functions. Also shown is a different baseline (blue), suppressed at small film thicknesses, which corresponds qualitatively to the data reported in (*2*). (**Bottom**) Schematic drawing for an experiment that tests the superconducting properties of such films.

An oscillatory dependence of T_c on film thickness is a far more convincing proof for quantum size effects. Some prior studies suggested such oscillatory behavior (*7*, *8*), but the report by Guo *et al.* (*2*) is the first definitive and quantitative demonstration. Using atomically uniform films of lead with exactly known numbers of atomic layers deposited on a silicon (111) surface (see the figure), the authors observed oscillations in T_c that correlated well with the confined electronic structure. Their work has elevated this type of measurement to a new level of precision and sophistication.

Quantum oscillations can be understood by analogy to the systematic property variations of chemical elements. The number of confined electrons in a film increases as the film gets thicker. These electrons fill quantum well states, just as the electrons in atoms fill successive shells. However, in contrast to the spherical geometry of atoms, the films are planar. The properties therefore vary with film thickness. The period at which they do so is fixed for each system and equals one-half of the bulk Fermi wavelength (which is related to the average electron density and the crystal structure) (*4*).

For lead films on silicon (111) surfaces, the period of variation is 2.2 atomic layers. Because this is close to 2 atomic layers, physical properties (including T_c) should oscillate between films with even and odd numbers of layers. However, the slight difference between 2.2 and 2 layers leads to a beating effect (see the figure, where a flat baseline is assumed).

The atoms at each surface or interface of a film amount to $1/N$ of the total number of atoms in the film. These atoms are perturbed by the surface or interface much more than the rest of the film is. The effect

The author is in the Department of Physics and the Frederick Seitz Materials Research Laboratory, University of Illinois, Urbana, IL 61801, USA. E-mail: chiang@mrl.uiuc.edu

on the physical properties should therefore, on average, scale as ~1/N (*5*, *6*). The result is a baseline function, which can have a positive or negative sign depending on the specifics of the system.

For 20 to 30 atomic layers, the measured T_cs reported in (*2*) show even-odd oscillations within one lobe of the envelope function (see the figure). However, they are all lower than the bulk value. This reduction can be attributed to a suppressed baseline function with an approximately –1/N dependence, as schematically illustrated in the figure. Under suitable conditions (for example when a different substrate material is used), the baseline function could correspond to a +1/N dependence instead, resulting in an increase in T_c at small N.

Achieving a higher T_c in thin films than in the bulk will require a thorough understanding of the underlying physics. For lead on silicon, detailed measurements are needed to quantitatively link the observed T_c variations to fundamental quantities, such as the density of states and electron-phonon coupling. The superconducting gap should also be measured for each quantum well state; this gap enables zero electrical resistance and can vary between different quantum well states in the same film. These data are important for testing and refining theories of superconductivity in thin films.

Quantum oscillations such as those reported by Guo *et al*. (*2*) may lead to improved properties at selected film thicknesses, but baseline variations can also play a useful role, especially if they improve film properties. For example, silver films prepared on certain substrates exhibit enhanced electron-phonon coupling (*5*, *6*), implying the possibility of a higher T_c at small film thickness. It would be remarkable if materials that are not superconducting in the bulk—such as silver—could be changed into superconductors by quantum engineering (*10*). As the search for better superconducting materials continues, quantum size effects are an important avenue toward this goal.

References and Notes

1. J. M. Blatt, C. J. Thompson, *Phys. Rev. Lett.* **10**, 332 (1963).
2. Y. Guo *et al.*, *Science* **306**, 1915 (2004).
3. T.-C. Chiang, *Surf. Sci. Rep.* **39**, 181 (2000).
4. C. M. Wei, M. Y. Chou, *Phys. Rev. B* **66**, 233408 (2002).
5. T. Valla *et al.*, *J. Phys. Condens. Matter* **12**, L477 (2000).
6. D.-A. Luh, T. Miller, J. J. Paggel, T.-C. Chiang, *Phys. Rev. Lett.* **88**, 256802 (2002).
7. O. Pfennigstorf, A. Petkova, H. L. Guenter, M. Henzler, *Phys. Rev. B* **65**, 045412 (2002).
8. B. G. Orr, H. M. Jaeger, A. M. Goldman, *Phys. Rev. Lett.* **53**, 2046 (1984).
9. A. M. Goldman, N. Marković, *Phys. Today* **51**, 39 (November 1998).
10. Superconductivity has been reported in silver films on germanium (*11*), but the sample surface in that study may have been oxidized as a result of air exposure, and the results have not been reproduced.
11. M. J. Burns *et al.*, *Solid State Commun.* **51**, 865 (1984).

10.1126/science.1106675

NEUROSCIENCE

Addiction as Compulsive Reward Prediction

Serge H. Ahmed

Drug addicts are often portrayed as irrational persons who fail to maximize future rewards. Despite heavy costs, they seem to prefer to engage in drug-seeking behavior over more rewarding courses of action. But are addicts really irrational? To prove that addiction is an irrational behavior, one needs to show that addicts would be better off if they had been prevented from taking drugs in the first place—a difficult study to conduct. Research programs that look at the welfare of addicts versus nonaddicts are not sufficiently informative because they presuppose that addicts are average individuals before becoming addicted to drugs. Fortunately, in the absence of relevant facts, researchers can still resort to theory and computer simulation to tackle the problem.

Over the past 30 years, economists have developed a sophisticated theory of addiction that complies with the rationality principle of classical economics. In this counterintuitive theory, addicts are presented as efficient decision-makers who try to maximize future rewards by using drugs as self-medication (*1*–*3*). On page 1944 of this issue, Redish (*4*) presents a neurobiological computational model of cocaine choice that challenges the rational theory of addiction. In this model, cocaine is a disease agent that corrupts optimal decision-making by hijacking the brain circuitry responsible for learning about rewards.

Redish's model is an abstract variant of temporal-difference reward learning models that have been used to elucidate the function of the neurotransmitter dopamine in the brain (*5*, *6*). In this class of learning models, transient changes in the output of midbrain dopamine cells are hypothesized to signal to the forebrain discrepancies or errors between prediction of reward and occurrence of reward—and not, as originally thought, the hedonic experience of reward consumption itself. Schultz (*7*) has shown in monkeys that midbrain dopamine cells respond to reward as if they were effectively coding a reward-prediction error: Dopamine neurons fire in response to a surprising reward, such as fruit juice (error > 0), but stop responding to the same reward after learning to anticipate the juice (error = 0). During the progression of learning, the dopamine error signal is driven to zero and is shifted backward to cues or actions that precede and predict reward consumption. This graded correction of reward-prediction error has two main functions: (i) It allows the subject to ignore redundant reward predictors in the environment, a process critical to keeping memory unsaturated; and (ii) it permits the maximization of future rewards by attributing more weight or value to those future actions that will pay the most (*8*, *9*). The latter evaluation is at the heart of Redish's computational model of addiction.

In a normal situation involving a choice, say, between a slice of pizza and a hamburger, the subject learns through prediction error-correction to assign the greatest value to the action that leads to the more rewarding food, here the pizza (see the figure, top left panel). In other words, the subject learns to match the value of alternative actions with their real utility. At a neurobiological level, this differential evaluation process would correspond to a differential activation of dopamine neurons during contemplation of alternative actions, which biases the probability of selection in favor of the action with the best outcome (see the figure, top right panel). This stochastic theory of behavioral choice predicts that the subject will allocate behavior to the two actions according to their respective utility rather than exclusively foraging for the preferred food, a prediction consistent with the facts (*10*, *11*).

With dazzling insight, Redish realized that this balanced evaluation should fail in situations involving a choice between cocaine and an alternative nondrug reward, even though the latter produces more satisfaction than the available dose of cocaine. Indeed, unlike ordinary rewards, cocaine directly boosts dopamine activity regardless of whether cocaine use is anticipated or not by the subject. Cocaine generates a false, fixed reward-prediction error that cannot be corrected during learning. As a result, the value assigned to future cocaine use increases

The author is at CNRS UMR 5541, Université Victor-Segalen Bordeaux 2, Bordeaux, France. E-mail: sahmed@lnpb.u-bordeaux2.fr

without being bound to an amount that no longer matches the real utility of the drug. This unbounded evaluation makes cocaine choice more likely in the future, despite the increase in cost and a more rewarding alternative (see the figure, middle panels). Thus, the long-term effect of cocaine use is a decrease in total future reward, an outcome that represents a genuine violation of rationality.

Redish's model represents a significant advance in the dopamine theory of cocaine addiction. The model explains irrational drug choice as a failure of dopamine neurons to correctly predict variations in drug reward. Consequently, the model generates several unique predictions including an inability to ignore redundant predictors of drug reward (a phenomenon that may explain an addict's obsession with cocaine as well as anomalous observations in stimulant conditioning) (*12*). Nevertheless, as with other dopamine hypotheses of cocaine addiction (*13*–*15*), the computational model of Redish rests on the strong postulate that addiction results from a dopamine-dependent alteration in the attribution of value to reward-seeking actions without changes in the hedonic experience of rewards per se—which is presumed to be independent of dopamine. Thus, cocaine addicts would experience the same level of pleasure from a unit of either drug or alternative reward prior to becoming addicted. We do not have to accept this "hedonic constancy" postulate, however. In fact, there is now evidence that hedonic processing is compromised in both cocaine-addicted animals and humans (*16*–*20*). This hedonic deficit eventually may lead to a devaluation of alternative nondrug rewards, which biases action selection in favor of drug-seeking behavior (see the figure, bottom panels) (*20*). Heyman has shown using Herrnstein's theory of choice (*10*) that devaluing alternative rewards can indeed suffice to precipitate progression toward excessive drug choice (*11*). From this perspective, drug use acquires more value with repeated experience, not because of abnormal dopamine-dependent value learning as argued by Redish (*4*) and others (*13*–*15*), but because of a blunted hedonic reaction to alternative rewards. Addicts thus would behave rationally by preferring cocaine over decreased alternative rewards, a conclusion opposite to that reached by the Redish model. This discussion shows that the same pattern of drug choice can be interpreted differently depending on whether one postulates hedonic stability or not. Thus, a significant challenge for future computational research in addiction will be to better analyze how changes in value attribution and in hedonic processing interact to precipitate the transition to addiction. In this context, the Redish model of addiction may serve as a seed to crystallize future research in this direction.

In the long-run, the value of the Redish model will depend on its ability to cope with two important challenges. The Redish model must take into account (i) addictions to ordinary rewards, such as fatty foods, which, unlike cocaine, produce a dopamine signal that can be accomodated, and (ii) addictions to nonstimulant substances, such as alcohol and opiates, the self-administration of which is not critically dependent on mesolimbic dopamine. Another significant challenge for the model concerns the role of impulsivity in addiction. Impulsivity defines the preference for immediate, smaller gratifications over delayed, larger ones and is thought to result from hyperbolic discounting of future rewards (*21*). Although Redish's computational model predicts hyperbolic discounting, it considers impulsivity neither as a cause nor as an effect of addiction. This contrasts with previous theories and with recent data showing that addicts discount the future more heavily than nonaddicted individuals (*22*). Finally, the model will have to cope with the general challenge of explaining not only why individuals get hooked on drugs but also why they eventually desire to become sober, sometimes eagerly. The flip-flop conflict between the tendency to take drugs and the tendency to abstain suggests that the evaluation of future drug use is not as consistent over time as suggested by Redish's work. The next generation of models inspired by Redish's computation will have to consider this motivational conflict if they are to provide a more realistic picture of addiction.

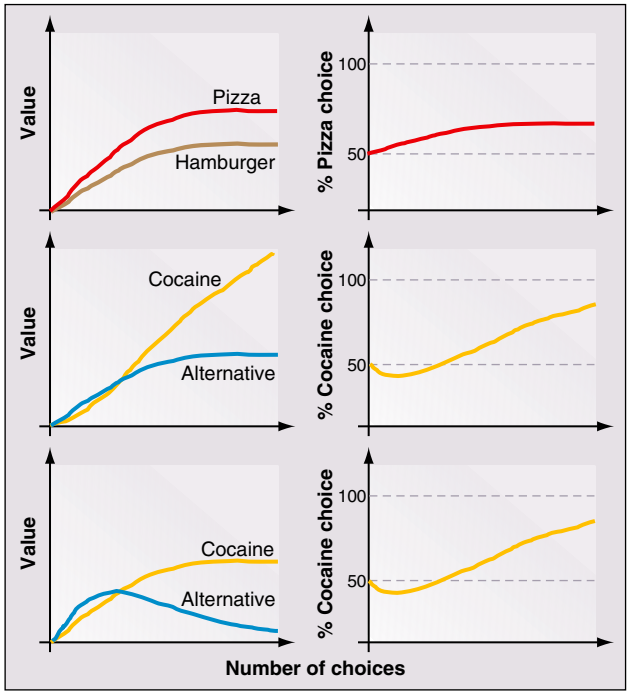

The dynamics of drug choice. (Left) Value learning during successive choices and (right) the percent choice of food or drug reward (50% represents the indifference level). (**Top**) Choice between two ordinary foods. During learning, the subject assigns progressively more value to the pizza—the consumption of which induces the greatest satisfaction—than to the hamburger, until a maximum, stable value is assigned to each option. This bounded, differential evaluation is reflected by the development of a nonexclusive preference for pizza consumption over hamburger consumption. (**Middle**) Choice between cocaine and a more rewarding, nondrug alternative, as extrapolated from Redish's computational model of addiction (*4*). During learning, the subject is hypothesized to initially assign greater value to the more rewarding alternative, which explains why the alternative is initially more likely to be chosen. However, due to an inability to correct the reward-error signal induced by cocaine, the value attributed to future cocaine use continues to increase above the maximum value assigned to the alternative. As a result, cocaine becomes the preferred choice. (**Bottom**) Choice between cocaine and a more rewarding nondrug alternative, as predicted by hedonic dysregulation hypotheses of addiction. As in (the middle panel), the subject begins to attribute more value to the alternative than to cocaine. However, with repeated drug use, the value of the alternative gradually decreases below the value of future cocaine use, thereby explaining the transition to excessive cocaine choice. In this last model, the value assigned to cocaine is finite.

References

1. G. J. Stigler, G. S. Becker, *Am. Econ. Rev.* **67**, 78 (1977).
2. G. S. Becker, K. M. Murphy, *J. Polit. Econ.* **96**, 675 (1988).
3. J. F. Bridges, *Eur. Addict. Res.* **7**, 78 (2001).
4. A. D. Redish, *Science* **306**, 1944 (2004).
5. P. R. Montague *et al.*, *J. Neurosci.* **16**, 1936 (1996).
6. W. Schultz *et al.*, *Science* **275**, 1593 (1997).
7. W. Schultz, *J. Neurophysiol.* **80**, 1 (1998).
8. D. M. Egelman *et al.*, *J. Cogn. Neurosci.* **10**, 623, (1998).
9. S. M. McClure *et al.*, *Trends Neurosci.* **26**, 423 (2003).
10. R. J. Herrnstein, D. Prelec, *J. Econ. Perspect.* **5**, 137 (1991).
11. G. M. Heyman, *Behav. Brain Sci.* **19**, 561 (1996).
12. S. H. Ahmed *et al.*, *Behav. Neurosci.* **112**, 1167 (1998).
13. T. E. Robinson, K. C. Berridge, *Brain Res. Rev.* **18**, 247 (1993).
14. G. Di Chiara, *Eur. J. Pharmacol.* **375**, 13 (1999).
15. J. D. Berke, S. E. Hyman, *Neuron* **25**, 515 (2000).
16. G. F. Koob, M. Le Moal, *Science* **278**, 52 (1997).
17. N. D. Volkow *et al.*, *Mol. Psychiat.* **9**, 557 (2004).
18. H. Garavan *et al.*, *Am. J. Psychiat.* **157**, 1789 (2000).
19. S. H. Ahmed, G. F. Koob, *Science* **282**, 298 (1998).
20. S. H. Ahmed *et al.*, *Nature Neurosci.* **5**, 625 (2002).
21. G. Ainslie, *Psychol. Bull.* **82**, 463 (1975).
22. W. K. Bickel, L. A. Marsch, *Addiction* **96**, 73 (2001).

10.1126/science.1107071

The Mentality of Crows: Convergent Evolution of Intelligence in Corvids and Apes

Nathan J. Emery[1]* and Nicola S. Clayton[2]

Discussions of the evolution of intelligence have focused on monkeys and apes because of their close evolutionary relationship to humans. Other large-brained social animals, such as corvids, also understand their physical and social worlds. Here we review recent studies of tool manufacture, mental time travel, and social cognition in corvids, and suggest that complex cognition depends on a "tool kit" consisting of causal reasoning, flexibility, imagination, and prospection. Because corvids and apes share these cognitive tools, we argue that complex cognitive abilities evolved multiple times in distantly related species with vastly different brain structures in order to solve similar socioecological problems.

In Aesop's fable, a thirsty crow spied a pitcher containing a small amount of water. Unfortunately, the water was out of reach of the crow's bill, but next to the pitcher was a pile of stones. The crow began placing the stones in the pitcher, thereby raising the water until it could drink. Did the crow understand that its actions would increase the water level?

Throughout folklore, the corvids (crows, jays, ravens, and jackdaws) (Fig. 1) have been credited with intelligence. Recent experiments investigating the cognitive abilities of corvids have begun to reveal that this reputation has a factual basis. These studies have found that some corvids are not only superior in intelligence to birds of other avian species (perhaps with the exception of some parrots), but also rival many nonhuman primates. Traditionally, studies of complex cognition have focused on monkeys and apes (*1*). However, there is no reason to assume that complex cognition is restricted only to the primates (*2*). Indeed, the social intelligence hypothesis (*3*) states that intelligence evolved not to solve physical problems, but to process and use social information, such as who is allied with whom and who is related to whom, and to use this information for deception (*4*). There is evidence that some other large-brained social animals, such as cetaceans, demonstrate similar levels of intelligence as primates (*5*). Corvids also appear to meet many of the criteria for the use of social knowledge in their interactions with conspecifics (*6*).

[1]Sub-Department of Animal Behaviour, University of Cambridge, CB3 8AA, UK. [2]Department of Experimental Psychology, University of Cambridge, CB2 3EB, UK.

*To whom correspondence should be addressed. E-mail: nje23@cam.ac.uk

Do Corvids Have the Brains for Complex Cognition?

The crow has a brain significantly larger than would be predicted for its body size (*7*), and it is relatively the same size as the chimpanzee brain. The relative size of the forebrain in corvids is significantly larger than in other birds (with the exception of some parrots) (*2*), particularly those areas thought to be analogous to the mammalian prefrontal cortex: the nidopallium and mesopallium (Fig. 2B) (*8*, *9*). This enlargement of the "avian prefrontal cortex" may reflect an increase in primate-like intelligence in corvids (*10*, *11*).

An Overview of Corvid Cognitive Psychology

To fully appreciate how corvid and ape psychology are similar, it is important to describe how corvids may represent their physical and social worlds, and how these forms of mental representation may be similar or dissimilar to those used by apes in solving similar problems. We use the term "understanding" to convey the idea that corvids and apes reason about a domain (physical or social) in a way that transcends basic associative and reinforcement processes.

Tool use and manufacture. Tool use is defined as "the use of an external object as a functional extension of mouth, beak, hand, or claw, in the attainment of an immediate goal" (*12*). Although many birds, primates, and other animals use tools, it is not clear whether any of these species appreciate how tools work and the forces underlying their function. Perhaps the most convincing candidates are New Caledonian crows, who display extraordinary skills in making and using tools to acquire otherwise unobtainable foods. In the wild, they make two types of tools. Hook tools are crafted from twigs by trimming and sculpting until a functional hook has been fashioned (*13*) and are used to poke out insect larvae from holes in trees using slow deliberate movements (*14*).

The crows also manufacture stepped-cut *Pandanus* leaves (*14*), which are used to probe for prey under leaf detritus, using a series of rapid back-and-forth movements or slow deliberate movements that spear the prey onto the sharpened end or the barbs of the leaf, if the prey is located in a hole. These tools are consistently made to a standardized pattern and are carried around on foraging expeditions (*15*). The manufacture of stepped tools appears to be lateralized at the population level (*16*) and tool use at the individual level (*17*, *18*).

Observations of the crows' tool use in the wild suggest complex cognition. For example, there is potential cumulative evolution in the complexity of stepped tools (increasing the number of steps required to make a more complex tool), which are analogous to minor technological innovations in humans (*19*). There are also population differences in the types of tools manufactured (*19*), seemingly independent of ecological variability, which has been suggested as a form of culture in chimpanzees (*20*).

Laboratory experiments have confirmed the sophisticated cognitive abilities of these crows. One of them, Betty, appears to be capable of reasoning by analogy with her previous experience with hooks, by modifying nonfunctional novel material (metal wire) into hook-like shapes to retrieve food in a bucket inside a vertical tube (*21*). Furthermore, she chooses the correct length or diameter of tool out of a "tool box" containing tools of different lengths and widths to reach normally inaccessible food (*22*, *23*).

Traveling mentally in time and space. Many corvids cache food for future consumption; either a large amount of seeds cached over a wide area, which are stored seasonally, or a smaller amount of higher-quality, perishable material, which is recovered hours or days later. These differences may require different cognitive abilities for successful retrieval. Clark's nutcrackers living at high elevations cache up to 30,000 pine seeds over a wide area and can recover them up to

6 months later (*24*). By contrast, western scrub jays living in more temperate environments cache fewer of a wider variety of food items that differ in their level of perishability and are recovered after much shorter periods (*25*).

Cache recovery may require more than simply remembering where their caches are hidden, for species that cache many types of food. These species may need to process information about the location of the cache site, the type and perishability of the cached item, and the social context of caching (*26*). When caching perishable food, it is prudent to learn something about the decay rates of the food, and if two or more perishable foods are cached, to learn their relative decay rates, in order to recover food when it is still fresh and edible. Laboratory studies have capitalized on the fact that western scrub jays readily cache perishable foods but will not consume these items when they have degraded.

When jays were allowed to cache perishable and nonperishable foods, they were able to remember not only which foods they cached where, but also how long ago they had cached them. If a short time had elapsed between caching and recovery, then they recovered the perishable food. But if they had cached a long time ago, they did not attempt to recover the rotten degraded food and selectively searched for the nonperishable caches (*27*, *28*). Furthermore, they could recall when they cached different foods in the same location and could even distinguish between two caches of the same food type that had been cached at different times (*29*). These results suggest that scrub jays remember the "what, where, and when" of specific caching events (episodic-like memory). This representation of the time since caching is essential for the efficient recovery of perishable food items (*25*, *26*).

Social cognition of cache protection and pilfering. Food storers should also be sensitive to the social context of caching, because caches are susceptible to pilfering (*30*). For pilferers, the ability to quickly and efficiently locate caches made by others may be the difference between successful pilfering and attack by the storer. A number of corvids observe conspecifics caching and demonstrate excellent observational spatial memory for the location of another bird's caches (*25*, *31*, *32*).

The use of observational spatial memory as a pilfering strategy may differ between species depending on level of sociality, and as such may be an adaptive specialization (*33*). Do social pinyon and Mexican jays, and territorial Clark's nutcrackers, remember where another bird has cached (*31*, *34*)? Pinyon jays remembered the specific location of others' caches after 1 and 2 days, as did Mexican jays, whereas Clark's nutcrackers were only as accurate as chance after 1 day. After 2 days, the Clark's nutcrackers were only accurate at recovering their own caches, not those they had observed. (*34*). This finding supports the adaptive specialization of the social learning hypothesis in corvids; however, another study is more ambiguous (*35*). Furthermore, western scrub jays are semiterritorial, and they have highly accurate observational spatial memories (*25*).

The social context of caching may be viewed as an arms race between storers and pilferers, in which storers use counterstrategies to minimize the risk of having their caches pilfered (*36*). However, individual birds can play both roles. Storers engage in a number of cache protection strategies, which may or may not be dependent on cognitive processes. Examples of such strategies include hiding food behind barriers so that pilferers cannot see them (*37*, *38*), waiting until pilferers are distracted before resuming caching (*32*, *39*), leading competitors away from the location of caches (*40*), or making false caches that contain either an inedible item, such as a stone, or nothing at all (*41*). Some corvids return alone to caches they had hidden in the presence of conspecifics and readily recache them in new places unknown to the potential thief (*41*, *42*).

One strategy that may decrease the probability that a pilferer will successfully

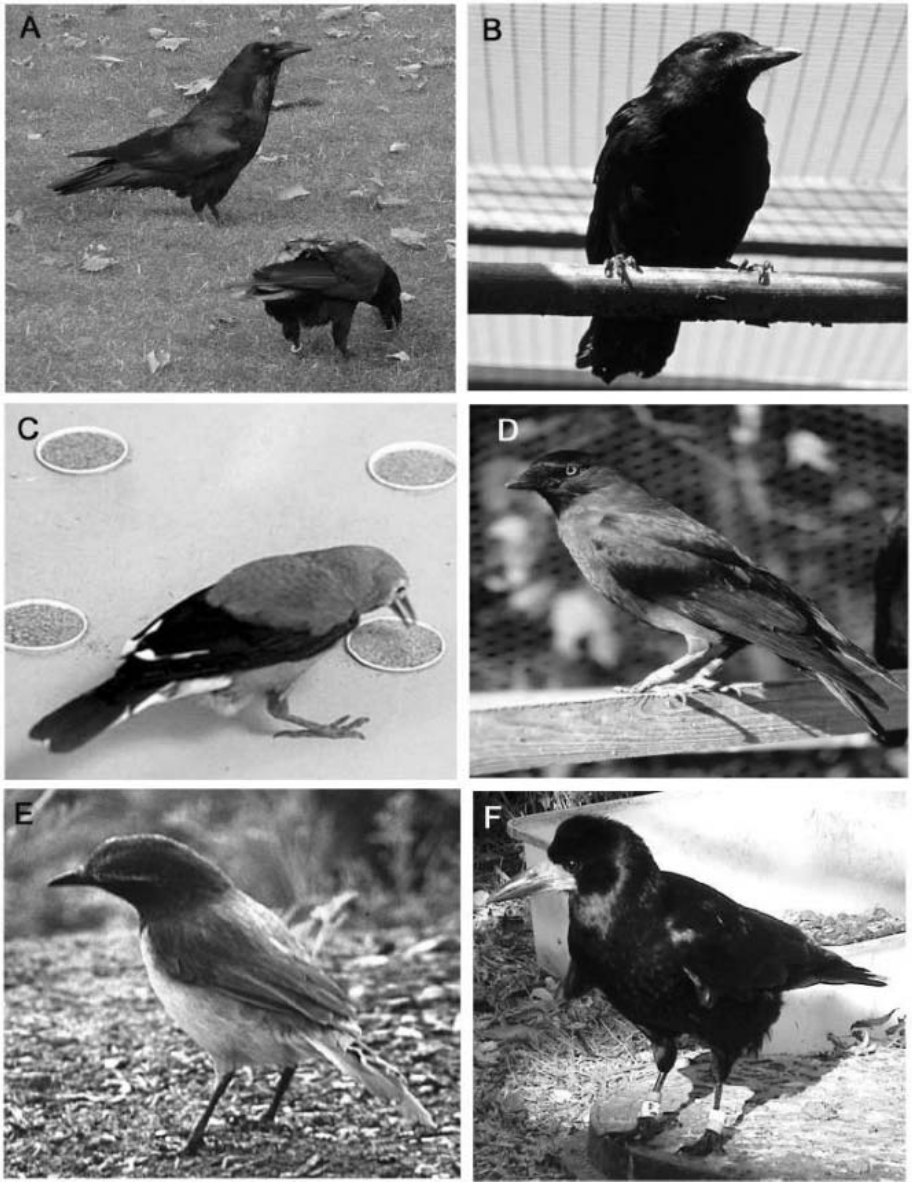

Fig. 1. Photographs of representatives of the crow-like Corvidae (ravens, crows, rooks, jackdaws, magpies, and jays) family of passerine birds. There are approximately 120 species of corvids, dispersed all over the world except in the polar regions. (**A**) Raven. [Photograph by N. Emery] (**B**) New Caledonian crow. [Photograph by A. Weir and A. Kacelnik] (**C**) Clark's nutcracker. [Photograph by R. Balda] (**D**) Jackdaw. [Photograph by A. von Bayern] (**E**) Western scrub jay. [Photograph by S. de Kort] (**F**) Rook. [Photograph by A. Seed]

steal another's caches is to eliminate or reduce the information available to the pilferer at the time of caching, such as caching behind a barrier (*37*). Of course, this behavior could be explained as ''out of sight, out of mind'' (that is, cache when you no longer see others present), as opposed to understanding what another can or cannot see. There is some evidence, however, that when given a choice of two cache sites that an observer can see, storers prefer to cache in the sites least visible to the observer, such as in a darkened part of a cage as compared to an illuminated part (*43*).

An experimental approach is crucial for understanding the processes underlying these behaviors and determining the effects of experience, particularly in relation to theory of mind. Consider the observation of birds moving food they had hidden in the presence of other individuals and recaching the items in new places when those observers were no longer present. In the wild, one might explain the presence or absence of another bird as being purely coincidental to the caching and recaching events. To test this, hand-raised western scrub jays were allowed to cache either in private or while a conspecific was watching and then recover their caches in private (*42*). Individuals with prior experience of pilfering another bird's caches subsequently recached food in new sites, but only when they had been observed during caching. Because the two conditions were identical at the time of recovery, the birds had to remember whether or not they had been watched during caching, and if so, whether to recache during recovery and whether in new or old sites. Note that jays without experience of themselves being pilferers did not move their caches to new sites. The inference is that these birds, who had been thieves in the past, engage in experience projection (*2*); that is, they relate information about their previous experience as a pilferer to the possibility of future stealing by another individual, and modify their recovery strategy appropriately. By focusing on the counterstrategies of the storer when previously observed by a potential thief, this experiment raises the possibility that recaching behavior is based on simulation of another's viewpoint (one form of mental attribution) (*2*).

A Cognitive Tool Kit for Corvids and Apes?

Our review of corvid cognition suggests that these birds display similar intelligent behavior as the great apes. However, is the content of the cognitive processes based on a similar or different mental foundation? One reason why the processes may be similar is that corvids and apes face many of the same socioecological challenges, such as locating perishable food distributed in time and space or understanding the relationships between different individuals within large social groups. We suggest that these environmental problems are solved by using four cognitive tools that have driven the evolution of complex cognition in corvids and apes: causal reasoning, flexibility, imagination, and prospection (Fig. 3).

Causal reasoning. Some of the examples of tool use and manipulation described earlier suggest that some corvids, like apes, may understand the causal relationships by which these tools operate or are effective. In the absence of detailed knowledge about the acquisition of tool use in the wild, the role of basic instrumental conditioning processes remains unclear (*44*). However, what may suggest that corvid tool use transcends such noncognitive processes is Betty's innovative tool manufacture in the lab (*21*). The fact that she transformed a novel piece of wire into a hook-like tool suggests some appreciation of mechanical causation.

Although an understanding of physical causation suffices for interactions with inanimate objects, transactions within the social realm also require representations of mental causation. Do animals also realize that mental states (beliefs, desires, and intentions) can be causally effective? This question is best studied in the sphere of social cognition by investigating whether an animal can represent the behavior of conspecifics (or heterospecifics) as caused by their intentions, beliefs, and desires; in other words, can represent that these animate beings are intentional agents. Animate beings are distinct from inanimate objects: Although they can be acted on by external forces, they also have mental states. This is an essential precursor for predicting a conspecific's or heterospecific's behavior and manipulating another for personal benefit (tactical deception). Although still controversial, corvids and apes appear to demonstrate a similar propensity for representing animate beings as causal agents (*6*, *45*, *46*).

Flexibility. The ability to act on information flexibly is one of the cornerstones of intelligent behavior. Deployment of flexible learning strategies may form the basis for creativity as demonstrated in social and object play (*47*) and innovation (*48*). Here we focus on experimental evidence. In the food perishability experiments described earlier, scrub jays integrated information about the what, where, and when of a trial-unique caching event to influence their cache recovery decisions (*29*). However, for a bird that caches perishable food items in fluctuating temperatures (ranging from cold to extreme heat), it is critical that the bird be able to update its knowledge about decay rates and apply this knowledge to information already encoded. To investigate this, scrub jays were allowed to cache preferred, perishable crickets and less preferred, nonperishable peanuts (*49*). After caching, but before recovery, the jays gained new information that the crickets decayed more quickly than they had expected when they had cached them. When tested, the scrub jays used this new information and switched to recovering the peanuts rather than the now-inedible crickets.

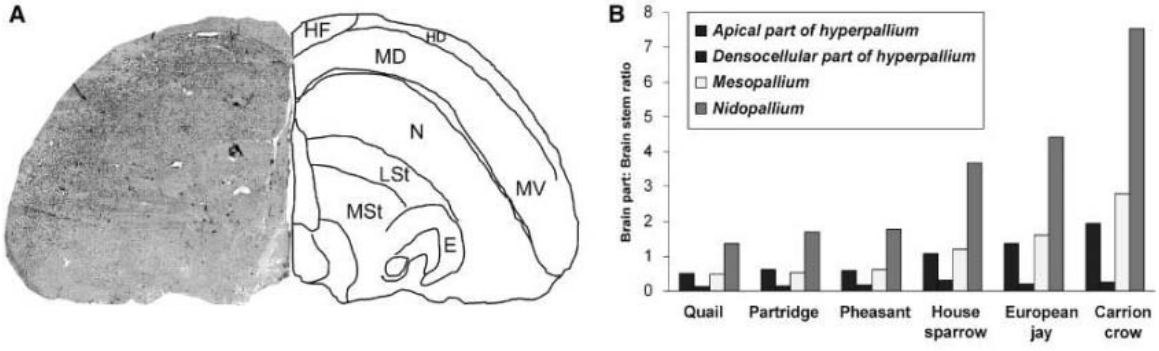

Fig. 2. (**A**) (Left) A low-power photograph of a coronal section through a rook telencephalon, stained with a Nissl stain. (Right) A line drawing of the corresponding half of the same section showing the location of the major parts of the telencephalon. HF, hippocampal formation; HD, densocellular part of the hyperpallium; MD, dorsal mesopallium; MV, ventral mesopallium; N, nidopallium; MSt, medial striatum; LSt, lateral striatum; E, entopallium. Abbreviations are from (*8*). (The brain section was kindly provided by S. Healy and J. Krebs.) (**B**) Graph displaying how the relative size of the apical part of the hyperpallium, densocellular part of the hyperpallium, mesopallium, and nidopallium are relatively larger in passerines and particularly in the corvids (Eurasian jay and carrion crow) than in quail, partridge, and pheasant. Brain data are from (*9*).

One important aspect underlying all flexible behavior is the ability to generalize learned rules in order to apply them to novel stimuli or situations. This ability to solve transfer problems by abstracting general rules is what distinguishes rule learners from rote learners. When presented with a series of different discriminations to learn, corvids (blue jays, rooks, jackdaws, and Eurasian jays), like monkeys and apes, extract the general rule, such as win-stay, lose-shift rather than having to learn each new discrimination afresh. By contrast, pigeons appeared to be rote learners, solving the task eventually by learning each discrimination individually (*50*, *51*).

Corvids also demonstrate superior abilities in other transfer problems. One case is the ability of some corvids (pinyon jays and western scrub jays) to solve transitive inference problems (A > B > C > D), in which the birds are trained on an ordered set of various pairwise comparisons (such as A+ B–, B+ C–, etc.). When tested, they must transfer information about the dyadic relationships to novel pairs (such as B versus D) to solve the task. Pinyon jays outperform scrub jays on some aspects of this task (although their learning curves are similar), which has been attributed to differences in sociality (*52*). Indeed, pinyon jays appear to use transitive inference to rank unknown individuals in a dominance hierarchy and use this information in their subsequent social interactions (*53*). Finally, corvids are proficient in transferring to novel stimuli in matching and oddity discriminations. Rooks, jays, and jackdaws outperform pigeons on these problems (*51*). What is common to these various transfer tasks—from learning sets to transitive inference—is the ability to abstract general rules or relationships that transcend the basic learning experience. Abstraction might be an important process underlying this flexibility.

Imagination. Imagination refers to the process by which scenarios and situations that are not currently available to perception are formed in the mind's eye. One advantage of imagination is that possible situations can be practiced internally (simulated) before they are actually performed, which may be important when encountering novel stimuli within a familiar context. The ability to form representations of objects that are outside of perception (object permanence) may be a precursor of imagination. In food-caching corvids, object permanence is essential for the successful recovery of cached food; in young magpies, it develops around the same time as caching (*54*).

Insight, cognitive maps, and experience projection are three candidates that indicate the use of imagination. In a classic study of insight, a group of chimpanzees was presented with a problem (a banana hanging on string out of their reach), some sticks, and a series of boxes (*55*), which they appeared to spontaneously use to reach the banana. The implication has been that the chimpanzees imagined the solution to the problem before performing it, although this explanation has been disregarded as trial-and-error learning (*44*). Recent experiments in ravens may provide clearer evidence. Hand-raised ravens encountered a novel problem (meat attached to string hanging from a perch) (*56*). The only successful method was to pull the string up, place the foot on the

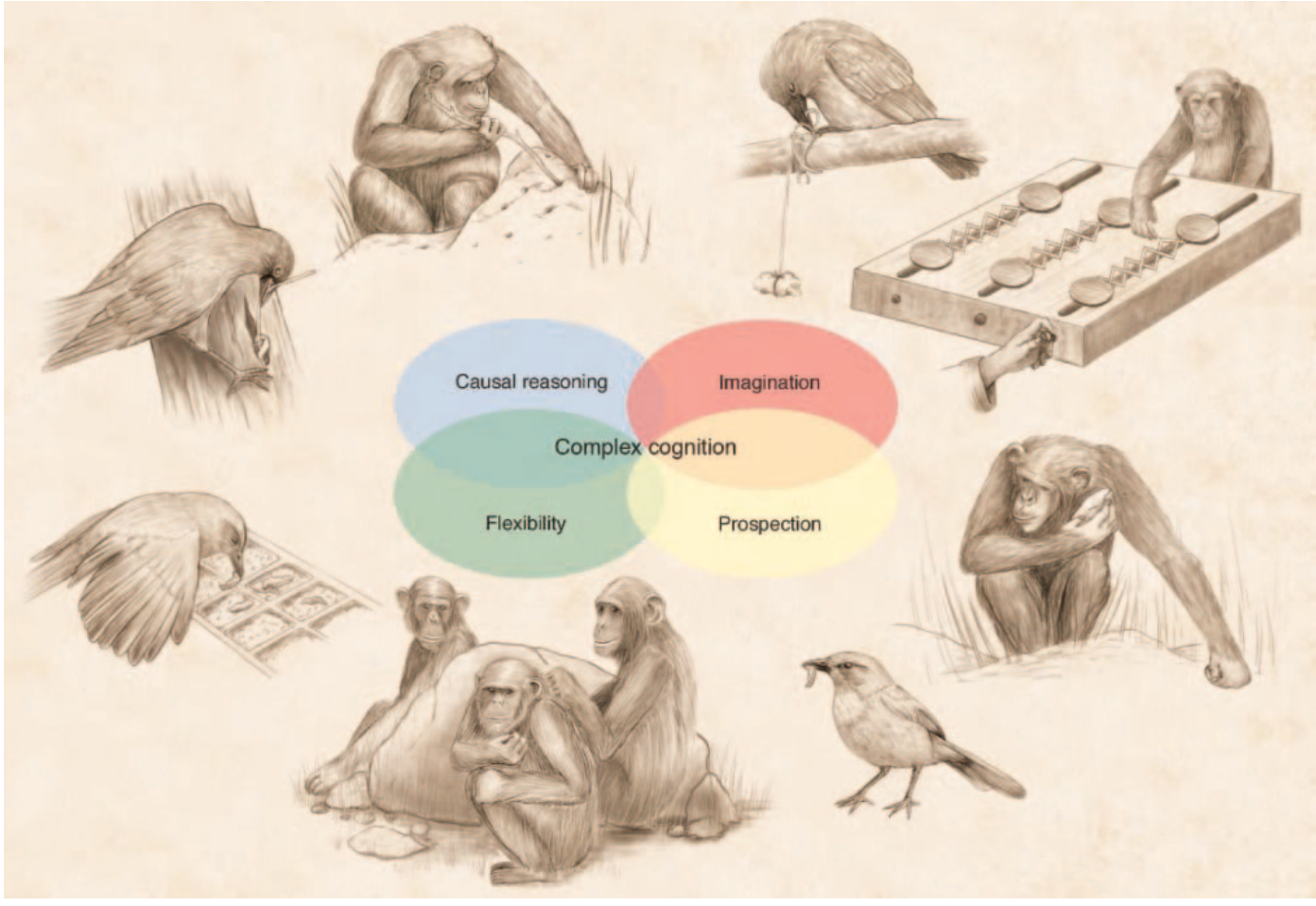

Fig. 3. Illustration of the four nonverbal cognitive tools displayed by corvids and apes, which are proposed as the basis for complex cognition: causal reasoning (New Caledonian crow and chimpanzee tool use), imagination (insight in ravens and role taking in chimpanzees), flexibility (western scrub jays' flexible memory for degraded and fresh food items and tactical deception in apes), and prospection (western scrub jays recaching food and chimpanzees carrying stone tools). These cognitive tools interact in different ways to produce complex cognition. [Drawing by C. Cain]

string after each pull up, and repeat this multiple times until the food was in reach, a solution some ravens reached on the first trial (that is, without recourse to trial-and-error learning). Furthermore, the ravens chose the correct string from a number of alternatives, choosing the string attached to the food, as opposed to a similarly sized stone. They did not fly off with the attached food, nor did they attempt to pull up items that were too heavy.

A second candidate for imagination is the use of a cognitive map (a mental representation of the major landmarks in the environment) to aid in navigation, particularly when novel routes are required. Although the issue of whether animals possess cognitive maps remains controversial (*57*), the enhanced spatial memory of the food-caching corvids might be a prime candidate for indicating their existence. It has been suggested that Clark's nutcrackers may use something akin to a cognitive map to locate a hidden goal object, even when the position of the fixed distal landmarks changed with respect to the local landmarks and the goal (*58*).

A final candidate for imagination is experience projection or role taking, in which an individual simulates another's experiences and perspective (*2*). This ability implies that an observer forms a representation of a model's perspective or experiences that are similar to or different from their own. In a cooperative task to investigate role taking, chimpanzees, but not rhesus monkeys, reversed the roles they were trained on (*59*, *60*), suggesting that the chimpanzees may have taken their partner's perspective; however, both monkeys and chimpanzees failed to immediately transfer to the opposite role on the first trial (*61*).

The example of recaching demonstrated by western scrub jays may present a case for imagination, because the jays needed to have remembered the relevant previous social context, used their own experience of having been a thief to predict the behavior of a pilferer, and determined the safest course of action to protect the caches from pilferage (*42*).

Prospection. In the previous discussion of imagination, an agent could simulate scenarios with respect to past events; however, one function of simulation may be to imagine possible future events, so-called prospection. Although various behaviors have been proposed as examples of future thinking, it is important to distinguish between those behaviors that are tuned to current thinking and motivational states and those that are tuned to future thinking and motivational states (*62*, *63*). Caching would appear to provide a natural example of future planning. Food is hidden in the present to provide sustenance for the future. However, if caching is controled by hunger, then this current motivational state may facilitate caching without any appreciation of becoming hungry in the future (*63*).

The example of recaching by scrub jays may also provide the best evidence for prospection (*42*). Recaching items in new sites when an observer saw the placement of caches, but not when the caches were made in private, suggests that the jays were using a strategy to protect their caches from future cache pilfering, not because of hunger levels. It is important to stress that prospection is highly reliant on retrospection (*63*).

Conclusions

There are many aspects of corvid and ape cognition that appear to use the same cognitive tool kit: causal reasoning, flexibility, imagination, and prospection. We suggest that nonverbal complex cognition may be constructed through a combination of these tools. Although corvids and apes may share these cognitive tools, this convergent evolution of cognition has not been built on a convergent evolution of brains. Although the ape neocortex and corvid nidopallium are both significantly enlarged, their structures are very different, with the ape neocortex having a laminar arrangement and the avian pallium having a nuclear arrangement (*2*). It is unclear what implications these structural differences have. However, cognition in corvids and apes must have evolved through a process of divergent brain evolution with convergent mental evolution. This conclusion has important implications for understanding the evolution of intelligence, given that it can evolve in the absence of a prefrontal cortex.

References and Notes

1. M. Tomasello, J. Call, *Primate Cognition* (Oxford Univ. Press, New York, 1997).
2. N. J. Emery, N. S. Clayton, in *Comparative Vertebrate Cognition: Are Primates Superior to Non-Primates?* L. J. Rogers, G. Kaplan, Eds. (Kluwer Academic, New York, 2004), pp. 3–55.
3. N. K. Humphrey, in *Growing Points in Ethology*, P. P. G. Bateson, R. A. Hinde, Eds. (Cambridge Univ. Press, Cambridge, 1976), pp. 303–317.
4. R. W. Byrne, A. Whiten, *Machiavellian Intelligence: Social Evolution in Monkeys, Apes and Humans* (Clarendon Press, Oxford, 1988).
5. L. Marino, *Brain Behav. Evol.* **59**, 21 (2002).
6. N. J. Emery, in *Comparative Analysis of Mind*, S. Watanabe, Ed. (Keio Univ. Press, Tokyo, 2004), pp. 181–213.
7. H. J. Jerison, *Evolution of the Brain and Intelligence* (Academic Press, New York, 1973).
8. A. Reiner *et al.*, *J. Comp. Neurol.* **473**, 377 (2004).
9. G. Rehkamper, H. D. Frahm, Z. Zilles, *Brain Behav. Evol.* **37**, 125 (1991).
10. L. Lefebvre, N. Nicolakakis, D. Boire, *Behaviour* **139**, 939 (2002).
11. L. Lefebvre, P. Whittle, E. Lascaris, A. Finkelstein, *Anim. Behav.* **53**, 549 (1997).
12. J. van Lawick-Goodall, *Adv. Study Behav.* **3**, 195 (1970).
13. G. R. Hunt, R. D. Gray, *Proc. R. Soc. London Ser. B* **271**, 88 (2004).
14. G. R. Hunt, *Nature* **379**, 249 (1996).
15. G. R. Hunt, *Proc. R. Soc. London Ser. B.* **267**, 403 (2000).
16. G. R. Hunt, R. D. Gray, M. C. Corballis, *Nature* **414**, 707 (2001).
17. R. Rutledge, G. R. Hunt, *Anim. Behav.* **67**, 327 (2004).
18. A. A. S. Weir, B. Kenward, J. Chappell, A. Kacelnik, *Proc R. Soc. London Ser B Biol. Lett.* **271**, 344 (2004).
19. G. R. Hunt, R. D. Gray, *Proc. R. Soc. London Ser. B* **270**, 867 (2003).
20. A. Whiten *et al.*, *Nature* **399**, 682 (1999).
21. A. A. S. Weir, J. Chappell, A. Kacelnik, *Science* **297**, 981 (2002).
22. J. Chappell, A. Kacelnik, *Anim. Cognit.* **5**, 71 (2002).
23. J. Chappell, A. Kacelnik, *Anim. Cognit.* **7**, 121 (2004).
24. R. P. Balda, A. C. Kamil, *Anim. Behav.* **44**, 761 (1992).
25. N. S. Clayton, D. P. Griffiths, N. J. Emery, A. Dickinson, *Philos. Trans. R. Soc. London Ser. B* **356**, 1483 (2001).
26. S. R. de Kort, S. Tebbich, J. M. Dally, N. J. Emery, N. S. Clayton, in *Comparative Cognition*, T. R. Zentall, E. Wasserman, Eds. (Oxford Univ. Press, New York, in press).
27. N. S. Clayton, A. Dickinson, *Nature* **395**, 272 (1998).
28. N. S. Clayton, A. Dickinson, *J. Comp. Psychol.* **113**, 403 (1999).
29. N. S. Clayton, K. Yu, A. Dickinson, *J. Exp. Psychol. Anim. Behav. Process.* **27**, 17 (2001).
30. S. B. Vander Wall, *Food Hoarding in Animals* (Univ. of Chicago Press, Chicago, 1990).
31. P. A. Bednekoff, R. P. Balda, *Behaviour* **133**, 807 (1996).
32. B. Heinrich, J. W. Pepper, *Anim. Behav.* **56**, 1083 (1998).
33. R. P. Balda, A. C. Kamil, P. A. Bednekoff, in *Current Ornithology*, V. Nolan, E. D. Ketterson, Eds. (Plenum, New York, 1996), vol. 13, pp. 33–66.
34. P. A. Bednekoff, R. P. Balda, *Anim. Behav.* **52**, 833 (1996).
35. J. J. Templeton, A. C. Kamil, R. P. Balda, *J. Comp. Psychol.* **113**, 450 (1999).
36. N. J. Emery, J. M. Dally, N. S. Clayton, *Anim. Cognit.* **7**, 37 (2004).
37. J. M. Dally, N. J. Emery, N. S. Clayton, *Anim. Behav.*, in press.
38. T. Bugnyar, K. Kotrschal, *Anim. Behav.* **64**, 185 (2002).
39. H. Kallander, *Anser Suppl.* **3**, 124 (1978).
40. T. Bugnyar, K. Kotrschal, *Anim. Cognit.* **7**, 69 (2004).
41. B. Heinrich, *Mind of the Raven* (Harper Collins, New York, 1999).
42. N. J. Emery, N. S. Clayton, *Nature* **414**, 443 (2001).
43. J. M. Dally, N. J. Emery, N. S. Clayton, *Proc. R. Soc. London Ser. B Biol. Lett.*, in press.
44. D. J. Povinelli, *Folk Physics for Apes* (Oxford Univ. Press, New York, 2000).
45. B. Hare, J. Call, B. Agnetta, M. Tomasello, *Anim. Behav.* **59**, 771 (2000).
46. B. Hare, J. Call, M. Tomasello, *Anim. Behav.* **61**, 139 (2001).
47. J. Diamond, A. B. Bond, *Behaviour* **140**, 1091 (2003).
48. S. M. Reader, K. N. Laland, in *Animal Innovation*, S. M. Reader, K. N. Laland, Eds. (Oxford Univ. Press, Oxford, 2003), pp. 3–35.
49. N. S. Clayton, K. S. Yu, A. Dickinson, *J. Exp. Psychol. Anim. Behav. Process.* **29**, 14 (2003).
50. M. W. Hunter, A. C. Kamil, *Psychon. Sci.* **22**, 271 (1971).
51. B. Wilson, N. J. Mackintosh, R. A. Boakes, *Q. J. Exp. Psychol. B* **37**, 313 (1985).
52. A. B. Bond, A. C. Kamil, R. P. Balda, *Anim. Behav.* **65**, 479 (2003).
53. G. Pas-y-Mino, C. A. B. Bond, A. C. Kamil, R. P. Balda, *Nature* **430**, 778 (2004).
54. B. Pollok, H. Prior, O. Gunturkun, *J. Comp. Psychol.* **114**, 148 (2000).
55. W. Kohler, *The Mentality of Apes* (Vontage Books, New York, ed. 2, 1927).
56. B. Heinrich, *Auk* **112**, 994 (1995).
57. A. D. Bennett, *J. Exp. Biol.* **199**, 219 (1996).
58. B. M. Gibson, A. C. Kamil, *J. Comp. Psychol.* **115**, 403 (2001).
59. D. J. Povinelli, J. E. Nelson, S. T. Boysen, *Anim. Behav.* **43**, 633 (1992).
60. D. J. Povinelli, K. A. Parks, M. A. Novak, *Anim. Behav.* **44**, 269 (1991).
61. C. M. Heyes, *Behav. Brain Sci.* **21**, 101 (1998).
62. T. Suddendorf, M. C. Corballis, *Genet. Soc. Gen. Psychol. Monogr.* **123**, 133 (1997).
63. N. S. Clayton, T. J. Bussey, A. Dickinson, *Nat. Rev. Neurosci.* **4**, 685 (2003).

64. N.J.E. is supported by a Royal Society Research Fellowship. The writing of this review was supported by grants from the Biotechnology and Biological Sciences Research Council (grants S16565 and BBS/B/05354), the Royal Society, and the University of Cambridge. We thank A. Dickinson, S. de Kort, C. Rutte, G. Hunt, and A. Kacelnik for comments on the manuscript.

10.1126/science.1098410

Institutional Site License Available

Q What can *Science* STKE give me?

A The definitive resource on cellular regulation

STKE – Signal Transduction Knowledge Environment offers:

- A weekly electronic journal
- Information management tools
- A lab manual to help you organize your research
- An interactive database of signaling pathways

STKE gives you essential tools to power your understanding of cell signaling. It is also a vibrant virtual community, where researchers from around the world come together to exchange information and ideas. For more information go to www.stke.org

To sign up today, visit promo.aaas.org/stkeas

Sitewide access is available for institutions.
To find out more e-mail stkelicense@aaas.org

Science stke AAAS

Capuchin Stone Tool Use in Caatinga Dry Forest

A. C. de A. Moura[1,2*] and P. C. Lee[2]

The abilities of capuchin monkeys (*Cebus* spp.) to use tools and to solve problems in captivity are notable (*1*). Despite decades of field observation, however, reports of tool use in the wild have been remarkably rare (*2*, *3*). We report on the almost daily use of feeding tools by *Cebus apella libidinosus*, including digging stones, from the Caatinga dry forests of northeastern Brazil (Fig. 1).

The lack of tool use by wild capuchins, in contrast to their captive abilities, has been explained by their limited terrestrial foraging or by dexterous manipulation without the need for tools (*4*, *5*). However, food bottlenecks can create contexts for deriving benefits from technology. When tool use improves foraging efficiency and allows the retrieval of otherwise inaccessible resources, the exploitation of foods with high nutritional value becomes possible (*6*). The benefits of tool use could be high when time for foraging is inadequate for nutrient acquisition or where there is limited food abundance, as in the Caatinga dry forest. In this habitat, capuchins forage terrestrially for embedded foods such as tubers during the extended dry season.

The Serra da Capivara National Park is located 7°30′S and 41°30′W in the state of Piaui, in northeastern Brazil. Yearly precipitation in the Caatinga dry forest averages ~800 mm, with extreme variance between areas and years (*7*). Over 7 years (1995–2001), the study site mean was 781 mm (coefficient of variation, 98.2 to 154.8). There is a marked dry season from May to mid-October, and erratic rainfall affects primary productivity with limited, highly seasonal fruit production (*8*). Our Oitenta study group consisted of 10 animals (2 males, 5 females, and 3 juveniles); other groups were censused and surveyed on a monthly basis (*8*).

We observed the use of feeding tools in three groups ranging throughout a 40-km^2 study area. Evidence of tool use by a fourth group—a stone hammer and scattered cracked seeds of *Manihot* around a wooden anvil—was also found. Feeding tools were used in three contexts: (i) digging, (ii) cracking, and (iii) probing. A total of 154 feeding tool-use events were systematically observed from October 2000 to March 2002. Here we analyze tool use (n = 134 events, 0.43 events per hour or 5.1 per observation day in the Oitenta study group) during 312 contact hours between January and December 2001.

The most frequent type of tool use (65% of the observed events) was digging with stones, which was observed in groups >20 km apart. The customary use of stones to dig up tubers, roots, or insects has yet to be described for any primate population in the wild or captivity (*9*), other than humans. The most versatile technology was cracking (19%). Monkeys used stones to crack open seeds (38% of the cracking events), to open hollow branches (16%), and to break tubers (from the *Manihot* and *Thiloa* species) into pieces small enough for consumption (46%). Occasionally, cracking or pulverizing was used to obtain vertebrate prey such as lizards or to process cactus (*Pilosocereus piauhyensis*) to consume the soft inner pith. In addition, branches or twigs were used to probe tree holes and rock crevices for insects, honey, or water (14% of tool-use events), and monkeys modified the twigs on 43% of occasions, removing leaves or stems before using their tools.

Fig. 1. (**A**) A capuchin monkey foraging and (**B**) a general view of the Caatinga during the dry season. The low food abundance and starvation risk could prompt innovative behavior such as tool use (movie S1).

Stone digging and hammer tools did not appear to be limited to any specific size or shape, although detailed measurements of their lithic properties have yet to be made. The weight of digging and hammer stones ranged from 10 to 625 g (n = 14 stones). Tools were selected from the rocky substrate or soils nearby and could be reused when found close to hand during a digging event (digging was seen in 4% of all foraging events, n = 867). Monkeys typically held the stone with one hand and hit the ground quickly 3 to 6 times, while simultaneously scooping away the soil with the other hand; they then released the stone to dig with both hands or reused the stone again.

These monkeys use 41 plant species as foods; tool use probably increased the consumption of at least three: *Thiloa glaucocarpa* (underground tubers), *Manihot* sp. (seeds), and *Hymenaea courbaril* (fruits). The use of stones for cracking and digging enhanced access to resources such as high-carbohydrate tubers and protein-rich insects. When digging with tools, the monkeys terminated their activity by obtaining a tuber or root in 41% of the cases. Tools, when easy to obtain and simple to use, can potentially reduce the time costs of processing large or embedded foods (*10*) and thus increase return rates in a time- and energy-limited environment. We suggest that capuchin destructive foraging for embedded resources in areas of energy bottlenecks is facilitated by innovative tool use.

References and Notes

1. G. C. Westegaard, S. J. Suomi, *J. Anthropol. Res.* **51**, 1 (1995).
2. D. Fragaszy *et al.*, *Am. J. Primatol.*, in press.
3. A. Langguth, C. Alonso, *Neotrop. Primates* **5**, 77 (1997).
4. E. B. Ottoni, M. Mannu, *Int. J. Primatol.* **22**, 310 (2001).
5. E. Visalberghi, *Folia Primatol.* **49**, 168 (1987).
6. G. Yamakoshi, *Am. J. Phys. Anthropol.* **106**, 283 (1998).
7. A. C. de S. Reis, *An. Acad. Brasil. Ciên.* **48**, 325 (1976).
8. A. C. de A. Moura, thesis, University of Cambridge (2004).
9. A. Lanjouw, in *Behavioural Diversity in Chimpanzees and Bonobos*, C. Boesch *et al.*, Eds. (Cambridge Univ. Press, Cambridge, 2002), pp. 52–60.
10. S. T. Parker, K. R. Gibson, *J. Hum. Evol.* **6**, 623 (1977).
11. We thank N. Guidon for support during fieldwork. Supported by a Brazilian Research Council (CNPq) scholarship and by Darwin College, Cambridge. Research permission was from Instituto Brasileiro do Meio Ambiente e dos Recursos Naturais Renováveis (IBAMA).

Supporting Online Material

www.sciencemag.org/cgi/content/full/306/5703/1909/DC1

Movie S1

9 July 2004; accepted 13 October 2004
10.1126/science.1102558

[1]Darwin College, University of Cambridge, Silver Street, Cambridge CB3 9EU, UK. [2]Department of Biological Anthropology, University of Cambridge, Downing Street, Cambridge CB2 3DZ, UK.

*To whom correspondence should be addressed. E-mail: acdam2@cam.ac.uk

Observation of the Spin Hall Effect in Semiconductors

Y. K. Kato, R. C. Myers, A. C. Gossard, D. D. Awschalom*

Electrically induced electron-spin polarization near the edges of a semiconductor channel was detected and imaged with the use of Kerr rotation microscopy. The polarization is out-of-plane and has opposite sign for the two edges, consistent with the predictions of the spin Hall effect. Measurements of unstrained gallium arsenide and strained indium gallium arsenide samples reveal that strain modifies spin accumulation at zero magnetic field. A weak dependence on crystal orientation for the strained samples suggests that the mechanism is the extrinsic spin Hall effect.

The Hall effect (*1*, *2*) has proved to be a convenient and useful tool for probing charge transport properties in the solid state and is routinely used as a standard materials characterization method. It finds widespread application in magnetic field sensors (*2*) and has led to a wealth of new phenomena, such as the integer and fractional quantum Hall effects in two-dimensional systems (*3*, *4*), the anomalous Hall effect in ferromagnetic systems (*1*, *5*), and the spin-dependent Hall effect (*6*). In analogy to the conventional Hall effect, the spin Hall effect has been proposed to occur in paramagnetic systems as a result of spin-orbit interaction, and refers to the generation of a pure spin current transverse to an applied electric field even in the absence of applied magnetic fields. A pure spin current can be thought of as a combination of a current of spin-up electrons in one direction and a current of spin-down electrons in the opposite direction, resulting in a flow of spin angular momentum with no net charge current. Similar to the charge accumulation at the sample edges, which causes a Hall voltage in the conventional Hall effect, spin accumulation is expected at the sample edges in the spin Hall effect. Early theoretical studies predicted a spin Hall effect originating from asymmetries in scattering for up and down spins (*7*–*10*), which is referred to as an extrinsic spin Hall effect. More recently, it has been pointed out that there may exist an intrinsic spin Hall effect that arises as a result of the band structure, even in the absence of scattering (*11*, *12*). This idea has led to much theoretical discussion (*13*–*16*), but experimental evidence of the spin Hall effect has been lacking.

We report on the optical detection of the spin Hall effect in thin films of the semiconductors GaAs and InGaAs. Scanning Kerr rotation measurements show the presence of electron spin accumulation at the edges of the samples, consistent with the prediction of a spin current transverse to the applied electric field. We investigated the effect in both unstrained and strained samples and found that an applied in-plane magnetic field can play a critical role in the appearance of the spin accumulation. No marked crystal direction dependence is observed in the strained samples, which suggests that the contribution from the extrinsic spin Hall effect is dominant.

Experimental details. Experiments were performed on a series of samples fabricated from *n*-GaAs and *n*-$In_{0.07}Ga_{0.93}As$ films grown on (001) semi-insulating GaAs substrate by molecular beam epitaxy. Our results are obtained from samples fabricated from two wafers. The unstrained GaAs sample consists of 2 μm of *n*-GaAs grown on top of 2 μm of undoped $Al_{0.4}Ga_{0.6}As$, whereas the strained InGaAs sample has 500 nm of *n*-$In_{0.07}Ga_{0.93}As$ capped with 100 nm of undoped GaAs. In both wafers, the *n*-type layers are Si doped for $n = 3 \times 10^{16}$ cm^{-3} to achieve long spin lifetimes (*17*). Standard photolithography and wet etching are used to define a semiconductor channel, and the *n*-type layers are contacted with annealed Au/Ni/Au/Ge/Ni. All the samples are left attached to the 500-μm-thick substrate to minimize unintentional strain from sample mounting. Samples are placed in a low-temperature Kerr microscope (*18*) with the channel oriented perpendicular to the externally applied in-plane magnetic field B_{ext} (Fig. 1A).

Static Kerr rotation (KR) probes the electron spin polarization in the sample. A mode-locked Ti:sapphire laser produces ~150-fs pulses at a repetition rate of 76 MHz and is tuned to the absorption edge of the semiconductor. A linearly polarized beam is directed along the *z* axis and is incident normal to the sample through an objective lens with a numerical aperture of 0.73, focusing the beam to a circular spot with a full width at half-maximum of 1.1 μm. The polarization axis of the reflected beam rotates by an amount proportional to the net magnetization of the

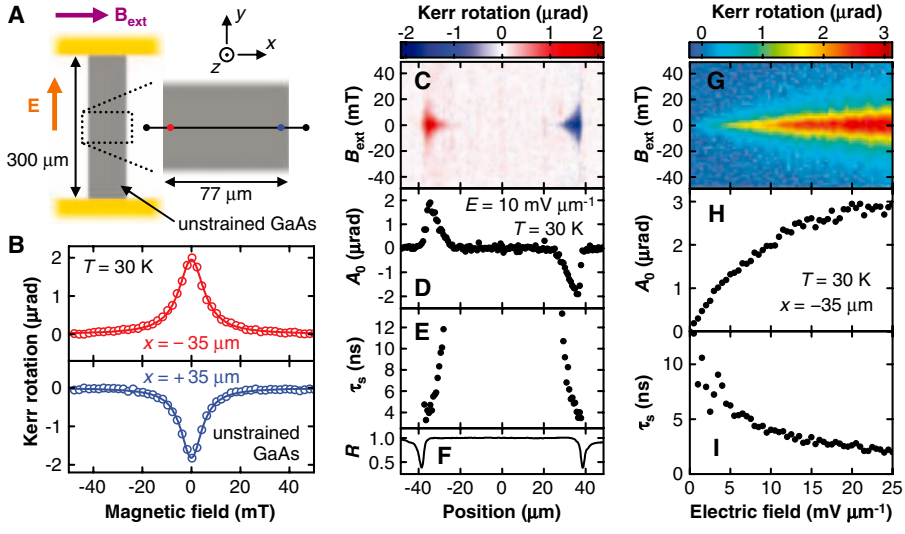

Fig. 1. The spin Hall effect in unstrained GaAs. Data are taken at $T = 30$ K; a linear background has been subtracted from each B_{ext} scan. (**A**) Schematic of the unstrained GaAs sample and the experimental geometry. (**B**) Typical measurement of KR as a function of B_{ext} for $x = -35$ μm (red circles) and $x = +35$ μm (blue circles) for $E = 10$ mV μm^{-1}. Solid lines are fits as explained in text. (**C**) KR as a function of x and B_{ext} for $E = 10$ mV μm^{-1}. (**D** and **E**) Spatial dependence of peak KR A_0 and spin lifetime τ_s across the channel, respectively, obtained from fits to data in (C). (**F**) Reflectivity R as a function of x. R is normalized to the value on the GaAs channel. The two dips indicate the position of the edges and the width of the dips gives an approximate spatial resolution. (**G**) KR as a function of E and B_{ext} at $x = -35$ μm. (**H** and **I**) E dependence of A_0 and τ_s, respectively, obtained from fits to data in (G).

Center for Spintronics and Quantum Computation, University of California, Santa Barbara, CA 93106, USA.

*To whom correspondence should be addressed. E-mail: awsch@physics.ucsb.edu

electron spins along the laser propagation direction (*19*). The KR is detected with the use of a balanced photodiode bridge with a noise equivalent power of 600 fW $Hz^{-1/2}$ in the difference channel. We apply a square wave voltage with a frequency f_E = 1.169 kHz to the two contacts, producing an alternating electric field with amplitude E for lock-in detection. Measurements are done at a temperature T = 30 K unless otherwise noted.

Detecting spin currents. An unstrained GaAs sample with a channel parallel to [110] with a width w = 77 μm, a length l = 300 μm, and a mesa height h = 2.3 μm was prepared (Fig. 1A) and was measured using a wavelength of 825 nm and an average incident laser power of 130 μW. We took the origin of our coordinate system to be the center of the channel. In Fig. 1B, typical KR data for scans of B_{ext} are shown. The red curve is taken at position x = –35 μm; the blue curve is taken at x = +35 μm, corresponding to the two edges of the channel. These curves can be understood as the projection of the spin polarization along the z axis, which diminishes with an applied transverse magnetic field because of spin precession; this is known as the Hanle effect (*8*, *20*). The data are well fit to a Lorentzian function $A_0/[(\omega_L\tau_s)^2 + 1]$, where A_0 is the peak KR, $\omega_L = g\mu_B B_{ext}/\hbar$ is the electron Larmor precession frequency, τ_s is the electron spin lifetime, g is the electron g factor (*21*), μ_B is the Bohr magneton, and $\hbar$ is the Planck constant.

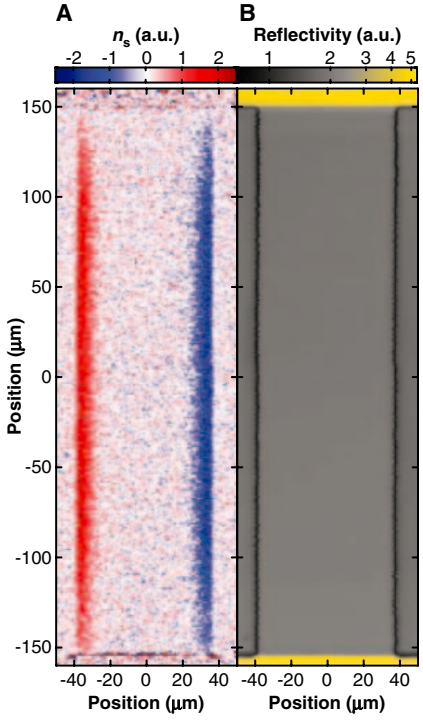

Fig. 2. (**A** and **B**) Two-dimensional images of spin density n_s and reflectivity R, respectively, for the unstrained GaAs sample measured at T = 30 K and E = 10 mV μm^{-1}.

Strikingly, the signal changes sign for the two edges of the sample, indicating an accumulation of electron spins polarized in the $+z$ direction at x = –35 μm and in the $-z$ direction at x = +35 μm. This is a strong signature of the spin Hall effect, as the spin polarization is expected to be out-of-plane and change sign for opposing edges (*7*–*12*). A one-dimensional spatial profile of the spin accumulation across the channel is mapped out by repeating B_{ext} scans at each position (Fig. 1C). It is seen that A_0, which is a measure of the spin density, is at a maximum at the two edges and falls off rapidly with distance from the edge, disappearing at the center of the channel (Fig. 1D) as expected for the spin Hall effect (*10*, *11*). We note that equilibrium spin polarization due to current-induced magnetic fields cannot explain this spatial profile; moreover, such polarization is estimated to be less than 10^{-6}, which is below our detection capability.

An interesting observation is that the width of the Lorentzian becomes narrower as the distance from the edge increases, corresponding to an apparent increase in the spin lifetime (Fig. 1E). It is possible that the finite time required for the spins to diffuse from the edge to the measurement position changes the lineshape of B_{ext} scans. Another conceivable explanation is the actual change in τ_s for spins that have diffused away from the edge. Because these spins have scattered predominantly toward the center of the channel, spin relaxation due to the D'yakonov-Perel mechanism (*20*) may be affected. In Fig. 1G, B_{ext} scans at x = –35 μm for a range of E are shown. Increasing E leads to larger spin accumulation (Fig. 1H), but the polarization saturates because of shorter τ_s for larger E (Fig. 1I). The suppression of τ_s with increasing E is consistent with previous observations (*22*).

The homogeneity of the effect is addressed by taking a two-dimensional image of the entire sample (Fig. 2, A and B). Here, instead of taking a full B_{ext} scan, B_{ext} is sinusoidally modulated at f_B = 3.3 Hz with an amplitude of 30 mT, and signal is detected at $f_E \pm 2f_B$. The measured signal is then proportional to the second derivative of a B_{ext} scan around B_{ext} = 0 mT and can be regarded as a measure of the spin density n_s. The image shows polarization localized at the two edges of the sample and having opposite sign, as discussed above. The polarization at the edges is uniform over a length of 150 μm but decreases near the contacts. The latter is expected as unpolarized electrons are injected at the contacts.

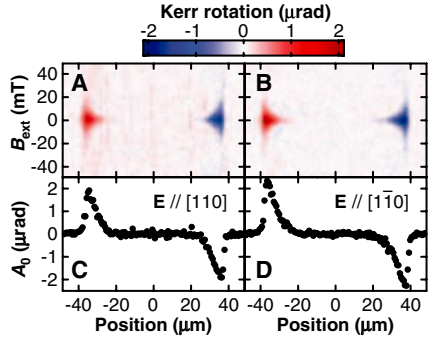

Fig. 3. Crystal orientation dependence of the spin Hall effect in the unstrained GaAs sample with w = 77 μm. (**A** and **B**) KR as a function of x and B_{ext} for E // [110] and E // [1$\bar{1}$0], respectively, with E = 10 mV μm^{-1}. A linear background has been subtracted from each B_{ext} scan. (**C** and **D**) Spatial profile of A_0 for E // [110] and E // [1$\bar{1}$0], respectively.

The origin of the observed spin Hall effect is likely to be extrinsic, as the intrinsic effect is only expected in systems with spin splitting that depends on electron wave vector k. Although k^3 spin splitting in bulk GaAs (*23*) may give rise to an intrinsic spin Hall effect, this is unlikely because negligible spin splitting has been observed in unstrained n-GaAs (*24*). Measurements were also performed on another sample with a channel parallel to [1$\bar{1}$0], and essentially the same behavior was reproduced (Fig. 3).

Effects of strain. The strained InGaAs sample, in contrast, offers the possibility of displaying the intrinsic spin Hall effect in addition to the extrinsic effect. The lattice mismatch causes strain in the InGaAs layer (*25*), and partial strain relaxation causes the in-plane strain to be anisotropic (*26*). Using reciprocal space mapping with x-ray diffraction at room temperature, we determined the in-plane strain along [110] and [1$\bar{1}$0] to be –0.24% and –0.60%, respectively, and the strain along [001] to be +0.13%. These strained layers show electron spin precession at zero applied magnetic field when optically injected electron spins are dragged with a lateral electric field (*24*), which is due to an effective internal magnetic field B_{int} perpendicular to both the growth direction and the electric field (Fig. 4A). A possible explanation for such behavior may be strain-induced k-linear spin splitting terms in the Hamiltonian, which is expected to give rise to the intrinsic spin Hall effect (*16*).

The strained InGaAs sample was processed into a channel oriented along [110] with w = 33 μm, l = 300 μm, and h = 0.9 μm. A laser wavelength of 873 nm and an incident power of 130 μW were used for this measurement, and typical results are shown in Fig. 4B. Surprisingly, the spin polarization is suppressed at B_{ext} = 0 mT, and we observe two peaks offset from B_{ext} = 0 mT. We attribute this behavior to the presence of B_{int}. Because electron spins respond to the sum of B_{ext} and B_{int}, the spin polarization is maximum at $B_{ext} = -B_{int}$ when B_{ext} cancels out B_{int}. The application of a square-wave voltage causes the signal to arise from both positive and negative electric-field directions, resulting in a double-peak structure. Although the spin polarization reverses direc-

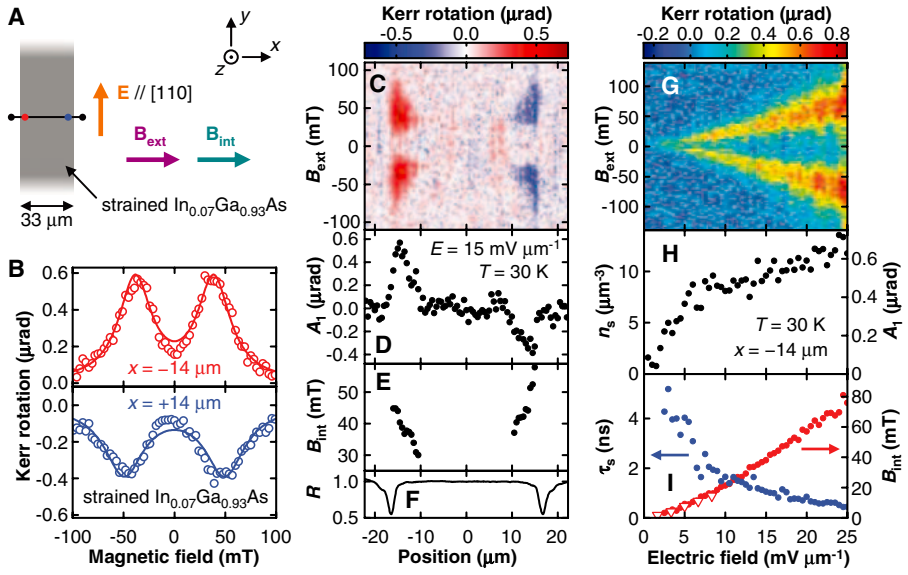

Fig. 4. The spin Hall effect in strained $In_{0.07}Ga_{0.93}As$. Data are taken at T = 30 K; a linear background has been subtracted from each B_{ext} scan. (**A**) Schematic of the strained InGaAs sample and the geometry of electric and magnetic fields. (**B**) Typical measurement of KR as a function of B_{ext} for x = −14 μm (red circles) and x = +14 μm (blue circles) for E = 15 mV μm^{-1}. Solid lines are fits as explained in text. (**C**) KR as a function of x and B_{ext} for E = 15 mV μm^{-1}. (**D** and **E**) Spatial dependence of A_1 and B_{int} across the channel, respectively, obtained from fits to data in (C). (**F**) R, normalized to the value on the InGaAs channel, as a function of x. (**G**) KR as a function of E and B_{ext} at x = −14 μm. (**H**) E dependence of n_s obtained from fits to data in (G). Corresponding A_1 are given on the right axis (*27*). (**I**) E dependence of τ_s (blue circles) and B_{int} (red circles) obtained from fits to data in (G). Red open triangles indicate B_{int} measured by spin drag experiments (*24*) on another chip from the same wafer.

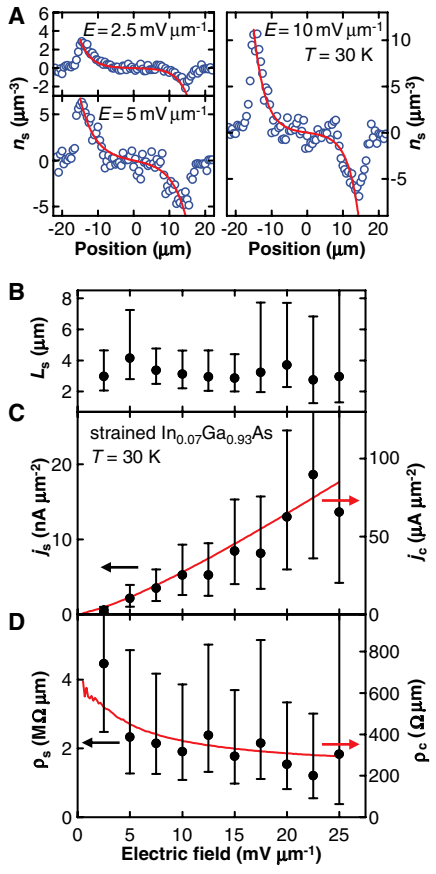

Fig. 5. (**A**) Spatial profiles of n_s for E = 2.5, 5, and 10 mV μm^{-1} at T = 30 K in the strained InGaAs sample. Blue circles are data; red lines are fits as explained in text. (**B**) L_s as a function of E obtained from fits including those shown in (A). (**C**) Spin current density j_s (black circles) and charge current density j_c (red line) as a function of E in the strained InGaAs sample. For the calculation of j_c from the total charge current measurements, an effective film thickness of 400 nm is used to take surface depletion effects into account. (**D**) Spin Hall resistivity ρ_s (black circles) and longitudinal charge resistivity ρ_c (red line) as a function of E. Changes in ρ_c with E are due to changes in the mobility originating from electronic heating, as inferred from conventional Hall measurements. The error bars in (C) and (D) include the systematic error from the calibration of n_s (*27*).

tion for opposing electric field directions, the two peaks have the same sign. This is because lock-in measurement detects the signal difference between the two electric field directions, so both positive polarization at positive E and negative polarization at negative E produce positive signal. The data are fit to $A_1/[(\omega_+\tau_s)^2 + 1] + A_1/[(\omega_-\tau_s)^2 + 1]$, where A_1 is the peak KR, and $\omega_+ = g\mu_B(B_{ext} + B_{int})/\hbar$ and $\omega_- = g\mu_B(B_{ext} - B_{int})/\hbar$ are the precession frequencies when B_{int} adds to and subtracts from B_{ext}, respectively (*21*). We note that the spatially uniform current-induced spin polarization (*22*) is not detected in this geometry, as this polarization is parallel to B_{ext}.

Spatial dependence in this sample (Fig. 4C) reproduces the characteristic signatures of the spin Hall effect. The polarization is localized at the channel edges and has opposite sign for the two edges, disappearing at the center (Fig. 4D). The slight asymmetry of the spin polarization for the two edges may be due to inhomogeneous strain. The peak width narrows as the distance from the channel edge increases, reproducing the apparent increase of τ_s in this sample as well. In addition, we find that the splitting of the two peaks decreases with increasing distance from the channel edge (Fig. 4E). A possible explanation is that the spins detected far away from the edge have average k, which has some component transverse to E; in this case, B_{int} will have a smaller component along B_{ext}, causing the splitting to decrease. The electric field dependence (Fig. 4G) exhibits similarity to the unstrained GaAs sample, showing polarization saturation (Fig. 4H) as the spin lifetime diminishes (Fig. 4I). In this sample, it is possible to correlate the KR angle to the actual spin density. We define the spin density $n_s = \langle\sigma_z\rangle n$, where $\langle\sigma_z\rangle$ is the expectation value of the Pauli operator and n is the electron density. To obtain a calibration for n_s, we used the Kerr microscope to measure the current-induced spin polarization in a sample from the same wafer with known characteristics (*27*). The peak spin density reaches 10 μm^{-3}, a value comparable to that of current-induced spin polarization. The electric field dependence of B_{int} is also plotted in Fig. 4I, and it shows very similar values to the B_{int} measured by spin drag experiments (*24*) on another chip from the same wafer. Additional measurements between 10 K < T < 60 K with E = 15 mV μm^{-1} show no marked changes in the spin polarization or its spatial profile.

It is possible to calculate the spin current from the values of the accumulated spin density. In a simple picture ignoring the position dependence of τ_s, the solution to the spin drift-diffusion equation (*10*, *11*) is $n_0 \sinh(x/L_s)/\cosh[w/(2L_s)]$, where $n_0 = \iota_s\tau_s/L_s$ is the spin density at the edge, $L_s = (D_s\tau_s)^{1/2}$ is the spin diffusion length, D_s is the spin diffusion coefficient, $\iota_s = \langle\sigma_z v\rangle n$ is the spin current density, and v is the velocity operator. By fitting the spatial dependence for various values of E (Fig. 5A), we obtain both n_0 and L_s. Values of τ_s are averaged between 10 μm < x < 15 μm for the calculations of ι_s. We note that L_s does not change noticeably with E (Fig. 5B), whereas τ_s decreases with increasing E. This implies that D_s increases with E, consistent with previous measurements (*24*). In Fig. 5C, we plot the spin current density $j_s = e\iota_s$, where e is the unit charge. The spin current is converted into units of charge current to allow comparison with the longitudinal charge current density j_c, which is also plotted in Fig. 5C. The spin Hall resistivity $\rho_s = E/j_s$ and the longitudinal charge resistivity $\rho_c = E/j_c$ are plotted in Fig. 5D. The intrinsic spin Hall resistivity,

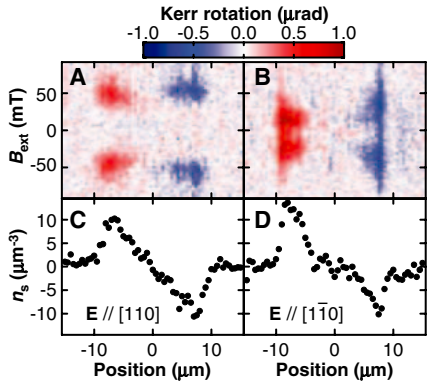

Fig. 6. Crystal orientation dependence of the spin Hall effect in the strained InGaAs sample with w = 18 μm. (**A** and **B**) KR as a function of x and B_{ext} for E // [110] and E // [1$\bar{1}$0], respectively, with E = 15 mV μm^{-1}. A linear background has been subtracted from each B_{ext} scan. (**C** and **D**) Spatial profile of n_s obtained from the fits for E // [110] and E // [1$\bar{1}$0], respectively.

when neglecting the effect of scattering, is predicted to be $4\pi^2\hbar/(e^2k_F) = 1.69$ kilohm·μm, where k_F is the Fermi wave vector (*16*); the measured values are ~2 megohm·μm. We estimate the effect of scattering by noting that a factor of $(\Delta\tau/\hbar)^2$ enters the expression for spin current (*14*), where Δ is the spin splitting at the Fermi energy and τ is the momentum relaxation time. Although this result is derived for other systems, this factor is ~10^{-6} for our samples and may explain why the observed spin current is small.

In an effort to identify a possible contribution from the intrinsic effect, we investigated crystal orientation dependence. The spin splitting in these strained InGaAs samples has crystal anisotropy (*24*), and therefore the intrinsic contribution should be sensitive to the crystal axis. Samples oriented along [110] and [1$\bar{1}$0] were fabricated on a single chip to minimize the effect of inhomogeneous strain. The results are shown in Fig. 6, where we observe that the splitting of the two peaks is smaller for E // [1$\bar{1}$0] because B_{int} is smaller in this direction (*24*), whereas no marked difference in n_s is seen, which suggests that the extrinsic effect is also dominant in the strained InGaAs samples.

Conclusion. The observed spin Hall effect provides new opportunities for manipulating electron spins in nonmagnetic semiconductors without the application of magnetic fields. The spin current and spin accumulation induced by the spin Hall effect may be used to route spin-polarized current depending on its spin, or to amplify spin polarization by splitting a channel into two and cascading such structures. In addition, the suppression of spin accumulation at B_{ext} = 0 mT caused by B_{int} is an important aspect that has not been considered previously and may possibly allow control of the spin accumulation by means of, for example, gate voltage control of the Rashba effect (*28*).

References and Notes

1. C. L. Chien, C. R. Westgate, Eds., *The Hall Effect and Its Applications* (Plenum, New York, 1980).
2. R. S. Popovic, *Hall Effect Devices* (Institute of Physics, Bristol, UK, ed. 2, 2004).
3. B. Huckestein, *Rev. Mod. Phys.* **67**, 357 (1995).
4. H. L. Stormer, D. C. Tsui, A. C. Gossard, *Rev. Mod. Phys.* **71**, S298 (1999).
5. W. L. Lee, S. Watauchi, V. L. Miller, R. J. Cava, N. P. Ong, *Science* **303**, 1647 (2004).
6. J. N. Chazalviel, *Phys. Rev. B* **11**, 3918 (1975).
7. M. I. D'yakonov, V. I. Perel, *JETP Lett.* **13**, 467 (1971).
8. M. I. D'yakonov, V. I. Perel, *Phys. Lett. A* **35**, 459 (1971).
9. J. E. Hirsch, *Phys. Rev. Lett.* **83**, 1834 (1999).
10. S. Zhang, *Phys. Rev. Lett.* **85**, 393 (2000).
11. S. Murakami, N. Nagaosa, S. C. Zhang, *Science* **301**, 1348 (2003).
12. J. Sinova *et al.*, *Phys. Rev. Lett.* **92**, 126603 (2004).
13. E. I. Rashba, *Phys. Rev. B* **68**, 241315(R) (2003).
14. J. Schliemann, D. Loss, *Phys. Rev. B* **69**, 165315 (2004).
15. J. Inoue, G. E. W. Bauer, L. W. Molenkamp, *Phys. Rev. B* **70**, 041303(R) (2004).
16. B. A. Bernevig, S. C. Zhang, www.arXiv.org/abs/cond-mat/0408442 (2004).
17. J. M. Kikkawa, D. D. Awschalom, *Phys. Rev. Lett.* **80**, 4313 (1998).
18. J. Stephens *et al.*, *Phys. Rev. B* **68**, 041307(R) (2003).
19. S. A. Crooker, D. D. Awschalom, J. J. Baumberg, F. Flack, N. Samarth, *Phys. Rev. B* **56**, 7574 (1997).
20. F. Meier, B. P. Zakharchenya, Eds., *Optical Orientation* (Elsevier, Amsterdam, 1984).
21. The electron g factor is –0.44 for the unstrained GaAs sample and –0.63 for the strained InGaAs sample, as determined by time-resolved Faraday rotation measurements (*19*).
22. Y. K. Kato, R. C. Myers, A. C. Gossard, D. D. Awschalom, *Phys. Rev. Lett.* **93**, 176601 (2004).
23. G. Dresselhaus, *Phys. Rev.* **100**, 580 (1955).
24. Y. Kato, R. C. Myers, A. C. Gossard, D. D. Awschalom, *Nature* **427**, 50 (2004).
25. S. C. Jain, M. Willander, H. Maes, *Semicond. Sci. Technol.* **11**, 641 (1996).
26. K. L. Kavanagh *et al.*, *J. Appl. Phys.* **64**, 4843 (1988).
27. The strained InGaAs sample is the sample E used in previous work (*22*, *24*). We use the value of current-induced spin polarization efficiency η as defined in (*22*) to obtain the calibration, and assume that the ratio of KR to spin polarization is within 10% on the samples from the same wafer that are measured in these experiments. The systematic error introduced in this calibration is +48%/–38%.
28. J. Nitta, T. Akazaki, H. Takayanagi, T. Enoki, *Phys. Rev. Lett.* **78**, 1335 (1997).

29. Supported by the Defense Advanced Research Projects Agency, the Defense Microelectronics Activity, and NSF.

21 September 2004; accepted 28 October 2004
Published online 11 November 2004;
10.1126/science.1105514
Include this information when citing this paper.

REPORTS

Transient Interface Sharpening in Miscible Alloys

Zoltán Erdélyi,[1]* Marcel Sladecek,[3] Lorenz-M. Stadler,[3] Ivo Zizak,[4] Gábor A. Langer,[1] Miklós Kis-Varga,[2] Desző L. Beke,[1] Bogdan Sepiol[3]

We observed that diffuse interfaces sharpen rather than broaden in completely miscible ideal binary systems. This is shown in situ during heat treatments at gradually increasing temperatures by scattering of synchrotron radiation in coherent Mo/V multilayers containing initially diffuse interfaces. This effect provides a useful tool for the improvement of interfaces and offers a way to fabricate better x-ray or neutron mirrors, microelectronic devices, or multilayers with giant magnetic resistance.

Computer simulations have recently shown (*1*, *2*) that on the nanoscale, for strongly composition-dependent diffusion coefficients, an initially diffuse interface of species A and B can become chemically abrupt even in ideal (either crystalline or amorphous) systems with complete mutual solubility. This sharpening is surprising at first sight, because the direction of diffusion is always opposite to the direction of the composition gradient: $J = -D$ grad c, where J is the atomic flux, D is the diffusion coefficient, and c is the concentration. Indeed, for constant D, the composition profile will gradually decay and a broadening of the interface is expected. However, when the diffusion coefficient is strongly dependent on the local composition, the flux distribution can lead to a sharpening of the interface (Fig. 1). For example, the sharpening can occur when the diffusion of A and B in B is much faster than the diffusion of either in A. The sharpening can be qualitatively predicted from the classical Fick I law, although it is not able to provide correct kinetics on the nanoscale (*1*, *3*).

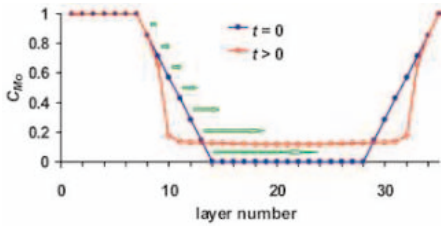

Fig. 1. Composition [atomic fraction (C_{Mo})] distribution during intermixing in one period of a Mo/V multilayer calculated from an atomistic model, as in (*1*). The arrows represent schematically the "flux distribution" (i.e., their lengths are proportional to the absolute value of the atomic flux).

This effect is not only interesting from a fundamental point of view but also of practical interest. For many devices, the chemical abruptness of the interfaces is key (e.g., x-ray and neutron mirrors and conductors, semiconductor bi- and multilayers, and giant magnetic resistance technology), but most fabricated interfaces are more or less diffuse initially. For example, in Si-Ge multilayers grown by molecular beam epitaxy, the Ge/Si interface produced by the deposition of Si on Ge is always more diffuse than the Si/Ge interface due to mixing driven by Ge segregation during the growth (*4*, *5*).

We studied Mo/V multilayers because the materials are completely miscible. The structures (20 bilayers with a modulation length ≈ 5 to 6 nm) were produced by magnetron sputtering (*6*, *7*). The pure Mo and V layers were separated by a diffuse interface about 1 nm thick with a constant composition gradient (*7*). The microstructural characterization of the samples was accomplished by a standard x-ray diffraction instrument with a Siemens Cu anode.

To follow the change of the composition profiles in situ during heat treatments, x-ray measurements were performed at the KMC2 beamline at the Berlin electron storage ring compound for synchrotron radiation (BESSY), with the use of brilliance much higher than that used at the x-ray source in the lab. The samples were placed on a heater inside a hemispherical Be window under high-vacuum conditions. Measurements were carried out at temperatures that gradually increased from 293 K up to about 973 K in 10 steps. At each temperature, consecutive symmetrical scans between 53° and 66° of the scattering angle 2θ were performed, measuring the scattering intensity around the (002) Bragg reflection of the Mo/V multilayer structure. The sample was held at each temperature until no change in the diffraction pattern could be observed, and this required a minimum of 2 hours.

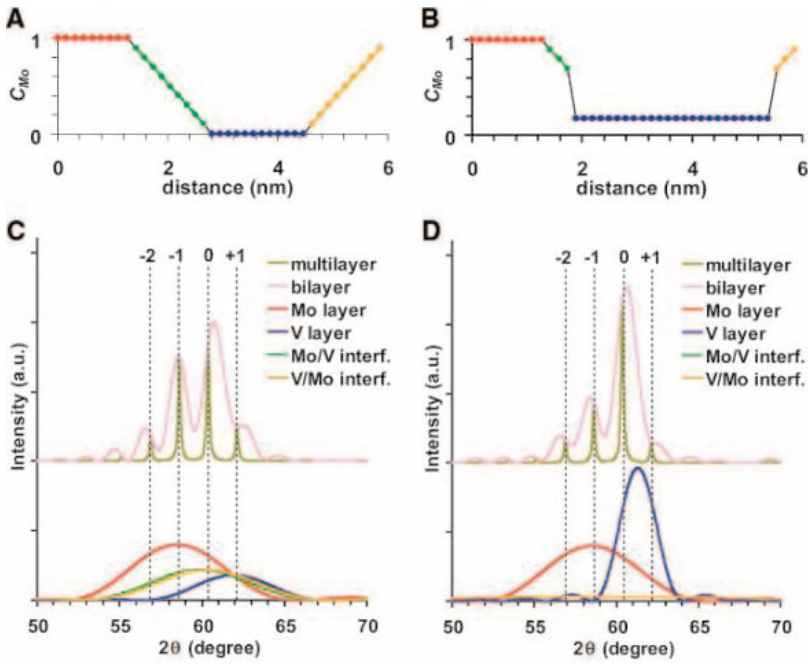

Fig. 2. Composition profiles in the initial state (**A**) and after some sharpening (**B**) and the calculated corresponding diffraction patterns (**C** and **D**). The four curves at the bottom of (C) and (D) represent the square of the scattering amplitudes (intensities) from the pure Mo (I^{Mo}), and V (I^{V}), as well as from the Mo/V ($I^{Mo/V}$) and V/Mo ($I^{V/Mo}$) interfaces. The two curves at the top of (C) and (D) are the square of the scattering amplitudes from one bilayer and from the whole multilayer, respectively. The dashed lines show the peak positions. It can be seen that during sharpening, the heights of the higher order peaks decrease as compared with the height of the 0th-order peak. a.u., arbitrary units.

The x-ray diffraction patterns were reconstructed with two models based on the works of Stearns (*8*) and Fullerton *et al*. (*9*). However, because the shapes shown in Fig. 1 for $t > 0$ could not be handled in these models, we had to modify them (*7*).

During sharpening, the Mo layer remains intact. The V layer fills up with Mo and thus its scattering factor increases and the composition profile has an abrupt break in the interface region. Hence, the following important changes, shown in Fig. 2, are expected in the diffraction patterns: (i) The intensity of all satellite peaks decreases as compared with the 0th-order peak; (ii) the –1st-order peak changes most markedly; (iii) the +1st-order peak decreases faster than the –2nd-order peak. In other words, the ratio I^0/I^i increases ($i = -2, -1, +1$), whereas I^{+1}/I^{-2} decreases. In Fig. 2, the contributions of the four different parts (pure Mo, pure V, and the Mo/V and V/Mo interfaces) of the multilayer to the total intensity are also shown. It can be seen that during sharpening I^V becomes larger and narrower, and because of the increase of the lattice parameter of the V-rich layer, the corresponding I^V curve shifts to smaller angles. At the same time, the interfaces sharpen (their thicknesses decrease), $I^{Mo/V}$ and $I^{V/Mo}$ decrease markedly and broaden. Furthermore, they shift to smaller angles because the average lattice parameter of the interface region increases (given that there are fewer V atoms).

This result can be surprising at first sight, because usually the "sharper interfaces, larger satellite peaks" rule (*10*, *11*) is accepted in the literature. Indeed, it is easy to show from a similar analysis to the one above—assuming that only the interface sharpness increases, but its shape and the composition in the layers do not change—that the intensity at the satellite positions should be larger for sharper interfaces. For instance, in (*10*), such interface sharpness was controlled by the substrate temperature during the deposition.

Figure 3 shows the diffraction patterns measured during heat treatment and their fits by the modified Stearns model. As can be seen, we could reproduce the measured diffraction patterns almost perfectly. Within the error limits, both models gave the same layer and interface thicknesses (Fig. 4). We found that initially the Mo/V interfaces were slightly thicker than the V/Mo ones, and this difference decreased during sharpening. This observation is in accordance with the results

[1]Department of Solid State Physics, University of Debrecen, Post Office Box 2, H-4010 Debrecen, Hungary. [2]Nuclear Research Institute of the Hungarian Academy of Sciences, Post Office Box 51, H-4100 Debrecen, Hungary. [3]Institut für Materialphysik, Universität Wien, Strudlhofgasse 4, A-1090 Wien, Austria. [4]Hahn-Meitner-Institut Berlin, Glienicker Straße 100, D-14109 Berlin, Germany.

*To whom correspondence should be addressed. E-mail: zerdelyi@dragon.unideb.hu

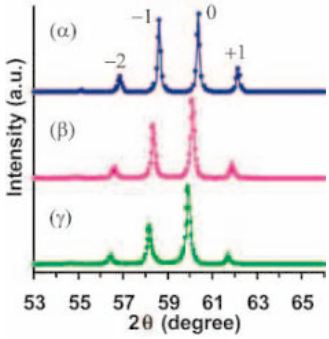

Fig. 3. Diffraction patterns measured (circles) during the heat treatments and their reconstructions by the modified Stearns model (solid line): (α) room temperature, (β) 903 K, and (γ) 953 K. a.u., arbitrary units.

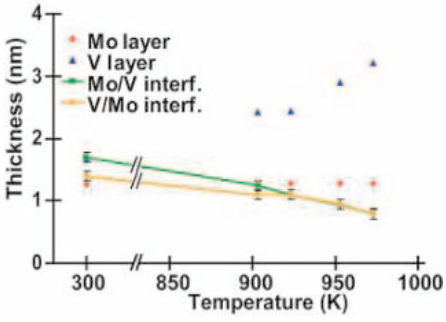

Fig. 4. Thickness of the interfaces as well as the pure Mo and V layers, as obtained from the fits. Error bars show the estimated errors of fitting. In case of the pure Mo and V layer, respectively, error bars are comparable to the symbol sizes. The solid curves are to guide the eye. interf., interface.

obtained in Si/Ge (*4*, *5*) and Au/Ni (*10*, *12*) multilayers. During deposition of one element (e.g., A) having a segregation tendency on the surface of the other (B), a segregation-assisted intermixing takes place and the B/A interface is more diffuse than the A/B interface.

Because the fits resulted in a decreasing interface thickness (i.e., the increase of I^0/I^i, with $i = -2, -1, +1$, and the decrease of I^{+1}/I^{-2}), we conclude that the interface sharpened during the heat treatment. The most notable feature of the reconstructions is the reproduction of changes of the intensity ratios with increasing temperature.

Finally, at a fixed temperature no more changes were observed after a certain time (i.e., a gradually increasing temperature was necessary), which also supports that the interfaces sharpen. Because the interface is sharper, the Mo atoms are bound more strongly in the interface (the interface is more and more Mo rich), and consequently their diffusion into the V is slower (Fig. 1). Thus, to counterbalance this effect, we had to increase the temperature slightly (the diffusivity has exponential dependence on both the temperature and the composition).

One may argue that other effects could produce a similar evolution. For example, stress development and relaxation during intermixing could be one of the most relevant effects. However, as was shown in (*2*), the composition profile develops similarly to that of a stress-free case, and only the time scale of the process is expected to be slightly different.

We successfully followed in situ interface sharpening in coherent Mo/V multilayers. As data in Fig. 4 show, the thickness of the Mo layers did not change, apart from a tiny increase caused by thermal expansion. In contrast, the V-rich layers became much thicker, which cannot be explained solely by thermal expansion. The interface thicknesses decreased by about a factor of 2 (from 1.7 and 1.4 nm, respectively, to 0.78 nm), confirming the sharpening effect.

References and Notes

1. Z. Erdélyi, I. A. Szabó, D. L. Beke, *Phys. Rev. Lett.* **89**, 165901 (2002).
2. Z. Erdélyi, D. L. Beke, *Phys. Rev. B* **68**, 092102 (2003).
3. Z. Erdélyi *et al.*, *Surf. Sci.* **496**, 129 (2002).
4. D. E. Jesson, in *Handbook of Thin Film Process Technology*, D. A. Glocker, S. I. Shah, Eds. (Institute of Physics, Bristol, UK, 1997), vol. F, pp. F1:1–F1:10.
5. T. Walther, C. J. Humphreys, D. J. Robbins, *Forum* **143**, 1135 (1997).
6. A. Dudás *et al.*, *J. Appl. Phys.* **86**, 2008 (1999).
7. Materials and methods are available as supporting material on *Science* Online.
8. M. B. Stearns, *Phys. Rev. B* **38**, 8109 (1988).
9. E. E. Fullerton, I. K. Schuller, H. Vanderstraeten, Y. Bruynseraede, *Phys. Rev. B* **45**, 9292 (1992).
10. H. Kano *et al.*, *Appl. Phys. Lett.* **63**, 2839 (1993).
11. M. Xu *et al.*, *J. Cryst. Growth* **212**, 291 (2000).
12. S. Labat, P. Gerguad, O. Thomas, B. Gilles, A. Marty, *Appl. Phys. Lett.* **75**, 914 (1999).
13. We thank G. Vogl for helpful discussions. This work was financially supported by the Austrian Federal Ministry for Education, Science and Culture, project GZ 45.529/2-VI/B/7a/2002, by the FWF project P15421, and by the OTKA Board of Hungary (nos. F043372, T043464, T038125). Z.E. is a grantee of the Bolyai János scholarship.

Supporting Online Material

www.sciencemag.org/cgi/content/full/306/5703/1913/DC1
Materials and Methods
Fig. S1
References

23 August 2004; accepted 10 November 2004
10.1126/science.1104400

Superconductivity Modulated by Quantum Size Effects

Yang Guo,[1]* Yan-Feng Zhang,[1]* Xin-Yu Bao,[1]* Tie-Zhu Han,[1] Zhe Tang,[1] Li-Xin Zhang,[1] Wen-Guang Zhu,[1] E. G. Wang,[1] Qian Niu,[2] Z. Q. Qiu,[3] Jin-Feng Jia,[1] Zhong-Xian Zhao,[1] Qi-Kun Xue[1]†

We have fabricated ultrathin lead films on silicon substrates with atomic-scale control of the thickness over a macroscopic area. We observed oscillatory behavior of the superconducting transition temperature when the film thickness was increased by one atomic layer at a time. This oscillating behavior was shown to be a manifestation of the Fabry-Pérot interference modes of electron de Broglie waves (quantum well states) in the films, which modulate the electron density of states near the Fermi level and the electron-phonon coupling, which are the two factors that control superconductivity transitions. This result suggests the possibility of modifying superconductivity and other physical properties of a thin film by exploiting well-controlled and thickness-dependent quantum size effects.

Modern electronic and opto-electronic devices are often made of thin films. Ideally, following the textbook description for quantum particles in a box, electrons confined in a perfectly uniform thin film are quantized into discrete energy levels in the vertical direction, forming standing-wave–like eigenstates, or quantum well states (QWSs), similar to the Fabry-Pérot modes in an optical interferometer (*1*, *2*). Such electron interference is very sensitive to film thickness and smoothness because of the very short wavelength of electron waves (~1 nm) and has been shown to modulate the electronic distribution near the Fermi level (E_F), thus substantially affecting the physical and chemical properties of a thin film (*3*, *4*). We report on the effect of electron-wave interference on the superconductivity property of two-dimensional (2D) thin films.

Traditionally, 2D thin-film superconductors are defined as those whose material size is less than the coherence length in one di-

[1]Beijing National Laboratory for Condensed Matter Physics, Institute of Physics, Chinese Academy of Sciences, Beijing 100080, China. [2]Department of Physics, University of Texas at Austin, Austin, TX 78712, USA. [3]Department of Physics, University of California at Berkeley, Berkeley, CA 94720, USA.

*These authors contributed equally to this work.
†To whom correspondence should be addressed. E-mail: qkxue@aphy.iphy.ac.cn

mension (*5*). For conventional superconductors such as Pb, the coherence length ξ_0 (83 nm for Pb) (*6*) is very large compared to atomic dimensions and the electron Fermi wavelength (λ_F ~1.06 nm). Therefore, 2D superconductors are still made of 3D electrons; only the condensate wave function for the Cooper pairs may be regarded as 2D. A common trend of such 2D superconductors is that the superconducting transition temperature (T_c) is continuously reduced as the film thickness is decreased. This reduction of T_c is caused by enhanced quantum fluctuations of the phase of the condensate wave function for thinner films (*7*, *8*). Oscillatory behavior in T_c from the quantum size effect (QSE) was suggested in early theoretical works (*9*, *10*), and experimental observation of such an effect was claimed in a study of thin Sn films (*11*). However, the observed T_c oscillations differed quantitatively from the theoretical predictions, and there was no corresponding oscillation in the normal-state resistivity as expected. These results were explained later (*12*, *13*) as due to QSEs in the grain structures of the films, which were typically polycrystalline and granular in nature. Conductance measurement of ultrathin Pb films on Si(111) showed clear variations in T_c, but the data were insufficient to establish an oscillating period (*14*).

We were able to grow ultrathin crystalline Pb films on Si(111) substrates with atomic-scale uniformity in thickness over a macroscopic area. We were therefore able to make transport measurements on the films and identify T_c as a function of the number of atomic layers in a well-controlled manner (*18*).

Scanning tunneling microscope (STM) topographic images are shown of the Pb films with 23 and 24 atomic monolayers (MLs) (Fig. 1), which typify the surface morphology of all the films discussed in this paper. The steps seen in the images originate from the Si substrate, and there is exactly the same number of Pb atomic layers on each terrace. Such high-quality films are crucial for electron coherence, because the wavelength of electrons in Pb is only 1.06 nm. We found that when the thickness was smaller than 22 MLs, only stable odd-layered films were obtained; the intervening even-layered films and the films thinner than 12 MLs tended to be rough. Such "magic" thicknesses are due to QWSs, whose discrete energy levels are known to strongly regulate the relative stability of such films (*15*–*17*). Above 21 MLs, we were able to achieve layer-by-layer growth with the perfect uniformity mentioned above.

One expects that with films of almost perfectly uniform thickness (Fig. 1), the electronic motion in the vertical direction should be frozen into a small number of quantized levels (QWSs), and motion in the horizontal directions should remain free. This is indeed

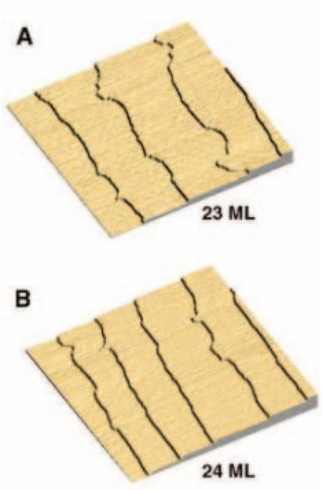

Fig. 1. Room temperature STM images (2000 × 2000 nm) of the Pb films at the completion of 23 (**A**) and 24 (**B**) MLs, grown at a deposition rate of 0.2 ML/min on Si(111) substrates held at 145 K. All the Pb films discussed in this paper exhibit essentially the same morphology.

observed. The thickness-dependent photoemission spectra measured in situ from these samples (Fig. 2) show clearly well-defined QWS peaks, which shift progressively in energy as the film thickness is increased by each atomic layer. In contrast, the spectrum for a film of 26.85 MLs, which deviates only slightly from the ideal case of 27 MLs, shows a considerable contribution from the spectrum of 26 MLs. The observation of the clean QWS peaks is therefore another good indication of the high quality of the films. Because the QWSs progress in energy as a function of film thickness, and because of the discrete nature of the film thickness, the position of the highest occupied QWS (marked by crosses) oscillates with respect to E_F (0.0 eV) between the odd and even layers. This is further confirmed by our first-principles calculations, which show the same oscillatory behavior with a higher density of states near E_F for the odd layers and lower ones for the even layers (*18*). According to our photoemission spectra, the total intensity (density of states) between neighboring even and odd layers changes by ~5, 10, and 20% within energy ranges of 10, 20, and 30 meV below the Fermi level, respectively (fig. S2). Because most physical properties such as transport and superconductivity depend strongly on the distribution of electrons near E_F, we expect that these properties will also be modulated as a function of film thickness.

Figure 3 shows T_c (black solid balls) as a function of film thickness. Here, T_c is defined as the temperature at which the film resistance becomes half of the normal-state resistance at T = 8 K, as indicated by the arrow in the inset of Fig. 3. We can see that

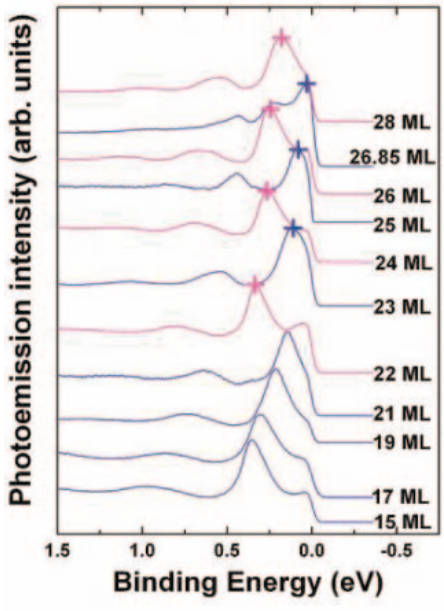

Fig. 2. Monolayer thickness–resolved normal-emission photoemission spectra of the Pb thin films measured in situ at 75 K. The crosses highlight the peaks of the highest occupied QWSs for the odd-layered (blue) and even-layered (pink) films, respectively, showing an oscillatory thickness dependence in the density of states near E_F (0.0 eV). The photoemission spectra were collected with a Gammadata Scienta SES-2002 analyzer with a HeI light source of 21.2 eV. arb., arbitrary.

there is an overall trend of increasing T_c with increasing film thickness, which is consistent with the behavior of conventional 2D superconductors. There is an oscillatory behavior in T_c above 21 MLs, with an oscillating period of 2 MLs, with a higher T_c for the even-numbered thicknesses and a lower T_c for the odd-numbered thicknesses. Monotonic behavior below 21 MLs is observed, but the intervening even layers are missing there.

According to the Bardeen-Cooper-Schrieffer (BCS) theory of superconductivity (*19*), T_c depends exponentially on the electron density of states $N(E_F)$ at the Fermi energy and on the phonon-mediated attractive interaction V between the electrons in the form of

$$T_c = 1.14T_D\exp[-1/N(E_F)V] \qquad (1)$$

where T_D is the Debye temperature characterizing the energies of the phonons. From Fig. 2, we know that the presence of QWSs can strongly modulate the density of states $N(E_F)$, and thus the oscillatory T_c should be closely related to the formation of QWSs in the films. For a system in which the QSE is involved, $N(E_F)$ oscillates as $N(E_F) = (m^*/\pi\hbar^2 t)[2t/\lambda_F]$, as a function of the film thickness t, where m^* is the effective mass of electrons, $\hbar$ is $(h/2\pi)$(where h is Planck's constant), and $[2t/\lambda_F]$ is the integer part of $2t/\lambda_F$ (*11*). In our case, the Fermi wavelength λ_F of Pb is

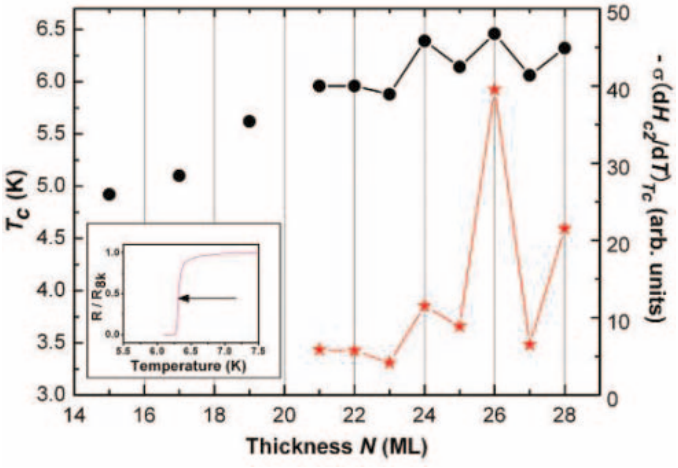

Fig. 3. T_c (black solid dots) and the density of states $N(E_F) \propto -\sigma(dHc_2/dT)_{T_c}$ (red stars) as a function of Pb film thickness, demonstrating a nonmonotonic oscillatory behavior in both T_c and $N(E_F)$. The inset shows the resistance as a function of temperature measured from the 28-ML film, which reveals a sharp transition to superconductivity at 6.32 K, as indicated by the arrow. The vertical scale is normalized with the resistance at 8 K. The measurements were carried out with a Quantum Design Magnetic Property Measurement System (MPMS-5).

about 4 MLs, which corresponds to an oscillating period of 2 MLs (*16*). When the film thickness fits to an integer multiple of half wavelength, resonance of QWSs occurs.

To further identify the role of the QWS-modulated density of states in T_c, we performed magnetoresistance measurements to estimate more accurately the density of states near the superconducting state. The photoemission data in Fig. 2 could not be directly used for this purpose for two reasons. First, those data were collected along the normal-emission direction (perpendicular to the sample surface), which is an incomplete measurement of the density of states. Second, those data were obtained in situ for the bare Pb films without Au coverage (T_c was obtained with an Au cap cover). Preliminary theoretical and experimental studies show that Au coverage can significantly shift the energy positions of the QWSs in the Pb films because of the change of boundary conditions. According to the Ginzburg-Landau-Abricosov-Gorkov theory, $N(E_F)$ of a Pb film is proportional to the slope of the upper critical field, H_{c2}, in its temperature dependence near T_c (*20*)

$$N(E_F) \propto -\sigma(dH_{c2}/dT)_{T_c} \qquad (2)$$

where σ is the normal-state conductivity. We measured the film resistance R as a function of applied magnetic field H along the surface-normal direction at different temperatures, and obtained H_{c2} as the magnetic field at which R reached half of the normal-state resistance at the onset point for the superconducting transition. In order to remove the influence from the Au cap layer, the normal-state relative conductivity of the Pb films was estimated from the resistance at T_c on the R-T curves. The measured value (red stars) of $-\sigma(dH_{c2}/dT)_{T_c}$, which is proportional to the density of states $N(E_F)$, is plotted in Fig. 2, and a one-to-one correspondence between the thickness dependence of $N(E_F)$ and T_c was observed (*21*).

The electron density of states is not the only factor affecting T_c. For a conventional superconductor such as Pb, electron-electron attraction, which is necessary for the binding of Cooper pairs, is ultimately due to electron-phonon interactions (*22*). As we mentioned earlier, QWSs strongly regulate the mechanical stability of films at different thicknesses, and they can cause expansion and shrinkage of interlayer spacing (*23*). Both of these facts indicate the possibility of modulating electron-phonon coupling by QSEs. Here we present more direct spectroscopic evidence of QSEs in electron-phonon coupling.

According to the more elaborate Eliashberg-McMillan theory (*24*), $\lambda = \frac{1}{2\pi k_B}\frac{d\Delta E}{dT}$ replaces $N(E_F)V$ in the BCS theory (Eq. 1) as the major parameter controlling T_c, where ΔE is the quasiparticle linewidth due to phonon broadening. We estimated ΔE from the QWS peak widths at high temperatures where phonon broadening dominates (*25*–*27*), and the QWS peaks were fitted by the Voigt profiles with the Lorentzian lineshape (fig. S3). We carried out variable temperature photoemission spectroscopy measurements for all stable films with thickness smaller than 25 MLs (fig. S4), and obtained λ (fig. S5) by the method described in (*26*). For thicknesses above 21 MLs, an oscillatory λ as a function of thickness was again seen. The overall similar oscillatory behavior and one-to-one correspondence in terms of the number of atomic layers in λ, $N(E_F)$, and T_c demonstrate that QWSs could greatly modulate the electron-phonon coupling as well. However, the relevance of the λ value, which is estimated from the QWSs at different binding energies, to T_c remains a question for further study.

Because the formation of QWSs greatly modulates electronic structure near the Fermi level of the films, we speculate that many other properties such as work function, friction force, thermal properties, electron mobility, Curie temperature (for magnetic materials), and catalytic properties can be modulated as well as superconductivity.

References and Notes

1. T.-C. Chiang, *Surf. Sci. Rep.* **39**, 181 (2000).
2. J. J. Paggel, T. Miller, T.-C. Chiang, *Science* **283**, 1709 (1999).
3. M. Jalochowski, E. Bauer, *Phys. Rev. B* **38**, 5272 (1988).
4. I. Vilfan, M. Henzler, O. Pfennigstorf, H. Pfnür, *Phys. Rev. B* **66**, 241306 (2002).
5. W. J. Skocpol, M. Tinkham, *Rep. Prog. Phys.* **38**, 1049 (1975).
6. J. Bardeen, J. R. Schrieffer, *Recent Developments in Superconductivity* (North-Holland, Amsterdam, 1991).
7. D. B. Haviland, Y. Liu, A. M. Goldman, *Phys. Rev. Lett.* **62**, 2180 (1989).
8. H. M. Jaeger, D. B. Haviland, B. G. Orr, A. M. Goldman, *Phys. Rev. B* **40**, 182 (1989).
9. J. M. Blatt, C. J. Thompson, *Phys. Rev. Lett.* **10**, 332 (1963).
10. M. Yu, M. Strongin, A. Paskin, *Phys. Rev. B* **14**, 996 (1976).
11. B. G. Orr, H. M. Jaeger, A. M. Goldman, *Phys. Rev. Lett.* **53**, 2046 (1984).
12. A. Paskin, M. Strongin, *Phys. Rev. Lett.* **55**, 139 (1985).
13. A. Frydman, *Phys. C* **391**, 189 (2003).
14. O. Pfennigstorf, A. Petkova, H. L. Guenter, M. Henzler, *Phys. Rev. B* **65**, 045412 (2002).
15. W. B. Su *et al.*, *Phys. Rev. Lett.* **86**, 5116 (2001).
16. M. H. Upton, C. M. Wei, M. Y. Chou, T. Miller, T.-C. Chiang, *Phys. Rev. Lett.* **93**, 026802 (2004).
17. Z. Zhang, Q. Niu, C. K. Shih, *Phys. Rev. Lett.* **80**, 5381 (1998).
18. Materials and methods are available as supporting material on *Science* Online.
19. J. Bardeen, L. N. Cooper, J. R. Schrieffer, *Phys. Rev.* **108**, 1175 (1957).
20. M. V. Sadovskii, *Superconductivity and Localization* (World Scientific Publishing, Singapore, 2000).
21. For the ex situ transport measurements, ~4 MLs of Au was deposited on clean Pb thin films in a molecular beam epitaxy chamber to avoid air contamination. The Au film can also grow in layer-by-layer mode, and the surface morphology after Au deposition, which is shown by our STM data, is essentially the same as that of the Pb film shown in Fig. 1. The critical transition temperature T_c at zero magnetic field extrapolated from the H_{c2}-T curve shows the same oscillatory behavior as the T_c value in the R-T measurement. The results from the magnetic and resistance measurements are consistent, so that the effects from the Au cover layer are eliminated.
22. B. Allen, R. C. Dynes, *Phys. Rev. B* **12**, 905 (1975).
23. A. Crottini *et al.*, *Phys. Rev. Lett.* **79**, 1527 (1997).
24. G. Grimvall, *The Electron-Phonon Interaction in Metals* (North-Holland, Amsterdam, 1981).
25. J. J. Paggel, D.-A. Luh, T. Miller, T.-C. Chiang, *Phys. Rev. Lett.* **92**, 186803 (2004).
26. D.-A. Luh, T. Miller, J. J. Paggel, T.-C. Chiang, *Phys. Rev. Lett.* **88**, 256802 (2002).
27. T. Balasubramanian, E. Jensen, X. L. Wu, S. L. Hulbert, *Phys. Rev. B* **57**, R6866 (1998).

28. The work at the Chinese Academy of Sciences was supported by the National Science Foundation and the Ministry of Science and Technology of China. Q.N. was supported by NSF through grant no. DMR-0306239 and by the Welch Foundation.

Supporting Online Material

www.sciencemag.org/cgi/content/full/306/5703/1915/DC1
Materials and Methods
Figs. S1 to S5

10 September 2004; accepted 25 October 2004
10.1126/science.1105130

Transient Uplift After a 17th-Century Earthquake Along the Kuril Subduction Zone

Yuki Sawai,[1]* Kenji Satake,[1] Takanobu Kamataki,[1] Hiroo Nasu,[1,2] Masanobu Shishikura,[1] Brian F. Atwater,[3] Benjamin P. Horton,[4] Harvey M. Kelsey,[5] Tamotsu Nagumo,[6] Masaaki Yamaguchi[7]

In eastern Hokkaido, 60 to 80 kilometers above a subducting oceanic plate, tidal mudflats changed into freshwater forests during the first decades after a 17th-century tsunami. The mudflats gradually rose by a meter, as judged from fossil diatom assemblages. Both the tsunami and the ensuing uplift exceeded any in the region's 200 years of written history, and both resulted from a shallow plate-boundary earthquake of unusually large size along the Kuril subduction zone. This earthquake probably induced more creep farther down the plate boundary than did any of the region's historical events.

Large shallow earthquakes at subduction zones commonly warp Earth's surface. Although the most dramatic deformation accompanies the earthquakes, additional, transient warping can follow in response to fault creep, mantle relaxation, or both (*1*). Small postseismic transients at subduction zones have produced days, weeks, months, or even years of horizontal motion detectable by satellite geodesy (*2*–*4*). The largest recorded transients, induced by giant earthquakes during the 1960s in Chile and Alaska, continue today and have thus far produced as much as a meter or two of gradual coastal uplift, according to eyewitnesses, tide gauges, and estuarine ecology (*5*–*9*).

Postseismic uplift has a long-recognized potential for resolving a glaring conflict between geologic uplift and geodetic subsidence along the Kuril subduction zone. The subduction zone conveys the Pacific plate beneath Asia at rates averaging 8 to 9 m per century (*10*) (Fig. 1A). In eastern Hokkaido, 60 to 80 km above the top of the subducting plate, uplifted marine terraces somehow coexist with subsiding tide gauges and bench marks. The geology requires 20 to 50 m of net uplift in the past 125,000 years (*11*), but the geodesy shows as much as 1 m of subsidence in the past 100 years (*12*, *13*). The subsidence probably results from subduction; currently locked to the overriding plate (*14*), the subducting Pacific plate drags eastern Hokkaido downward. In 1973, when a shallow earthquake of moment magnitude (M_w) 7.8 broke the plate boundary offshore (Fig. 1B), geophysicists expected decimeters of rebound (*15*, *16*). However, no onshore uplift coincided with the earthquake and less than 0.1 m followed (*17*). Similarly, an adjacent earthquake of M_w 8.0 in 2003 was accompanied by onshore subsidence and was followed by just centimeters of onshore uplift (*18*). Little, if any, other uplift is known from the rest of eastern Hokkaido's written history, which includes an earthquake of M_w 8.2 in 1952 (*19*) and several other magnitude-8 events from the past 200 years (*20*).

Eastern Hokkaido's geologic history of the past 3000 years, however, indicates episodic uplift perhaps related to unusually large earthquakes. The uplift, which repeatedly changed muddy estuaries into lowland forests, amounted to about 1 m per episode (*21*–*23*). The outsize earthquakes, inferred from unusually large tsunamis that spread sand kilometers inland, probably resulted from seismic ruptures at least twice as long as those in 1973 and 2003 (*24*). Both for the episodic uplift and the outsize earthquakes, hundreds of years elapsed between events, and the most recent event occurred in the 17th century. Do unusually large plate-boundary earthquakes provide the long-sought mechanism for eastern Hokkaido's terrace uplift?

We address this question by using stratigraphy and paleoecology to learn whether the 17th-century uplift episode shortly followed the outsize 17th-century tsunami. The tsunami deposited a sand sheet, commonly 10 cm thick, on lowlands along the open Pacific coast. The sheet was previously unknown from the sheltered arms of estuaries where the 17th-century uplift is recorded by an upward change from tidal mud to forest peat. We recently found tsunami sand sheets within such mud-to-peat sequences at two estuaries beside the Pacific coast: Mochirippu (Fig. 2), described below, and the south end of Kiritappu marsh, described in supporting material (*25*) (fig. S1).

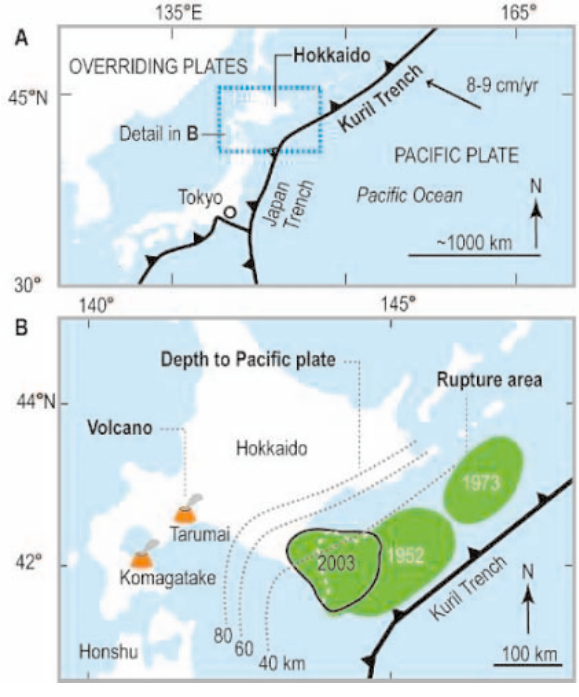

Fig. 1. Study area. (**A**) Kuril and Japan trenches. (**B**) Hokkaido, showing volcanoes responsible for tephra layers in Fig. 2 (*26*), depths to the Pacific plate (*37*), and rupture areas of instrumentally recorded earthquakes on the plate boundary off eastern Hokkaido (*4*, *19*, *28*). Heavy lines in (A) and (B) denote seafloor trenches, which mark seaward edges of subduction zones; triangles point down the fault plane.

[1]Active Fault Research Center, Geological Survey of Japan, National Institute of Advanced Industrial Science and Technology, Site C7 1-1-1 Higashi, Tsukuba 305-8567, Japan. [2]International Research Center for Japanese Studies, 3-2 Oeyama-cho, Goryo, Nishikyo-ku, Kyoto, 610-1192, Japan. [3]U.S. Geological Survey, University of Washington, Seattle, WA 98195–1310, USA. [4]Sea Level Research Laboratory, Department of Earth and Environmental Sciences, University of Pennsylvania, Philadelphia, PA 19104–6316, USA. [5]Department of Geology, Humboldt State University, Arcata, CA 95521, USA. [6]Department of Biology, The Nippon Dental University, Fujimi, Chiyoda-ku, Tokyo 102-8159, Japan. [7]Graduate School of Frontier Science, The University of Tokyo, 7-3-1 Hongo, Bunkyo-ku, Tokyo 113-0033, Japan.

*To whom correspondence should be addressed. E-mail: yuki.sawai@aist.go.jp

Mochirippu consists of a bay and fringing tidal marshes that together extend 3 km inland from a narrow inlet through a beach berm (Fig. 2A). In dozens of cores 2.0 to 2.5 km inland from the beach, we found no sand from historical tsunamis. However, we consistently found two prehistoric tsunami sand sheets (Figs. 2B). The younger sheet, mainly 2 to 5 cm thick, is widely bounded by mud that contains tidal-flat diatom assemblages (Fig. 2, C and D). As much as 5 cm of mud overlies the younger sheet. This mud grades upward into peat that formed on a forest floor. Dates of regional volcanic-ash layers (*26*) show that the tidal flat changed into the forest by 1667 and that the forest persisted through 1739 (Fig. 2C).

We quantify this 17th-century emergence at Mochirippu, and elsewhere, by means of diatom assemblages that we relate to modern environments through transfer functions (*25*, *27*). The results imply several decimeters of gradual pre-tsunami subsidence, no detectable change around the time of the tsunami, and at least 1 m of subsequent uplift (Fig. 2D). The uplift began around the time of the tsunami (which has not been dated exactly), continued to 1667, and ended by 1694. A core from the southern Kiritappu marsh shows a similar uplift history (fig. S1), as do sites elsewhere in eastern Hokkaido (red triangles in Fig. 3A). Written records provide evidence against more than 2 m of 17th-century uplift at Akkeshi-ko (*23*).

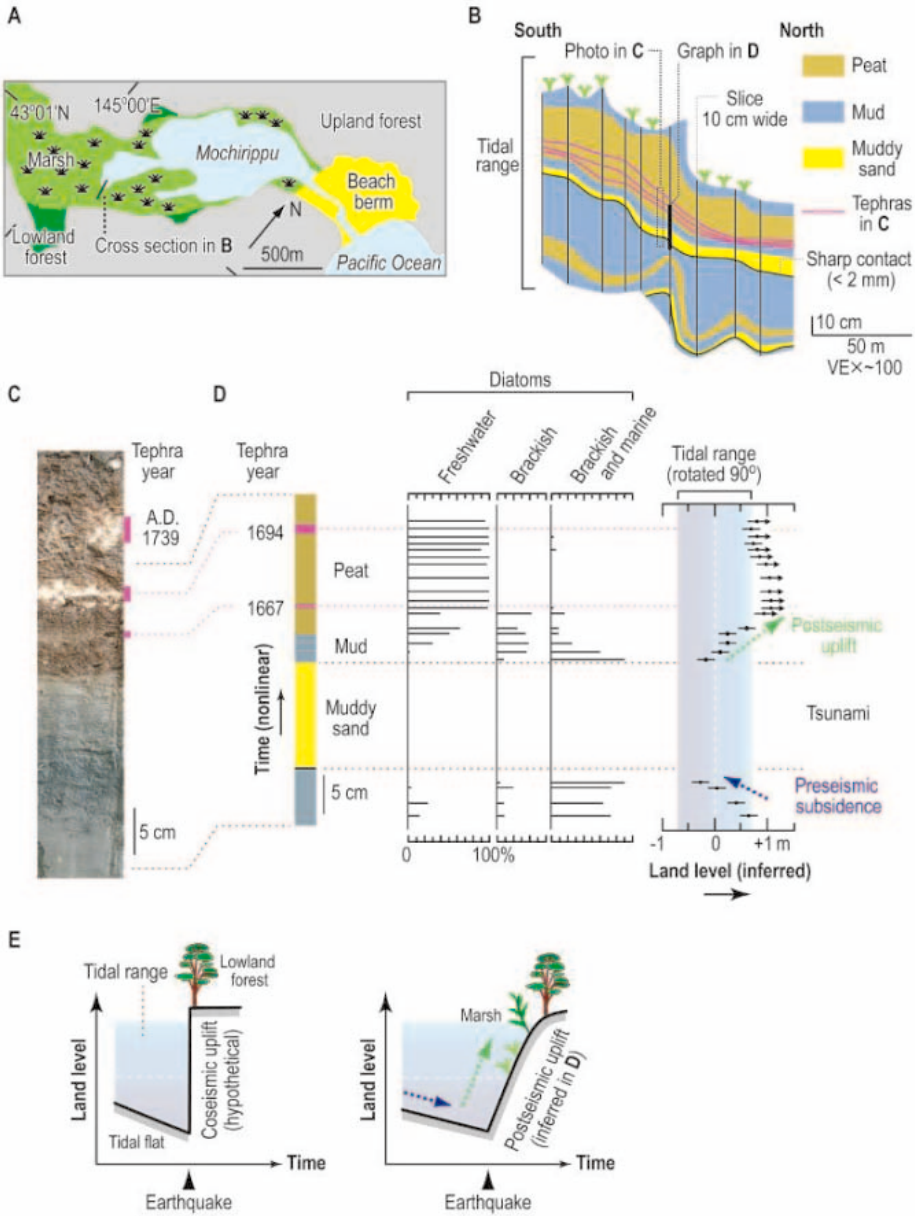

Fig. 2. Geologic evidence for postseismic coastal uplift at Mochirippu (location, Fig. 3A). (**A**) Index map. (**B**) Stratigraphic cross section. (See figs. S1 and S2 for additional cross sections.) (**C**) Example of change from tidal-flat mud to lowland-forest peat, punctuated by a tsunami deposit and by volcanic-ash layers. (**D**) Land-level changes inferred from diatom assemblages in a core near the one in (C). Stratigraphy (left) and relative abundance of diatoms, which are grouped by ecology, in a core near the one in (C) (middle), and land-level changes inferred from the diatom assemblages (right). Error bars for height estimates span 2 SD. Arrow in (D) denotes limiting-minimum height estimated from diatom assemblage typical of lowland forests above high tides (*27*). (**E**) Changes in land level and depositional environment in response to coseismic uplift (left) and postseismic uplift (right).

Stratigraphy and paleoecology thus imply that a 17th-century earthquake off eastern Hokkaido generated both an outsize tsunami and an ensuing episode of gradual coastal uplift. Had the earthquake accompanied the uplift, the tsunami would have coincided with an abrupt change from tidal flat to lowland forest (Fig. 2E, left). Instead, the uplift happened gradually in the first decades after the tsunami (Fig. 2E, right).

How did the 17th-century earthquake induce uplift that historical earthquakes failed to trigger? In the most likely series of events, an unusually large earthquake broke the plate boundary offshore, and this rupture induced unusual amounts of postseismic slip farther down the plate boundary, beneath eastern Hokkaido. Satellite geodesy suggests that the plate boundary is currently locked beneath most of the continental shelf and slope. Modeled for an elastic Earth, the locked zone extends down the plate boundary to a depth of 55 km (*14*). The 1973 rupture broke this part of the plate boundary no deeper than about 30 km (*28*), and the 1952 and 2003 ruptures reached depths of 50 km along only a few tens of kilometers of rupture length (Fig. 1B). The 17th-century uplift, however, followed an earthquake that probably broke the combined areas of the 1952 and 1973 ruptures, for a rupture length of at least 300 km (*24*). We assume that such widespread rupture, if it reached the lower limit of the locked zone, would release the plate boundary for afterslip farther downdip, beneath eastern Hokkaido. In addition, because uplift usually occurs above the area of slip on a thrust fault (*29*), meters of plate-boundary creep beneath eastern Hokkaido should raise the coast, as simulated by the simple dislocation model in Fig. 3, B and C (*30*, *31*). Such afterslip, on a much smaller scale, probably generated Hokkaido's postseismic uplift in 2003 (*4*, *18*).

Relaxation of stress in the continental mantle also may have contributed to eastern Hokkaido's 17th-century uplift. During a shallow plate-boundary earthquake, seaward displacement of the overriding plate stresses the mantle wedge behind and below it. The mantle, as a viscoelastic material, then catches up with this displacement by flowing seaward and upward beneath the coast (*1*). This kind of deep deformation, be-

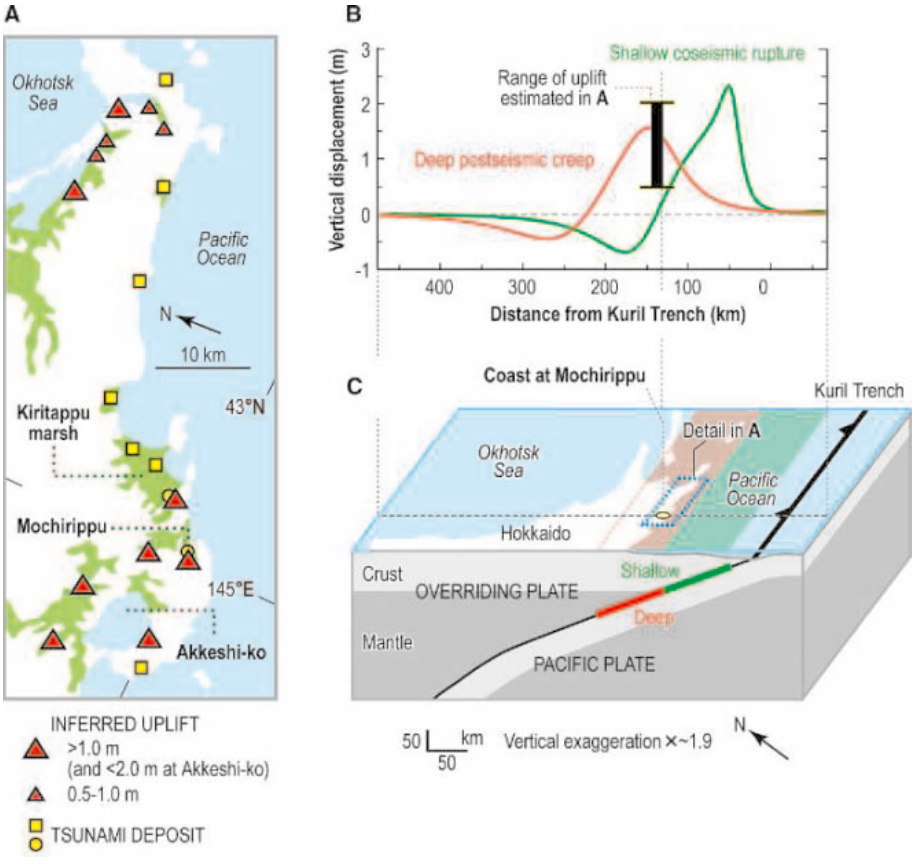

Fig. 3. Afterslip hypothesis for eastern Hokkaido. (**A**) Distribution of 17th-century evidence for an unusually large tsunami (yellow) and uplift (red). Tsunami sites shown by squares are from Nanayama *et al*. (*24*); circles, this study. Uplift amounts were estimated as in Fig. 2D and fig. S3C. (**B**) Vertical displacement computed by elastic-dislocation modeling (*29*) of fault slip assumed in (C). (**C**) Modeled slip at the plate boundary (front panel) and corresponding areas of computed uplift at Earth's surface (color bands viewed obliquely). Green, shallow seismic rupture of the interseismic locked zone (*14*) at 15 to 55 km depth. Red, deep afterslip at 55 to 85 km, downdip from full interplate coupling. Uplift profiles in (B).

lieved to be going on today in the region of the 1960 Chile earthquake, can be difficult to distinguish observationally from afterslip (*32*).

Do the postseismic effects of outsize earthquakes produce enough uplift to negate interseismic subsidence in eastern Hokkaido? An uplift deficit persists if the interseismic subsidence accumulates at nearly 1 m per 100 years and if the postseismic uplift averages just 1 to 2 m in 500 years. However, a definitive answer will require a clear picture of entire deformation cycles between outsize earthquakes. That picture will depend on the interseismic subsidence rates (*33*, *34*), land-level changes that accompany the outsize earthquakes, the size and duration of ensuing transients, the coseismic and postseismic effects of lesser earthquakes, and the recurrence intervals of the various earthquakes themselves.

References and Notes

1. K. Wang, in *The Seismogenic Zone Experiment*, T. Dixon, Ed. (Columbia Univ. Press, New York, in press).
2. K. Heki, S. Miyazaki, H. Tsuji, *Nature* **386**, 595 (1997).
3. T. I. Melbourne, F. H. Webb, J. M. Stock, C. Reigher, *J. Geophys. Res.* **107**, 2241 (2002); http://dx.doi.org/10.1029/2001JB000555.
4. S. Ozawa, M. Kaidzu, M. Murakam, T. Imakiire, Y. Hatanaka, *Earth Planets Space* **56**, 675 (2004).
5. S. E. Barrientos, G. Plafker, E. Lorca, *Geophys. Res. Lett.* **19**, 701 (1992).
6. S. C. Cohen, J. T. Freymueller, *J. Geophys. Res.* **102**, 20479 (1997).
7. Y. Zong, I. Shennan, R. A. Combellick, S. L. Hamilton, M. M. Rutherford, *Holocene* **13**, 7 (2003).
8. J. P. Guilbault, J. J. Clague, M. Lapointe, *Quat. Sci. Rev.* **15**, 913 (1996).
9. Uplift since the 1964 Alaska earthquake, known mainly from tide-gauge records (*6*), is also evident as changes in diatom and pollen assemblages of estuarine deposits (*7*). Similarly, postseismic uplift induced by the 1700 Cascadia earthquake has been inferred from foraminifera (*8*). In both cases, and also in southwest Japan (*10*), the uplift occurred in areas that subsided during the earthquake, and the amount of coseismic subsidence exceeded the amount of postseismic uplift. The 17th-century uplift in eastern Hokkaido, by contrast, more nearly resembles the postseismic uplift in Chile (*5*) insofar as the Chilean uplift occurred arcward of the area of coseismic subsidence.
10. C. DeMets, *J. Geophys. Res.* **97**, 17,615 (1992).
11. K. Okumura, *Geog. Rep. Tokyo Metrop. Univ.* **31**, 19 (1996).
12. K. Shimazaki, *Phys. Earth Planet. Inter.* **8**, 148 (1974).
13. S. Ozawa, M. Hashimoto, T. Tada, *Bull. Geog. Surv. Inst.* **43**, 1 (1997).
14. S. Mazzotti, X. Le Pichon, P. Henry, S.-I. Miyazaki, *J. Geophys. Res.* **105**, 13159 (2000).
15. K. Shimazaki, *Phys. Earth Planet. Inter.* **9**, 314 (1974).
16. K. Kasahara, *Pure Appl. Geophys.* **113**, 127 (1975).
17. K. Kasahara, T. Kato, *Pure Appl. Geophys.* **119**, 392 (1980/1981).
18. Y. Yamanaka, M. Kikuchi, *Earth Planets Space* **55**, e21 (2003).
19. K. Hirata, E. L. Geist, K. Satake, Y. Tanioka, S. Yamaki, *J. Geophys. Res.* **108**, 2196 (2003); http://dx.doi.org/10.1029/2002JB001976.
20. An offshore earthquake in 1894 was followed, between 1894 and 1905, by as much as 0.2 m of coastal uplift in easternmost Hokkaido (*15*, *16*). This estimate is based on incomplete records of a tide gauge.
21. Y. Sawai, *Quat. Res.* **56**, 231 (2001).
22. Y. Sawai, H. Nasu, Y. Yasuda, *J. Quat. Sci.* **17**, 602 (2002).
23. B. F. Atwater *et al.*, *Holocene* **14**, 487 (2004).
24. F. Nanayama *et al.*, *Nature* **424**, 660 (2003).
25. Materials and methods are available as supporting material on *Science* Online.
26. R. Furukawa, M. Yoshimoto, K. Yamagata, K. Wada, T. Ui, *Kazan* **42**, 269 (1997).
27. Y. Sawai, B. P. Horton, T. Nagumo, *Quat. Sci. Rev.* **23**, 2467 (2004); http://dx.doi.org/10.1016/j.quascirev.2004.05.006.
28. A. Nakanishi *et al.*, *J. Geophys. Res.* **109**, 5305 (2004); http://dx.doi.org/10.1029/2003JB002574.
29. J. C. Savage, *J. Geophys. Res.* **88**, 4984 (1983).
30. Y. Okada, *Bull. Seismol. Soc. Am.* **75**, 1135 (1985).
31. Vertical displacement of ground surface was computed for a dislocation model (*29*) in which the fault extends from 15 to 55 km depth on the subducting plate (dip angle 20°) for coseismic rupture and 55 to 85 km depth for deep postseismic creep. The average coseismic slip is 5 m (*23*), and the same amount is assumed for the deep postseismic slip.
32. Y. Hu, K. Wang, J. He, J. Klotz, G. Khazaradze, *J. Geophys. Res.*, in press.
33. The estimate of nearly 1 m per 100 years exaggerates eastern Hokkaido's 20th-century subsidence. At the region's two tide gauges, Hanasaki and Kushiro, the Pacific coast sank relative to the sea by 8 to 9 mm/year on average from 1958 to 1995 (*13*). However, sea level in northeast Japan has risen more than 2 mm/year, on average, in the past few decades (*35*, 36). Subtraction of sea-level rise from the tide-gauge rates decreases the amount of terrace uplift that remains to be explained.
34. Subduction erosion may also contribute to modern subsidence in eastern Hokkaido (*36*). However, if it has occurred steadily throughout the late Quaternary, subduction erosion does not diminish the amount of uplift needed to raise the region's marine terraces.
35. A. Cazenave, R. S. Nerem, *Rev. Geophys.* **42**, RG3001 (2004).
36. K. Heki, *Earth Planet. Sci. Lett.* **219**, 13 (2004).
37. K. Katsumata, N. Wada, M. Kasahara, *J. Geophys. Res.* **108**, 2565 (2003); http://dx.doi.org/10.1029/2002JB002175.

38. We thank K. Wang for improving the geophysical model, B. Sherrod for field help, J. Bourgeois, J. Clague, T. Kato, T. Sagiya, K. Shimazaki, H. Sekiguchi, Y. Tanioka, W. Thatcher, S. Toda, K. Wang, and two anonymous referees for reviews and E. Davis, A. J. Long, and I. Shennan for discussion. Part of the work was supported by grants from the Japanese Ministry of Education, Science, and Culture (nos. 10007549 and 13007536) to Y.S. Authors are grouped by affiliation in the by-line. Their responsibilities: field work, Y.S., T.K., H.N., M.Y.; diatom analysis, Y.S., T.N., B.H.; afterslip model, K.S., H.K.; manuscript preparation, B.A., K.S., Y.S.

Supporting Online Material

www.sciencemag.org/cgi/content/full/306/5703/1918/DC1
Materials and Methods
Fig. S1
References

7 September 2004; accepted 10 November 2004
10.1126/science.1104895

Organic Aerosol Growth Mechanisms and Their Climate-Forcing Implications

Steven F. Maria,[1] Lynn M. Russell,[3]* Mary K. Gilles,[4] Satish C. B. Myneni[2,5]

Surface- and volume-limited chemical reactions on and in atmospheric aerosol particles cause growth while changing organic composition by 13 to 24% per day. Many of these particles contain carbonaceous components from mineral dust and combustion emissions in Africa, Asia, and North America and reveal reaction rates that are three times slower than those typically used in climate models. These slower rates for converting from volatile or hydrophobic to condensed and hygroscopic organic compounds increase carbonaceous particle burdens in climate models by 70%, producing organic aerosol climate forcings of as much as –0.8 watt per square meter cooling and +0.3 watt per square meter warming.

Aerosol particles enter Earth's atmosphere by direct emission of particles and by condensation of vapor-phase species. Heterogeneous and multiphase reactions in the atmosphere change chemical and physical properties of aerosol particles, but these processes are not understood well enough to predict accurately the evolution of the gas and particle-phase composition of the troposphere (*1*). Carbonaceous aerosol particles compose ~37% of global submicrometer particle emissions (*2*), yet climate models have used an oxidation reaction rate equivalent to 60% of organic particle mass per day for these particles because atmospheric observations have not been available (*3*, *4*). This assumption controls the associated lifetime, burden, and climate forcing predicted for atmospheric carbonaceous particles.

Because gas-to-particle conversion and heterogeneous chemistry control the composition of carbonaceous particles in ways that are poorly understood, the organic composition of atmospheric particles is also not well known (*5*). The oxidation of vapor-phase organic compounds, in which the number of alkyl bonds is reduced and the number of alcohol and carbonyl bonds is increased, produces compounds that may have sufficiently low vapor pressures to condense onto preexisting particle surfaces to form secondary organic aerosol (SOA). This condensation pathway accounts for an estimated 10% of global organic aerosol (*4*) and increases the fractional concentrations of the condensing species more rapidly for smaller than for larger particles because of larger surface area–to–volume ratios in smaller particles.

Condensed organic compounds originating from the vapor phase or from direct particulate emissions can become oxidized through heterogeneous reactions that are surface-limited or volume-limited (*6*). Typically these mechanisms are represented by a single lumped rate in climate models (*4*). Mixtures of large molecular-weight organic compounds with elemental carbon are also oxidized by atmospheric reactions. Volume-limited oxidation occurs when particle-phase diffusion of reactants is fast compared with the kinetics of chemical reaction. A uniform reaction extent results in an equally increased carbonyl carbon concentration for all particles regardless of size. Surface-limited oxidation may indicate efficient surface reactivity or highly viscous or solid aerosols, and the localization of the reaction at the surface results in larger concentrations of carbonyl carbon for smaller aerosol particles with larger surface area–to–volume ratios than for larger particles. Condensation of organic compounds from the gas phase to the particle phase, oxidation of those organic compounds on particles surfaces, and oxidation of compounds that have diffused into particle volumes, as well as combina-

[1]Department of Chemical Engineering, [2]Department of Geosciences, Princeton University, Princeton, NJ 08544, USA. [3]Scripps Institution of Oceanography, University of California San Diego, La Jolla, CA 92093, USA. [4]Chemical Sciences Division, [5]Advanced Light Source, Lawrence Berkeley National Laboratory, Berkeley, CA 94720, USA.

*To whom correspondence should be addressed. E-mail: lmrussell@ucsd.edu

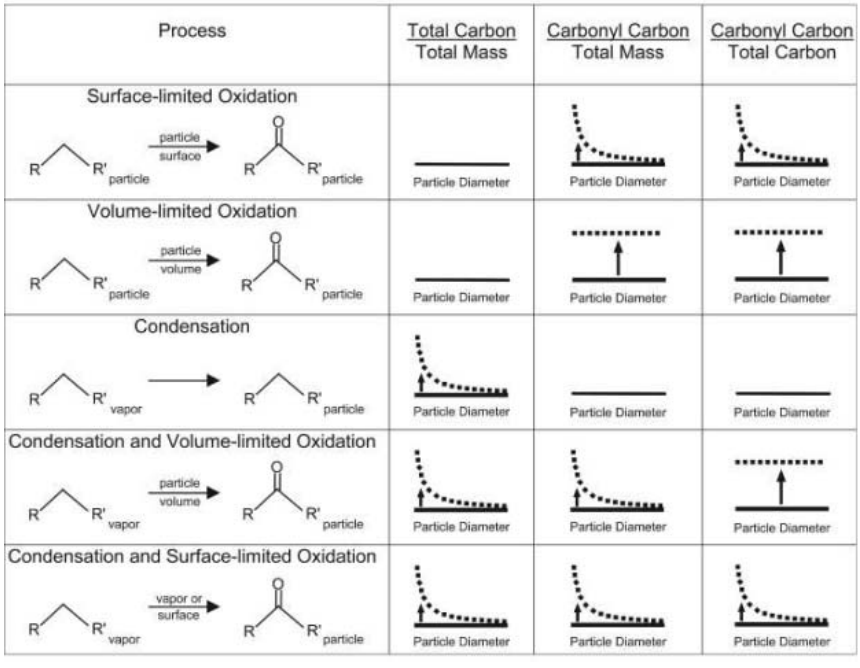

Fig. 1. Theoretical diagrams showing the effects of five oxidation and condensation mechanisms on organic mass composition ratios as functions of particle diameter. In each diagram, the vertical axis represents a unitless ratio and the horizontal axis represents particle size with diameters increasing toward the right for the size range from 0.4 to 5 μm in diameter. The exact size scale for each diagram varies with atmospheric parameters including processing time, temperature, and vapor-phase concentrations of the reacting or condensing species. Condensation, volume-limited oxidation, and surface-limited oxidation mechanisms can be distinguished with use of the three STXM variables shown here: the total carbon–to–total mass ratio, the carbonyl carbon–to–total mass ratio, and the carbonyl carbon–to–total carbon ratio. In all diagrams, R and R′ indicate aliphatic chains, hydrogen atoms, or alcohol groups. Subscripts refer to the reactant phase, and arrow labels indicate the reaction phase where oxidation occurs. Condensation followed by surface-limited vapor-phase reaction has the same organic composition dependence on size as the condensation of oxygenated organic compounds oxidized in the vapor phase. The particle-phase reaction of vapor-phase reactants can occur if vapor-phase reactants absorb or condense onto aerosol particles before reacting.

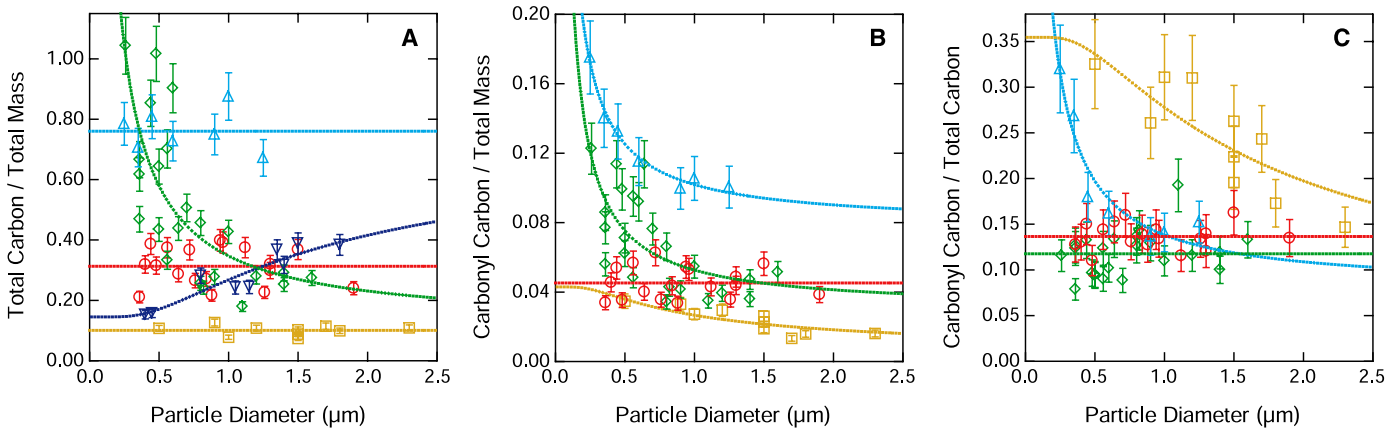

Fig. 2. For individual particles, the (**A**) total carbon–to–total mass ratio, (**B**) carbonyl carbon–to–total mass ratio, and (**C**) carbonyl carbon–to–total carbon ratio are shown as a function of particle diameter. Light blue triangles represent the organic mode of Asian mixed combustion aerosol particles collected during the Aerosol Characterization Experiment (ACE)–Asia project over the Sea of Japan on 27 April 2001, dark blue inverted triangles [only in (A)] represent the sulfate mode of Asian mixed combustion aerosol particles collected over the Sea of Japan on 27 April 2001, brown squares represent African mineral dust collected over the Caribbean Sea on 21 July 2000, red circles represent eastern U.S. combustion particles collected in New Jersey under clear conditions on 12 August 2003, and green diamonds represent eastern U.S. combustion particles collected in New Jersey under foggy conditions on 7 August 2003. Error bars represent the uncertainty associated with the calibration from absorbance ratios to mass ratios. Dotted lines represent curve fits to the data. The sulfate mode of the Asian mixed combustion particles has been removed from (B) and (C) because the large variability associated with this mode masks any underlying atmospheric processes. These particles did not show a dependence of organic composition with size that was consistent with any single dominant condensation or oxidation mechanism.

tions of these processes, are summarized (Fig. 1). The reaction mechanisms and the phase origin of the reactants can be distinguished by using size-resolved aerosol chemical composition measurements of organic functional groups.

Soft x-ray spectromicroscopy studies in the transmission mode (scanning transmission x-ray microscopy, or STXM) can detect organic functional groups within individual particles with a resolution below 0.1 μm (*7*). By using this technique, data from four atmospheric aerosol samples (Asian mixed combustion over the Sea of Japan, African mineral dust over the Caribbean Sea, and U.S. combustion in New Jersey) were analyzed (Fig. 2). Details for each sample are also summarized (Fig. 3). For each aerosol sample, two-dimensional maps of particle composition and morphology were compiled from STXM measurements (*8*). In Fig. 2, STXM absorbance ratios were converted to absolute mass ratios by using the Fourier transform infrared–measured compositions of simultaneously collected bulk submicrometer aerosol samples for calibration (*9*). Spatial distributions of measured composition ratios (Fig. 4) illustrate four different particle morphologies and mixing states. The four samples provide examples of the aerosol organic reaction mechanisms described in Fig. 1.

Evidence of surface-limited oxidation is reflected in the chemical composition of Asian mixed combustion aerosol collected at 1500 m over the Sea of Japan. This sample contains two aerosol modes evident from the particle maps in Fig. 4, A and B, and the total carbon–to–total mass ratio in Fig. 2A: a carbonaceous mode and a mode containing

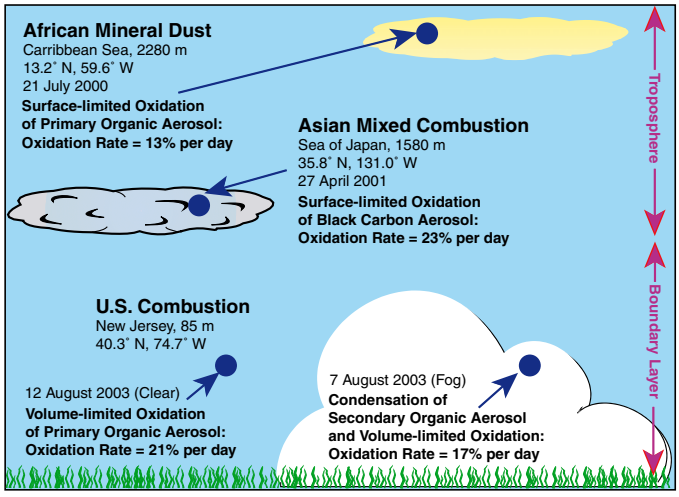

Fig. 3. Source type, STXM composition, and mechanism information for the four aerosol samples. All compositions are mass-average values from single-particle measurements. The Asian mixed combustion aerosol included two distinct modes, and the STXM results shown here are for the organic mode only. The oxidation rate in mass percent per day was calculated by using back trajectories to estimate aerosol age and assuming a primary carbonyl–to–total carbon ratio of 10%. This value was chosen by extrapolating time since emission and composition data for the four aerosol samples to the time of emission.

very low carbon concentrations. The carbonaceous mode composition has a size dependence in Fig. 2, B and C, and does not in Fig. 2A, consistent with a surface-limited oxidation mechanism (Fig. 1). The lack of size dependence of the total carbon–to–total mass ratio suggests that organic compounds were incorporated in the particle phase before the particles were emitted from their sources.

In the Asian mixed combustion particles, the strong absorption by carbon-carbon double bonds is consistent with products of incomplete combustion including polycyclic aromatic hydrocarbons and graphitic elemental carbon, components whose light-absorbing properties have earned the popular appellation of black carbon (abbreviated in this work as BC). The particles were sampled in dry conditions more than 30 hours after emission (*8*) and may have been crystalline or amorphous solids. Particle composition is consistent with an oxidation rate of 24% of carbon mass per day, increasing the carbonyl–to–total carbon ratio by 5.5% per day. In Fig. 4H, the organic mode particles have larger carbonyl carbon–to–total carbon ratios at particle edges, with ratios near 0.2 occurring exclusively in edge regions. Bulk filter analysis shows that the Asian mixed combustion submicrometer particles consist of organic compounds and sulfate with substantial BC and almost no dust (*10*). The mode with low carbon concentrations is probably largely sulfate. Particles from both modes are

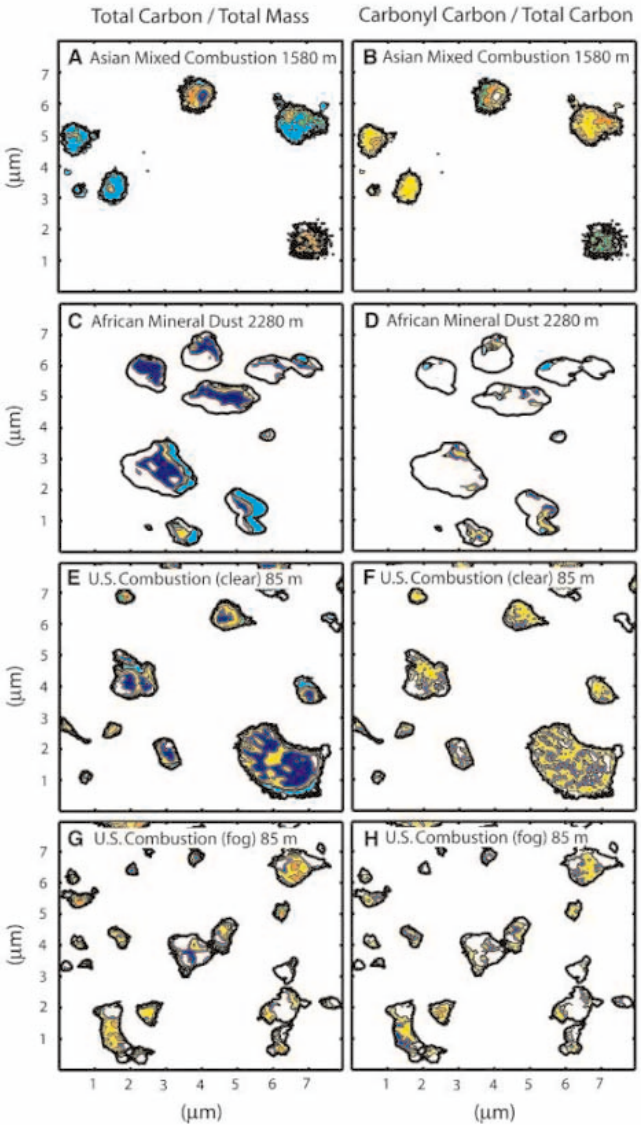

Fig. 4. Two-dimensional spectrally resolved maps of organic composition for particles representative of the four aerosol samples shown in Fig. 2. The total carbon–to–total mass ratios are plotted [(**A**),(**C**),(**E**), and (**G**)], demonstrating ratios of 0.02 to 0.2 (dark blue), 0.2 to 0.4 (yellow), 0.4 to 0.6 (orange), 0.6 to 0.8 (green), and >0.8 (light blue). The carbonyl–to–total carbon ratio is plotted [(**B**), (**D**), (**F**), and (**H**)], demonstrating ratios of 0.02 to 0.08 (dark blue), 0.08 to 0.16 (yellow), 0.16 to 0.24 (orange), 0.24 to 0.32 (green), and >0.32 (light blue). For chemically heterogeneous particles, regions of enhanced carbon and carbonyl concentrations can be identified as orange, green, or light blue areas in the plots shown here. The samples shown are [(A) and (B)] Asian combustion over the Sea of Japan on 27 April 2001, [(C) and (D)] African mineral dust over the Caribbean Sea on 21 July 2000, [(E) and (F)] eastern U.S. combustion in New Jersey on 12 August 2003, and [(G) and (H)] eastern U.S. combustion during fog in New Jersey on 7 August 2003. For all panels, black outlines indicate regions where the total mass is above the detection limit. The total mass detection limit and the particle edges are effectively coincident to within the precision of the STXM measurement. White regions indicate that total carbon or carbonyl carbon signatures are below detection.

evident in Fig. 4A, with the low carbon mode containing 20 to 40% carbon by mass. The total carbon–to–total mass ratio of the low carbon mode increases with size (Fig. 2A).

Surface-limited oxidation signatures are also evident in the African mineral dust sample collected in the lower troposphere over the Caribbean Sea (*11*). The size dependence of the dust composition is similar to that of the carbonaceous mode of the Asian mixed combustion aerosol, providing evidence of surface-limited oxidation reactions without condensation processes (compare Fig. 2 to Fig. 1). The carbonyl carbon–to–total carbon ratio and the carbonyl carbon–to–total mass ratio both increase with decreasing particle size (Fig. 2, B and C), and the total carbon–to–total mass ratio is independent of particle size (Fig. 2A). The carbonyl carbon–to–total mass ratio is near 0.04 for 0.5-μm-diameter particles and 0.02 for 2.0-μm-diameter particles, whereas the carbonyl carbon–to–total carbon ratio is near 0.3 for 0.5-μm-diameter particles and 0.2 for 2.0-μm-diameter particles. Surface-limited heterogeneous reactions have been reported previously in laboratory measurements on dust, including the uptake of acetaldehyde on mineral oxides (*12*), consistent with the observations for these particles.

The constant value of the total carbon–to–total mass ratio across all particle sizes (Fig. 2C) suggests that the organic compounds in the African mineral dust did not form by condensation. The organic carbon compounds, composing 10% of total mass (Fig. 2A), were most likely associated with the dust source and subsequently oxidized on the dust particles during transport. Spatial distributions (Fig. 4, C and D) demonstrate the resulting enhancement of carbonyl carbon concentrations at the edges of particles. Carbonyl carbon is only above the detectable absorbance near particle edges, where it represents up to 40% of total carbon. From Fig. 2C, the carbonyl carbon–to–total carbon ratio of 0.3 for 0.5-μm-diameter particles is roughly three times larger than the average ratio of 0.1 for eastern U.S. combustion particles collected in the lower tropospheric boundary layer. The substantial oxidized fraction of carbon is consistent with the long atmospheric processing time associated with the dust particles that crossed the Atlantic before being sampled. The age of the mineral dust particles, sampled 5 days of transport from their source, is consistent with an oxidation reaction rate of 13% of organic compound mass per day, increasing the carbonyl carbon–to–total carbon ratio by 3% per day.

Volume-limited oxidation signatures are observable in the boundary layer U.S. combustion sample collected in New Jersey on 12 August 2003 in the absence of precipitation or fog. The chemical composition of this aerosol is constant across all measured sizes (Fig. 2) with an average carbonyl carbon–to–total carbon ratio of 0.1. The lack of sensitivity to particle size indicates that the carbon distribution was not controlled by surface-limited processes (compare Fig. 2 to Fig. 1). Relative humidity (RH) was high (>75%) on 12 August 2003 with particles containing some condensed water, and this aqueous phase may have facilitated the diffusion of reactants within particles for volume-limited reactions. The carbonyl–to–total carbon ratio is spatially uniform with similar values within particles and at particle edges (Fig. 4F), consistent with volume-limited oxidation. Isentropic back trajectories suggest that the boundary layer particles were collected at least 10 to 15 hours after emission (*8*). The estimated times since emission of these particles are consistent with an oxidation rate of 21% of organic compound mass per day, increasing the carbonyl carbon–to–total carbon ratio by 4.8% per day.

Volume-limited oxidation also occurred in the U.S. aerosol collected during a fog event on 7 August 2003 with similar emission sources as on 12 August 2003 (*8*). The size dependence of the total carbon–to–total mass ratio in Fig. 2A, near 0.5 for 0.8-μm-diameter particles and 1 for 0.3-μm-diameter particles, indicates organic condensation. The similar size dependence of the carbonyl carbon–to–total mass ratio in Fig. 2B, ranging up to 0.1 for a diameter of 0.3 μm, suggests that the condensed organic compounds were oxidized. The uniformity of the carbonyl carbon–to–total carbon ratio in Fig. 2C, 0.1 for all particle sizes, demonstrates that the organic compounds were oxidized uniformly regardless of the original phase or proximity to the particle surface. The spatial distribution of the carbonyl carbon–to–total carbon ratio (Fig. 4H) during the fog event shows fairly uniform values near 0.1, consist-

ent with Fig. 2C. These three trends of composition with size are consistent with condensation and volume-limited oxidation (Fig. 1).

On 7 and 12 August 2003, similar U.S. combustion sources produced particles with very different organic compositions: one with a strong size dependence and the other with none. The similarity of sources means that the observed differences in composition result from condensation and reaction processes that occurred after emission. The high RH and the presence of fog on 7 August 2003 suggest that most of the aerosol particles on that day contained substantial water. Condensation and volume-limited oxidation during fog events are consistent with the mechanism proposed for oxalic acid formation in cloud droplets (*13*). The close correspondence between the observed particle-composition size dependence during the fog event and the expected theoretical relationships for condensation (Fig. 2, A and B) and volume-limited oxidation (Fig. 2C) provides evidence supporting this pathway for forming the organic fraction of this aerosol. The particle ages are consistent with an SOA formation rate equivalent to 17% of the primary organic compound mass per day, increasing the carbonyl carbon–to–total carbon ratio by 4% per day.

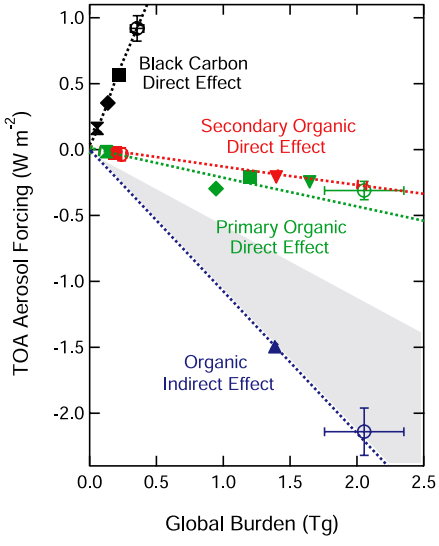

Fig. 5. Estimated TOA radiative forcing for four major effects of measured reaction rates for globally averaged carbonaceous aerosol burdens. Open circles show burden and forcing predictions calculated with use of the measured secondary organic aerosol (red), primary organic aerosol (green), and black carbon (black) oxidation rates. The carbonyl carbon–to–total carbon ratio of 0.3 was used for oxidation products, consistent with the measured ratio in particles dominated by oxidation products (aged African mineral dust particles and small condensation-dominated eastern U.S. combustion particles from 7 August 2003 in Fig. 2). Error bars represent the range of predictions associated with carbonyl–to–total carbon ratios from 0.2 to 0.5. Dotted lines are linear fits to the model predictions for each type of forcing. Solid symbols represent burden and forcing predictions, with squares (*4*), diamonds (*17*), inverted triangles (*18*), hourglasses (*19*), and triangles (*16*) representing carbonaceous aerosol burdens and TOA forcing from published estimates. TOA forcing estimates were extrapolated linearly from modeled values (*4*). The gray region indicates the large uncertainty associated with the indirect effect of organic aerosol, bounded by the estimate given here.

The four aerosol chemical signatures illustrate differences in atmospheric processing, with evidence for four mechanisms of condensation and reaction in the atmosphere. Volume-limited oxidation reactions were observed in boundary layer aerosol in which particles were largely aqueous. Surface-limited oxidation reactions were observed in particles at higher altitudes where lower RH and insoluble components were present. All four distinct aerosol compositions from different regions and with competing reaction mechanisms consistently demonstrate an oxidation rate that is a factor of 3 or more lower than the values currently used in climate model calculations. Because oxidation is the removal mechanism for hydrophobic organic and BC particles in climate models (*4*), larger predicted carbonaceous aerosol lifetimes and burdens result from the slower oxidation rates.

The direct effects of carbonaceous aerosol cause cooling by light scattering and warming by absorption, both of which increase nearly proportionally with the aerosol burden (*4*). The carbonyl groups associated with organic molecules exert influence on cloud properties (*14*), affecting cloud formation in what is termed an indirect forcing. Figure 5 shows simple estimates of changes in global burdens and associated top-of-atmosphere (TOA) forcings for the measured oxidation rates of 24% per day for BC and 13 to 21% for organic aerosol. The estimated direct effects assume constant hygroscopicity and scavenging with organic composition. More detailed calculations including the changes in these properties are not possible because an accurate global characterization of the variability of these properties with location and oxidation state does not exist.

The much slower oxidation rates mean that organic aerosol will be less hygroscopic, reflecting more radiation because of increased atmospheric lifetimes and an estimated 70% increase of the organic aerosol burden. This change in average SOA, primary organic aerosol, and BC burdens is calculated from the atmospheric oxidation rates of the samples measured here with use of a global model of parameterized burden derived from detailed climate model calculations (*4*). By incorporating similar parameterizations of the direct and indirect effects, the result is a direct organic aerosol forcing increase of up to –0.1 W m^{-2}, an indirect forcing increase of up to –0.7 W m^{-2} (*15*), and a BC forcing increase of up to +0.3 W m^{-2} (Fig. 5). The combined increases of cooling by 47% and warming by 61% represent an absolute difference of 1.1 W m^{-2} associated with uncertainties in the oxidation rate of carbonaceous aerosols, comparable to the total uncertainty in aerosol forcing and half of the magnitude of the forcing change from doubling CO_2 (+2.2 W m^{-2}).

References and Notes

1. A. R. Ravishankara, *Science* **276**, 1058 (1997).
2. V. Ramaswamy *et al.*, *Climate Change 2001: The Scientific Basis. Contribution of Working Group I to the Third Assessment Report of the Intergovernmental Panel on Climate Change* (Cambridge Univ. Press, New York, 2001), pp. 289–416.
3. W. F. Cooke, C. Liousse, H. Cachier, J. Feichter, *J. Geophys. Res.* **104**, 22137 (1999).
4. S. H. Chung, J. H. Seinfeld, *J. Geophys. Res.* **107**, 10.1029/2001JD00397 (2002).
5. E. E. Gard *et al.*, *Science* **279**, 1184 (1998).
6. D. R. Worsnop, J. W. Morris, Q. Shi, P. Davidovits, C. E. Kolb, *Geophys. Res. Lett.* **29**, 10.1029/2002GL015542 (2002).
7. L. M. Russell, S. F. Maria, S. C. B. Myneni, *Geophys. Res. Lett.* **29**, 10.1029/2002GL014874 (2002).
8. Materials and methods are available as supporting material on *Science* Online.
9. The average total carbon–to–total mass absorption ratio for each STXM sample was calibrated to the bulk aerosol organic carbon mass fraction. This calibration is rigorous for 0.2- to 2.0-μm-diameter STXM particle populations with mass average compositions that are equivalent to the submicrometer aerosol mass average measured for each sample.
10. S. F. Maria *et al.*, *J. Geophys. Res.* **108**, 10.1029/2003JD003703 (2003).
11. T. J. Garrett, L. M. Russell, V. Ramaswamy, S. F. Maria, B. J. Huebert, *J. Geophys. Res.* **108**, 10.1029/2002JD002228 (2003).
12. V. H. Grassian, *Int. Rev. Phys. Chem.* **20**, 467 (2001).
13. K. K. Crahan, D. Hegg, D. S. Covert, H. Jonsson, *Atmos. Environ.* **38**, 3757 (2004).
14. R. J. Charlson *et al.*, *Science* **292**, 2025 (2001).
15. Organic compounds may account for up to 63% of cloud condensation nuclei (*16*), corresponding to an indirect forcing estimated to be –1.5 W m^{-2}. The longer lifetime of hydrophobic organic compounds predicted here would magnify this effect, increasing the organic fraction of cloud droplets from 63% to 75% and increasing the global organic indirect effect to –2.2 W m^{-2} (*2*). This estimated indirect effect gives an order-of-magnitude calculation by extending a limited set of observations and provides an upper bound on the forcing magnitude (gray region in Fig. 5).
16. T. Novakov, J. E. Penner, *Nature* **365**, 823 (1993).
17. D. Koch, *J. Geophys. Res.* **106**, 20311 (2001).
18. M. Kanakidou, K. Tsigaridis, F. J. Dentener, P. J. Crutzen, *J. Geophys. Res.* **105**, 9243 (2000).
19. W. F. Cooke, V. Ramaswamy, P. Kasibhatla, *J. Geophys. Res.* **107**, 10.1029/2001JD001274 (2002).

20. Support for this research was provided by NSF grant ATM-0408501 and the James S. McDonnell Foundation. The authors thank A. L. D. Kilcoyne and Lawrence Berkeley National Laboratory for usage and support of Advanced Light Source Beamline 5.3.2.

Supporting Online Material

www.sciencemag.org/cgi/content/full/306/5703/1921/DC1
Materials and Methods
Figs. S1 and S2
Table S1
References

2 August 2004; accepted 11 November 2004
10.1126/science.1103491

Langmuir Supercells: A Mechanism for Sediment Resuspension and Transport in Shallow Seas

A. Gargett,* J. Wells, A. E. Tejada-Martínez, C. E. Grosch

Recent measurements at a cabled sea-floor node in 15 meters of water off the coast of New Jersey suggest that Langmuir supercells, Langmuir circulations that achieve vertical scales equal to the water depth under extended storms, are an important mechanism for major sediment resuspension events on the extensive shallow shelves off the eastern U.S. coast. Because sediment resuspension is a prelude to transport, supercell events are a necessary condition for major sediment transport. Such events may also contribute to shelf-sea exchange and to offshore gradation of benthic community structure in shallow seas.

In wind- and wave-driven surface layers of lakes and oceans, Langmuir circulations (LC) are parallel counterrotating vortices oriented roughly downwind, with maximum downwind velocities at the surface convergences between vortex pairs. LC are believed to be generated by interaction between Stokes drift, associated with finite amplitude surface gravity waves, and vertical vorticity, associated with wind-driven "mean" currents (*1*) and/or turbulence generated by breaking surface waves (*2*): Both mechanisms require the presence of surface gravity waves. Since the initial elucidation of LC by Langmuir (*3*), observational (*4*–*6*), theoretical (*1*, *2*, *7*), and computational (*8*–*11*) studies have defined many characteristic features. Maximum downwelling velocities, w_{dn}, occur at middepth of the cells and exceed maximum upwelling velocities (*4*, *5*); hence upwelling limbs of cells are wider than downwelling limbs. Horizontal scales of Langmuir cells (defined here as a vortex pair) are roughly three times larger than vertical (*5*). In homogeneous water under fully developed seas, w_{dn} is predicted to scale with wind speed U_w measured at 10-m height as $w_{dn} \approx 0.008U_w$, and the maximum depth to which LC penetrate a linearly stratified water column is predicted to be $d = 1.7w_{dn}N^{-1}$, where $N = [-g\rho_o^{-1}(\partial\overline{\rho}/\partial z)]^{1/2}$ is buoyancy frequency (*11*).

Despite continuing interest in open-ocean LC, curiously little observational attention has been given to the situation in which the vertical scale of LC reaches the full depth of the water column. Yet our observations suggest that episodic occurrence of such situations is associated with major sediment resuspension, and hence transport, in shallow seas.

Department of Ocean, Earth, and Atmospheric Sciences, Old Dominion University, Norfolk, VA 23529, USA.

*To whom correspondence should be addressed. E-mail: gargett@ccpo.odu.edu

A five-beam turbulence VADCP (vertical-beam acoustic Doppler current profiler), installed on a bottom platform at the LEO-15 cabled ocean observatory off the coast of New Jersey, recorded velocity profiles roughly every second from 25 April to 31 October 2003. The vertical beam provided unambiguous measurement of vertical velocity w from ~1 m above the seabed to the sea surface, and slant-beam pairs provided standard estimates of horizontal velocity components. The deployment included the full annual variation of water column stability and tidal and atmospheric forcing as well as passage of a hurricane, spanning the full range of turbulence-generating processes at the site.

Turbulent velocities are extracted from much larger velocities associated with surface waves by low-pass filtering (*12*). During the deployment, major episodes of sediment resuspension (characterized by clouds of high backscatter originating at the bottom and extending to near the surface) occurred when vertical velocity fields characteristic of LC extended over the full water column. The example in Fig. 1 occurred when a high pressure system brought strong winds from the northeast on 16 and 17 May 2004. Over the first 4 to 5 hours shown, wind direction rotated from easterly to northeasterly, and wind stress rose rapidly, thereafter fluctuating only slightly about 0.1 N/m^2 for the next 24 hours. An estimate of peak-to-trough surface wave height (*13*) grew to an order of 1 m by ~1200 and thereafter remained relatively constant, suggesting that seas had reached an equilibrium state. Surface buoyancy flux, dominated by the heat flux shown here (*14*), changed from weakly stabilizing ($Q_T < 0$) during the day to weakly destabilizing overnight: Net heat flux over the period shown was very close to zero. The relative (*15*) backscatter amplitude field, A_s, indicates the onset of major bottom sediment resuspension around 1800 on 16 May 2004. Figure 1B enlarges A_s and w fields for the shaded period of Fig. 1A, when the sediment resuspension process is fully developed. At this time, the upper water column contains regions of high near-surface backscatter occurring in the downwelling limbs (coded blue in the w field) of what we will argue are LC. Such signatures are known to arise from air microbubbles deposited near the surface by wave breaking and redistributed to depth by LC (*6*, *16*). In the lower water column, the A_s record shows high backscatter clouds originating from the bottom, associated with upward-going limbs (coded yellow in the w field) of LC that extend over the full depth of the water column.

Identification of these observations as LC results from examination of both the forcing fields and in-water observational data, as well as associated large-eddy simulations (LES) of unstratified surface stress–driven Couette flow with and without Langmuir forcing (*17*). First, other potential explanations for the observations are eliminated. The observed cells are not generated by normal bottom boundary layer processes, because they are observed first near the sea surface (left of Fig. 1A) and only progressively extend to the bottom. They are not (primarily) driven by unstable buoyancy forcing, because they persist, and indeed reach bottom, while buoyancy forcing is stabilizing during daytime. Lastly, conservation of water column heat content throughout the record (*18*) suggests that onset and deepening of the cells are not advective effects. Next, we summarize features of the observations at the time of Fig. 1B that agree with those commonly accepted as characteristic of LC.

1) When horizontal fluctuation velocities (*19*) are rotated into components parallel (u_τ) and perpendicular ($u_\perp$) to the vector wind stress τ, the three-dimensional velocity field (Fig. 2) illustrates many flow features considered characteristic of LC. As cartooned in Fig. 3, mean water velocity U (30 cm s^{-1}) at the time of the measurements in Fig. 2 was slightly to the left of the wind stress, so cross-wind drift of cells past a fixed point P on the bottom is toward the left. As a downwelling region approaches P, the horizontal cross-wind component ($u_\perp > 0$ in the direction of $\tau_\perp$) near the bottom should first be positive then switch to negative at the center of the downwelling, the relationship observed between w and $u_\perp$ in Fig. 2, A and B. The observed field of $u_\perp$ does not show expected convergent flow near surface, because the upper 20% of the mean water column (shaded area in Fig. 3) could not be sampled during this period of large surface waves (*12*, *19*). Lack of convergent flow in the sampled domain implies that the actual convergent flow is surface-intensified, as

illustrated (Fig. 3) and found in other studies (*5*, *10*). The observed u_τ field (Fig. 2C) also exhibits characteristic "jets," enhanced downwind flow centered over downwelling regions, balanced by slower flow over upwelling regions.

2) As illustrated in Fig. 4A, downward vertical velocities are maximum at middepth and exceed upward velocities in magnitude (*4*). Observed middepth downward (–6.4 cm s^{-1}) and upward (4.3 cm s^{-1}) velocities predict a length scale ratio of upwelling to downwelling regions of ~1.5, in good agreement with a middepth ratio of 1.6 from our LES (*17*).

3) Horizontal cross-wind extents of the largest cells, calculated from time required to advect past the VADCP at mean cross-wind water velocity $U_\perp = 0.07$ ms^{-1}, were ~45 to 70 m, roughly three times their vertical extent (*5*).

4) Observed $w_{dn} \cong 6$ cm s^{-1} (Fig. 4A) agrees well with $w_{dn} \approx 0.008 U_w = 6.2$ cm s^{-1} predicted for a homogeneous water column under fully developed seas with the use of the observed wind speed $U_w = 7.8$ m s^{-1}. Agreement here, when seas are not quite fully developed (*13*), likely results from the weak (1/3 power) dependence of predicted w_{dn} on surface wave parameters (*11*).

5) Data from conductivity-temperature-depth (CTD) profiles and a thermistor chain confirm typical density homogenization over the vertical extent of water column occupied by structures with LC characteristics (*4*).

With the use of N values from 0.02 to 0.04 s^{-1} that were estimated from a CTD profile while cells were still confined near the surface and $w_{dn} \cong 6$ cm s^{-1} observed at that time, depths of LC penetration predicted with use of $d = 1.7\,|w_{dn}|N^{-1}$ (*11*) are only 2.5 to 5 m, far smaller than the full water column depth eventually occupied by the cells. It thus appears that the cells themselves were not responsible for homogenization of the entire water column in the example shown here. Instead, the vertical cell size constantly adjusted to fill a mixed layer deepening as a result of shear instability, a picture consistent with sporadic occurrence of Richardson number (*20*) $Ri \sim 1/4$ across the base of the density-mixed surface layer until its disappearance. In other episodes with comparable wind stress but lower initial N values, predicted LC mixing depths exceed the fluid depth and the Langmuir cells themselves can drive mixing to the bottom.

A major difference from LC observed in deepwater regimes is the strong bottom intensification (Fig. 2C) of otherwise characteristic LC "jets" parallel to the wind direction. We find similar bottom intensification of these jets in LES of surface stress–driven Couette channel flow only when the vortex force (*8*, *9*) used to model wind wave forcing of Langmuir cells is added to the surface stress forcing (fig. S1). Although both direct numerical simulation (*21*) and our own LES of basic turbulent Couette channel flow (CF in fig. S1, A to C) reveal the presence of coherent vortices that are elongated in the flow direction, as are the LC that replace them when Langmuir forcing is added to the model (LCF in fig. S1, D to F), these CF vortices have weaker velocities and smaller horizontal spatial scales than LC. In addition, streamwise jets in the LCF are bottom-intensified, in contrast to the CF.

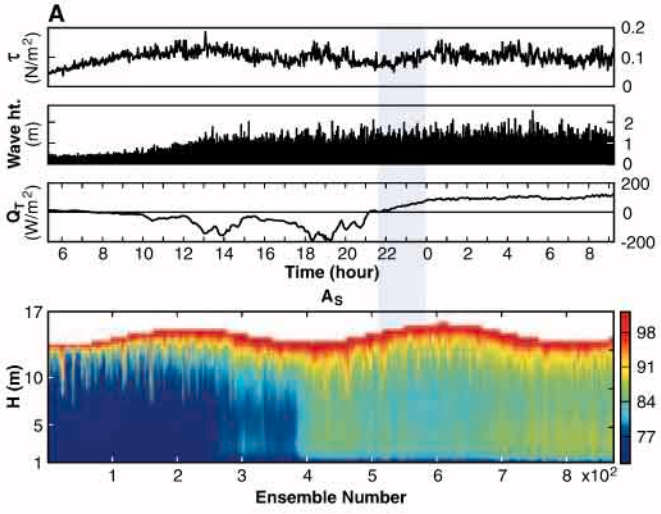

Fig. 1. (**A**) Atmospheric forcing (wind stress τ and net heat flux Q_T positive for ocean heat loss) and wave height spanning a period of increase in water column backscatter A_s on 16 May 2003. Local time (Eastern Standard Time) is time minus 5 hours. H is height above bottom. (**B**) Patterns of vertical velocity w and backscatter amplitude A_s from the shaded period in (A) are consistent with Langmuir circulations that have extended to full water column depth.

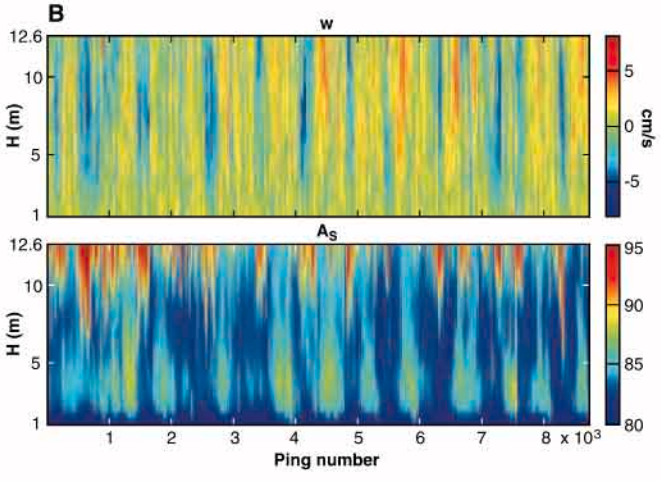

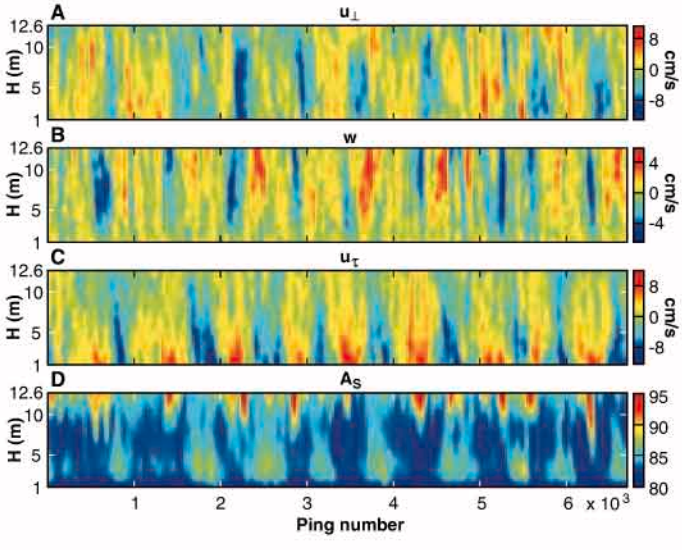

Fig. 2. Fields of horizontal velocity components perpendicular (**A**) ($u_\perp$) and parallel (**C**) (u_τ) to the wind stress vector τ, vertical velocity (**B**) (w), and backscatter amplitude (**D**) (A_s) for a subset of the record in Fig. 1B.

Lastly, the character of the trajectory of observed invariants of the Reynolds stress tensor in the Lumley triangle (*22*) (Fig. 4C) is only reproduced by the LES when Langmuir forcing is included (fig. S2B): The invariant trajectory of basic CF lies instead along the right-hand straight boundary of the triangle (fig. S2A). We are thus confident that the dominant velocity structures observed to fill the entire water column coincident with major sediment resuspension at the time of Fig. 2B are indeed LC.

Whether one views these LC as responsible for sediment resupension depends upon the vertical scale involved. At the time and place of our observations, velocities associated with the dominant surface waves (length ~ 90 m) extend to the bottom, producing an oscillatory "wave" boundary layer immediately adjacent to the bottom. Although turbulence within this highly sheared wave boundary layer is presumeably the means of detaching individual sediment grains from the bottom, the wave boundary layer is thin, reaching only ~10 to 30 cm in height (well below our first measurement bin) under strong waves (*23*): Resuspension on such small scales doesn't move the sediment far from the boundary. A major (large-scale) sediment resuspension event, in which bottom sediment is found throughout the water column, requires that sediment delivered by wave boundary layer processes be moved the full extent of the water column by turbulent structures in the overlying water column. In our observations, these structures are the relatively organized flows associated with Langmuir supercells, full-depth LC. In the larger data set available to us, such major sediment resuspension occurs whenever supercells appear and only when such structures are present (*24*).

The term "supercell" acknowledges the major impacts associated with LC that occupy the full water column. On the basis of vertical extent and level of backscatter signal originating from the bottom, supercell episodes lasting from 9 to 42 hours were the major sediment resuspension events during more than 6 months of measurements at LEO-15. Such large-scale resuspension is a necessary prelude to major sediment transport; sediment that is moved out of low-speed, near-bottom flow and into stronger interior flows will be transported much further than sediment remaining near the bottom. Thus, it appears that supercells are a major control on sediment transport in this and similar shallow environments. Acceptance of the strong likelihood that Langmuir cells occasionally intersect, and hence interact with, the bottom in shallow seas can explain other recent observations of particle structures within the water column. Glider-based observations on the New Jersey shelf (*25*) occasionally sampled localized regions where high backscatter is found throughout the water column, a likely signature of sediment resuspension by supercells. Recent observations on a shallow shelf surrounding the Bahamas (*26*) revealed a 400-km^2 region in which negatively buoyant brown algae were concentrated on the bottom in long downwind rows with horizontal spacing about three times the local water depth, again suggesting the action of supercells. Where shallow shelves extend to the shelf break, supercells driven by offshore winds can deliver sediment and bioactive material episodically to the deep sea. Transport in supercells driven by onshore winds offers a possible mechanism for resupply of biological material (resting spores, larvae) to shallow inner shelves. Langmuir supercells also have potential structuring effects on shallow-shelf benthic ecosystems, because benthic organisms dwelling where the bottom is semiregularly disrupted by supercell events must have far different characteristics than those whose homes are not typically within reach. Thus Langmuir supercells may be a major determinant of biogeochemical as well as physical functioning of shallow seas.

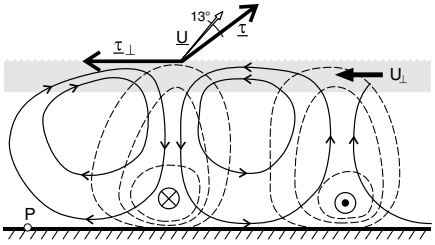

Fig. 3. Basic features of Langmuir circulations in shallow water, shown with the geometry of wind stress τ and mean current *U* at the time of the record in Fig. 2.

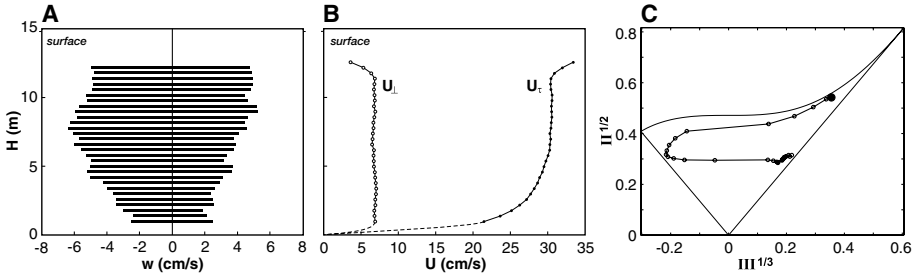

Fig. 4. Features characteristic of LC for the record in Fig. 2. (**A**) Downward vertical velocities exceed upward; maximum downward velocities occur several meters below the surface. (**B**) Mean profiles of horizontal velocity components (and density, not shown) tend to become homogenized over depth. (**C**) Depth trajectory of Lumley invariants (*22*) of the observed flow field is characteristic of Langmuir turbulence in LES (*17*). The filled circle (upper right) is the measurement closest to the bottom.

References and Notes

1. A. D. D. Craik, S. Leibovich, *J. Fluid Mech.* **73**, 401 (1976).
2. M. A. C. Teixeira, S. E. Belcher, *J. Fluid Mech.* **458**, 229 (2002).
3. I. Langmuir, *Science* **87**, 119 (1938).
4. R. A. Weller, J. F. Price, *Deep Sea Res.* **35**, 711 (1988).
5. J. Smith, R. Pinkel, R. A. Weller, *J. Phys. Oceanogr.* **17**, 425 (1987).
6. L. Zedel, D. M. Farmer, *J. Geophys. Res.* **96**, 8889 (1991).
7. A. Gnanadesikan, *J. Fluid Mech.* **322**, 81 (1996).
8. E. D. Skyllingstad, D. W. Denbo, *J. Geophys. Res.* **100**, 8501 (1995).
9. J. C. McWilliams, P. P. Sullivan, C.-H. Moeng, *J. Fluid Mech.* **334**, 1 (1997).
10. M. Li, C. Garrett, *J. Mar. Res.* **51**, 737 (1993).
11. M. Li, C. Garrett, *J. Phys. Oceanogr.* **27**, 121 (1997).
12. Dominant surface waves at the time of the data in Fig. 1B had period ~ 8 s and wavelength Λ ~ 90 m. With $D/\Lambda \sim 1/6$ (D is the water column depth), the waves were technically of intermediate type, with a phase speed ~ 10.5 m s^{-1}. Because surface waves pass the fixed instrument at this phase speed, whereas turbulent velocity structures are advected past at the speed of mean horizontal flow at the site (typically ~0.2 m s^{-1} or less), surface wave signatures appear at much higher frequencies and hence can be separated from the velocity signatures of turbulent structures of comparable or larger scales by low-pass filtering. Figure 1B presents data resulting from application of a ninth-order Butterworth filter with a frequency cutoff corresponding to ~1/4 the peak surface wave frequency. Even lower cutoffs (used for example to further smooth fields for Fig. 2) can be used without modifying the results presented here. Because time-domain filtering requires uniform time series, both tidal and surface wave excursions of the ocean surface affect the range over which data may be filtered. Only bins below the minimum identified surface level within a data segment are filtered and hence available for display in Figs. 1B, 2, and 4.
13. In Fig. 1A, wave height equals 2|ζ| where ζ is instantaneous wave height, an estimator that emphasizes the larger waves. For the time period of data in Fig. 1B, root mean square wave height ~ 0.3 m and significant wave height ~ 1.2 m are close to values (~0.4 m and 1.6 m, respectively) expected for fully developed seas with U_w = 7.8 m/s (*27*, *28*).
14. During the observations reported here, buoyancy flux was dominated by heat flux, with evaporation at most a 10% correction. Heat flux is calculated with standard routines (http://woodshole.er.usgs.gov/operations/sea-mat/index.html) with the use of wind; solar insolation; and air temperature, humidity, and pressure measurements from the Rutgers Marine Field Station tower.
15. Backscatter amplitude has been corrected for geometric spreading and absorption effects but not calibrated to absolute amplitude. In Fig. 1A, A_s is ensemble-averaged over ~120 s. In Fig. 1B, both A_s and w fields have been time-filtered (*12*) then block-averaged with a Hanning neighborhood of 31 pings and 3 bins. In order to measure as close to the bottom as possible, a shorter-than-normal blanking interval after acoustic transmission was used. This results in decreased amplitude in the lowest (closest to the transducer) bins but has no discernible effect on the Doppler determination of beam velocities.

16. S. A. Thorpe, A. J. Hall, *Cont. Shelf Res.* **1**, 353 (1983).
17. Method and flow parameter values used in the LES, as well as relevant results, are available on *Science* Online.
18. At the beginning of the record shown in Fig. 1A, a thermistor chain moored 95 m from the VADCP showed a surface layer well mixed in temperature over the depth range containing the cell-like velocity and backscatter signatures; below was a sharp thermocline (~2°C over less than 1 m) above a thinner well-mixed bottom layer. After deepening episodically for several hours, this thermocline disappeared from the depth range covered by the thermistor chain over a short period of time around 1100. The total heat content of the water column was unchanged by this event (indeed over the entire time shown in Fig. 1A), suggesting that homogenization of the water column was the result of local vertical mixing rather than advection.
19. Fields in Fig. 2 have been time-filtered more heavily than those in Fig. 1B in order to emphasize the largest-scale cell structures. Horizontal components of the velocity field are determined from slant beam radial velocity measurements under the assumption of velocity homogeneity over the beam spread R. In fields that include turbulence, this requires $R \ll L/2$, where L is a typical horizontal wavelength of the energy-containing eddies. Estimates of $L \sim U_{\perp}T \sim$ 45 to 70 m result from the periods ($T \sim$ 500 to 1000 s) associated with a broad spectral peak in the observed vertical velocity spectrum and the crosswind component ($U_{\perp}$ = 0.07 m s^{-1}) of the mean current. Maximum beam spread of $R_{max} \sim$ 13 m occurs at the maximum range included in the filtered data. Although cells with $L/2 \sim R_{max}$ will be affected by aliasing at the largest ranges (although not at smaller, nearer-bottom, ranges), the largest energy-containing cells at least marginally meet the requirement $R \ll L/2$ over the entire range. An independent check (made by comparing the field of w measured directly by the vertical beam with w_s, an estimate made from the four slant beams assuming homogeneity of the total velocity field over the beam spread) confirms that the assumption of velocity homogeneity is adequate for the largest cells. Despite potential for sidelobe contamination of horizontal velocity components in the upper 15% of the water column, the extremely rough surface at the time of the measurements shown in Fig. 2 appears to be a rather poor reflector, and horizontal velocities calculated over the full range available do not exhibit obvious contamination: The horizontal velocities calculated in the top three to four bins should nonetheless be considered cautiously.
20. $Ri \equiv (N^2/\overline{U}_z^2)$, where $N^2 = -g\rho_0^{-1}(\partial\overline{\rho}/\partial z)$ and $\overline{U}_z^2 = (U_z^2 + V_z^2)$. We estimated $\overline{\rho}$ by using thermistor chain measurements of T and the T/S relationship from CTD casts at 0130 and 1230 on 16 May 2004. Vertical gradients of both density and shear were computed as centered first differences of values interpolated to 0.5 m [from 0.4 m for shear and 0.25 m for $\rho(T,S)$], resulting in a Ri calculated over 1 m.
21. D. V. Papavassiliou, T. J. Hanratty, *Int. J. Heat Fluid Flow* **18**, 55 (1997).
22. Anisotropy of turbulent flow is characterized by only two invariants, II = $b_{ij}b_{ji}$ and III = $b_{ij}b_{jk}b_{ki}$, where $b_{ij} = \langle u_i' u_j' \rangle / 2K - \delta_{ij}/3$ and K is the turbulent kinetic energy (*29*, *30*). Invariants of realizable flows fall within the Lumley triangle (so called, although its upper boundary is not a straight line).
23. W. D. Grant, O. S. Madsen, *Annu. Rev. Fluid Mech.* **18**, 265 (1986).
24. A single exception may be the fall transition, a relatively abrupt and short-lived event that marked the end of strong summer stratification at LEO. This transition, possibly advective in origin, was accompanied by strong backscatter signal throughout the water column but did not display clear characteristics of LC.
25. S. Glenn *et al.*, *Oceanography* **17**, 86 (2004).
26. D. Burdige, R. Zimmerman, personal communication.
27. M. A. Donelan, J. Hamilton, W. H. Hui, *Philos. Trans. R. Soc. London* **A315** (1985).
28. M. S. Longuet-Higgins, *J. Mar. Res.* **11**, 245 (1952).
29. J. L. Lumley, *Adv. Appl. Mech.* **18**, 123 (1978).
30. S. B. Pope, *Turbulent Flows* (Cambridge Univ. Press, Cambridge, 2000), pp. 393–395.
31. We are grateful for research support from NSF (grant OCE-0136403) and NOAA (grant NA06RU0139) and generous support from S. Glenn, O. Schofield, and E. Creed. The success of the LEO-15 deployment was due to R. Petrecca and staff of the Rutgers Marine Field Station and the technical expertise of C. Powell. S. Huang provided essential data handling and access programming.

Supporting Online Material
www.sciencemag.org/cgi/content/full/306/5703/1925/DC1
Materials and Methods
Figs. S1 and S2
References

28 May 2004; accepted 5 November 2004
10.1126/science.1100849

Frequent Recombination in a Saltern Population of *Halorubrum*

R. Thane Papke,[1]* Jeremy E. Koenig,[1] Francísco Rodríguez-Valera,[2] W. Ford Doolittle[1]

Sex and recombination are driving forces in the evolution of eukaryotes. Homologous recombination is known to be the dominant process in the divergence of many bacterial species. For Archaea, the only direct evidence bearing on the importance or natural occurrence of homologous recombination is anecdotal reports of mosaicism from comparative genomic studies. Genetic studies, however, reveal that recombination may play a significant role in generating diversity among members of at least one archaeal group, the haloarchaea. We used multi-locus sequence typing to demonstrate that haloarchaea exchange genetic information promiscuously, exhibiting a degree of linkage equilibrium approaching that of a sexual population.

The evidence that haloarchaea are potentially sexual organisms comes from laboratory studies. Prototrophic recombinants of the genus *Haloferax* can be obtained when auxotrophic strains are filtered together and plated on growth medium (*1*, *2*), a process that may involve the formation of intercellular bridges. Transformation can be artificially induced in several species, and recombination occurs readily between chromosomes and introduced homologous DNA fragments (*3*–*5*). In nature, haloarchaea, which prefer elevated salt concentrations, are characteristically prominent in multipond solar salterns, where seawater is concentrated in stages from 4 to 37% sodium chloride (NaCl). Using ribosomal RNA (rRNA) genes (*6*, *7*), we have identified multiple clusters of related (conspecific) ribotypes in the salterns at Santa Pola, near Alicante, Spain. In these salterns, apparent species diversity decreased with increasing salinity but microdiversity increased. Diversity at a scale finer than that accessible to rRNA-based methods can be revealed by multi-locus sequence typing (MLST), which also offers a window into genetic exchange processes (*8*, *9*).

We undertook an MLST survey of haloarchaea isolated from different salinity ponds at this site (*10*). Polymerase chain reaction (PCR) was used to amplify a 325–base pair (bp) stretch of small subunit (SSU) rRNA genes. Sequenced PCR products showed few ambiguities, suggesting that the strains did not harbor multiple SSU rRNA genes of substantially different sequences, as some species of haloarchaea clearly do (*11*). In total, 122 strains were characterized and could be assigned to five clusters, corresponding to four named haloarchaeal genera and one novel haloarchaeal assemblage. Sixty-nine of the strains assignable to the *Halorubrum* cluster had SSU rRNA sequences identical to each other and to an Australian isolate [*Halobacterium sp.* AUS1 (JCM9573)] (*12*). Thirty-six of these isoribotypes were selected for MLST analysis. Primers were designed with reference to the sequenced genome of *Halobacterium* NRC-1 and individual GenBank entries (*13*) to generate products of approximately 500 bp from *atpB*, *ef-2*, *radA* (*10*), and *secY* genes. For each gene, each different sequence obtained was considered an allele and assigned a number (Table 1). Alleles at each locus were also analyzed phylogenetically and assigned to one of two to four clades (fig. S1).

Among the isolates, allelic profiles were highly mosaic; all loci (except for SSU rRNA) were polymorphic with 8 to 15 alleles and 30 to 61 polymorphic nucleotide sites per locus. We estimated the genetic

[1]Department of Biochemistry and Molecular Biology, Dalhousie University, 5859 University Avenue, Halifax, Nova Scotia B3H 4H7, Canada. [2]División de Microbiologia, Unívesidad Miguel Hernández, Campus de San Juan, 03550 San Juan de Alicante, Spain.

*To whom correspondence should be addressed. E-mail: rpapke@dal.ca

diversity as $H = 1 - \Sigma x_i^2$, where x is the relative frequency of the ith allele, and we averaged the values to obtain the average genetic diversity in our sample set (*14*). The estimated value for the entire data set was $H = 0.69$. For the 36 and 23% salinity ponds, separately, we estimated the average genetic diversity to be 0.83 and 0.57, respectively. All values were higher than the average genetic diversity of 0.47 reported for *Escherichia coli*, which itself is approximately five times higher than that of typical eukaryotic species (*14*).

Strain phylogenies based on the different genes were incongruent, which was expected if recombination had occurred during the divergence of these organisms (fig. S1). Comparison of isolate-specific allelic profiles (Table 1) using linkage disequilibrium freeware (*15*, *16*) also demonstrated recombination. This freeware measures the variance in allelic profiles in all pairwise combinations and contrasts it to the value obtained from 1000 randomizations ($P = 0.001$) of the data set (simulating a freely recombining population). If the observed variance is greater than the maximum variance obtained from randomizing the data set, then the association of alleles is not random: There is linkage disequilibrium, and recombination may be rare. However, if the measured variance is less than the maximum value obtained from randomization, then alleles are arbitrarily associated: the population is more likely to be freely recombining and in linkage equilibrium (*15*, *16*). Linkage analysis of our entire data set revealed that the observed variance of 0.92 was lower than the maximum variance of 1.26 and close to the mean variance of 0.83 obtained in 1000 randomized data. When isolates cultured from ponds of different salinities were analyzed as separate data sets, even wider differences in variance were measured. From the 36% salinity pond, the observed variance was 0.510 and the maximum and mean variances for 1000 trials were 1.30 and 0.69, respectively. From the 23% salinity pond, the observed variance was 0.707 and the maximum and mean variances for 1000 randomizations were 1.31 and 0.77, respectively. This analysis suggests that the *Halorubrum* population is near linkage equilibrium and that random mating and recombination occur both within and (possibly at a somewhat reduced rate) between ponds of different salinities.

Table 1. Members of different allele clades differ by 6 to 43 nucleotides at any locus and are represented by different colors for heuristic value (fig. S1). Column P shows recombination detected by phylogenetic analysis. Column S shows recombination detected by SLV analysis.

Isolate	16S rRNA	*atp B*	*ef-2*	*rad A*	*sec Y*	P	S
018	1	1	1	1	1		
020	1	2	2	2	2		
026	1	1	3	3	3		•
028	1	3	4	2	4		
034	1	4	3	4	5		
045	1	5	3	5	5		
054	1	6	4	6	6		
055	1	2	5	7	7	•	
056	1	7	5	8	8	•	
071	1	9	2	6	5	•	
094	1	4	3	4	5		
105	1	8	3	3	3		
135	1	8	6*	3	5		•
143	1	7	4	9	9		
145	1	8	3	2	3	•	•
146	1	8	3	2	10	•	•
148	1	8	3	2	6	•	•
149	1	1	3	2	11	•	
153	1	8	3	1	12		
154	1	8	5	8	13	•	
159	1	5	3	5	14		
160	1	8	3	10	10		
162	1	8	7	11	10		
175	1	8	3	12*	3		•
189	1	8	3	3	3		
192	1	8	7	1	15		
196	1	8	3	3	5		•
198	1	8	8	11	10		
202	1	4	3	3	3		•
208	1	8	3	13	5		
209	1	8	3	10	3		•
217	1	1	3	10	5		
227	1	8	3	3	12		•
228	1	8	3	3	3		
252	1	8	3	3	3		
254	1	8	3	10	10		

*Alleles found in additional data set not presented in Table 1.

It is also possible to quantify the relative contributions to diversity of mutation and recombination using rules of procedure based on single-locus variation (SLV) developed in MLST studies on bacteria (*17*). SLV, a situation in which two strains are identical at all alleles except for one, can arise by either mutation or recombination. Mutational alterations are single-nucleotide changes and are unique in a data set, whereas recombination events can have single or multiple nucleotide changes and are encountered several times, independently. In either case, uniqueness, direction of change, and independence of occurrence can be mapped against a clonal complex model (fig. S2). We noted 87 nucleotide changes in 10 alleles that likely arose from recombination and two nucleotide changes in 2 alleles that likely arose from mutation.

For certain pathogenic bacterial species, comparable excesses of recombination over mutation as source of variation have been reported (*17*, *18*), leading to a radical rethinking of mechanisms of bacterial adaptation and diversification. Adaptive sweeps do occur, reducing variation within a population. But such variants arise within populations that are interrelated in complex weblike patterns through recombination, and may come to dominate because they bear favorable combinations of preexisting alleles, rather than because they carry novel mutations (*9*). Much recombination may occur within so-called "species boundaries," but there may be no absolute barrier to recombination between species. Some of the recombination events we documented involved sequences differing by more than 7% and may have transgressed such boundaries.

Recombination, our results show, can be an important force in the generation of diversity and adaptive novelty in Archaea. Although the underlying cellular mechanisms are as yet poorly known, cytoplasmic connections (*1*) may represent an evolved gene exchange system within the Euryarchaeota. There is also evidence for natural conjugative mechanisms for gene exchange and recombination in species of *Sulfolobus,* a member of the second major division of Archaea, the Crenarchaeota (*19*–*21*).

References and Notes

1. I. Rosenshine, R. Tchelet, M. Mevarech, *Science* **245**, 1387 (1989).
2. M. Dyall-Smith, S. L. Tang, C. Bath, *Res. Microbiol.* **154**, 309 (2003).
3. S. W. Cline, W. F. Doolittle, *J. Bacteriol.* **174**, 1076 (1992).
4. S. W. Cline, F. Pfeifer, W. F. Doolittle, in *Archaea: A Laboratory Manual*, F. T. Robb *et al.*, Eds. (Cold Spring Harbor Laboratory Press, Cold Spring Harbor, NY, 1995), protocol 29, pp. 197–204.
5. G. Wang, S. P. Kennedy, S. Fasiludeen, C. Rensing, S. DasSarma, *J. Bacteriol.* **186**, 3187 (2004).
6. S. Benlloch *et al.*, *Environ. Microbiol.* **4**, 349 (2002).
7. E. O. Casamayor *et al.*, *Environ. Microbiol.* **4**, 338 (2002).
8. E. J. Feil, M. C. J. Maiden, M. Achtman, B. G. Spratt, *Mol. Biol. Evol.* **16**, 1496 (1999).
9. E. J. Feil, B. G. Spratt, *Annu. Rev. Microbiol.* **55**, 561 (2001).
10. Materials and methods are available as supporting material on *Science* Online.
11. Y. Boucher *et al.*, *J. Bacteriol.* **186**, 3980 (2004).
12. Y. Mukohata, Y. Sugiyama, K. Ihara, M. Yoshida, *Biochem. Biophys. Res. Commun.* **151**, 1339 (1988).
13. GenBank accession numbers for data generated in this manuscript are as follows: AJ851294-AJ851329, AJ851333-AJ851368, AJ851895-AJ851930, and AJ851932-AJ852003.
14. R. K. Selander, B. R. Levin, *Science* **210**, 545 (1980).
15. The Multi-Locus Sequence Typing Web site (http://www.mlst.net) was developed by Man-Suen Chan and David Aanensen and funded by the Wellcome Trust.
16. J. Maynard Smith, N. H. Smith, M. O'Rourke, B. G. Spratt, *Proc. Natl. Acad. Sci. U.S.A.* **90**, 4384 (1993).
17. E. J. Feil, J. Maynard Smith, M. C. Enright, B. G. Spratt, *Genetics* **154**, 1439 (2000).
18. E. J. Feil, C. J. Maiden, M. Achtman, B. G. Spratt, *Mol. Biol. Evol.* **16**, 1496 (1999).
19. D. Prangishvili *et al.*, *Plasmid* **40**, 190 (1998).
20. M. S. Reilly, D. W. Grogan, *J. Bacteriol.* **183**, 2943 (2001).
21. M. Jonuscheit, E. Martusewitsch, K. M. Stedman, C. Schleper, *Mol. Microbiol.* **48**, 1241 (2003).

22. We thank the Canadian Institutes for Health Research and Genome Atlantic for supporting this research. Isolation of strains was carried out at F.R.V.'s laboratory and funded by grant PM99-0078 from the Spanish Ministry of Science and Technology.

Supporting Online Material

www.sciencemag.org/cgi/content/full/306/5703/1928/DC1
Materials and Methods
References
Figs. S1 and S2

27 July 2004; accepted 20 October 2004
10.1126/science.1103289

Targeting Malaria Virulence and Remodeling Proteins to the Host Erythrocyte

Matthias Marti,* Robert T. Good,* Melanie Rug, Ellen Knuepfer, Alan F. Cowman†

To establish infection in the host, malaria parasites export remodeling and virulence proteins into the erythrocyte. These proteins can traverse a series of membranes, including the parasite membrane, the parasitophorous vacuole membrane, and the erythrocyte membrane. We show that a conserved pentameric sequence plays a central role in protein export into the host cell and predict the exported proteome in *Plasmodium falciparum*. We identified 400 putative erythrocyte-targeted proteins corresponding to ~8% of all predicted genes, with 225 virulence proteins and a further 160 proteins likely to be involved in remodeling of the host erythrocyte. The conservation of this signal across *Plasmodium* species has implications for the development of new antimalarials.

Species of the genus *Plasmodium* are obligate intracellular parasites of the phylum Apicomplexa that switch between an arthropod vector and a vertebrate host, where they undergo cycles of asexual reproduction in blood cells. Each year, several hundred million people become infected with *P. falciparum*, which causes the most severe form of malaria in humans, and 1 to 2 million die from complications. Once the parasite is in the blood, its continuous asexual multiplication inside erythrocytes is responsible for clinical symptoms of malaria and the associated morbidity and mortality. Asexual stages reside in a parasitophorous vacuole, and they elaborate a membranous network in the erythrocyte cytoplasm, including Maurer's clefts. Moreover, the surface of the infected erythrocyte membrane is also remodeled with electron-dense elevations called knobs. The 85- to 110-kD knob-associated histidine-rich protein (KAHRP) is present on the cytoplasmic side of the knob structure (*1*), and the 200- to 300-kD antigen PfEMP1 is located on the exterior surface (*2*). PfEMP1 is encoded by ~60 *var* genes per parasite (*3*), and monoallelic expression of variant forms of the protein is responsible for antigenic variation (*4*). The primary structure of PfEMP1 consists of a large N-terminal ecto-

Walter and Eliza Hall Institute of Medical Research, Melbourne, Victoria 3050, Australia.

*These authors contributed equally to this work.
†To whom correspondence should be addressed. E-mail: cowman@wehi.edu.au

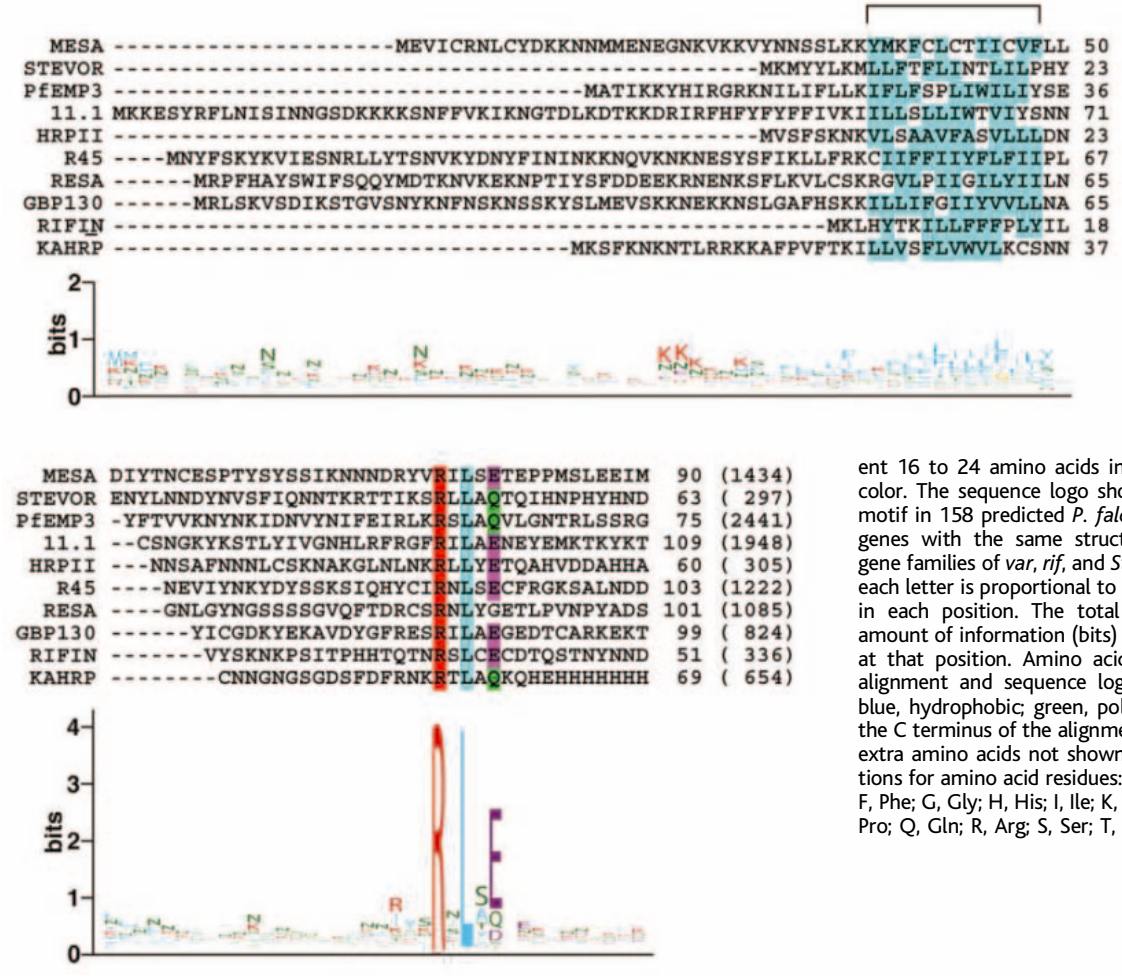

Fig. 1. Identification of a novel motif in exported *P. falciparum* proteins. Multiple sequence alignment of the N-terminal portion of 10 exported *P. falciparum* proteins shows that gene structure is conserved with a hydrophobic signal sequence (see bracket; hydrophobic amino acids are highlighted in blue) encoded in exon 1 (upper panel) and a highly variable sequence encoded in exon 2 (lower panel). However, a conserved pentameric motif is present 16 to 24 amino acids into exon 2, as highlighted in color. The sequence logo shows the conservation of this motif in 158 predicted *P. falciparum* proteins encoded by genes with the same structure, excluding the multiple gene families of *var*, *rif*, and *Stevor* (fig. S1A). The height of each letter is proportional to the frequency of amino acids in each position. The total letter height indicates the amount of information (bits) contained in the amino acids at that position. Amino acid color coding for both the alignment and sequence logo: red, basic; purple, acidic; blue, hydrophobic; green, polar amino acids. Numbers at the C terminus of the alignment (lower panel) indicate the extra amino acids not shown in the alignment. Abbreviations for amino acid residues: A, Ala; C, Cys; D, Asp; E, Glu; F, Phe; G, Gly; H, His; I, Ile; K, Lys; L, Leu; M, Met; N, Asn; P, Pro; Q, Gln; R, Arg; S, Ser; T, Thr; V, Val; W, Trp; Y, Tyr.

domain containing a variable number of duffy-binding-like (DBL) domains that mediate cytoadherence to various host cell receptors (*5*). The cytoadhesion of parasite-infected erythrocytes to a number of host cells is a causative factor in severe pathology of malaria, and PfEMP1 is considered the major virulence determinant of *P. falciparum*. Remodeling of the anucleated erythrocyte requires targeting of parasite proteins beyond the plasma membrane and translocation across the parasitophorous vacuole membrane. Proteins exported through this route, such as KAHRP, are trafficked through the parasite's secretory pathway by virtue of a hydrophobic signal and secreted into the parasitophorous vacuole (*6*). Further transport across the parasitophorous vacuole membrane requires additional targeting signals located within 60 amino acids downstream of the signal sequence, at least in the case of KAHRP (*6*) or HRPII (*7*). Interestingly, in most known exported proteins (such as KAHRP, GBP130, the Rifin and Stevor families, RESA, MESA, HRPII/III, R45, and protein 11.1), the signal sequence is encoded in a first exon while the remaining portion of the protein is encoded in the second exon (*8*).

To identify sequences involved in protein translocation through the parasitophorous vacuole membrane and into the erythrocyte cytoplasm, we aligned the N-terminal sequences of these proteins (Fig. 1). Although the N-terminal region of the mature proteins shows no overall conservation (Fig. 1), we identified a pentameric motif present in the N-terminal portion of all these proteins. It consists of a positively charged, hydrophilic amino acid in position 1 (Arg or Lys), a hydrophobic amino acid in position 3 (Leu or Ile), and another less conserved amino acid in position 5 (predominantly Asp, Glu, or Gln), with noncharged amino acids in positions 2 and 4 (Fig. 1). To investigate the role of this motif in protein export, we fused the N termini of two exported proteins, KAHRP and GBP130 (i.e., the portions shown in the alignment of Fig. 1), to green and yellow fluorescent reporter proteins (GFP and YFP), respectively, and generated a series of modifications (Fig. 2). The soluble fusions that included the wild-type motif were efficiently exported and evenly distributed throughout the erythrocyte cytoplasm. When the motif was either mutated or deleted, the reporters were accumulated in the parasitophorous vacuole; this result shows that the motif is required for export of soluble proteins in *P. falciparum* (*9*). We termed this motif Pexel (short for *Plasmodium* export element).

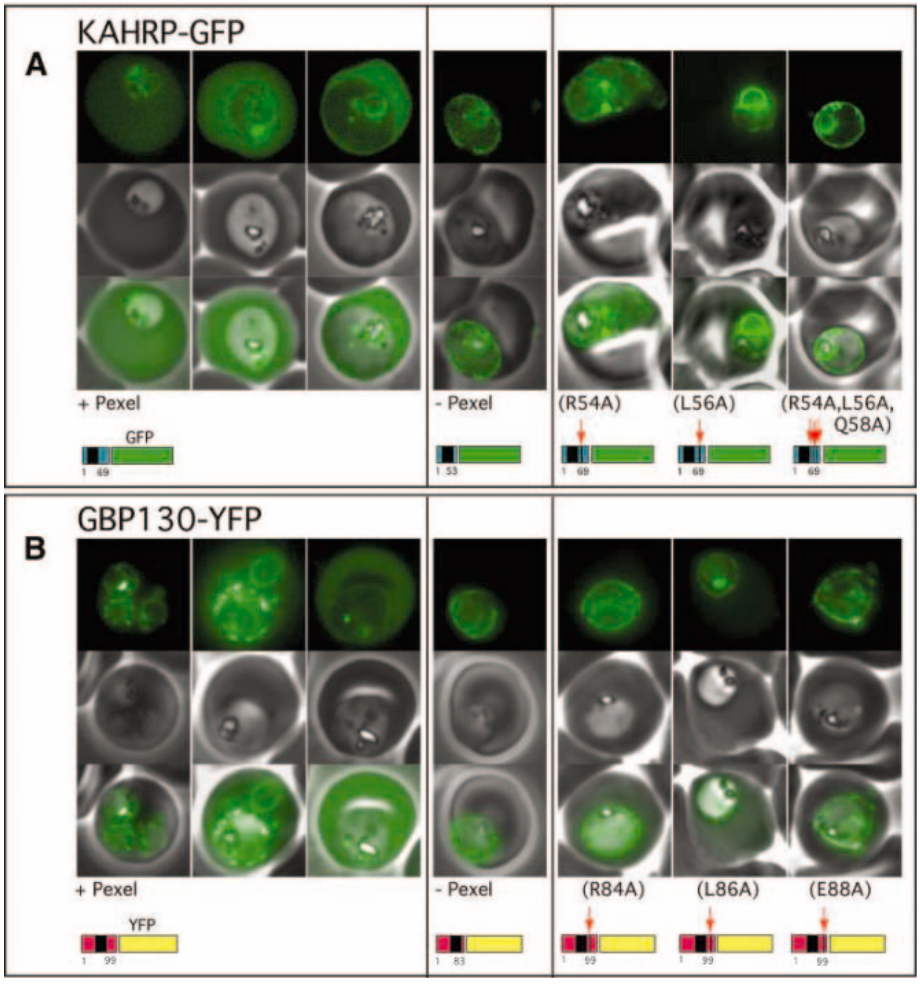

Fig. 2. The Pexel motif is necessary for export of soluble proteins in *P. falciparum*. The reporter is exported only when fused to the N terminus of KAHRP (**A**) or GBP130 (**B**) including the complete Pexel motif (left panel, +Pexel); complete truncations of the motif result in accumulation of the reporter in the parasitophorous vacuole (for construct details, see fig. S2). Representative cells expressing the exported reporter (+Pexel) are shown in ring stage (left), early (center), and late trophozoites (right). Note that KAHRP-GFP is already exported into the host cell in early stages, whereas GBP130-YFP is retained in the parasitophorous vacuole and released after development into mature trophozoite stages, perhaps because of its unusually recessed or embedded signal sequence (see also fig. S3). Coloring of the schematic representation of fusion proteins: black, hydrophobic signal sequence; blue, KAHRP N terminus; green, GFP; red, GBP130 N terminus; yellow, YFP. Arrows indicate positions of mutated amino acids, e.g., R54A for mutation of R (Arg) to A (Ala) in position 54 of KAHRP.

To determine whether the Pexel motif was also required for transport of membrane-bound surface proteins out of the parasitophorous vacuole, we replaced the ectodomain of a Rifin variant, a member of a superfamily (~160 genes in the *P. falciparum* genome), with YFP (Fig. 3A). As expected, the reporter was transported into the host cell only when the Pexel motif was present, whereas truncations of the motif completely blocked export. Mutation of the Pexel motif also blocked export; hence, it is required for transport of the Rifin proteins across the parasitophorous vacuole membrane and into the erythrocyte.

These data show that the Pexel motif is required for protein export in *P. falciparum* for both soluble and membrane proteins such as KAHRP, GBP130, and Rifin family members. The virulence protein PfEMP1 was also exported; however, it lacks a signal sequence at the N terminus but has a putative C-terminal transmembrane region. Alignment of the N terminus (preceding the first DBL domain) of the 60 PfEMP1 proteins encoded in the *P. falciparum* genome sequence revealed the presence of a conserved motif that shares features of the Pexel motif (Fig. 3C) (fig. S1, B and C). To determine whether export of PfEMP1 was dependent on the presence of a functional Pexel motif, we fused portions of the *var* gene sequence (PFL1960w) to YFP. Specifically, the N-terminal portion of PfEMP1 including the putative Pexel motif was fused to the PfEMP1 transmembrane domain and the acidic terminal segment (ATS), and YFP (added at the C terminus). Control constructs lacking the putative Pexel motif were used, as in the pre-

vious experiments (Figs. 2 and 3A). Additionally, we specifically mutated the Pexel motif to Ala residues. Again, in support of the hypothesis that this motif is a general export signal for translocation across the parasitophorous vacuole membrane and into the host erythrocyte, only PfEMP1-YFP fusions containing a functional signal were exported into the erythrocyte while the control proteins accumulated in the parasitophorous vacuole (Fig. 3B). Similar to Rif-YFP, PfEMP1-YFP was initially localized to Maurer's clefts in the erythrocyte cytosol, and a rim fluorescence pattern suggestive of surface localization later emerged at the erythrocyte membrane, although we have not shown that this PfEMP1 chimera was in the correct orientation on the red cell membrane surface. Our data support previous evidence that Maurer's clefts function as intermediate compartments for proteins destined for the erythrocyte surface (*6*). Recently, we found that the KAHRP Pexel sequence can complement the equivalent PfEMP1 motif for export across the parasitophorous vacuole membrane and (with the putative transmembrane region) can provide the information for insertion into the erythrocyte membrane and localization of the exodomain on the outside surface of the infected host cell (*10*).

If we assume that parasite protein export via a Pexel-mediated translocation process is the predominant entry into the erythrocyte cytoplasm, the in vivo experiments also confirm that the exported *P. falciparum* proteome can be predicted in silico. Some proteins such as SBP1 (*11*) are exported, although they show a different gene structure and appear to lack a Pexel motif; this observation suggests other mechanisms such as escorters (*12*). Apart from the proteins encoded by the *var* (60 paralogs), *Rifin* (140 paralogs), and *Stevor* (25 paralogs) gene families, a motif search of the *P. falciparum* genome (*13*) at www.plasmodb.org revealed the existence of ~160 genes with (i) a short first exon encoding a signal sequence, and (ii) a Pexel motif encoded close to the start of the second exon (Fig. 1) (fig. S1A). Together, these findings suggest that ~400 *P. falciparum* proteins (i.e., ~8% of its proteome) are exported into the host erythrocyte, where they are involved in antigenic and structural alterations of the erythrocyte membrane and cytoplasm, mediate nutrient import from the red blood cell into the parasite, and provide the machinery for protein export to the erythrocyte (*14*). These exported proteins appear to be unique to *Plasmodium*, because most show no sequence homology to known protein domains. An exception is the RESA protein family, whose members have a DNAJ-like protein-binding domain. Interestingly, the vast majority of the corresponding genes are located in subtelomeric regions of the 14 chromosomes in close apposition to members of the *var* and *Rifin* gene families (Fig. 4A). This finding supports the idea that genes encoding factors involved in host-parasite interactions are located on chromosome ends,

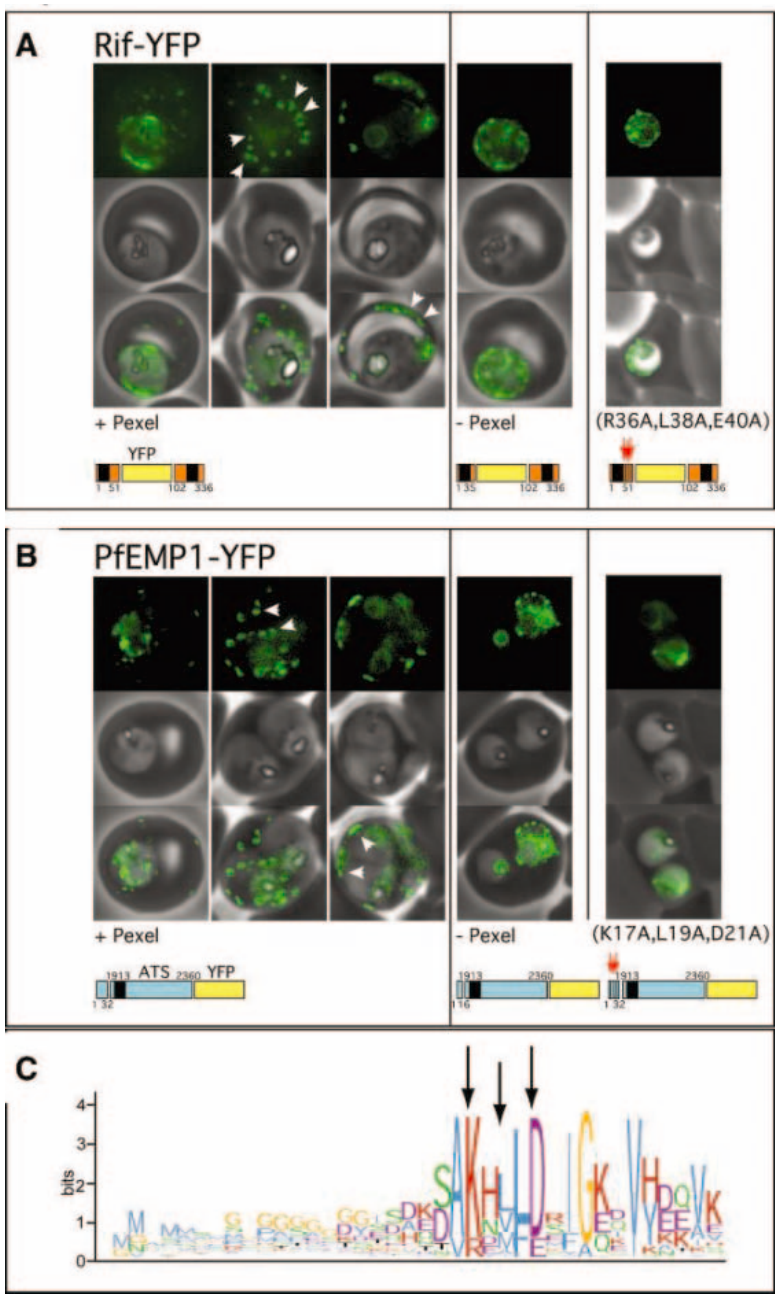

Fig. 3. Export of Rifin surface antigens and of the major *P. falciparum* virulence factor, PfEMP1, depends on a functional Pexel motif. (**A**) A Rifin-YFP fusion including the Pexel motif is exported into the erythrocyte while truncated versions accumulate in the parasitophorous vacuole membrane. Arrowheads indicate the localization of the reporter to punctate structures reminiscent of Maurer's clefts (left panel, center) and later to the surface. Coloring of the schematic representation of fusion proteins: black, hydrophobic stretches (N-terminal signal sequence and C-terminal transmembrane domain); orange, N-terminal and C-terminal portion of the Rifin protein; yellow, YFP. Arrows indicate positions of mutated amino acids. (**B**) Export of PfEMP1-YFP also depends on a functional Pexel motif. As for the Rifin-YFP fusion, the reporter transiently localizes to structures similar to Maurer's clefts, followed by a rim fluorescence suggestive of surface localization. For construct details, see fig. S2. Coloring of the schematic representation of fusion proteins: black, hydrophobic PfEMP1 transmembrane domain; blue, PfEMP1 N terminus and ATS; yellow, YFP. Arrows indicate positions of mutated amino acids. (**C**) Logo alignment (based on the ClustalX alignment of fig. S1B) of all 60 PfEMP1 variants encoded in the genome of *P. falciparum* strain 3D7, indicating the conservation of the Pexel motif. Note that the amino acid residues surrounding the Pexel motif are more conserved in PfEMP1 because it is a more recently radiated gene family. Arrows indicate positions 1, 3, and 5 of the Pexel motif. Amino acid color coding is the same as in Fig. 1.

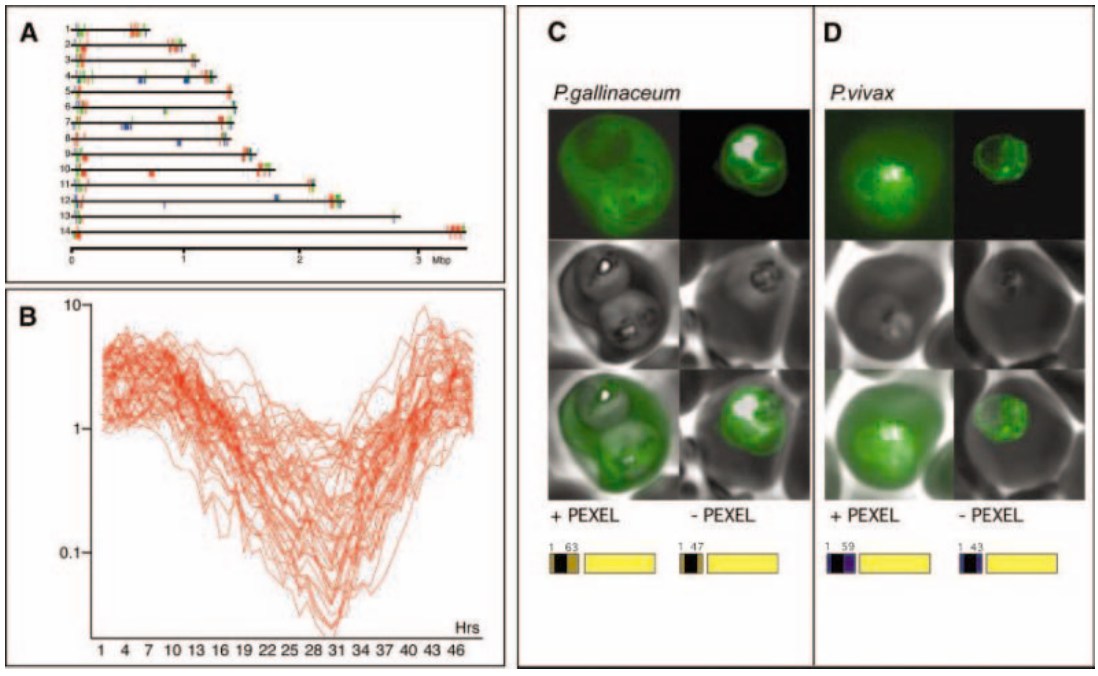

Fig. 4. Defining *Plasmodium* proteins exported into host erythrocytes. (**A**) Chromosomal map of *P. falciparum* strain 3D7, showing the positions of predicted proteins containing Pexel motifs, demonstrates the subtelomeric location of the majority of exported proteins. Bars represent individual genes: 60 *var* (blue), 165 *rif/stevor* (green), and 158 other proteins containing a Pexel motif (red). (**B**) Normalized transcriptional expression profiles during the asexual cycle of 90 Pexel genes [red bars in (A)], visualized on a time course as described (*17*). The set was selected on the criterion that the control expression value of each gene was at least 10 in the Affymetrix microarray experiments (for original microarray data, see fig. S4). Export of predicted surface antigens from *P. gallinaceum* (**C**) and *P. vivax* (**D**) depends on a functional Pexel motif when expressed in *P. falciparum*. Coloring of the schematic representation of fusion proteins: black, hydrophobic signal sequence; olive, N terminus of a predicted *P. gallinaceum* surface antigen; dark blue, N terminus of a predicted *P. vivax* surface antigen; yellow, YFP.

because these regions exhibit the highest genomic plasticity and therefore allow rapid adaptation of the parasite to the host (*15*).

Microarray experiments reveal that the overall transcription patterns of these ~400 genes show peak levels between late ring and early trophozoite stages of development (Fig. 4B) (fig. S4), a time during which most host cell remodeling occurs; this is in agreement with other microarray studies of the *P. falciparum* transcriptome (*16*, *17*). However, some predicted exported proteins are expressed exclusively in sporozoite or gametocyte stages (*18*, *19*), and there is evidence that protein 11.1 is exported in early gametocytes (*20*) (tables S1 and S2). The presence of Pexel-containing proteins in intrahepatocytic stages indicates that the machinery for protein translocation across the parasitophorous vacuole membrane is functional in different host cell types.

A bioinformatic survey of the (uncompleted) genomes of other *Plasmodium* species—the human parasite *P. vivax*, the rodent parasites *P. yoelii* (*21*) and *P. berghei*, and the avian parasite *P. gallinaceum*—revealed a remarkable radiation of the "export element" consisting of the first exon encoding the signal sequence, the intron, and the second exon encoding the Pexel motif (fig. S5). Moreover, we identified a number of large species-specific gene families encoding putative surface antigens in the genomes of *P. vivax*, *P. berghei*, and *P. gallinaceum* (fig. S5). On the basis of their structural similarity to PfEMP1, Rifin, and Stevor in *P. falciparum* (i.e., a highly variable N-terminal exodomain, a putative transmembrane domain, and a conserved cytoplasmic tail), these antigens are predicted to be virulence factors on the surface of the corresponding host cells. Accordingly, we show that the N termini including the Pexel motif of members of these families from *P. gallinaceum* (Fig. 4C) and *P. vivax* (Fig. 4D) are necessary to target YFP to the erythrocyte when transfected into *P. falciparum*. Hence, the Pexel motif is conserved in *Plasmodium* spp. Although many exported proteins are prime candidates for vaccine development or therapeutic intervention, their usefulness is limited by antigenic variation and strain-specific differences. The identification of an export mechanism unique to *Plasmodium* spp. raises the possibility of developing completely novel strategies to interfere with multiple aspects of parasite development through a single target.

References and Notes

1. L. G. Pologe, A. Pavlovec, H. Shio, J. V. Ravetch, *Proc. Natl. Acad. Sci. U.S.A.* **84**, 7139 (1987).
2. D. I. Baruch *et al.*, *Cell* **82**, 77 (1995).
3. X. Z. Su *et al.*, *Cell* **82**, 89 (1995).
4. J. D. Smith *et al.*, *Cell* **82**, 101 (1995).
5. S. Kyes, P. Horrocks, C. Newbold, *Annu. Rev. Microbiol.* **55**, 673 (2001).
6. M. E. Wickham *et al.*, *EMBO J.* **20**, 1 (2001).
7. C. Lopez-Estrano, S. Bhattacharjee, T. Harrison, K. Haldar, *Proc. Natl. Acad. Sci. U.S.A.* **100**, 12402 (2003).
8. M. Foley, L. Tilley, *Int. J. Parasitol.* **28**, 1671 (1998).
9. See supporting data on *Science* Online.
10. E. Knuepfer, M. Rug, N. Klonis, L. Tilley, A. F. Cowman, unpublished data.
11. T. Blisnick *et al.*, *Mol. Biochem. Parasitol.* **111**, 107 (2000).
12. D. L. Baldi *et al.*, *EMBO J.* **19**, 1 (2000).
13. M. J. Gardner *et al.*, *Nature* **419**, 498 (2002).
14. K. Haldar *et al.*, *Cell. Microbiol.* **4**, 383 (2002).
15. L. H. Freitas-Junior *et al.*, *Nature* **407**, 1018 (2000).
16. K. G. Le Roch *et al.*, *Science* **301**, 1503 (2003); published online 31 July 2003 (10.1126/science.1087025).
17. Z. Bozdech *et al.*, *Genome Biol.* **4**, R9 (2003).
18. L. Florens *et al.*, *Nature* **419**, 520 (2002).
19. E. Lasonder *et al.*, *Nature* **419**, 537 (2002).
20. A. Scherf *et al.*, *EMBO J.* **11**, 2293 (1992).
21. J. M. Carlton *et al.*, *Nature* **419**, 512 (2002).

22. The genome sequence data for *P. berghei* and *P. gallinaceum* were produced by the Pathogen Sequencing Unit at the Wellcome Trust Sanger Institute (ftp://ftp.sanger.ac.uk/pub/pathogens/Plasmodium). Sequence data for *P. vivax* and *P. yoelii* were obtained from The Institute for Genomic Research (TIGR; www.tigr.org). The *P. vivax* sequences used in this study were performed by TIGR and funded by the National Institute of Allergy and Infectious Diseases and the U.S. Department of Defense. Corresponding PlasmoDB (for 3D7) and GenBank (for all other strains) accession numbers can be found at *Science* Online. We thank J. Healer, A. B. Hehl, G. I. McFadden, L. Tilley, and B. S. Crabb for comments, and the Red Cross Blood Service (Australia) for blood. Supported by a postdoctoral fellowship from the Swiss National Science Foundation (M.M.), a Wellcome Trust International Traveling Fellowship (E.K.), NIH grant R01-A144008-04A1, the Wellcome Trust, and the National Health and Medical Research Council (Australia). A.F.C. is an International Scholar of the Howard Hughes Medical Institute.

Supporting Online Material

www.sciencemag.org/cgi/content/full/306/5703/1930/DC1
Materials and Methods
Figs. S1 to S5
Table S1
References

19 August 2004; accepted 22 October 2004
10.1126/science.1102452

A Host-Targeting Signal in Virulence Proteins Reveals a Secretome in Malarial Infection

N. Luisa Hiller, Souvik Bhattacharjee, Christiaan van Ooij, Konstantinos Liolios, Travis Harrison, Carlos Lopez-Estraño,* Kasturi Haldar†

Malaria parasites secrete proteins across the vacuolar membrane into the erythrocyte, inducing modifications linked to disease and parasite survival. We identified an 11–amino acid signal required for the secretion of proteins from the *Plasmodium falciparum* vacuole to the human erythrocyte. Bioinformatics predicted a secretome of >320 proteins and conservation of the signal across parasite species. Functional studies indicated the predictive value of the signal and its role in targeting virulence proteins to the erythrocyte and implicated its recognition by a receptor/transporter. Erythrocyte modification by the parasite may involve plasmodial heat shock proteins and be vastly more complex than hitherto realized.

P. falciparum causes the most virulent form of human malaria. Blood stage parasites that infect mature erythrocytes are responsible for all the symptoms and pathologies of the disease (*1*). Proteins secreted from the parasite to the host erythrocyte are responsible for many disease pathologies and death (*1*). They are also thought to underlie structural and transport changes in the erythrocyte required for parasite survival (*2*, *3*). Thus, secreted protein families such as subtelomeric variable open reading frame (STEVOR), repetitive interspersed family (RIFIN), and *P. falciparum* erythrocyte membrane protein 1 (PfEMP1) are responsible for antigenic and adhesive changes in the infected erythrocyte (*4*). PfEMP1s are the major virulence determinants in cerebral and placental malaria commonly seen in young children and pregnant women [the groups most vulnerable to malaria (*4*, *5*)]. Despite advances in proteomics (*6*, *7*), parasite proteins that underlie multiple phenotypic modifications in the erythrocyte membrane, as well as the number of exported proteins, remain enigmatic (*2*, *3*). We investigated whether critical, conserved transport signals target proteins from the parasite to the erythrocyte to establish the presence of a major host-targeting pathway in malarial infection and to enable recognition of a wide range of proteins (a "secretome") that present high-value candidate effectors of disease and infection.

Departments of Pathology and Microbiology-Immunology, Feinberg School of Medicine, Northwestern University, 303 East Chicago Avenue, Chicago, IL 60611, USA.

*Present address: Department of Microbiology and Molecular Cell Sciences, University of Memphis, 3774 Walker Avenue, 409B Life Sciences Building, Memphis, TN 38152, USA.

†To whom correspondence should be addressed. E-mail: k-haldar@northwestern.edu

Within the erythrocyte, *P. falciparum* resides and develops surrounded by a parasitophorous vacuolar membrane. Several studies have established that a cleavable endoplasmic reticulum (ER)–type signal sequence (SS) is sufficient for protein recruitment into the secretory pathway within the parasite, as well as release at the parasite plasma membrane and into the lumen of the parasitophorous vacuole (*8*–*10*). We have recently demonstrated that for two histidine-rich proteins [the knob-associated histidine-rich protein or histidine-rich protein I (HRPI) as well as histidine-rich protein II (HRPII)], cleavage of the ER-type SS reveals a vacuolar transport signal (VTS) that resides within the next 40 amino acids of each protein (*11*). The VTS is required to export a reporter such as green fluorescent protein (GFP) from the lumen of the parasitophorous vacuole to the erythrocyte cytoplasm and must be exposed at the N terminus (*11*). We now show (Fig. 1A) VTSs located within 60 amino acids downstream from the SS cleavage site of non–histidine-rich proteins [such as PfEMP2 (*12*) and glycophorin-binding protein 130 (GBP 130) (*13*) that are known to be exported to the erythrocyte].

Multiple Expectation Maximization for Motif Elicitation (MEME) analysis revealed the presence of a primary pattern common in five experimentally validated VTS sequences (fig. S1, A and B) (*14*). Reiterative use of MEME and of the Motif Alignment and Search Tool (MAST) (fig. S1) (*14*) in the *P. falciparum* database yielded an optimized MEME motif of RxSRILAExxx (*15*) (blue bar in Fig. 1B; the positional value indicated by x is elaborated in fig. S1A). This motif was detected in 259 parasite proteins, 8 of which were removed by hand curation, leav-

Table 1. Summary of predicted secretome based on table S1.

Category	No. of proteins	Notable characteristics	Annotation source
Unknowns	91	No annotation	None
Protein families	8	Range between two to four sequences from predicted secretome per family	This report
Protein rich in internal repeats	10	Repeats	This report
Proteins highly enriched in one or more amino acids	11	At least one residue is highly enriched over expected frequencies	This report
RIFINs	119	Variant antigens	PlasmoDB
STEVORs	22	Variant antigens	PlasmoDB
Candidate phosphatases	3	Aminopeptidase/α/β hydrolase	PlasmoDB, this report
		α/β hydrolase	PlasmoDB, this report
		Calcineurin-like phosphoesterase	This paper
Candidate serine-threonine kinases	3	3.8 protein	PlasmoDB
		Kinase	This report
		Kinase	This report
Predicted heat shock proteins	3	hsp40 homolog	PlasmoDB, this report
		DNAJ	PlasmoDB, this report
		DNAJ domain	PlasmoDB, this report
Predicted ARF	1	Missing one domain critical for guanosine 5′-triphosphate binding	PlasmoDB
Presence of glycophorin-binding repeats	3	GBP 130	PlasmoDB
		Five repeats	PlasmoDB
		Seven repeats	PlasmoDB
Putative ABC transporter	1	Transporter	PlasmoDB
Proteins in the input	5	GBP 130	PlasmoDB
		HRP I	PlasmoDB
		HRP II	NCBI
		Erythrocyte membrane protein 2	PlasmoDB
		Erythrocyte membrane protein 3	PlasmoDB
PfEMP1	67	Absence of N-terminal SS	PlasmoDB

ing 251 parasite proteins (fig. S1A). These included our original input of five soluble proteins, a surprisingly large number of hypothetical proteins (Table 1 and table S1), and known exported antigens (*16*–*18*) not in our original input (thereby validating the MAST). Prominent among the known proteins were 119 and 22 membrane-bound RIFINs and STEVORs, respectively, even though our original input contained only soluble exported proteins. Consistent with the location of STEVORs in erythrocytic "cleft" structures (*16*), expression of a full-length STEVOR fused at its C terminus to GFP resulted in detection of green fluorescence in punctate domains in the erythrocyte (Fig. 1Ca). Notably, the first 60 amino acids downstream of STEVOR SS (but lacking the transmembrane domains) constitute a VTS and export the GFP reporter to the erythrocyte cytosol (Fig. 1Cb), suggesting a shared function for the motif in both soluble and membrane antigens. Additional signals must localize full-length STEVORs to punctate domains in the erythrocyte.

A sequence logo (*19*) of the MEME motif and its surrounding region is presented in Fig. 2A. It reveals the high information content of the 11 amino acids in the motif. It indicates that Arg in position 4 and Leu in position 6 are the most highly conserved residues in the motif. It also shows the lower but finite positional value of the three C-terminal residues represented as "xxx" in the linearized motif RxSRILAExxx. Placing an Ala in position 4 or in position 6 in the PfHRPII VTS blocks export of GFP to the erythrocyte (Fig. 2B), indicating that the motif provides a signal for protein export from the vacuole to the erythrocyte. Inhibition of export upon single amino acid replacement implicates recognition of the signal by a receptor/transporter.

To independently test the predictive power of the motif in identifying unknown exported proteins, we investigated whether a hypothetical protein in the MAST output (fig. S1A) contained a functional export signal. We selected a protein (PFE1615c) expressed during blood stage infection (as determined by transcriptome analysis) (*20*, *21*) with no National Center for Biotechnology Information (NCBI) homologs or Pfam pattern recognized in silico. Furthermore, it is only present in the second MAST output and not in the first (fig. S1A). Although still included in the matrix, its motif (THSRILKQLEF) differs from that of PfHRPII (LNKRLLHETQA) (and all of the initial experimental data set). PFE1615c contains a vacuolar translocation signal (Fig. 2Ca) that can export GFP to the erythrocyte, but this export is blocked by replacement of RILKQLE in its motif with LNAKALA (Fig. 2Cb). Thus, the motif

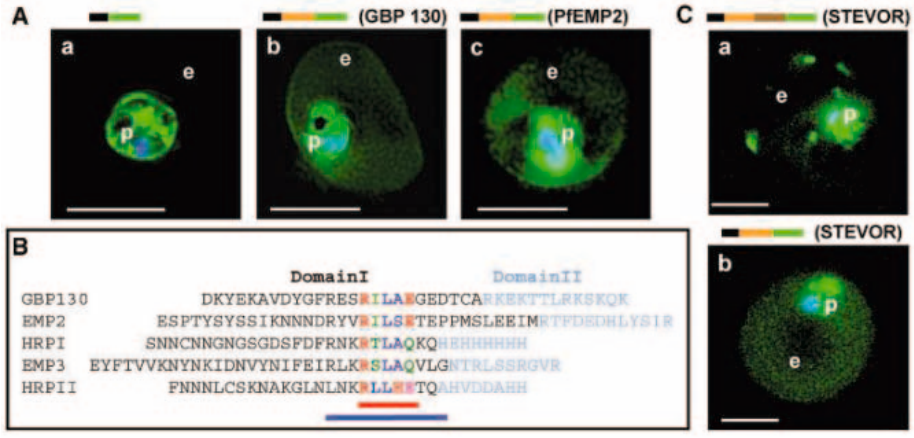

Fig. 1. Identification of a conserved motif of 11 amino acids in VTSs of parasite proteins exported to the erythrocyte. (**A**) VTS of proteins PfGBP 130 and PfEMP2 target GFP to the erythrocyte. Projections (0°) of live cells expressing GFP chimeras of a SS alone (a), SSVTSGBP130 (b), and SSVTSEMP2 (c). (**B**) Alignment of MEME motifs in VTSs of indicated five exported soluble proteins. Red bar underlines 5–amino acid MEME motif 1. Blue bar underlines 11–amino acid MEME motif 2. (**C**) Projections (0°) of live cells expressing GFP chimeras of full-length STEVOR (a) and SSVTSSTEVOR (b). (A) and (C) were detected by digitized fluorescence microscopy. Parasite (p) nucleus is Hoechst stained (blue). Green, GFP; e, erythrocyte. Schematic above panels indicate constructs containing SS (black), VTS (orange) of the indicated proteins, and GFP (green). STEVOR sequences downstream of the VTS are indicated in brown in (C). Scale bars, 5 μm.

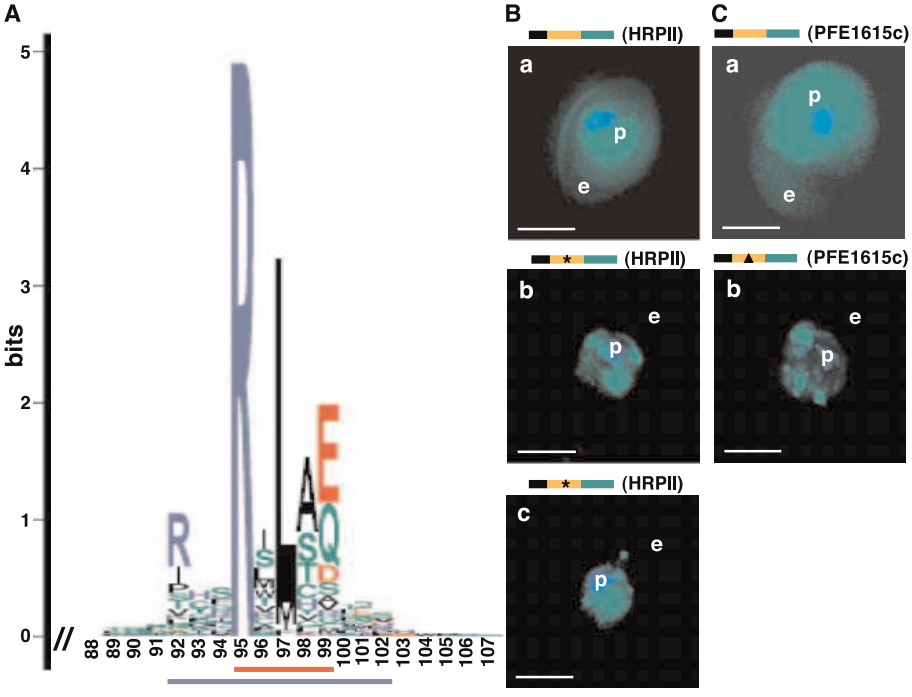

Fig. 2. The VTS motif is a signal for vacuolar protein export and shows high value in identification of unknown parasite proteins exported to the erythrocyte. (**A**) Sequence logo derived from the predicted secretome. Amino acids are represented by one-letter abbreviations and color coded as follows: blue, basic; red, acidic; black, hydrophobic; green, polar. Height of amino acids is proportional to the fraction of the observed frequency relative to the expected frequency in *P. falciparum* proteins. (**B**) Projections (0°) of live cells expressing GFP chimeras of SSHRPIIVTS with no change (a) or motif point mutants R4A (b) or L6A (c), where 4 and 6 indicate position in the signal. Export of green fluorescence (GFP) to erythrocyte (e) is abrogated in both point mutants. (**C**) Projections (0°) of live cells expressing GFP chimeras of SSVTSPFE1615c with intact motif (a), or replacement of motif sequences RILKQLE with LNAKALA (b). Replacement of motif residues blocks export of green fluorescence to the erythrocyte. (B) and (C) were detected by digitized fluorescence microscopy. Parasite (p) nucleus is Hoechst stained (blue). Schematics above panels indicate constructs containing SS (black), VTS (orange) of the indicated proteins, and GFP (green). Stars indicate single amino acid substitutions and the triangle indicates seven-residue replacement. Scale bars, 5 μm.

provides a vacuolar export signal in unknown proteins, shows high predictive value in identifying hitherto unknown parasite proteins exported to the erythrocyte, and is conserved across parasite species (fig. S4) (*22*).

Arguably, the most important of known parasite protein families exported to the erythrocyte is the PfEMP1 family (*1*). However, PfEMP1s lack a leader SS and are presumably recruited into the parasite secretory pathway by means of an internal SS that serves as membrane anchor for these type I membrane proteins (*23*). Thus, PfEMP1s were not included in our initial database subjected to MAST (fig. S1 series). We therefore investigated the presence of the MEME motif in a data set that contained *P. falciparum* proteins that lack a predicted N-terminal ER-type SS (fig. S2). Three predicted PfEMP1 sequences containing QFFRWFSEWSE or IGKRVHAQVQN were detected in the MAST (fig. S2A). IGKRVHAQVQN was present in only two proteins, whereas QFFRWFSEWSE is a highly conserved sequence in all PfEMP1s (Fig. 3A and fig. S2B). We reasoned that an export motif should be preserved in the family. Unfortunately, because of their size, full-length PfEMP1s cannot be cloned and expressed as transgenes. Nonetheless, we successfully synthesized a "minitransgene" containing the motif that is present in full-length PfEMP1s beyond amino acid 200 but before the cysteine-rich interdomain region α (Fig. 3, A and B). The synthetic PfEMP1 also contained the conserved transmembrane and C-terminal cytoplasmic domains (amino acids 1521 to 2042 of *P. falciparum* PfEMP1, NCBI accession number AAB09769.1), but most of the PfEMP1 adhesive domains were replaced by GFP (Fig. 3B). Expression of this transgene resulted in the export of green fluorescence primarily to "spots" (possibly reflecting clefts) in the erythrocyte (Fig. 3Ca). When FFRWFSEWS in the motif was replaced by AASTDIAST (Fig. 3Cb) or the N-terminal fragment was deleted (Fig. 3Cc), green fluorescence remained with the parasite. This provides the first identification of a conserved sequence in the virulence membrane protein PfEMP1 that can signal protein export to the erythrocyte. This is likely to occur without exporting the membrane protein into the erythrocyte cytosol. Although the exact step of vacuolar export catalyzed by the signal in transmembrane proteins is not yet delineated, the motif clearly provides a host/erythrocyte-targeting signal in PfEMP1 transport. The experimentally validated PfEMP1 signal QFFRWFSEWSE can be incorporated into the MEME and MAST analysis in fig. S1A to optimize the plasmodial host–targeting (PlasmoHT) pattern (*22*).

The presence of the host-targeting signal in putative parasite phosphatases and kinases expressed during blood stage infection (Table 1 and table S1) suggests that these activities modify the erythrocyte, consistent with previous data suggesting export of these parasite functions to the erythrocyte (*24*). A putative parasite adenosine 5′-diphosphate–ribosylation factor (ARF) or ARF-like protein is also predicted to be exported, the functional evaluation of which may reveal whether the parasite exports both the machinery and cargo underlying erythrocyte modification. Notably, our study provides the first prediction for the export of parasite-encoded heat shock proteins to the erythrocyte. Moreover, evidence that a GFP fusion of a soluble heat shock protein 40 (HSP40) (with motif TSLRSLAEFNS) is exported to the erythrocyte (fig. S3) strongly supports a role for these parasite chaperones in the process of protein export and/or erythrocyte modification.

The vacuolar export/host-targeting signal is also present in 91 unknown proteins (Table 1). Conservative estimates project that at least 50 of these unknowns are expressed during blood stage infection (table S1), suggesting the possibility that the parasite induces substantial complex molecular changes in the erythrocyte, of which we remain largely ignorant. Importantly, they provide high-value candidate effectors, the functional analyses of which may yield further insights into mechanisms underlying virulence and disease associated with blood stage malarial infection as well as the ability of the parasite to survive within the erythrocyte.

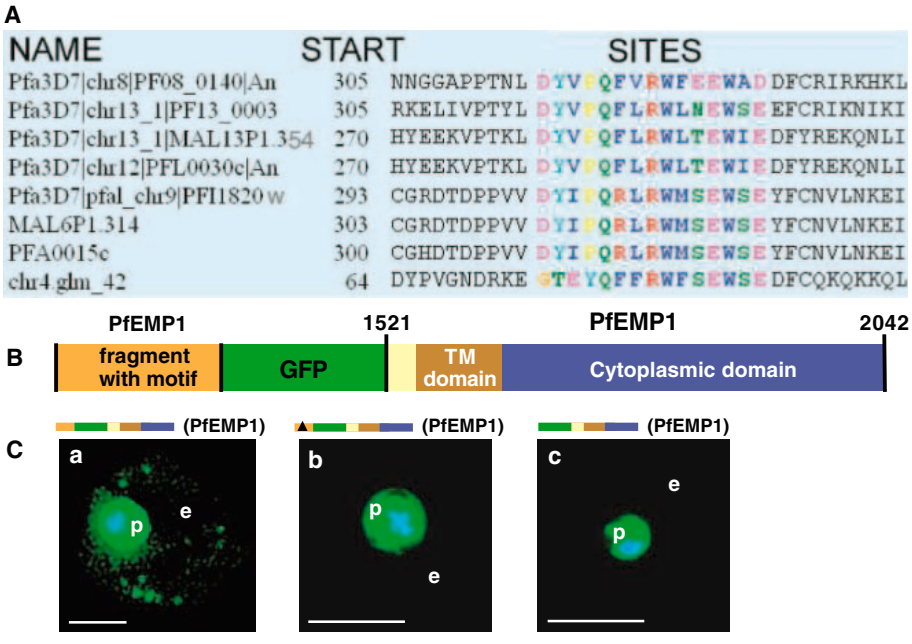

Fig. 3. A host-targeting signal is detected in the virulence membrane protein PfEMP1. (**A**) Alignment of multiple predicted PfEMP1 sequences with colored amino acids highlighting the MEME of the conserved region (*14*), in which the last 11 colored amino acids correspond to a predicted export signal. (**B**) Schematic representation of a PfEMP1 minigene–GFP chimera containing PfEMP1 domain (orange) with the MEME motif as well as transmembrane and cytosolic domain (amino acids 1521 to 2042 from PfEMP1 AAB09769.1) (yellow, brown, and blue). (**C**) Projections (0°) of live cells expressing the PfEMP1 minigene–GFP chimera with no change (a), nine-residue replacement (triangle) of FFRWFSEWS in signal with AASTDIAST (b), and deletion of the 203-to-321 fragment (c), as detected by digitized fluorescence microscopy. Export of green fluorescence is primarily to "spots" (possibly reflecting clefts) in the erythrocyte in (a). This export is blocked by either replacement of indicated residues in the predicted signal or loss of the fragment (containing the motif). p, parasite; e, erythrocyte. Scale bars, 5 μm. Identification codes shown are from PlasmoDB.

References and Notes

1. L. H. Miller, D. I. Baruch, K. Marsh, O. K. Doumbo, *Nature* **415**, 673 (2002).
2. K. Haldar *et al.*, *Cell. Microbiol.* **4**, 383 (2002).
3. L. Aravind, L. M. Iyer, T. E. Wellems, L. H. Miller, *Cell* **115**, 771 (2003).
4. N. Rasti, M. Wahlgren, Q. Chen, *FEMS Immunol. Med. Microbiol.* **41**, 9 (2004).
5. M. Fried, P. E. Duffy, *Science* **272**, 1502 (1996).
6. L. Florens *et al.*, *Nature* **419**, 520 (2002).
7. N. Nirmalan, P. F. Sims, J. E. Hyde, *Mol. Microbiol.* **52**, 1187 (2004).
8. M. E. Wickham *et al.*, *EMBO J.* **20**, 5636 (2001).
9. P. Cheresh, T. Harrison, H. Fujioka, K. Haldar, *J. Biol. Chem.* **277**, 16265 (2002).
10. R. F. Waller, M. B. Reed, A. F. Cowman, G. I. McFadden, *EMBO J.* **19**, 1794 (2000).
11. C. Lopez-Estraño, S. Bhattacharjee, T. Harrison, K. Haldar, *Proc. Natl. Acad. Sci. U.S.A.* **100**, 12402 (2003).
12. S. Lustigman, R. Anders, G. Brown, R. L. Coppel, *Mol. Biochem. Parasitol.* **38**, 261 (1990).
13. M. Perkins, *Exp. Parasitol.* **65**, 61 (1988).
14. Materials and methods are available as supporting material on *Science* Online.
15. Single-letter abbreviations for the amino acid residues are as follows: A, Ala; C, Cys; D, Asp; E, Glu;

F, Phe; G, Gly; H, His; I, Ile; K, Lys; L, Leu; M, Met; N, Asn; P, Pro; Q, Gln; R, Arg; S, Ser; T, Thr; V, Val; W, Trp; and Y, Tyr.
16. M. Kaviratne, S. M. Khan, W. Jarra, P. R. Preiser, *Eukaryot. Cell* **1**, 926 (2002).
17. M. Haeggstrom *et al.*, *Mol. Biochem. Parasitol.* **133**, 1 (2004).
18. T. Y. Sam-Yellowe *et al.*, *Genome Res.* **14**, 1052 (2004).
19. J. Gorodkin, L. J. Heyer, S. Brunak, G. D. Stormo, *Comput. Appl. Biosci.* **13**, 583 (1997).
20. Z. Bozdech *et al.*, *PLoS Biol.* **1**, E5 (2003).
21. K. G. Le Roch *et al.*, *Science* **301**, 1503 (2003).
22. A search engine to identify proteins containing the PlasmoHT motif is available at www.haldarlab.northwestern.edu.
23. X.-Z. Su *et al.*, *Cell* **82**, 89 (1995).
24. J. F. Kun *et al.*, *Mol. Biochem. Parasitol.* **85**, 41 (1997).
25. We thank W. Kibbe, L. Zhu, V. Haztimanikatis, A. Vania Apkarian, and A. Chenn for helpful discussion. Supported by American Heart Association fellowship (0215246z to N.L.H.) and the NIH (HL69630, AI39071 to K.H.). PlasmoDB and GenBank identification codes, respectively: PFE1615c: NP_703661; PfHSP40: PFE0055c and NP_703357; PfEMP1 fragment chr4.glm_42. The PfEMP1 used for transmembrane domain and cytoplasmic tail has NCBI identification code AAB09769.1.

Supporting Online Material
www.sciencemag.org/cgi/content/full/306/5703/1934/DC1
Materials and Methods
Figs. S1 to S4
Table S1
Bioinformatic Data

13 July 2004; accepted 19 October 2004
10.1126/science.1102737

A Draft Sequence for the Genome of the Domesticated Silkworm (*Bombyx mori*)

Biology analysis group: Qingyou Xia,[1]*† Zeyang Zhou,[1]* Cheng Lu,[1]* Daojun Cheng,[1] Fangyin Dai,[1] Bin Li,[1] Ping Zhao,[1] Xingfu Zha,[1] Tingcai Cheng,[1] Chunli Chai,[1] Guoqing Pan,[1] Jinshan Xu,[1] Chun Liu,[1] Ying Lin,[1] Jifeng Qian,[1] Yong Hou,[1] Zhengli Wu,[1] Guanrong Li,[1] Minhui Pan,[1] Chunfeng Li,[1] Yihong Shen,[1] Xiqian Lan,[1] Lianwei Yuan,[1] Tian Li,[1] Hanfu Xu,[1] Guangwei Yang,[1] Yongji Wan,[1] Yong Zhu,[1] Maode Yu,[1] Weide Shen,[1] Dayang Wu,[1] Zhonghuai Xiang[1]†
Genome analysis group: Jun Yu,[2,3]*† Jun Wang,[2,3]* Ruiqiang Li,[2]* Jianping Shi,[2] Heng Li,[2] Guangyuan Li,[2] Jianning Su,[2] Xiaoling Wang,[2] Guoqing Li,[2] Zengjin Zhang,[2] Qingfa Wu,[2] Jun Li,[2] Qingpeng Zhang,[2] Ning Wei,[2] Jianzhe Xu,[2] Haibo Sun,[2] Le Dong,[2] Dongyuan Liu,[2] Shengli Zhao,[2] Xiaolan Zhao,[2] Qingshun Meng,[2] Fengdi Lan,[2] Xiangang Huang,[2] Yuanzhe Li,[2] Lin Fang,[2] Changfeng Li,[2] Dawei Li,[2] Yongqiao Sun,[2] Zhenpeng Zhang,[2] Zheng Yang,[2] Yanqing Huang,[2] Yan Xi,[2] Qiuhui Qi,[2] Dandan He,[2] Haiyan Huang,[2] Xiaowei Zhang,[2] Zhiqiang Wang,[2] Wenjie Li,[2] Yuzhu Cao,[2] Yingpu Yu,[3] Hong Yu,[3] Jinhong Li,[3] Jiehua Ye,[3] Huan Chen,[3] Yan Zhou,[3] Bin Liu,[2] Jing Wang,[2] Jia Ye,[3] Hai Ji,[2] Shengting Li,[2] Peixiang Ni,[2] Jianguo Zhang,[2] Yong Zhang,[2] Hongkun Zheng,[2] Bingyu Mao,[2] Wen Wang,[2] Chen Ye,[2] Songgang Li,[2] Jian Wang,[2,3] Gane Ka-Shu Wong,[2,3,4]† Huanming Yang[2,3]†

We report a draft sequence for the genome of the domesticated silkworm (*Bombyx mori*), covering 90.9% of all known silkworm genes. Our estimated gene count is 18,510, which exceeds the 13,379 genes reported for *Drosophila melanogaster*. Comparative analyses to fruitfly, mosquito, spider, and butterfly reveal both similarities and differences in gene content.

Silk fibers are derived from the cocoon of the silkworm *Bombyx mori*, which was domesticated over the past 5000 years from the wild progenitor *Bombyx mandarina* (*1*). Silkworms are second only to fruitfly as a model for insect genetics, owing to their ease of rearing, the availability of mutants from genetically homogeneous inbred lines, and the existence of a large body of information on their biology (*2*). There are about 400 visible phenotypes, and ~200 of these are assigned to linkage groups (*3*). Silkworms can also be used as a bioreactor for proteinaceous drugs and as a source of biomaterials. Here, we present a draft sequence of the silkworm genome with 5.9× coverage.

B. mori has 28 chromosomes. More than 1000 genetic markers have been mapped at an average spacing of 2 cM (~500 kb) (*4*). A physical map is being constructed through the fingerprinting and end sequencing of bacterial artificial chromosome (BAC) clones (*5*). Many expressed sequence tags (ESTs) have been produced (*6*), and a 3× draft sequence has just been announced by the International Lepidopteran Genome Project (*7*). Our project is independent of, but complementary to, that of the consortium. Our sequence has been submitted to the DNA Data Bank of Japan/European Molecular Biology Laboratory/GenBank (project accession number AADK00000000, version AADK01000000) and is also accessible from our Web site (http://silkworm.genomics.org.cn) (*8*). ESTs discussed in this Report can be found at GenBank (accession numbers CK484630 to CK565104).

DNA for genome sequencing is derived from an inbred domesticated variety, *Dazao* (posterior silk gland, fifth-instar day 3, on a mix of 1225 males). A whole-genome shotgun (*9*) technique was used, and our coverage is 5.9×. Including the unassembled reads, the total estimated genome size is 428.7 Mb, or 3.6 and 1.54 times larger than that of fruitfly (*10*) and mosquito (*11*). The N50 contig and scaffold sizes are 12.5 kb and 26.9 kb. Our assembly contains 90.9% of the 212 known silkworm genes (with full-length cDNA sequence), 90.9% of ~16,425 EST clusters, and 82.7% of the 554 known genes from other Lepidoptera. Additional details of our quality analyses are given in the supporting online material (fig. S1 and tables S1 to S6).

We developed a gene-finder algorithm *BGF* (BGI GeneFinder) (fig. S2), based on *GenScan* and *FgeneSH*. To determine a gene count for silkworm, one must correct for erroneous and partial predictions (Table 1). The final corrected gene count for silkworm is 18,510 genes, which far exceeds the official gene count of 13,379 for fruitfly

[1]Southwest Agricultural University, Chongqing Beibei, 400716, China. [2]Beijing Institute of Genomics of Chinese Academy of Sciences, Beijing Genomics Institute, Beijing Proteomics Institute, Beijing 101300, China. [3]James D. Watson Institute of Genome Sciences of Zhejiang University, Hangzhou Genomics Institute, Key Laboratory of Genomic Bioinformatics of Zhejiang Province, Hangzhou 310008, China. [4]University of Washington Genome Center, Department of Medicine, University of Washington, Seattle, WA 98195, USA.

*These authors contributed equally to this work.
†To whom correspondence should be addressed. E-mail: xiaqy@swau.cq.cn (Q.X.), xzh@swau.cq.cn (Z.X.), junyu@genomics.org.cn (J.Y.), gksw@genomics.org.cn (G.K-S.W.), yanghm@genomics.org.cn (H.Y.)

(our *BGF*-based procedures predict 13,366 genes for fruitfly). We find that 14.9% of predicted genes are confirmed by ESTs (based on aligning the ESTs to the genome and looking for a 100–base pair overlap with the predicted exons); 60.4% and 63.1% are confirmed by similarity to fruitfly genes and GenBank nonredundant proteins (*BlastP* at 10^{-6} E-value). Overall, 69.7% are confirmed by at least one method.

Not only did we find more genes in silkworm than in fruitfly, but we also found larger genes as a result of the insertion of transposable elements (TEs) in introns. For example, in *calcineurin B* (*cnb*), the silkworm gene was 12 times as large as that of fruitfly. To generalize, we compared annotations, found reciprocal best matches, and computed gene size ratios. Because prediction errors are unlikely to be alignable across species, we restricted our analysis to aligned regions, giving us a mean (median) ratio of 2.29 (2.75) (Fig. 1). This combination of more and bigger genes can explain 86% of the factor of 3.67 increase in genome size from fruitfly (116.8 Mb) to silkworm (428.7 Mb). Silkworm genes also had slightly more exons than fruitfly, with a mean (median) ratio of 1.15 (1.12) for number of exons per gene.

As shown by our TE annotations, most of this increase in the genome size of silkworm is relatively recent. Of the 21.1% of the genome that is recognizable as being of TE origins, 50.7% is from a single *gypsy-Ty3*–like retrotransposon (*12*) (table S7). Mean sequence divergence is 7.7%, which dates the initial appearance of this TE to 4.9 million years ago, if we use the fruitfly neutral rate of 15.6×10^{-9} substitutions per year (*13*). Most other TEs are comparably recent in origins (fig. S3). GC-rich regions contain a higher density of TEs, particularly LINEs (long interspersed nuclear elements), which is the exact opposite of what is reported for the human and mouse genomes.

Unlike silkworm, which is a lepidopteran, fruitfly and mosquito are dipterans. The two insect orders diverged about 280 to 350 million years ago (*14*). Comparisons of their genome content were done at the level of InterPro domains. Functional assignments were mapped according to Gene Ontology (GO). Domain clustering (*15*) (table S8) produced 8947 groups, with 2565 shared among insects and 1793 unique to silkworm (Fig. 2). Consistent with the observed TE expansion, domains like reverse transcriptase, integrase, and transposase stand out for their prevalence in silkworm. A complete list of predicted silkworm genes is shown in table S9, with a special indexing table for the genes discussed in this paper.

The silk gland, essentially a modified salivary gland, is a highly specialized organ whose function is to synthesize silk proteins. We identified a set of 1874 annotated genes that are confirmed by silk gland ESTs. Only 45 of these genes had been previously described in *B. mori*. GO function categories for silk gland and 11 other tissue libraries were compared (fig. S4). Several hormone-processing enzymes are active in silk gland, which is of interest because hormones participate in regulation of silk protein genes (*16*). Not counting low expressed genes undetectable at current EST depths, genes found only in silk gland include juvenile hormone (JH) esterase, ecdysone oxidase, and JH-inducible protein 1. Ecdysteroid UDP (uridine 5′-diphosphate)–glucosyl transferase is found in silk gland, testis, and ovary. Fibroin forms the bulk of the cocoon mass. It has two major components, a heavy (350 kD) and a light chain (25 kD). We found 1126 ESTs for the light chain, but only 4 ESTs for the heavy chain, suggesting that the one-to-one ratio for light and heavy chains is maintained at the post-transcription level. The heavy chain has five predominant amino acids: Gly (45.9%), Ala (30.3%), Ser (12.1%), Tyr (5.3%), and Val (1.8%). A complete tRNA gene set (table S10) was detected, including 41 Gly-tRNA and 41 Ala-tRNA, twice as many as in the other two insects and consistent with the requirements for fibroin production.

Another well-studied silk-secreting arthropod is the spider. We compared those 1874 genes expressed in *B. mori* silk gland with all available spider data (1482 from GenBank) and identified 107 homologs, including four *B. mori* counterparts for the major ampullate gland peroxidase in spider, which is involved in silk fiber formation (*17*).

We found 87 neuropeptide hormones, hormone receptors, and hormone-regulation genes. *Drosophila melanogaster* and *Anopheles gambiae* have 101 and 73 such genes, respectively. For *B. mori*, 52 genes were unknown, and 35 others were previously reported. Ecdysone oxidase and ecdysteroid UDP–glucosyl transferase (UGT) are implicated in ecdysone metabolism. We classified 20 UGT genes into five major clades (fig. S5), similar to the 34 UGT genes analyzed for *D. melanogaster* (*18*). Juvenile hormone (JH), ecdysone hormone (EH), and prothoracicotropic hormone (PTTH) work in coordination of ecdysis and metamorphosis. We identified 18 EH-sensitive receptors and receptor-like transcription factors. Four BRC Z4 genes contain intact DNA binding BTB domains. One has two additional zinc finger C2H2 type domains, with a zinc-coordinating cysteine pair and a histidine pair. These are involved in completing the larval-pupal transition, and later morphogenetic defects, or in programmed cell death of larval silk glands (*19*). We found many neuropeptide hormone genes too, like diapause hormone (DH), pheromone biosynthesis activating neuropeptide (PBAN), adipokinetic hormone (AKH), eclosion hormone, and bombyxin (4K-PTTH). In addition, diuretic hormone precursor and its receptor, allatotropin, and allatostatin were found. There was also a homolog to *Lymnaea stagnalis* neuropeptide Y precursor, a gene with pancreatic hormone activity that had not been detected in *D. melanogaster* and other insects and may therefore be new to silkworm.

Developmental genes for *D. melanogaster* have been extensively studied. We focused on 83 genes (*20*) that include 41 maternal genes, 12 gap genes, 9 pair-rule genes, 12 segment polarity genes, and 9 homeotic genes. The maternal genes are subdivided into four groups according to their function in patterning the early embryos (anterior, posterior, terminal, and dorsal-ventral). Only six genes [*oskar*, *swallow*, *trunk*, *fs(1)k10*, *gurken*, and *tube*], all from the maternal group, were not detected in *B. mori*. This confirms that the basic mechanism of development is largely conserved

Table 1. Number of predicted genes from *BGF*. We show the initial count, the number of erroneous predictions, and the gene count after likely errors are removed. There are four successive filters, which include rules to remove TEs and pseudogenes, as described in the SOM Text. The final gene count is computed as row 1 minus the sum of rows 2 to 5. Predictions are classified into single-exon genes, partial genes (no head = no start, no tail = no stop, neither) or complete genes. We correct for partial genes by stipulating that each is worth only half a gene. The final corrected gene count is then 18,510.

	Single exon	No head	No tail	Neither	Complete	All genes	Corrected
Total predicted	10,512	6,366	4,903	550	21,199	43,530	37,621
CDS < 100 bp or max exon score < 0.2	107	974	299	15	84	1,479	835
RepeatMasker TEs or copy number >10	7,334	2,233	2,111	124	7,575	19,377	17,143
Similarity to TE-associated proteins	132	71	68	7	294	572	499
Processed "single-exon" pseudogenes	314	146	179	8	153	800	634
Final annotated	2,625	2,942	2,246	396	13,093	21,302	18,510

across insects. It had been reported that *swallow* and *trunk* have no homologs in *A. gambiae*. We find that *tube* has no homolog in *A. gambiae*. Loss of the other three genes is interesting. Localization of the maternal determinant *oskar* at the posterior pole of the *D. melanogaster* oocyte provides positional information for pole plasm formation (*21*). *Gurken* encodes a ligand for *torpedo* (Egf-r), which triggers dorsal differentiation (*22*), whereas *fs(1)k10* is a probable negative regulator of *gurken* translation.

Lepidopteran wing patterning has stimulated a number of experimental studies. Although domesticated silkworm moths have long lost their ability to fly, as well as their colorful wing patterns, we expected that many of these genes would still be found in the sequence. We detected 18 silkworm homologs of wing-patterning genes from other Lepidoptera, primarily *Junonia coenia*. They include the *Distal-less* homeodomain gene, which affects eyespot number, positions, and sizes (*23*); *Ubx*, which represses *Distal-less* expression and leads to haltere formation in *D. melanogaster*, but may not act in the same manner in butterfly (*24*); Hh signaling pathway genes like *Hh*, *Ci*, *En*, and *Ptc*, which are important in eyespot focus formation; *Wg*, which plays a key role in band formation; and *EcR*, which is expressed in prospective eyespots and is coexpressed with *Distal-less* (*25*). Many of these genes are shared with the Diptera. Of the 323 wing-development genes known in *D. melanogaster*, 300 are found in silkworm. Most are well conserved, in that 87% and 56% align at E-values of better than 10^{-20} and 10^{-50}.

Silkworm is a female-heterogametic organism (ZZ in male, ZW in female). Sex in *B. mori* is determined by a dominant feminizing factor on W, as compared to the intricate X:A counting system known in *D. melanogaster*. A homolog of the *D. melanogaster* sex-determining gene *dsx* has been isolated in *B. mori*. It is called *Bmdsx*. Although structural features and splice sites are conserved in these two genes, regulatory mechanisms are not (*26*). The splicing regulator *tra* was not identified in *B. mori*. Neither was the TRA/TRA2 binding site for *Bmdsx*, suggesting that the upstream sex-determining cascade for *B. mori* and *D. melanogaster* differ. However, homologs for most known sex-determining factors can be found. Among *daughterless* (*da*), *hermaphrodite* (*her*), *extra macrochaetae* (*emc*), *groucho* (*gro*), *sisterless A* (*sisA*), *scute* (*sc*), *outstretched* (*os*), *deadpan* (*dpn*), and *runt* (*run*) (*27*), homologs for *da*, *emc*, *gro*, *sc*, *dpn*, and *run* were identified in *B. mori*. For *D. melanogaster*, dosage compensation is known to equalize transcription of X-chromosome genes between sexes. At least six genes (*msl-1*, *msl-2*, *msl-3*, *mle*, *mof*, *JIL-1*) are required, and of these, homologs of *mle*, *mof*, and *msl-3* were found in *B. mori*, despite the growing evidence for absence of Z-linked dosage compensation in *B. mori* (*28*). In these and other cases in which insect genes were not found in *B. mori*, we manually checked our automated procedures (see SOM Text). However, further experiments will be needed, given the incompleteness of the genome and the level of homology needed for detection.

Humoral immune factors together with wound healing, homeostasis, and adaptive humoral immune responses are important components of immunity and defense in insects (*29*). We identified a total of 69 such genes, including 34 antibacterial genes, of which 23 appear to be newly identified. They encode the innate immune factors synthesized in fat bodies and hemocytes, which kill bacteria by permeabilizing their membranes. One of them is the Lepidopteran *moricin*, a highly alkaline antibacterial peptide initially isolated from *B. mori*. A new cluster of 8 *moricin* genes was found, with amino acid sequence identities of greater than 90% among members, but only 20% similarity to known *moricins*. *Defensins* specific to Gram-positive bacteria were found, as were *cecropins* (*30*). We detected a previously unknown class of *cecropins*. Other found genes related to insect defense include *lysozymes*, *hemolin*, *lectins*, and *prophenoloxidases*. As a member of the immunoglobulin (Ig) family, *hemolin* is unique to the Lepidoptera. *Lectins* are abundant, with 29 found in *B. mori*, compared to 35 and 22 in *D. melanogaster* and *A. gambiae* (*31*), respectively. We also identified three *prophenoloxidases*, of which two were previously known.

Lepidoptera are unusual because they have holocentric chromosomes with diffuse kinetochores. This characteristic is a potential driver of evolution because of the ability to retain chromosome fragments through many cell divisions. The nematode also has diffuse kinetochores, and five key chromosomal proteins are known (*32*, *33*): *hcp-1*, *hcp-2*, *hcp-3*, *hcp-4*, and *hcp-6*. (The prefix *hcp* stands for "holocentric protein.") *Hcp-3* is detected in all eukaryotic centromeres, similar to histone H3 in its histone-fold domain, but dissimilar in its N-terminal region. It is also known as *Cse4p* in yeast, *Cid* in fruitfly, and *CENP-A* in human. Their proteins are highly diverged. The putative homolog in silkworm has only 23% identity to the histone-fold domain of *hcp-3*, but their lengths are similar: 268 amino acids for silkworm and 288 amino acids for nematode. There are many homologs of *hcp-1* and *hcp-2*—18 and 72, to be specific—making it difficult to determine which ones might be the true orthologs. We could not find a homolog for *hcp-4*, but we did identify a homolog for a related gene that is known as *CENP-C* and was previously found in human, mouse, and chicken. Finally, we were not able to identify the silkworm homolog for *hcp-6*.

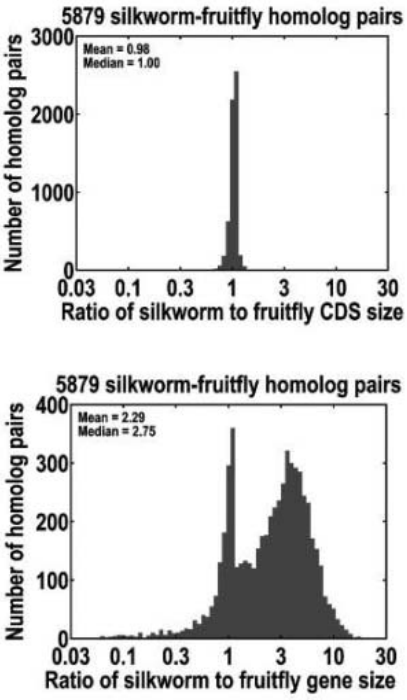

Fig. 1. Comparison of gene size in silkworm-fruitfly orthologs. We use reciprocal best matches, and calculate a ratio over the aligned portion. Size is shown with (gene size) or without (CDS size) introns. The minor peak is due to single-exon alignments.

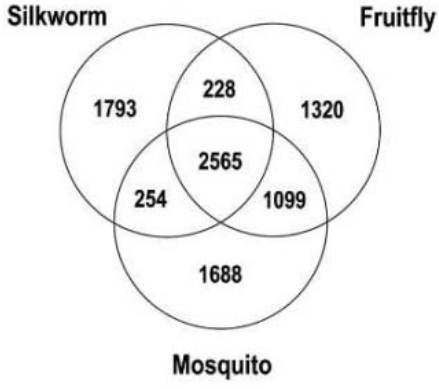

Fig. 2. InterPro domain clusters shared among or unique to all possible combinations of silkworm, fruitfly, and mosquito. Clusters are constructed with the algorithm detailed in table S8, which is based on a similar earlier analysis (*14*).

References and Notes

1. Y. Zhou, *General Entomology* (High Education Publication House, Beijing, ed. 2, 1958).
2. M. R. Goldsmith, in *Molecular Model Systems in the Lepidoptera*, M. R. Goldsmith, A. S. Wilkins, Eds. (Cambridge Univ. Press, Cambridge, 1995), pp. 21–76.

3. H. Doira, H. Fujii, Y. Kawaguchi, H. Kihara, Y. Banno, *Genetic Stocks and Mutations of Bombyx mori* (Institute of Genetic Resources, Kyushu University, Japan, 1992).
4. M. R. Goldsmith, T. Shimada, H. Abe, *Annu. Rev. Entomol.* 10.1146/annurev.ento.50.071803.130456 (2004).
5. C. Wu, S. Asakawa, N. Shimizu, S. Kawasaki, Y. Yasukochi, *Mol. Gen. Genet.* **261**, 698 (1999).
6. K. Mita *et al.*, *Proc. Natl. Acad. Sci. U.S.A.* **100**, 14121 (2003).
7. K. Mita *et al.*, *DNA Res.* **11**, 27 (2004).
8. J. Wang *et al.*, *Nucleic Acids Res.*, in press.
9. J. Yu *et al.*, *Science* **296**, 79 (2002).
10. M. D. Adams *et al.*, *Science* **287**, 2185 (2000).
11. R. A. Holt *et al.*, *Science* **298**, 129 (2002).
12. H. Abe *et al.*, *Mol. Gen. Genet.* **263**, 916 (2000).
13. W. H. Li, *Molecular Evolution* (Sinauer, Sunderland, MA, 1997).
14. M. W. Gaunt, M. A. Miles, *Mol. Biol. Evol.* **19**, 748 (2002).
15. G. M. Rubin *et al.*, *Science* **287**, 2204 (2000).
16. K. Grzelak, *Comp. Biochem. Physiol. B Biochem. Mol. Biol.* **110**, 671 (1995).
17. N. N. Pouchkina, B. S. Stanchev, S. J. McQueen-Mason, *Insect Biochem. Mol. Biol.* **33**, 229 (2003).
18. T. Luque, D. R. O'Reilly, *Insect Biochem. Mol. Biol.* **32**, 1597 (2002).
19. M. Uhlirova *et al.*, *Proc. Natl. Acad. Sci. U.S.A.* **100**, 15607 (2003).
20. T. Brody, *Trends Genet.* **15**, 333 (1999); http://flybase.bio.indiana.edu/allied-data/lk/interactive-fly.
21. N. F. Vanzo, A. Ephrussi, *Development* **129**, 3705 (2002).
22. S. Roth, F. S. Neuman-Silberberg, G. Barcelo, T. Schupbach, *Cell* **81**, 967 (1995).
23. P. Beldade, P. M. Brakefield, A. D. Long, *Nature* **415**, 315 (2002).
24. W. O. McMillan, A. Monteiro, D. D. Kapan, *Trends Ecol. Evol.* **17**, 125 (2002).
25. P. B. Koch, R. Merk, R. Reinhardt, P. Weber, *Dev. Genes Evol.* **212**, 571 (2003).
26. M. G. Suzuki, F. Ohbayashi, K. Mita, T. Shimada, *Insect Biochem. Mol. Biol.* **31**, 1201 (2001).
27. C. Schutt, R. Nothiger, *Development* **127**, 667 (2000).
28. M. G. Suzuki, T. Shimada, M. Kobayashi, *Heredity* **81**, 275 (1998).
29. A. B. Mulnix, P. E. Dunn, in *Molecular Model Systems in the Lepidoptera*, M. R. Goldsmith, A. S. Wilkins, Eds. (Cambridge Univ. Press, Cambridge, 1995), pp. 369–395.
30. H. Steiner, D. Hultmark, A. Engstrom, H. Bennich, H. G. Boman, *Nature* **292**, 246 (1981).
31. G. K. Christophides *et al.*, *Science* **298**, 159 (2002).
32. L. L. Moore, M. B. Roth, *J. Cell Biol.* **153**, 1199 (2001).
33. J. H. Stear, M. B. Roth, *Genes Dev.* **16**, 1498 (2002).
34. This project was supported by Chinese Academy of Sciences, National Development and Reform Commission, Ministry of Science and Technology, National Natural Science Foundation of China, Ministry of Agriculture, Chongqing Municipal Government, Beijing Municipal Government, Zhejiang Provincial Government, Hangzhou Municipal Government, and Zhejiang University. Additional funding came from National Human Genome Research Institute (grant 1 P50 HG02351).

Supporting Online Material

www.sciencemag.org/cgi/content/full/306/5703/1937/DC1
SOM Text
Figs. S1 to S5
Tables S1 to S10

1 July 2004; accepted 20 October 2004
10.1126/science.1102210

By Carrot or by Stick: Cognitive Reinforcement Learning in Parkinsonism

Michael J. Frank,[1]* Lauren C. Seeberger,[2] Randall C. O'Reilly[1]*

To what extent do we learn from the positive versus negative outcomes of our decisions? The neuromodulator dopamine plays a key role in these reinforcement learning processes. Patients with Parkinson's disease, who have depleted dopamine in the basal ganglia, are impaired in tasks that require learning from trial and error. Here, we show, using two cognitive procedural learning tasks, that Parkinson's patients off medication are better at learning to avoid choices that lead to negative outcomes than they are at learning from positive outcomes. Dopamine medication reverses this bias, making patients more sensitive to positive than negative outcomes. This pattern was predicted by our biologically based computational model of basal ganglia–dopamine interactions in cognition, which has separate pathways for "Go" and "NoGo" responses that are differentially modulated by positive and negative reinforcement.

Should you shout at your dog for soiling the carpet or praise him when he does his business in the yard? Most dog trainers will tell you that the answer is both. The proverbial "carrot-and-stick" motivational approach refers to the use of a combination of positive and negative reinforcement: One can persuade a donkey to move either by dangling a carrot in front of it or by striking it with a stick. Both carrots and sticks are important for instilling appropriate behaviors in humans. For instance, when mulling over a decision, one considers both pros and cons of various options, which are implicitly influenced by positive and negative outcomes of similar decisions made in the past. Here, we report that whether one learns more from positive or negative outcomes varies with alterations in dopamine levels caused by Parkinson's disease and the medications used to treat it.

To better understand how healthy people learn from their decisions (both good and bad), it is instructive to examine under what conditions this learning is degraded. Notably, patients with Parkinson's disease are impaired in cognitive tasks that require learning from positive and negative feedback (*1*–*3*). A likely source of these deficits is depleted levels of the neuromodulator dopamine in the basal ganglia of Parkinson's patients (*4*), because dopamine plays a key role in reinforcement learning processes in animals (*5*). A simple prediction of this account is that cognitive performance should improve when patients take medication that elevates their dopamine levels. However, a somewhat puzzling result is that dopamine medication actually worsens performance in some cognitive tasks, despite improving it in others (*6*, *7*).

Computational models of the basal ganglia–dopamine system provide a unified account that reconciles the above pattern of results and makes explicit predictions about the effects of medication on carrot-and-stick learning (*8*, *9*). These models simulate transient changes in dopamine that occur during positive and negative reinforcement and their differential effects on two separate pathways within the basal ganglia system. Specifically, dopamine is excitatory on the direct or "Go" pathway, which helps facilitate responding, whereas it is inhibitory on the indirect or "NoGo" pathway, which suppresses responding (*10*–*13*). In animals, phasic bursts of dopamine cell firing are observed during positive reinforcement (*14*, *15*), which are thought to act as "teaching signals" that lead to the learning of rewarding behaviors (*14*, *16*). Conversely, choices that do not lead to reward [and aversive events, according to some studies (*17*)] are associated with dopamine dips that drop below baseline (*14*, *18*). Similar dopamine-dependent processes have been inferred to occur in humans during positive and negative reinforcement (*19*, *20*). In our models, dopamine bursts increase synaptic plasticity in the direct pathway while decreasing it in the indirect pathway (*21*, *22*), supporting Go learning to reinforce the good choice. Dips in dopamine have the opposite effect, supporting NoGo learning to avoid the bad choice (*8*, *9*).

A central prediction of our models is that nonmedicated Parkinson's patients are impaired at learning from positive feedback (bursts of dopamine; "carrots"), because of reduced levels of dopamine. However, the

[1]Department of Psychology and Center for Neuroscience, University of Colorado Boulder, Boulder, CO 80309–0345, USA. [2]Colorado Neurological Institute Movement Disorders Center, Englewood, CO 80113, USA.

*To whom correspondence should be addressed. E-mail: frankmj@psych.colorado.edu (M.J.F.); oreilly@psych.colorado.edu (R.C.O.).

models also make the counterintuitive prediction that patients should display enhanced learning from negative feedback (dips in dopamine; "sticks"), because of their low dopamine levels that facilitate this kind of learning. Conversely, we predict that patients on medication have sufficient dopamine to learn from positive feedback, but would be relatively impaired at learning from negative feedback because the medication blocks the effects of normal dopamine dips. This pattern of dopamine effects explains the existing puzzling results in the Parkinson's disease literature showing both cognitive enhancements and impairments from medication (*8*).

This report presents a more direct test of the model's predictions. We used "procedural learning" (i.e., trial-and-error) tasks (*23*) with 30 Parkinson's patients and 19 healthy seniors matched for age, education, and an estimate of verbal IQ [see table S1 in (*24*) for demographic details and the number of subjects per task condition]. Two different procedural learning tasks were used, one probabilistic and one deterministic, with the task selected at random for the first session. A subset of participants returned for a second session to perform the other task, and Parkinson's patients in this session abstained from taking their regular dose of dopamine medication for a mean of 18 hours before the experiment (*7*, *24*).

In the probabilistic selection task, three different stimulus pairs (AB, CD, EF) are presented in random order, and participants have to learn to choose one of the two stimuli (Fig. 1A). Feedback follows the choice to indicate whether it was correct or incorrect, but this feedback is probabilistic. In AB trials, a choice of stimulus A leads to correct (positive) feedback in 80% of AB trials, whereas a B choice leads to incorrect (negative) feedback in these trials (and vice versa for the remaining 20% of trials). CD and EF pairs are less reliable: Stimulus C is correct in 70% of CD trials, whereas E is correct in 60% of EF trials. Over the course of training, participants learn to choose stimuli A, C, and E more often than B, D, or F. Note that learning to choose A over B could be accomplished either by learning that choosing A leads to positive feedback, or that choosing B leads to negative feedback (or both). To evaluate whether participants learned more about positive or negative outcomes of their decisions, we subsequently tested them with novel combinations of stimulus pairs involving either an A (AC, AD, AE, AF) or a B (BC, BD, BE, BF); no feedback was provided. We predict that Parkinson's patients on medication, compared with those off medication, learn more from positive than negative feedback and should, therefore, reliably choose the best carrot (stimulus A) in all novel test pairs in which it is present. In contrast, those off medication should learn more from negative than positive feedback and, therefore, reliably avoid the worst stick (stimulus B).

In the implicit transitive inference task (*25*), the reinforcement for each stimulus pair is deterministic, but stimulus pairs are partially overlapping (Fig. 1A). Four pairs of stimuli are presented: A+B–, B+C–, C+D–, and D+E– where + and – indicate positive and negative feedback. A hierarchy (A > B > C > D > E) emerges in which stimuli near the top of the hierarchy develop net positive associative strengths, whereas those near the bottom develop net negative associative strengths (*25*–*27*). This explains why, when presented with novel combination BD, participants (and animals trained in similar paradigms) often correctly choose stimulus B, despite having no explicit awareness of any hierarchical structure among the items (*25*, *26*, *28*, *29*). On the basis of this associative account, we predicted that Parkinson's patients on medication, compared with those off medication, would learn

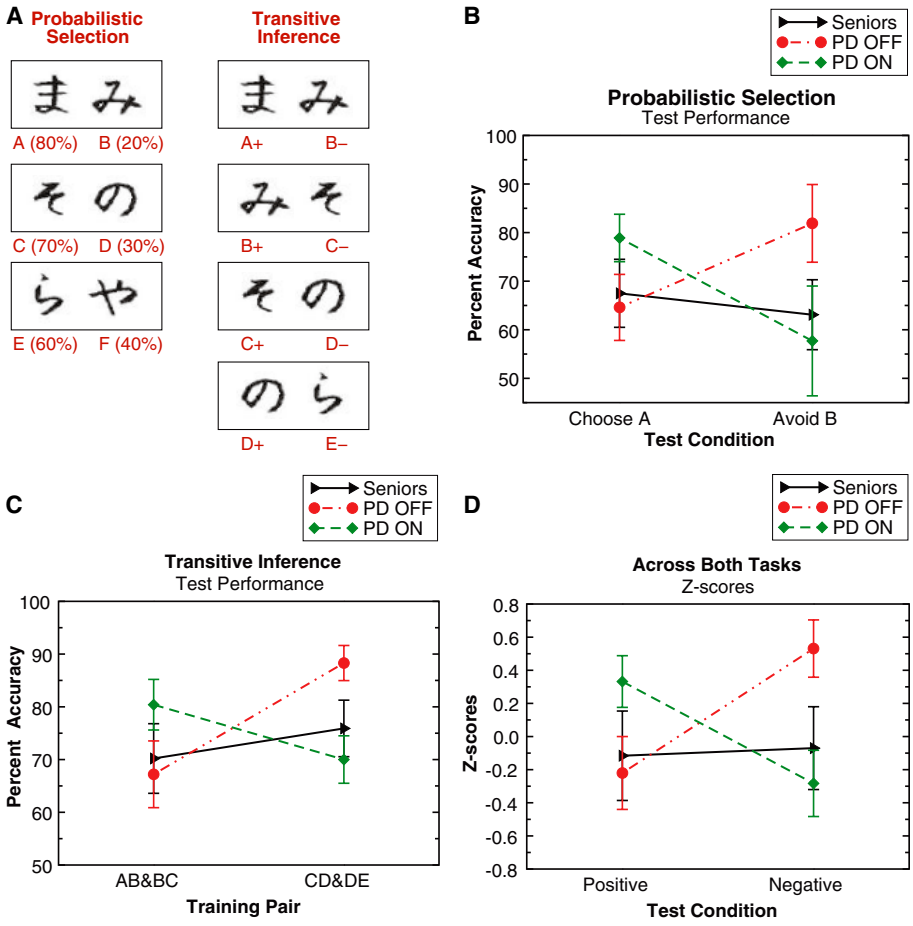

Fig. 1. (**A**) Example stimulus pairs (Hiragana characters) used in both cognitive procedural learning tasks, designed to minimize verbal encoding. One pair is presented per trial, and the participant makes a forced choice. In probabilistic selection, the frequency of positive feedback for each choice is shown. In transitive inference, feedback is deterministic and indicated by the +/− signs for each stimulus. Any of 12 keys on the left side of the keyboard selects the stimulus on the left, and vice versa for the right stimulus. The stimulus locations were randomized across trials, and assignment of Hiragana character to stimulus label (A to F) was randomized across participants. In actuality, different Hiragana characters were used across tasks. (**B**) Novel test-pair performance in the probabilistic selection task, where choosing A depends on having learned from positive feedback, whereas avoiding B depends on having learned from negative feedback. (**C**) Training pair performance during the test phase in the transitive inference task. Stimuli at the top of the hierarchy (A, B) have net positive associations, whereas those at the bottom (C, D) have net negative associations (*24*–*29*). Thus, learning from positive feedback benefits performance on AB and BC, while learning from negative feedback benefits CD and DE. Groups did not differ in novel test pairs AE and BD [not shown in figure; see (*24*)] which could be solved either by choosing stimuli with positive associations or avoiding those with negative associations. (**D**) The *z* scores across both probabilistic selection and transitive inference tasks. Positive and negative conditions correspond to A and B pairs in the probabilistic selection task, and AB/BC and CD/DE pairs in the transitive inference task. Error bars reflect standard error.

more about the positive associations at the top of the hierarchy, resulting in better performance on stimulus pairs AB and BC. Conversely, those off medication should learn more about the negative associations at the bottom of the hierarchy, which would result in better CD and DE performance. Note that because the choice for the novel BD pair could be made either by a positive B association or a negative D association, we did not predict a difference in BD performance between groups.

Results confirmed our predictions. Despite no main effect of medication, session, or test condition, the critical interaction between medication and test condition was significant for both the probabilistic selection [$F(1,26) = 4.3$, $P < 0.05$] and transitive inference [$F(1,39) = 5.5$, $P < 0.05$] tasks. In the probabilistic selection task (Fig. 1B), patients on medication tended to choose stimulus A, which indicated that they had found the best carrot in the bunch. In contrast, patients off medication had a greater tendency to avoid stimulus B, which indicated that they had learned to avoid the harshest stick. Age-matched controls did not differ in performance between A and B pairs. In the transitive inference task (Fig. 1C), patients on medication performed better at choosing positively associated stimuli at the upper end of the hierarchy, whereas those off medication more reliably avoided negative stimuli at the lower end. Finally, age-matched controls did not differ between performance on pairs at the high and low end of the stimulus hierarchy. There was also no effect of medication on performance on novel pairs AE and BD [$F(1,39) = 1.6$, n.s.].

To compare results across both tasks, we converted accuracy measures for both positive and negative conditions to z scores (Fig. 1D). This analysis confirmed a significant interaction between positive or negative condition and Parkinson's disease medication group [$F(1,68) = 10.4$, $P = 0.0019$]. Planned comparisons revealed that patients on medication chose positive stimuli more reliably than they avoided negative stimuli [$F(1,25) = 4.98$, $P < 0.05$] and chose them more reliably than the other two groups [$F(1,69) = 4.8$, $P < 0.05$]. Conversely, patients off medication avoided negative stimuli more reliably than they chose positive stimuli [$F(1,15) = 5.42$, $P < 0.05$] and more reliably than the other two groups [$F(1,69) = 7.6$, $P < 0.05$]. This was also true relative to healthy seniors alone [$F(1,69) = 4.6$, $P < 0.05$].

This last observation is a rare example of enhanced cognitive performance associated with neurological disease, as it suggests that nonmedicated patients made better use of negative feedback than either patients on medication or healthy seniors. Trial-to-trial analysis confirmed that a change of choice behavior in the probabilistic selection task (e.g., they chose C in a CD trial after having chosen D in the previous CD trial) was more often accounted for by negative feedback in the previous trial in patients off medication compared with those on medication [$F(1,26) = 5.62$, $P < 0.05$]. Medicated patients switched choices just as often during training but were not as influenced by negative feedback to do so. There was no difference between these groups in the efficacy of positive feedback to modify behavior on a trial-to-trial basis [$F(1,26) = 0.42$, not significant (n.s.)].

Taken together, these findings provide a mechanistic understanding of the nature of the cognitive sequelae of Parkinson's disease, which ties together a variety of other observations across multiple levels of analysis. First, we build on claims that learning from error feedback is primarily affected in Parkinson's disease (*3*), by showing that the direction of this effect interacts critically with the valence of the feedback and the medication status of the patient. Second, these results are consistent with neuroimaging studies showing that positive and negative feedback have differential effects on basal ganglia activity (*30*, *31*). Third, they help clarify the basis for why medication sometimes improves but sometimes impairs cognitive deficits in Parkinson's disease, depending on the task (*6*–*8*). Specifically, patients on medication displayed enhanced positive-feedback learning beyond even that of healthy participants, supporting the idea that medication results in higher-than-normal amounts of dopamine in ventral striatum, which is relatively spared in early-stage Parkinson's disease (*4*, *6*, *7*). Finally, our observation that nonmedicated patients display enhanced ability to avoid negative stimuli may provide the fundamental basis for reports of enhanced harm avoidance behavior in these patients (*32*, *33*).

An equally important contribution of this work is in its confirmation of very specific predictions made by our computational model of the basal ganglia system (*8*, *9*, *34*). Almost all of the basic mechanisms of this model have been postulated in various forms by other researchers. Nevertheless, it represents an integration of these mechanisms into a

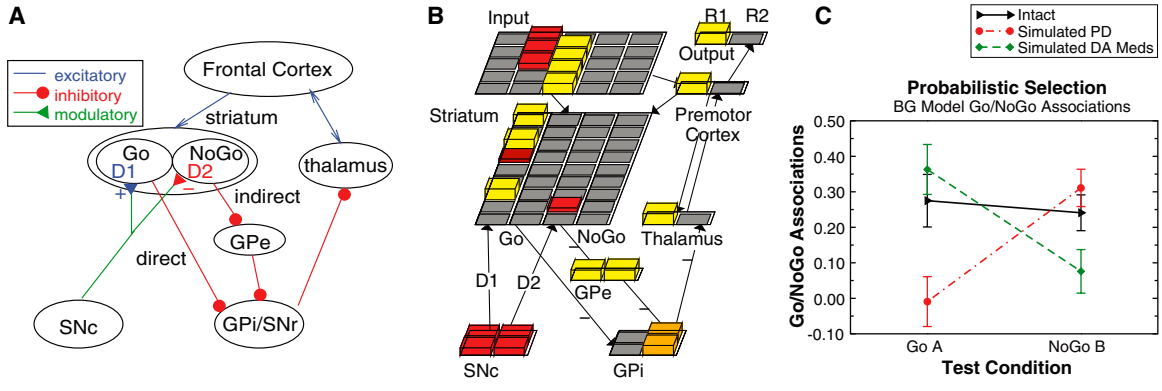

Fig. 2. (**A**) The cortico-striato-thalamo-cortical loops, including the direct (Go) and indirect (NoGo) pathways of the basal ganglia. The Go cells disinhibit the thalamus via the internal segment of globus pallidus (GPi) and thereby facilitate the execution of an action represented in cortex. The NoGo cells have an opposing effect by increasing inhibition of the thalamus, which suppresses actions and thereby keeps them from being executed. Dopamine from the substantia nigra pars compacta (SNc) projects to the dorsal striatum, causing excitation of Go cells via D1 receptors, and inhibition of NoGo via D2 receptors. GPe: external segment of globus pallidus; SNr: substantia nigra pars reticulata. (**B**) The Frank (in press) neural network model of this circuit (squares represent units, with height and color reflecting neural activity; yellow, most active; red, less active; gray, not active). The premotor cortex selects an output response via direct projections from the sensory input, and is modulated by the basal ganglia projections from thalamus. Go units are in the left half of the striatum layer; NoGo in the right half, with separate columns for the two responses [R1 (left button), R2 (right button)]. In the case shown, striatum Go is stronger than NoGo for R1, inhibiting GPi, disinhibiting thalamus, and facilitating execution of the response in cortex. A tonic level of dopamine is shown in SNc; a burst or dip ensues in a subsequent error feedback phase (not shown in figure), causing corresponding changes in Go/NoGo unit activations, which drive learning. (**C**) Predictions from the model for the probabilistic selection task, showing Go-NoGo associations for stimulus A and NoGo-Go associations for stimulus B. Error bars reflect standard error across 25 runs of the model with random initial weights.

coherent, mechanistically explicit system. At the most general level, the basal ganglia in our model modulates the selection of actions being considered in frontal cortex (*8*, *34–36*). More specifically, two main projection pathways from the striatum go through different basal ganglia output structures on the way to thalamus and up to cortex (Fig. 2A). Activity in the direct pathway sends a Go signal to facilitate the execution of a response considered in cortex, whereas activity in the indirect pathway sends a NoGo signal to suppress competing responses. Transient changes in dopamine levels that occur during positive and negative feedback have opposite effects on D1 and D2 (dopamine) receptors, which are relatively segregated in the direct and indirect pathways, respectively (*10–13*). Thus, the net effects of dopamine bursts during positive reinforcement are to activate the Go pathway and to deactivate the NoGo pathway, driving learning so that reinforced responses are subsequently facilitated. Conversely, decreases in dopamine during negative reinforcement have the opposite effect, driving NoGo learning so that incorrect responses are subsequently suppressed or avoided (*8*).

These dopamine modulation effects on the Go and NoGo pathways lead directly to the predictions that we confirmed in the experiments reported earlier, as revealed in computational simulations of these dynamics (Fig. 2, B and C) (*8*). To simulate Parkinson's disease, we decreased tonic and phasic dopamine levels in the substantia nigra pars compacta layer of the network, which reduced the ability to generate dopamine bursts during positive feedback. Therefore, the model was relatively impaired at reinforcing Go firing to correct responses. Furthermore, the low tonic dopamine levels produced a persistent bias on the system in favor of the NoGo pathway, which resulted in a corresponding bias to learn NoGo in response to negative feedback. Thus, in our simulation of the probabilistic selection task (Fig. 2C), the simulated Parkinson's model learned NoGo to B more often than Go to A. In contrast, intact models learned an even balance of Go to A and NoGo to B.

To simulate the effects of Parkinson's disease medication, we increased the dopamine levels (both tonic and phasic), but we also decreased the size of the phasic dopamine dips during negative feedback. The latter effect is included because D2 agonist medications taken by the vast majority of our Parkinson's patients (in addition to L-dopa) tonically bind to D2 receptors irrespective of phasic changes in dopamine firing, thereby "filling in" the dips. The net result is the opposite of our simulated Parkinson's model. The tonic elevation in dopamine receptor activation produced a Go bias in learning, whereas the diminished phasic dip decreased the model's ability to learn NoGo from negative feedback. These combined effects produced the clear crossover-interaction pattern that we observed in our studies (Fig. 2C). Similar results held for our simulation of the transitive inference experiment (*24*). Finally, reversal learning deficits observed in Parkinson's patients on medication (*6*, *7*) were also accounted for by this same model (*8*).

Nevertheless, the model does not capture the overall better performance of Parkinson's patients in our study relative to healthy senior controls. This result is somewhat surprising, given that patient impairments have been observed in previous studies (*1–3*). One potential reason for this discrepancy is the relative simplicity of our task relative to those used in previous studies. Furthermore, although our control group was matched to the patients in all of our demographic variables, other uncontrolled variables might have led to differences in overall performance levels. For example, because we had access to patient medical records, we may have successfully excluded more patients than seniors for other age-related neurological impairments. Alternatively, Parkinson's patients may have had greater motivation to perform well, given that they were aware that we were studying cognitive sequelae of their disease (the so-called Hawthorne effect). Further, although abstract neural models can make qualitative predictions (such as the crossover interactions observed in this study), the quantitative aspects of the predictions require more detailed knowledge of specific parameters of the neural system, along with the precise degree of dopamine depletion and remediation by medication in Parkinson's disease; these data are not available. Therefore, we argue that the most meaningful comparisons are the on-versus-off medication conditions, for which the model and data are in close agreement. In addition, the model accurately predicts that healthy seniors did not differ in their tendency to learn from positive versus negative feedback. Finally, we note that our model does not explicitly consider the uneven levels of dopamine depletion in ventral and dorsal striatum of Parkinson's patients (*4*), which are also thought to play a role in cognitive enhancements or impairments resulting from medication (*6–8*).

In summary, we have presented evidence for a mechanistic account of how the human brain implicitly learns to make choices that lead to good outcomes, while avoiding those that lead to bad outcomes. The consistent results across tasks (one probabilistic and the other deterministic) and in both medicated and nonmedicated Parkinson's patients provide substantial support for a dynamic dopamine model of cognitive reinforcement learning.

References and Notes

1. B. J. Knowlton, J. A. Mangels, L. R. Squire, *Science* **273**, 1399 (1996).
2. F. Ashby, L. Alfonso-Reese, A. Turken, E. Waldron, *Psychol. Rev.* **105**, 442 (1998).
3. D. Shohamy *et al.*, *Brain* **127**, 851 (2004).
4. S. Kish, K. Shannak, O. Hornykiewicz, *N. Engl. J. Med.* **318**, 876 (1988).
5. R. A. Wise, P.-P. Rompre, *Annu. Rev. Psychol.* **40**, 191 (1989).
6. R. Swainson *et al.*, *Neuropsychologia* **38**, 596 (2000).
7. R. Cools, R. Barker, B. Sahakian, T. Robbins, *Cereb. Cortex* **11**, 1136 (2001).
8. M. Frank, *J. Cognit. Neurosci.*, in press.
9. R. C. O'Reilly, M. J. Frank, *ICS Tech. Rep.,* University of Colorado Institute of Cognitive Science (2004).
10. C. Gerfen, *Annu. Rev. Neurosci.* **15**, 285 (1992).
11. I. Aubert, I. Ghorayeb, E. Normand, B. Bloch, *J. Comp. Neurol.* **418**, 22 (2000).
12. S. Hernandez-Lopez, J. Bargas, D. Surmeier, A. Reyes, E. Galarraga, *J. Neurosci.* **17**, 3334 (1997).
13. S. Hernandez-Lopez *et al.*, *J. Neurosci.* **20**, 8987 (2000).
14. W. Schultz, *Neuron* **36**, 241 (2002).
15. W. Schultz, P. Dayan, P. R. Montague, *Science* **275**, 1593 (1997).
16. J. Wickens, *Network Comput. Neural Syst.* **8**, R77 (1997).
17. M. Ungless, P. Magill, J. Bolam, *Science* **303**, 2040 (2004).
18. T. Satoh, S. Nakai, T. Sato, M. Kimura, *J. Neurosci.* **23**, 9913 (2003).
19. C. B. Holroyd, M. G. H. Coles, *Psychol. Rev.* **109**, 679 (2002).
20. D. Zald *et al.*, *J. Neurosci.* **24**, 4105 (2004).
21. A. Nishi, G. Snyder, P. Greengard, *J. Neurosci.* **17**, 8147 (1997).
22. D. Centonze, B. Picconi, P. Gubellini, G. Bernardi, P. Calabresi, *Eur. J. Neurosci.* **13**, 1071 (2001).
23. Note that, although participants may become aware of which stimulus they are actually choosing, they are likely not aware of the detailed influence of the history of positive and negative feedback on their choices. This is the sense in which we regard these as procedural or implicit learning tasks.
24. Materials and methods are available as supporting online material on *Science* Online.
25. M. Frank, J. Rudy, W. Levy, R. O'Reilly, *Mem. Cognit.,* in press.
26. M. Frank, J. Rudy, R. O'Reilly, *Hippocampus* **13**, 341 (2003).
27. L. von Fersen, C. D. L. Wynne, J. D. Delius, J. E. R. Staddon, *J. Exp. Psychol. Anim. Behav. Process.* **17**, 334 (1991).
28. C. Wynne, *Anim. Learn. Behav.* **23**, 207 (1995).
29. J. Delius, M. Siemann, *Behav. Processes* **42**, 107 (1998).
30. M. R. Delgado, H. M. Locke, V. Stenger, J. A. Fiez, *Cognit. Affect. Behav. Neurosci.* **3**, 27 (2003).
31. C. F. Zink, G. Pagnoni, M. E. Martin-Skurski, J. C. Chappelow, G. S. Berns, *Neuron* **42**, 509 (2004).
32. V. Kaasinen *et al.*, *Proc. Natl. Acad. Sci. U.S.A.* **98**, 13272 (2001).
33. R. Tomer, J. Aharon-Peretz, *J. Neurol. Neurosurg. Psychiatry* **75**, 972 (2004).
34. M. J. Frank, B. Loughry, R. C. O'Reilly, *Cognit. Affect. Behav. Neurosci.* **1**, 137 (2001).
35. J. Mink, *Prog. Neurobiol.* **50**, 381 (1996).
36. G. Chevalier, J. M. Deniau, *Trends Neurosci.* **13**, 277 (1990).

37. Supported by Office of Naval Research grants N00014-00-1-0246 and N00014-03-1-0428, and NIH grant MH069597-01. We thank the staff of the Colorado Neurological Institute for their assistance and K. Richardson for help in administering cognitive tasks to patients and senior participants. We also thank T. Curran, G. McClelland, and Y. Munakata for helpful comments.

19 July 2004; accepted 27 October 2004
Published online 4 November 2004;
10.1126/science.1102941
Include this information when citing this paper.

Addiction as a Computational Process Gone Awry

A. David Redish

Addictive drugs have been hypothesized to access the same neurophysiological mechanisms as natural learning systems. These natural learning systems can be modeled through temporal-difference reinforcement learning (TDRL), which requires a reward-error signal that has been hypothesized to be carried by dopamine. TDRL learns to predict reward by driving that reward-error signal to zero. By adding a noncompensable drug-induced dopamine increase to a TDRL model, a computational model of addiction is constructed that overselects actions leading to drug receipt. The model provides an explanation for important aspects of the addiction literature and provides a theoretic viewpoint with which to address other aspects.

If addiction accesses the same neurophysiological mechanisms used by normal reinforcement-learning systems (*1*–*3*), then it should be possible to construct a computational model based on current reinforcement-learning theories (*4*–*7*) that inappropriately selects an "addictive" stimulus. In this paper, I present a computational model of the behavioral consequences of one effect of drugs of abuse, which is increasing phasic dopamine levels through neuropharmacological means. Many drugs of abuse increase dopamine levels either directly [e.g., cocaine (*8*)] or indirectly [e.g., nicotine (*9*, *10*) and heroin (*11*)]. A neuropharmacologically driven increase in dopamine is not the sole effect of these drugs, nor is it likely to be the sole reason that drugs of abuse are addictive. However, this model provides an immediate explanation for several important aspects of the addiction literature, including the sensitivity of the probability of selection of drug receipt to prior drug experience, to the size of the contrasting nondrug reward, and the sensitivity but inelasticity of drugs of abuse to cost.

The proposed model has its basis in temporal-difference reinforcement models in which actions are selected so as to maximize future reward (*6*, *7*). This is done through the calculation of a value function $V[s(t)]$, dependent on the state of the world $s(t)$. The value function is defined as the expected future reward, discounted by the expected time to reward:

$$V(t) = \int_t^\infty \gamma^{\tau - t} E[R(\tau)] d\tau \qquad (1)$$

where $E[R(\tau)]$ is the expected reward at time τ and γ is a discounting factor ($0 < \gamma < 1$) reducing the value of delayed rewards. Equation 1 assumes exponential discounting in order to accommodate the learning algorithm (*6*, *7*); however, animals (including humans) show hyperbolic discounting of future rewards (*12*, *13*). This will be addressed by including multiple discounting time scales within the model (*14*).

In temporal-difference reinforcement learning (TDRL), an agent (the subject) traverses a world consisting of a limited number of explicit states. The state of the world can change because of the action of the agent or as a process inherent in the world (i.e., external to the agent). For example, a model of delay conditioning may include an interstimulus-interval state (indicated to the agent by the observation of an ongoing tone); after a set dwell time within that state, the world transitions to a reward state and delivers a reward to the agent. This is an example of changing state because of processes external to the agent. In contrast, in a model of FR1 conditioning, an agent may be in an action-available state (indicated by the observation of a lever available to the agent), and the world will remain in the action-available state until the agent takes the action (of pushing the lever), which will move the world into a reward state. For simplicity later, an available action will be written as $S_k \xrightarrow{a_i} S_l$, which indicates that the agent can achieve state S_l if it is in state S_k and selects action a_i. Although the model in this paper is phrased in terms of the agent taking "action" a_i, addicts have very flexible methods of finding drugs. It is not necessary for the model actions to be simple motor actions. $S_k \xrightarrow{a_i} S_l$ indicates the availability of achieving state S_l from state S_k. The agent selects actions proportional to the expected benefit that would be accrued from taking the action; the expected benefit can be determined from the expected change in value and reward (*4*, *6*, *14*, *15*).

The goal of TDRL is to correctly learn the value of each state. This can be learned by calculating the difference between expected and observed changes in value (*6*). This signal, termed δ, can be used to learn sequences that maximize the amount of reward received over time (*6*). δ is not equivalent to pleasure; instead, it is an internal signal indicative of the discrepancy between expectations and observations (*5*, *7*, *15*). Essentially, if the change in value or the achieved reward was better than expected ($\delta > 0$), then one should increase the value of the state that led to it. If it was no different from expected ($\delta = 0$), than the situation is well learned and nothing needs to be changed. Because δ transfers backward from reward states to anticipatory states with learning, actions can be chained together to learn sequences (*6*). This is the heart of the TDRL algorithm (*4*–*7*).

TDRL learns the value function by calculating two equations as the agent takes each action. If the agent leaves state S_k and enters state S_l at time t, at which time it receives reward $R(S_l)$, then

$$\delta(t) = \gamma^d [R(S_l) + V(S_l)] - V(S_k) \qquad (2)$$

where γ^d indicates raising the discounting factor γ by the delay d spent by the animal in state S_k (*14*). $V(S_k)$ is then updated as

$$V(S_k) \leftarrow V(S_k) + \eta_V \delta \qquad (3)$$

where η_V is a learning rate parameter.

Phasic increases in dopamine are seen after unexpected natural rewards (*16*); however, with learning, these phasic increases shift from the time of reward delivery to cuing stimuli (*16*). Transient increases in dopamine are now thought to signal changes in the expected future reward (i.e., unexpected changes in value) (*4*, *16*). These increases can occur either with unexpected reward or with unexpected cue stimuli known to signal reward (*16*) and have been hypothesized to signal δ (*4*, *7*, *16*). Models of dopamine signaling as δ have been found to be compatible with many aspects of the data (*4*, *5*, *16*, *17*).

The results simulated below follow from the incorporation of neuropharmacologically produced dopamine into temporal difference models. The figures below were generated from a simulation by using a TDRL instantiation that allows for action selection within a semi-Markov state space, enabling simulations of delay-related experiments (*14*). The model also produces hyperbolic discounting under normal conditions, consistent with experimental data (*12*, *13*), by a summation of multiple exponential discounting components (*14*), a hypothesis supported by recent functional magnetic resonance imaging data (*18*).

The key to TDRL is that, once the value function correctly predicts the reward, learning stops. The value function can be said to compensate for the reward: The change in

Department of Neuroscience, 6-145 Jackson Hall, 321 Church Street SE, University of Minnesota, Minneapolis, MN 55455, USA. E-mail: redish@ahc.umn.edu

value in taking action $S_k \xrightarrow{a_i} S_l$ counterbalances the reward achieved on entering state S_l. When this happens, $\delta = 0$. Taking transient dopamine as the δ signal (*4*, *5*, *7*) correctly predicted rewards produce no dopamine signal (*16*, *17*).

However, cocaine and other addictive drugs produce a transient increase in dopamine through neuropharmacological mechanisms (*1*, *2*, *8*). The concept of a neuropharmacologically produced dopamine surge can be modeled by assuming that these drugs induce an increase in δ that cannot be compensated by changes in the value (*19*). In other words, the effect of addictive drugs is to produce a positive δ independent of the change in value function, making it impossible for the agent to learn a value function that will cancel out the drug-induced increase in δ. Equation 2 is thus replaced with

$$\delta = \max\{\gamma^d[R(S_l) + V(S_l)] - V(S_k) + D(S_l),\ D(S_l)\} \quad (4)$$

where $D(S_l)$ indicates a dopamine surge occurring on entry into state S_l. Equation 4 reduces to normal TDRL (Eq. 2) when $D(S_l) = 0$ but decreases asymptotically to a minimum δ of $D(S_l)$ when $D(S_l) > 0$. This always produces a positive reward-error signal. Thus, the values of states leading to a dopamine surge, $D > 0$, will approach infinity.

When given a choice between two actions, $S_0 \xrightarrow{a_1} S_1$ and $S_0 \xrightarrow{a_2} S_2$, the agent chooses actions proportional to the values of the subsequent states, S_1 and S_2. The more valuable the state taking an action leads to, the more likely the agent is to take that action. In TDRL, the values of states leading to natural rewards asymptotically approach a finite value (the discounted, total expected future reward); however, in the modified model, the values of states leading to drug receipt increase without bound. Thus, the more the agent traverses the action sequence leading to drug receipt, the larger the value of the states leading to that sequence and the more likely the agent is to select an action leading to those states.

In this model, drug receipt produces a $\delta > 0$ signal, which produces an increase in the values of states leading to the drug receipt. Thus, the values of states leading to drug receipt increase without bound. In contrast, the values of states leading to natural reward increase asymptotically to a value approximating Eq. 1. This implies that the selection probability between actions leading to natural rewards will reach an asymptotic balance. However, the selection probability of actions leading to drug receipt will depend on the number of experiences. Simulations bear this out (Fig. 1).

In the simulations, drug receipt entails a normal-sized reward $R(s)$ that can be compensated by changes in value and a small dopamine signal $D(s)$ that cannot (*14*). Early use of drugs occurs because they are highly rewarding (*1*, *3*, *20*), but this use transitions to a compulsive use with time (*1*, *3*, *20*–*22*). In the model, the $R(s)$ term provides for the early rewarding component, whereas the gradual effect of the $D(s)$ term provides for the eventual transition to addiction. This model thus shows that a transition to addiction can occur without any explicit sensitization or tolerance to dopamine, at least in principle.

The unbounded increase in value of states leading to drug reward does not mean that with enough experience, drugs of abuse are always selected over nondrug rewards. Instead, it predicts that the likelihood of selecting the drug over a nondrug reward will depend on the size of the contrasting nondrug reward relative to the current value of the states leading to drug receipt (Fig. 1).

When animals are given a choice between food and cocaine, the probability of selecting cocaine depends on the amount of food available as an alternative and the cost of each choice (*23*, *24*). Similarly, humans given a choice between cocaine and money will decrease their cocaine selections with increased value of the alternative (*25*). This may explain the success of vouchers in treatment (*25*). This will continue to be true even in well-experienced (highly addicted) subjects, but the sensitivity to the alternate should decrease with experience (see below). This may explain the incompleteness of the success of vouchers (*25*).

Natural rewards are sensitive to cost in that animals (including humans) will work harder for more valuable rewards. This level of sensitivity is termed elasticity in economics. Addictive drugs are also sensitive to cost in that increased prices decrease usage (*26*, *27*). However, whereas the use of addictive drugs does show sensitivity to cost, that sensitivity is inelastic relative to similar measures applied to natural rewards (*26*, *28*). The TDRL model proposed here produces just such an effect: Both modeled drugs and natural rewards are sensitive to cost, but drug reward is less elastic than natural rewards (Fig. 2).

In TDRL, the values of states leading to natural rewards decrease asymptotically to a stable value that depends on the time to the reward, the reward level, and the discounting factors. However, in the modified TDRL model, the values of states leading to drug rewards increase without bound, producing a ratio of a constant cost to increasing values. This decreasing ratio predicts that the elasticity of drugs to cost should decrease with experience, whereas it should not for natural rewards (fig. S4).

The hypothesis that values of states leading to drug receipt increase without

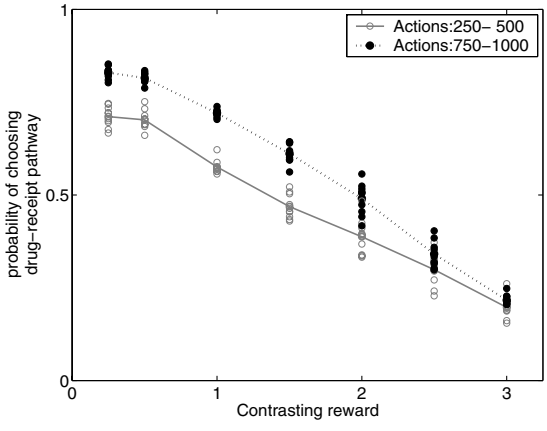

Fig. 1. Probability of selecting a drug-receipt pathway depends on an interaction between drug level, experience, and contrasting reward. Each line shows the average probability of selecting the drug-receipt pathway, $S_0 \xrightarrow{a_2} S_2$, over the contrasting reward pathway, $S_0 \xrightarrow{a_1} S_1$, as a function of the size of the contrasting reward $R(S_3)$. (State space is shown in fig. S1.) Drug receipt on entering state S_4 was $R(S_4) = 1.0$ and $D(S_4) = 0.025$. Individual simulations are shown by dots. Additional details provided in (*14*).

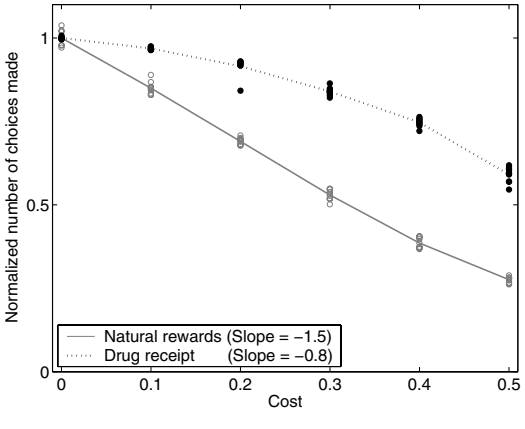

Fig. 2. Elasticity of drug receipt and natural rewards. Both drug receipt and natural rewards are sensitive to costs, but natural rewards are more elastic. Each dot indicates the number of choices made within a session. Sessions were limited by simulated time. The curves have been normalized to the mean number of choices made at zero cost.

bound implies that the elasticity to cost should decrease with use, whereas the elasticity of natural rewards should not. This also suggests that increasing the reward for not choosing the drug [such as vouchers (*25*)] will be most effective early in the transition from casual drug use to addiction.

The hypothesis that cocaine produces a $\delta > 0$ dopamine signal on drug receipt implies that cocaine should not show blocking. Blocking is an animal-learning phenomenon in which pairing a reinforcer with a conditioning stimulus does not show association if the reinforcer is already predicted by another stimulus (*17*, *29*, *30*). For example, if a reinforcer X is paired with cue A, animals will learn to respond to cue A. If X is subsequently paired with simultaneously presented cues A and B, animals will not learn to associate X with B. This is thought to occur because X is completely predicted by A, and there is no error signal ($\delta = 0$) to drive the learning (*17*, *29*, *30*). If cocaine is used as the reinforcer instead of natural rewards, the dopamine signal should always be present ($\delta > 0$), even for the AB stimulus. Thus, cocaine (and other drugs of abuse) should not show blocking.

The hypothesis that the release of dopamine by cocaine accesses TDRL systems implies that experienced animals will show a double dopamine signal in cued-response tasks (*14*). As with natural rewards, a transient dopamine signal should appear to a cuing signal that has been associated with reward (*16*). However, whereas natural rewards only produce dopamine release if unexpected (*16*, *17*), cocaine produces dopamine release directly (*8*), thus, after learning both the cue and the cocaine should produce dopamine (Fig. 3). Supporting this hypothesis, Phillips *et al.* (*31*) found by using fast-scan cyclic voltammetry that, in rats trained to associate an audiovisual signal with cocaine, both the audiovisual stimulus and the cocaine itself produced dramatic increases in the extracellular concentration of dopamine in the nucleus accumbens.

Substance abuse is a complex disorder. TDRL explains some phenomena that arise in addiction and makes testable predictions about other phenomena. The test of a theory such as this one is not whether it encompasses all phenomena associated with addiction, but whether the predictions that follow from it are confirmed.

This model has been built on assumptions about cocaine, but cocaine is far from the only substance that humans (and other animals) abuse. Many drugs of abuse indirectly produce dopamine signals, including nicotine (*10*) and heroin and other opiates (*11*). Although these drugs have other effects as well (*1*), the effects on dopamine should produce the consequences described above, leading to inelasticity and compulsion.

Historically, an important theoretical explanation of addictive behavior has been that of rational addiction (*32*), in which the user is assumed to maximize value or "utility" over time, but because long-term rewards for quitting are discounted more than short-term penalties, the maximized function entails remaining addicted. The TDRL theory proposed in this paper differs from that of rational addiction because TDRL proposes that addiction is inherently irrational: It uses the same mechanisms as natural rewards, but the system behaves in a nonoptimal way because of neuropharmacological effects on dopamine. Because the value function cannot compensate for the $D(s)$ component, the $D(s)$ component eventually overwhelms the $R(s)$ reward terms (from both drug and contrasting natural rewards). Eventually, the agent behaves irrationally and rejects the larger rewards in favor of the (less rewarding) addictive stimulus. The TDRL and rational-addiction theories make testably different predictions: Although rational addiction predicts that drugs of abuse will show elasticity to cost similar to those of natural rewards, the TDRL theory predicts that drugs of abuse will show increasing inelasticity with use.

The rational addiction theory (*32*) assumes exponential discounting of future rewards, whereas humans and other animals consistently show hyperbolic discounting of future rewards (*12*, *13*). Ainslie (*13*) has suggested that the "cross-over" effect that occurs with hyperbolic discounting explains many aspects of addiction. The TDRL model used here also shows hyperbolic discounting (*14*) and so accesses the results noted by Ainslie (*13*). However, in the theory proposed here, hyperbolic discounting is not the fundamental reason for the agent getting trapped in a nonoptimal state. Rather, the TDRL theory hypothesizes that it is the neuropharmacological effect of certain drugs on dopamine signals that drives the agent into the nonoptimal state.

Robinson and Berridge (*22*) have suggested that dopamine mediates the desire to achieve a goal ("wanting"), differentiating wanting from the hedonic desire of "liking." As noted by McClure *et al.* (*15*), Robinson and Berridge's concept of incentive salience (*22*) has a direct correspondence to variables in TDRL: the value of a state reachable by an action. If an agent is in state S_0 and can achieve state S_1 via action $S_0 \xrightarrow{a_i} S_1$ and if state S_1 has a much greater value than state S_0, then $S_0 \xrightarrow{a_i} S_1$ can be said to be a pathway with great incentive salience. The value function is a means of guiding decisions and thus is more similar to wanting than to liking in the terminology of Robinson and Berridge (*15*, *22*). In TDRL, dopamine does not directly encode wanting, but because learning an appropriate value function depends on an accurate δ signal, dopamine will be necessary for acquisition of wanting.

Many unmodeled phenomena play important roles in the compulsive self-administration of drugs of abuse (*1*), including titration of internal drug levels (*33*), sensitization and tolerance (*34*), withdrawal symptoms and release from them (*20*), and compensation mechanisms (*35*, *36*). Additionally, individuals show extensive interpersonal variability (*37*, *38*). Although these aspects are not addressed in the model presented here, many of these can be modeled by adding parameters to the model: for example, sensitization can be included by allowing the drug-induced δ parameter $D(s)$ to vary with experience.

TDRL forms a family of computational models with which to model addictive processes. Modifications of the model can be used to incorporate the unmodeled experimental results from the addiction literature. For example, an important question in this model is whether the values of states leading to drug receipt truly increase without bound.

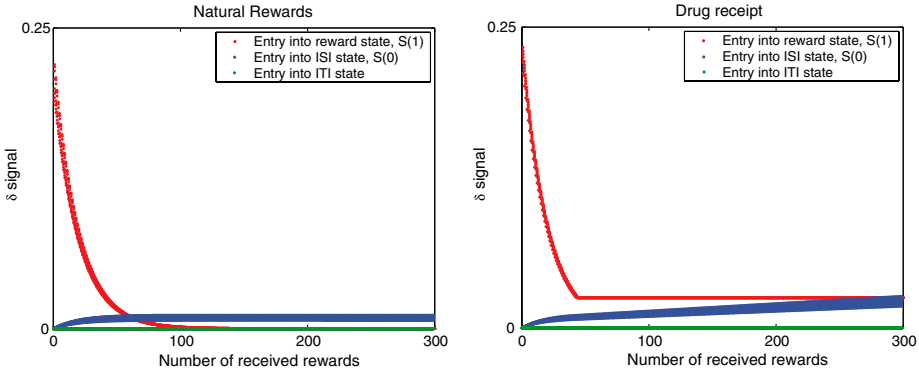

Fig. 3. Dopamine signals. (**Left**) With natural rewards, dopamine initially occurs primarily at reward receipt (on entry into reward state S_1) and shifts to the conditioned stimulus [on entry into interstimulus-interval (ISI) state S_0] with experience. (State space is shown in fig. S7.) (**Right**) With drugs that produce a dopamine signal neuropharmacologically, dopamine continues to occur at the drug receipt (on entry into reward state S_1) even after experience, as well as shifting to the conditioned stimulus (on entry into ISI state S_0), thus producing a double dopamine signal.

I find this highly unlikely. Biological compensation mechanisms (*35*, *36*) are likely to limit the maximal effect of cocaine on neural systems, including the value representation. This can be modeled in a number of ways, one of which is to include a global effectiveness-of-dopamine factor, which multiplies all $R(s)$ and $D(s)$ terms. If this factor decreased with each drug receipt, the values of all states would remain finite. Simulations based on an effectiveness-of-dopamine factor that decreases exponentially with each drug receipt (factor = 0.99^n, where n is the number of drug receipts) showed similar properties to those reported here, but the values of all states remained finite.

Another important issue in reinforcement learning is what happens when the reward or drug is removed. In normal TDRL, the value of states leading to reward decay back to zero when that reward is not delivered (*6*). This follows from the existence of a strongly negative δ signal in the absence of expected reward. Although firing of dopamine neurons is inhibited in the absence of expected reward (*16*), the inhibition is dramatically less than the corresponding excitation (*7*). In general, the simple decay of value seen in TDRL (*6*, *39*) does not model extinction very well, particularly in terms of reinstantiation after extinction (*40*). Modeling extinction (even for natural rewards) is likely to require additional components not included in current TDRL models, such as state-space expansion.

A theory of addiction that is compatible with a large literature of extant data and that makes explicitly testable predictions has been deduced from two simple hypotheses: (i) dopamine serves as a reward-error learning signal to produce temporal-difference learning in the normal brain and (ii) cocaine produces a phasic increase in dopamine directly (i.e., neuropharmacologically). A computational model was derived by adding a noncompensable δ signal to a TDRL model. The theory makes predictions about human behavior (developing inelasticity), animal behavior (resistance to blocking), and neurophysiology (dual dopamine signals in experienced users). Addiction is likely to be a complex process arising from transitions between learning algorithms (*3*, *20*, *22*). Bringing addiction theory into a computational realm will allow us to make these theories explicit and to directly explore these complex transitions.

References and Notes

1. J. H. Lowinson, P. Ruiz, R. B. Millman, J. G. Langrod, Eds., *Substance Abuse: A Comprehensive Textbook* (Williams and Wilkins, Baltimore, MD, ed. 3, 1997).
2. M. E. Wolf, S. Mangiavacchi, X. Sun, *Ann. N.Y. Acad. Sci.* **1003**, 241 (2003).
3. B. J. Everitt, A. Dickinson, T. W. Robbins, *Brain Res. Rev.* **36**, 129 (2001).
4. P. R. Montague, P. Dayan, T. J. Sejnowski, *J. Neurosci.* **16**, 1936 (1996).
5. W. Schultz, P. Dayan, P. R. Montague, *Science* **275**, 1593 (1997).
6. R. S. Sutton, A. G. Barto, *Reinforcement Learning: An Introduction* (MIT Press, Cambridge, MA, 1998).
7. N. D. Daw, thesis, Carnegie Mellon University, Pittsburgh, PA (2003).
8. M. C. Ritz, R. J. Lamb, S. R. Goldberg, M. J. Kuhar, *Science* **237**, 1219 (1987).
9. M. R. Picciotto, *Drug Alcohol Depend.* **51**, 165 (1998).
10. V. I. Pidoplichko, M. DeBiasi, J. T. Williams, J. A. Dani, *Nature* **390**, 401 (1997).
11. S. R. Laviolette, R. A. Gallegos, S. J. Henriksen, D. van der Kooy, *Nature Neurosci.* **7**, 160 (2004).
12. J. E. Mazur, *Psychol. Rev.* **108**, 96 (2001).
13. G. Ainslie, *Picoeconomics* (Cambridge Univ. Press, New York, 1992).
14. See materials and methods on *Science* Online.
15. S. M. McClure, N. D. Daw, P. R. Montague, *Trends Neurosci.* **26**, 423 (2003).
16. W. Schultz, *J. Neurophysiol.* **80**, 1 (1998).
17. P. Waelti, A. Dickinson, W. Schultz, *Nature* **412**, 43 (2001).
18. S. C. Tanaka *et al.*, *Nature Neurosci.* **7**, 887 (2004).
19. G. Di Chiara, *Eur. J. Pharmacol.* **375**, 13 (1999).
20. G. F. Koob, M. L. Moal, *Neuropsychopharmacology* **24**, 97 (2001).
21. L. J. M. J. Vanderschuren, B. J. Everitt, *Science* **305**, 1017 (2004).
22. T. E. Robinson, K. C. Berridge, *Annu. Rev. Psychol.* **54**, 25 (2003).
23. M. E. Carroll, S. T. Lac, S. L. Nygaard, *Psychopharmacology (Berlin)* **97**, 23 (1989).
24. M. A. Nader, W. L. Woolverton, *Psychopharmacology (Berlin)* **105**, 169 (1991).
25. S. T. Higgins, S. H. Heil, J. P. Lussier, *Annu. Rev. Psychol.* **55**, 431 (2004).
26. M. E. Carroll, *Drug Alcohol Depend.* **33**, 201 (1993).
27. M. Grossman, F. J. Chaloupka, *J. Health Econ.* **17**, 427 (1998).
28. W. K. Bickel, L. A. Marsch, *Addiction* **96**, 73 (2001).
29. R. A. Rescorla, A. R. Wagner, in *Classical Conditioning II: Current Research and Theory*, A. H. Black, W. F. Prokesy, Eds. (Appleton Century Crofts, New York, 1972), pp. 64–99.
30. A. Dickinson, *Contemporary Animal Learning Theory* (Cambridge Univ. Press, New York, 1980).
31. P. E. M. Phillips, G. D. Stuber, M. L. A. V. Heien, R. M. Wightman, R. M. Carelli, *Nature* **422**, 614 (2003).
32. G. S. Becker, K. M. Murphy, *J. Polit. Econ.* **96**, 675 (1988).
33. M. Woodward, H. Tunstall-Pedoe, *Addiction* **88**, 821 (1993).
34. C. W. Bradberry, *Neuroscientist* **8**, 315 (2002).
35. S. R. Letchworth, M. A. Nader, H. R. Smith, D. P. Friedman, L. J. Porrino, *J. Neurosci.* **21**, 2799 (2001).
36. F. J. White, P. W. Kalivas, *Drug Alcohol Depend.* **51**, 141 (1998).
37. N. Volkow, J. Fowler, G.-J. Wang, *Behav. Pharmacol.* **13**, 355 (2002).
38. V. Deroche-Gamonet, D. Belin, P. V. Piazza, *Science* **305**, 1014 (2004).
39. R. E. Suri, W. Schultz, *Neuroscience* **91**, 871 (1999).
40. M. E. Bouton, *Biol. Psychiatry* **52**, 976 (2002).

41. This work was supported by an Alfred P. Sloan Fellowship. I thank M. Thomas, E. Larson, M. Carroll, D. Hatsukami, J. Jackson, A. Johnson, N. Schmitzer-Torbert, and Z. Kurth-Nelson for comments on the manuscript and helpful discussions.

Supporting Online Material

www.sciencemag.org/cgi/content/full/306/5703/1944/DC1
Materials and Methods
Figs. S1 to S7

6 July 2004; accepted 19 October 2004
10.1126/science.1102384

The G_s-Linked Receptor GPR3 Maintains Meiotic Arrest in Mammalian Oocytes

Lisa M. Mehlmann,[1]* Yoshinaga Saeki,[2]† Shigeru Tanaka,[2]† Thomas J. Brennan,[3]‡ Alexei V. Evsikov,[4] Frank L. Pendola,[4] Barbara B. Knowles,[4] John J. Eppig,[4] Laurinda A. Jaffe[1]*

Mammalian oocytes are held in prophase arrest by an unknown signal from the surrounding somatic cells. Here we show that the orphan G_s-linked receptor GPR3, which is localized in the oocyte, maintains this arrest. Oocytes from *Gpr3* knockout mice resume meiosis within antral follicles, independently of an increase in luteinizing hormone, and this phenotype can be reversed by injection of *Gpr3* RNA into the oocytes. Thus, the GPR3 receptor is a link in communication between the somatic cells and oocyte of the ovarian follicle and is crucial for the regulation of meiosis.

Meiosis, which reduces the oocyte's chromosome number in preparation for fertilization, begins long before fertilization occurs. In most species, including mammals, DNA replication, entry into meiosis, and chromosomal recombination occur early in oogenesis, but then at late prophase, meiosis arrests. Much later, shortly before ovulation, meiosis resumes: the nuclear envelope breaks down, the chromosomes condense, and a metaphase spindle is formed. In vertebrates, this occurs in response to luteinizing hormone (LH) from the pituitary, which acts on the somatic (granulosa) cells that surround the oocyte in the ovarian follicle (*1*, *2*).

Throughout much of mammalian oogenesis, prophase arrest is maintained by inherent factors in the oocyte and correlates with low levels of activity by cell cycle regulatory proteins, including cyclin B and CDK1 (*1*). However, once the oocyte reaches its full size and an antral space begins to form between the granulosa cells, prophase arrest in the oocyte becomes dependent on unidentified signals from the granulosa cells. Oocytes that are removed from antral follicles resume meiosis spontaneously (*3*, *4*).

The maintenance of prophase arrest in oocytes within antral follicles requires the activity of signaling molecules within the

oocyte. In particular, the heterotrimeric G protein G_s is required; injection of oocytes with an inhibitory G_s antibody, or a dominant-negative form of G_s, causes meiosis to resume within the follicle (*5*, *6*). G_s stimulates adenylyl cyclase in the oocyte to keep cyclic adenosine monophosphate (cAMP) elevated (*7*), and this results, through activation of protein kinase A and subsequent incompletely understood steps, in the inhibition of the cyclin B–CDK1 complex that drives the prophase-to-metaphase transition (*8*–*11*). Because G_s by itself has no detectable constitutive activity (*12*), it is likely that a receptor in the oocyte membrane is required to keep G_s active.

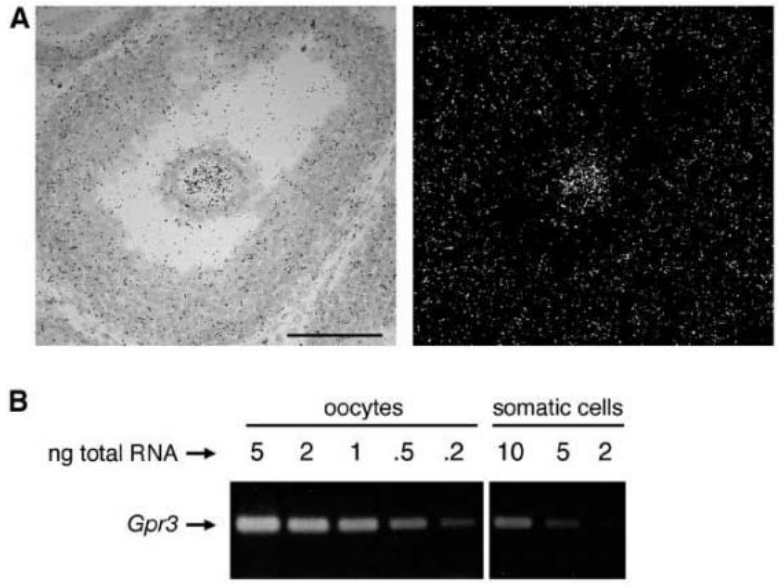

Fig. 1. *Gpr3* RNA is localized in the oocyte versus the somatic cells of antral follicles. (**A**) In situ hybridization of an ovarian section from a 22-day-old eCG-primed mouse, using a ^{33}P-labeled *Gpr3* antisense riboprobe. Left: A transmitted light image of a follicle. Right: A reflected light image of the silver grains in the overlying autoradiographic emulsion. Scale bar, 100 μm. Eight of eight follicles showed a similar distribution. (**B**) RT-PCR comparing the relative expression of *Gpr3* RNA in oocytes and somatic cells dissected from antral follicles. RT-PCR for *Gpr3* was performed with cDNA derived from the indicated amounts of total RNA from each tissue. Normalized to total RNA, oocytes contained 14 ± 7 times as much *Gpr3* RNA as somatic cells (mean ± SD for six RT-PCR experiments with cDNA from two separately collected sets of oocytes and somatic cells) (*13*).

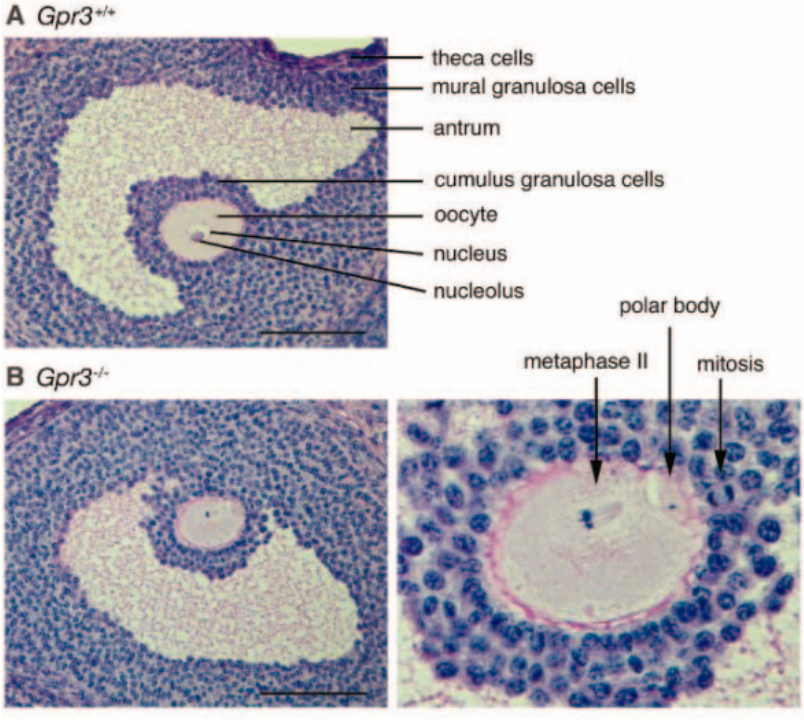

Fig. 2. Spontaneous resumption of meiosis in an oocyte within a $Gpr3^{-/-}$ antral follicle (adult mouse). (**A**) An antral follicle from a control $Gpr3^{+/+}$ ovary. The oocyte is arrested in prophase. (**B**) An antral follicle from a $Gpr3^{-/-}$ ovary. The oocyte has metaphase II chromosomes and a polar body. The right panel is an enlarged view of the left. Mitosis is ongoing in the somatic cells. Scale bars, 100 μm.

To identify such a receptor, we searched an expressed sequence tag (EST) database derived from a cDNA library of fully grown prophase-arrested mouse oocytes (*13*), looking for proteins predicted to be G protein–coupled receptors (GPCRs) because of their 7-transmembrane structure. Of the ~1000 mammalian genes that encode 7-transmembrane proteins, 15 were found in the oocyte EST database (table S1). One of these proteins, the orphan receptor GPR3, was of particular interest because it elevates cAMP when expressed in a variety of cultured cells (*14*–*16*), implying that GPR3 activates G_s.

Gpr3 RNA is found predominantly in the ovary, testis, and brain; it has not been found elsewhere, except at very low levels in kidney and lung (*14*, *17*–*19*). In situ hybridization of mouse ovarian sections showed that *Gpr3* RNA is localized in the oocyte (Fig. 1A), and reverse transcription polymerase chain reaction (RT-PCR) measurements indicated that *Gpr3* RNA expression is ~14 times higher in the oocyte than in the surrounding somatic cells (Fig. 1B).

To investigate whether the GPR3 receptor is required to maintain meiotic prophase arrest in mouse oocytes, we examined histological sections of ovaries from *Gpr3* knockout mice (*13*). The $Gpr3^{-/-}$ animals were indistinguishable from $Gpr3^{+/+}$ animals in external morphology, growth, and activity. Their ovaries were of normal size and had a distribution of preantral, early antral, and antral follicles similar to that seen in $Gpr3^{+/+}$ mice (fig. S1). The appearance and organization of the somatic cells in the $Gpr3^{-/-}$ follicles was similar to that in the $Gpr3^{+/+}$ follicles (Figs. 2, A and B; 3, A and B; and fig. S1).

However, although all of the oocytes within antral follicles of $Gpr3^{+/+}$ ovaries were in prophase, with an intact nuclear envelope and nucleolus (Fig. 2A; Fig. 3, A and D; and fig. S2), most of the oocytes within antral follicles

[1]Department of Cell Biology, University of Connecticut Health Center (UCHC), Farmington, CT 06032, USA. [2]Massachusetts General Hospital, Charleston, MA 02129, USA. [3]Deltagen Inc., San Carlos, CA 94070, USA. [4]The Jackson Laboratory, Bar Harbor, ME 04609, USA.

*To whom correspondence should be addressed. E-mail: lmehlmann@neuron.uchc.edu (L.M.M.); ljaffe@neuron.uchc.edu (L.A.J.)

†Present address: Ohio State University, Columbus, OH 43210, USA.

‡Present address: Toccata Therapeutics, Menlo Park, CA, 94025, USA.

of *Gpr3*$^{-/-}$ ovaries contained metaphase chromosomes, indicating that meiosis had resumed (Fig. 2B; Fig. 3, B and D; and fig. S2). For these studies, we primarily used ovaries from prepubertal (22- to 24-day-old) mice to avoid the complexity of the cycling adult ovary (*13*). In the prepubertal ovaries, 82% of the antral follicles contained oocytes that had resumed meiosis, compared with 0% in *Gpr3*$^{+/+}$ controls (Fig. 3D). The one adult *Gpr3*$^{-/-}$ ovary that we analyzed also showed that the majority of oocytes in antral follicles had resumed meiosis (Fig. 2B and fig. S2).

Among the *Gpr3*$^{-/-}$ antral follicles containing oocytes that had resumed meiosis, 42% were clearly at metaphase II, as indicated by the presence of a polar body (Figs. 2B and 3B). Oocytes that contained a metaphase spindle but lacked a visible polar body could have been at metaphase I or at metaphase II with a degenerated polar body. All oocytes within preantral follicles of *Gpr3*$^{+/+}$ and *Gpr3*$^{-/-}$ mice were arrested in prophase (Fig. 3D and fig. S2).

During the transition from preantral to antral, follicles go through an "early antral" stage, in which pockets of fluid appear between the granulosa cells; these pockets eventually coalesce to form the antrum. Near the early antral stage, oocytes become dependent on the somatic cells (*4*) and on cAMP (*7*, *20*), for the maintenance of prophase arrest. In the early antral follicles of prepubertal *Gpr3*$^{-/-}$ mice, 37% of the oocytes had resumed meiosis, as indicated by the presence of condensed chromosomes (Fig. 3, C and D); within the early antral category, oocytes in larger follicles showed a larger fraction of meiotic resumption (table S3). Most of these oocytes showed a metaphase spindle, although a few appeared to be at prometaphase; polar bodies were not observed (fig. S2 gives results from early antral follicles in adult mice).

To determine whether the oocytes in *Gpr3*$^{-/-}$ early antral and antral follicles that did not resume meiosis were competent to do so if removed from the follicle, we dissected follicles of comparable size ranges from *Gpr3*$^{-/-}$ ovaries (*13*). Thirty-six percent of the oocytes from *Gpr3*$^{-/-}$ early antral follicles had resumed meiosis at the time of isolation, and only a few additional oocytes had resumed meiosis by 5 hours after isolation (Fig. 3E). Thus, during follicle development, the maintenance of meiotic arrest becomes dependent on the GPR3 receptor at close to the same time that arrest becomes dependent on the somatic cells. Of the oocytes from *Gpr3*$^{-/-}$ antral follicles, 89% had resumed meiosis at the time of isolation, and this percentage increased to 99% by 5 hours after isolation (Fig. 3E). Possibly another G_s-linked receptor functions to maintain arrest in the small subgroup of *Gpr3*$^{-/-}$ oocytes that do not resume meiosis in their antral follicles.

The resumption of meiosis in *Gpr3*$^{-/-}$ follicles did not appear to result from an increase in LH, as could occur in a cycling adult mouse or potentially even in a prepubertal mouse if pituitary function was affected by the absence of GPR3. LH action on the mural granulosa cells causes extracellular matrix material to be deposited around the cumulus granulosa cells, resulting in an expansion of the cumulus mass in preparation for ovulation; cumulus expansion is evident by the time the oocyte reaches metaphase I (*21*, *22*) (Fig. 4A). However, no spontaneous cumulus expansion was seen in the *Gpr3*$^{-/-}$ follicles (Figs. 2B and 3B). Likewise, there was no spontaneous expansion of the follicle diameter (table S4), as is seen in response to LH (*23*). Thus, the presence of chromosomes aligned on metaphase I or II spindles in an oocyte within an unexpanded follicle with an unexpanded cumulus mass is not consistent with a response of the follicle to LH. Expression of an LH-dependent gene that encodes one of the proteins produced during cumulus expansion, chondroitin sulfate proteoglycan

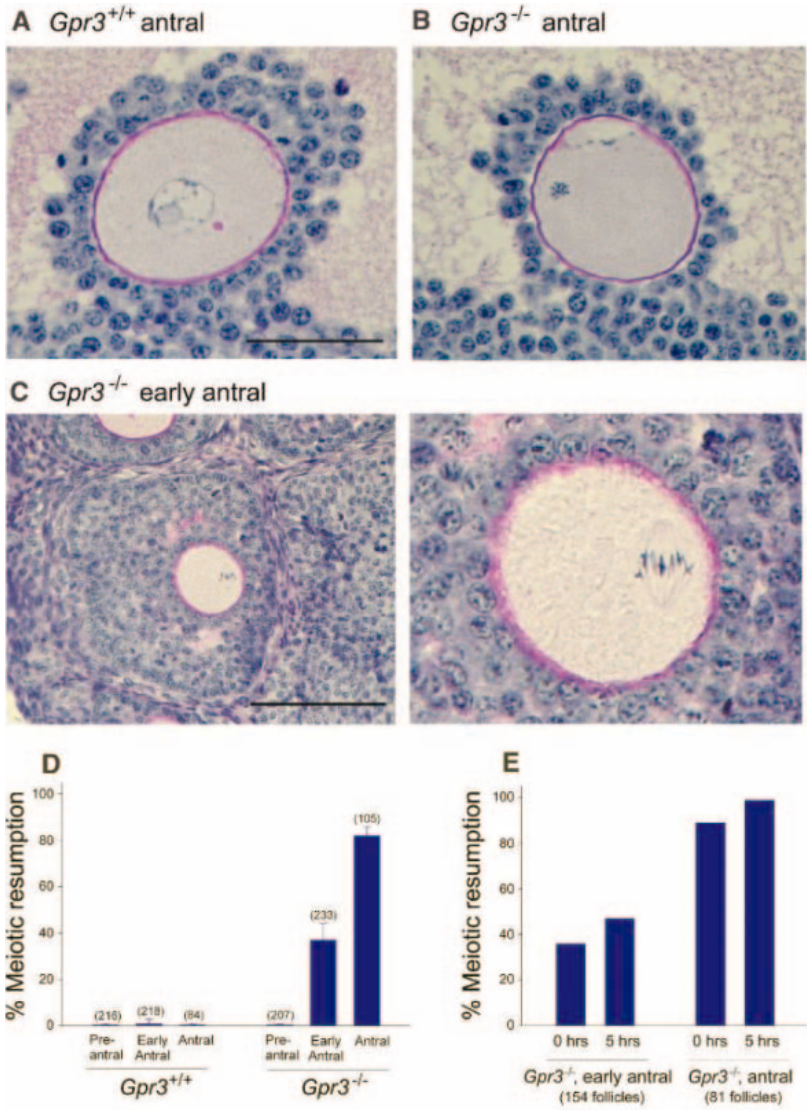

Fig. 3. Spontaneous resumption of meiosis in oocytes within *Gpr3*$^{-/-}$ antral and early antral follicles (of 22- to 24-day-old prepubertal mice). (**A**) A prophase-arrested oocyte within an antral follicle of a control *Gpr3*$^{+/+}$ ovary. Scale bar, 50 μm. (**B**) An oocyte with metaphase II chromosomes and a polar body, within an antral follicle of a *Gpr3*$^{-/-}$ ovary. Scale bar, 50 μm. (**C**) An early antral follicle from a *Gpr3*$^{-/-}$ ovary, showing metaphase I chromosomes. An enlarged view is on the right. Scale bar, 100 μm. (**D**) Percentages of oocytes that had resumed meiosis, counted in sections of ovaries from 22- to 24-day-old *Gpr3*$^{+/+}$ and *Gpr3*$^{-/-}$ mice. The graph shows the mean ± SD from analysis of ovaries from four *Gpr3*$^{+/+}$ and four *Gpr3*$^{-/-}$ mice; numbers above the bars indicate how many follicles were examined (*13*) (tables S3 to S5). (**E**) Percentages of *Gpr3*$^{-/-}$ oocytes that had resumed meiosis, at the time of removal from their follicles or 5 hours later (data obtained from five 22- to 24-day-old mice). For (E), "antral" includes follicles >250 μm in diameter; "early antral" includes follicles 140 to 250 μm in diameter.

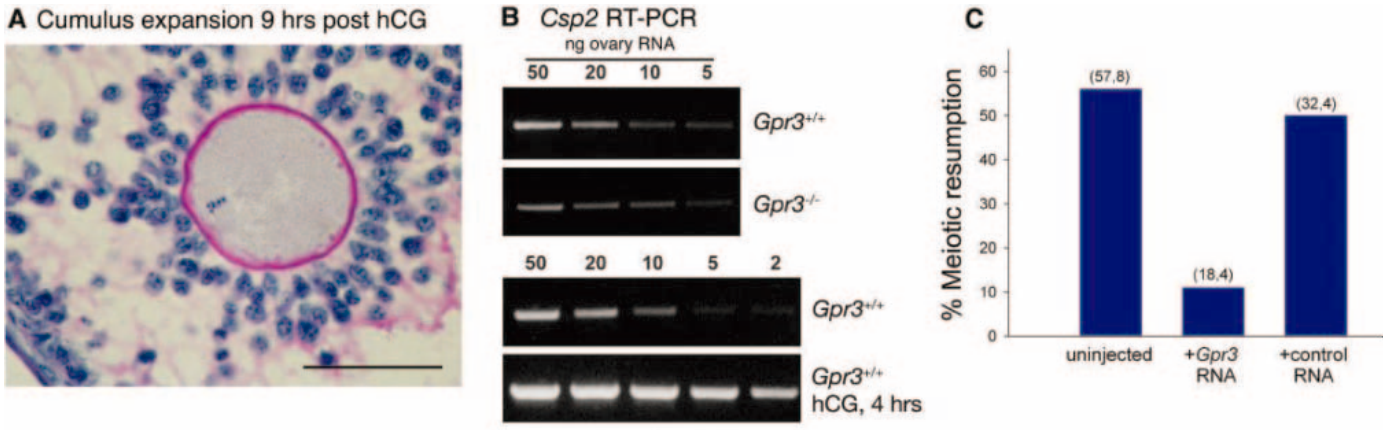

Fig. 4. Resumption of meiosis in *Gpr3*$^{-/-}$ ovaries is not due to elevation of LH and is prevented by injection of *Gpr3* RNA into the oocyte. (**A**) For comparison with the *Gpr3*$^{-/-}$ follicle shown in Fig. 3B, cumulus expansion in an antral follicle from a 22-day-old wild-type mouse injected 9 hours previously with the LH receptor agonist, hCG. Metaphase I chromosomes are present. Scale bar, 50 μm. In the *Gpr3*$^{-/-}$ follicles, oocytes reached metaphase II without cumulus expansion. (**B**) There was no increase in expression of an LH-dependent gene, *Csp2*, when *Gpr3*$^{-/-}$ and *Gpr3*$^{+/+}$ ovaries were compared. RT-PCR for *Csp2* was performed using cDNA derived from the indicated amounts of ovary RNA. Similar results were obtained in two experiments. For comparison, the lower panels show the increased expression of *Csp2* RNA in a *Gpr3*$^{+/+}$ ovary collected 4 hours after injection of the mouse with hCG, versus an unstimulated *Gpr3*$^{+/+}$ ovary; LH receptor stimulation increased expression of *Csp2* RNA by a factor of ~25. Previous work has shown that *Csp2* RNA increases by 2 hours after LH receptor stimulation and remains elevated for 16 hours (*22*). (**C**) Rescue of the ability to maintain meiotic arrest by injection of *Gpr3* RNA into prophase-arrested *Gpr3*$^{-/-}$ oocytes within preantral or very early antral follicles. After 4 days in culture, when antrum formation was occurring in most follicles, oocytes were isolated to determine if meiosis had resumed. Numbers above the bars indicate how many follicles and mice were analyzed. The percent meiotic resumption in the *Gpr3* RNA-injected oocytes was significantly different from that in uninjected oocytes and in control oocytes injected with RNA encoding red fluorescent protein (P = 0.0009 and 0.007, respectively, Fisher's exact test).

2 (CSP2 or versican V0) (*22*), was also not elevated in *Gpr3*$^{-/-}$ ovaries (Fig. 4B).

The resumption of meiosis in *Gpr3*$^{-/-}$ ovaries cannot be attributed to follicle atresia, because all of the *Gpr3*$^{-/-}$ follicles included in Fig. 3D appeared to be morphologically healthy, and mitosis was ongoing in the granulosa cells (Figs. 2B and 3B). A normal number of ovulated eggs was found in the oviducts of a *Gpr3*$^{-/-}$ mouse that had been injected 13 hours previously with the LH receptor agonist, human chorionic gonadotropin (hCG) (*24*), and sections of an ovary from an adult *Gpr3*$^{-/-}$ mouse showed corpora lutea (fig. S1). Thus, the pathways leading to ovulation and luteinization appear to be unimpaired in *Gpr3*$^{-/-}$ mice. The only detected defect in the *Gpr3*$^{-/-}$ ovary was the absence of the ability to maintain meiotic prophase arrest.

The predominant expression of *Gpr3* RNA in the oocyte versus the somatic cells of the follicle, and the dependence of meiotic arrest on oocyte G_s (*5*, *6*), support the conclusion that it is the GPR3 receptor in the oocyte, rather than in the somatic cells, that is primarily required to maintain meiotic arrest. To examine whether the spontaneous resumption of meiosis could be prevented by introducing GPR3 protein into *Gpr3*$^{-/-}$ oocytes, we injected prophase-arrested *Gpr3*$^{-/-}$ oocytes within preantral or very early antral follicles with *Gpr3* RNA and then cultured them under conditions that allowed antral formation (*25*) (Fig. 4C and fig. S3). After the culture period, about half of control *Gpr3*$^{-/-}$ oocytes had resumed meiosis, but only 11% of the *Gpr3*$^{-/-}$ oocytes that had been injected with *Gpr3* RNA had resumed meiosis (Fig. 4C). The reversal of the knockout phenotype by *Gpr3* RNA injection into the oocyte further indicates that the GPR3 receptor that maintains meiotic arrest is located primarily in the oocyte itself.

Although GPR3 has some ligand-independent activity (*14*–*16*), additional activation of GPR3 in the oocyte by an agonist from or on the granulosa cells could explain why meiosis remains arrested only if the oocyte is surrounded by granulosa cells. A GPR3 ligand that increases G_s activation remains to be discovered (table S1). Nevertheless, identification of GPR3 as a negative regulator of meiotic progression, through its activation of G_s and thus adenylyl cyclase, provides a key for identifying how the follicle acts to maintain meiotic arrest. It also provides clues about how LH might relieve the arrest and reinitiate meiosis.

References and Notes

1. J. J. Eppig, M. M. Viveiros, C. Marin Bivens, R. De La Fuente, in *The Ovary*, P. C. K. Leung, E. Y. Adashi, Eds. (Elsevier, Amsterdam, ed. 2, 2004), pp. 113–129.
2. J.-Y. Park *et al.*, *Science* **303**, 682 (2004).
3. G. Pincus, E. V. Enzmann, *J. Exp. Med.* **62**, 665 (1935).
4. G. F. Erickson, R. A. Sorensen, *J. Exp. Zool.* **190**, 123 (1974).
5. L. M. Mehlmann, T. L. Z. Jones, L. A. Jaffe, *Science* **297**, 1343 (2002).
6. R. R. Kalinowski *et al.*, *Dev. Biol.* **267**, 1 (2004).
7. K. Horner *et al.*, *Dev. Biol.* **258**, 385 (2003).
8. E. A. Bornslaeger, P. Mattei, R. M. Schultz, *Dev. Biol.* **114**, 453 (1986).
9. T. Choi *et al.*, *Development* **113**, 789 (1991).
10. B. C. Duckworth, J. S. Weaver, J. V. Ruderman, *Proc. Natl. Acad. Sci. U.S.A.* **99**, 16794 (2002).
11. A. J. Lincoln *et al.*, *Nature Genet.* **30**, 446 (2002).
12. T. Iiri, P. Herzmark, J. M. Nakamoto, C. Van Dop, H. R. Bourne, *Nature* **371**, 164 (1994).
13. Materials and methods are available as supporting material on *Science* Online.
14. D. Eggerickx *et al.*, *Biochem. J.* **309**, 837 (1995).
15. K. Uhlenbrock, H. Gassenhuber, E. Kostenis, *Cell. Signalling* **14**, 941 (2002).
16. J. N. Bresnick *et al.*, *Assay Drug Dev. Tech.* **1**, 239 (2003).
17. Y. Saeki *et al.*, *FEBS Lett.* **336**, 317 (1993).
18. T. P. Iismaa *et al.*, *Genomics* **24**, 391 (1994).
19. S. Tanaka, Y. Saeki, unpublished results.
20. E. A. Bornslaeger, P. M. Mattei, R. M. Schultz, *Mol. Reprod. Dev.* **1**, 19 (1988).
21. J. J. Eppig, *Dev. Biol.* **89**, 268 (1982).
22. D. L. Russell, S. A. Ochsner, M. Hsieh, S. Mulders, J. S. Richards, *Endocrinology* **144**, 1020 (2003).
23. A. Tsafriri, S.-Y. Chun, R. Reich, in *The Ovary*, E. Y. Adashi, P. C. K. Leung, Eds. (Raven, New York, 1993), pp. 227–244.
24. L. M. Mehlmann, L. A. Jaffe, unpublished results.
25. P. L. Nayadu, S. M. Osborn, *J. Reprod. Fertil.* **95**, 349 (1992).

26. We thank N. Ryan, S. J. Borch, L. Freudzon, L. Ross, and K. Kasai for technical assistance; A. F. Parlow and the National Hormone and Peptide Pituitary Program for providing equine chorionic gonadotropin (eCG) and follicle-stimulating hormone; R. Tsien for providing the mRFP1 red fluorescent protein cDNA and B. Kalinowski, G. Mandel, T. Jones, B. White, R. Berlin, and M. Terasaki for their continuing interest and advice. Supported by grants from the UCHC Center for Women's Health and the Patterson Trust (L.M.M.), from the Human Frontier Science Program (L.A.J.), and from NIH (L.M.M., Y.S., A.V.E., F.L.P., B.B.K., J.J.E., and L.A.J.).

Supporting Online Material

www.sciencemag.org/cgi/content/full/306/5703/1947/DC1
Materials and Methods
Figs. S1 to S3
Tables S1 to S5
References and Notes

12 August 2004; accepted 25 October 2004
10.1126/science.1103974

Defective Telomere Lagging Strand Synthesis in Cells Lacking WRN Helicase Activity

Laure Crabbe, Ramiro E. Verdun, Candy I. Haggblom, Jan Karlseder*

Cells from Werner syndrome patients are characterized by slow growth rates, premature senescence, accelerated telomere shortening rates, and genome instability. The syndrome is caused by the loss of the RecQ helicase WRN, but the underlying molecular mechanism is unclear. Here we report that cells lacking WRN exhibit deletion of telomeres from single sister chromatids. Only telomeres replicated by lagging strand synthesis were affected, and prevention of loss of individual telomeres was dependent on the helicase activity of WRN. Telomere loss could be counteracted by telomerase activity. We propose that WRN is necessary for efficient replication of G-rich telomeric DNA, preventing telomere dysfunction and consequent genomic instability.

Werner syndrome (WS) patients suffer from multiple signs of premature aging (*1*). A wide variety of cells are affected, which suggests a housekeeping dysfunction. Cells from WS patients grow poorly in culture and enter senescence prematurely, phenotypes that can be reversed by expression of the catalytic telomerase subunit human telomerase reverse transcriptase (hTERT) (*2*), therefore implicating a critical role for telomere integrity in WS pathogenesis.

Because of their G-rich nature, telomeres have been suggested to contain energetically stable non-B form DNA such as G-quadruplexes. WRN, previously found to associate with ALT-associated PML bodies (*3*), has been suggested as capable of unwinding such structures as well as resolving telomeric D-loops in vitro (*1*, *3*, *4*). This suggests that the role of WRN may be related to its ability to resolve G-rich structures during DNA replication. To investigate the potential involvement of WRN in telomere replication, we expressed wild-type WRN and a putative dominant negative WRN allele with an inhibitory mutation in the helicase domain (K577M) (*5*, *6*) in primary IMR90 fibroblasts and in HeLa cells. Fluorescent in situ hybridization (FISH) of metaphase telomeres (*7*) prepared from IMR90 fibroblasts and from HeLa cells expressing the helicase-deficient WRN allele revealed a number of chromosomes in which telomeric signals were only detected at a single chromatid, a phenotype we termed sister telomere loss (STL) (Fig. 1A). HeLa cells infected with a control virus or a virus expressing wild-type WRN displayed a low frequency of STL (0.8 events per cell) (*8*). STL increased significantly to 2.2 events per cell when the dominant negative WRN was expressed (Table 1). Consistent with telomerase alleviating the growth phenotypes in WS cells (*2*) and with the proposed preference of telomerase for critically short telomeres (*9*), inhibition of the catalytic subunit of telomerase (hTERT) (*10*, *11*) with a specific drug (BIBR1532) (*12*, *13*) led to a further increase of STL to 4.3 events per HeLa cell (Table 1). Expression of the helicase-deficient WRN allele in telomerase-deficient primary IMR90 fibroblasts also increased STL significantly to 4.1 events per cell (Table 1). Taken together, these data suggest that the helicase activity of WRN is required for proper telomere maintenance.

To test genetically the requirement of WRN for telomere stability, we looked for STL in primary fibroblasts from WS patients. Chromosomes with missing telomeres on single chromatids were readily detected in WS fibroblasts from the AG03141D and AG05229C cell lines (Fig. 1A), at a frequency of 2.8 and 1.7 events per cell, respectively (Table 1). No preference for p- or q-arm STL was observed, because single signals on both arms could be observed (Fig. 1B). Reconstitution of the AG05229C cells with wild-type WRN, a nuclease-deficient WRN-E84A allele (*14*), or helicase-deficient WRN-K577M (Fig. 1C) further supported the requirement of WRN helicase activity for telomere maintenance. Expression of WRN and WRN-E84A reduced the frequency of STL to a background level of 1 event per cell, whereas expression of WRN-K577M failed to reduce STL frequencies (Table 1). Expression of the catalytic subunit of telomerase markedly reduced the occurrence of STL (Table 1).

Excessive loss of telomeric DNA leads to induction of the DNA damage machinery (*15*–*17*). Twenty-eight percent of primary WS fibroblasts stained positively with an antibody directed against ataxia telangiectasia mutated (ATM) phosphorylated at serine 1981 (phospho-ATM) (Fig. 1D) (*18*). In comparison, despite a higher S phase index, only 6% of IMR90 fibroblasts showed such staining. Expression of wild-type WRN and nuclease-deficient WRN reduced the percentage of phospho-ATM–positive cells to 17% and 17.5% ($P < 0.0001$), respectively. Helicase-deficient WRN did not alter the percentage of cells with phospho-ATM foci, suggesting that the helicase activity of the protein is required to suppress the initiation of DNA damage signals. Expression of hTERT in WS fibroblasts, however, almost completely repressed ATM foci formation (Fig. 1D and fig. S1), consistent with our finding that telomerase expression lowers the frequency of STL (Table 1). Collectively, our data suggest that lack of WRN helicase activity leads to DNA damage signaling, likely because of telomere loss on single sister chromatids.

To establish whether STL leads to chromosome fusions, WS cells were analyzed for DNA bridges during anaphase (*19*). When the pRB and p53 pathways were suppressed by expression of the human papilloma virus sero-

Table 1. Effect of WRN on sister telomere loss (loss of the telomeric signal from one of two sister chromatids). At least 26 metaphases per cell line were analyzed. *P* values were determined by Wilcoxon two-sided ranks test analysis.

Cell line	STL/cell	Significance
HeLa control	0.8	
HeLa WRN	0.9	
HeLa WRN K577M	2.2	$P < 0.0001$
HeLa BIBR control*	1.1	
HeLa BIBR WRN	1.0	
HeLa BIBR WRN K577M	4.3	$P < 0.0001$
IMR90	0.8	
IMR90 WRN K577M	4.1	$P < 0.0001$
AG03141D control	2.8	
AG05229C control	1.7	
AG05229C WRN	1.2	$P < 0.0001$
AG05229C WRN E84A	1.1	$P < 0.0001$
AG05229C WRN K577M	2.0	$P < 0.0001$
AG05229C hTERT	0.4	$P < 0.0001$

*Cells were treated with BIBR1532 for 2 days before analysis.

The Salk Institute for Biological Studies, 10010 North Torrey Pines Road, La Jolla, CA 92037, USA.

*To whom correspondence should be addressed. E-mail: Karlseder@salk.edu

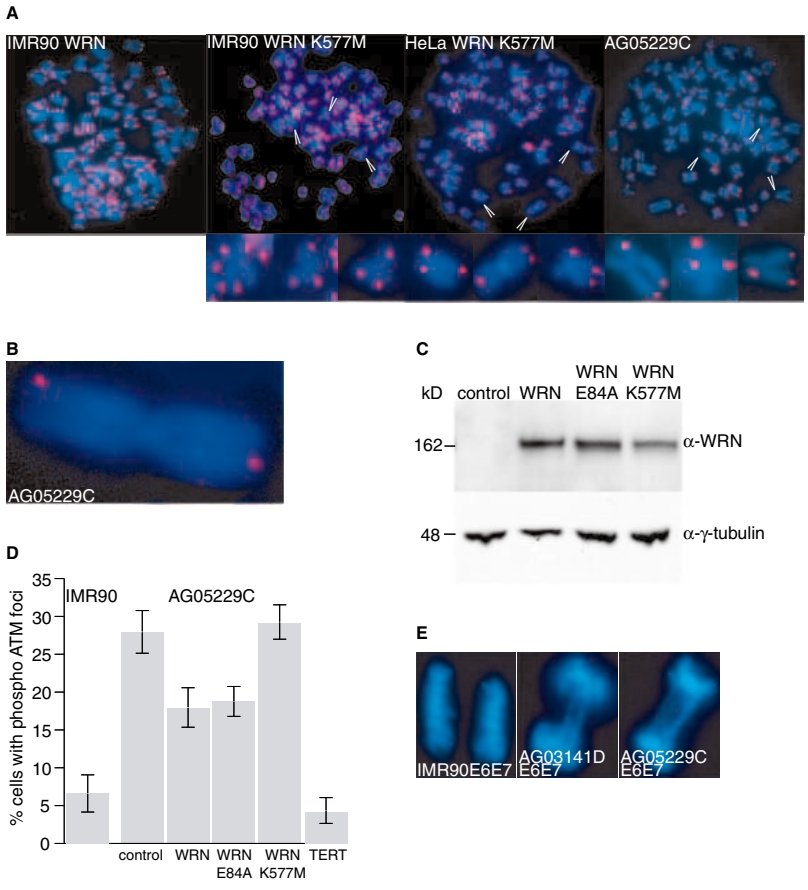

Fig. 1. Dysfunctional telomeres in WS cells. (**A**) FISH analysis of metaphase chromosomes (*8*) of IMR90 WRN, IMR90 WRN-K577M, HeLa WRN-K577M, and AG05229C primary WS fibroblasts. Telomeres were hybridized with a TRITC-$[TTAGGG]_4$ probe and are shown in the red channel; DNA was stained with 4′,6-diamidino-2-phenylindole (DAPI) and is shown in the blue channel. Arrows indicate missing telomeric staining from single sister chromatids. (**B**) An individual chromosome from an AG05229C WS fibroblast. (**C**) Western blot of WRN, WRN-E84A, and WRN-K577M in AG05229C WS fibroblasts. Antibodies to WRN and to γ-tubulin were used to detect the indicated proteins. (**D**) Quantification of cells showing staining with an antibody directed against ATM phosphorylated at serine 1981 (*8*). IMR90 fibroblasts infected with a control virus and primary WS cells were analyzed. Werner cells were infected with a control retrovirus or with viruses expressing WRN, nuclease-deficient WRN (E84A), or helicase-deficient WRN (K577M). Only cells with two or more prominent ATM foci were considered. (**E**) Anaphases from IMR90 cells and AG03141D and AG05229C Werner fibroblasts expressing HPV16 E6 and E7 oncoproteins. DNA has been stained with DAPI and is shown in blue.

type 16 (HPV16) E6 and E7 oncoproteins, the number of chromosome fusions, seen as anaphase bridges, was sharply elevated (Fig. 1E and table S1). Fusions were maintained in the checkpoint-suppressed cells, independently of the expression of WRN alleles. hTERT expression lowered the frequency of anaphase bridges by 75%, which stresses the importance of telomerase in alleviating defects in WS cells, as well as in telomerase-suppressed HeLa cells (table S1).

STL points to a dysfunction in telomere replication during S phase. Telomeric chromatin immunoprecipitation (ChIP) assays (*8*, *20*) with an antibody to WRN in primary IMR90 fibroblasts led to recovery of TTAGGG repeats in extracts from S phase cells (recovery of 5.5% of input telomeric DNA). No signal was detected in extracts from G2, M, and G1 cells. The S phase–specific association of WRN with telomeres was not due to cell cycle–regulated levels of WRN protein amounts (Fig. 2A). An alternative assessment of the association of WRN with telomeres, using immunostaining analysis (*8*) in IMR90 fibroblasts, uncovered similar results (fig. S2). In contrast, the duplex telomere-binding proteins TRF1 and TRF2 were associated with TTAGGG repeats throughout the cell cycle (Fig. 2, A and B). Thus, WRN has the ability to associate with telomeres and does so preferentially during the DNA synthesis phase of the cell cycle.

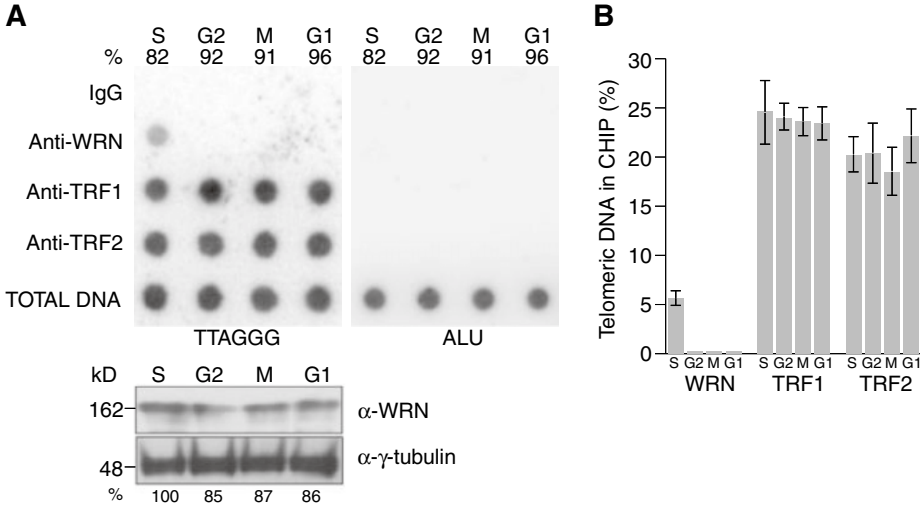

Fig. 2. S phase–specific telomeric association of WRN in primary human IMR90 fibroblasts. (**A**) ChIPs on IMR90 cells over the cell cycle. Immunoprecipitations were performed with the indicated antibodies and dot blots hybridized with TTAGGG and ALU probes (*8*, *20*). Fractions of cells in the according cell cycle phase are indicated in percentage. The same extracts were used for WRN and γ-tubulin Western blotting. Quantification of the Western blot is indicated in percentage of the S phase signal. IgG, immunoglobulin G. (**B**) Quantification of the data in (A), $n = 6$ independent ChIP experiments.

On the basis of our findings that WRN localizes to telomeres in primary cells in S phase and that WS cells show telomerase-dependent catastrophic loss of telomeres from single sister chromatids, we considered the possibility that WRN played a role in telomere replication. Telomeres replicated by either leading or lagging strand synthesis can be distinguished by chromosome orientation FISH (CO-FISH) (*21*) (Fig. 3A). HeLa 1.2.11 cells, which carry telomeres with an average length of 20 kb (*19*), showed clear signals after

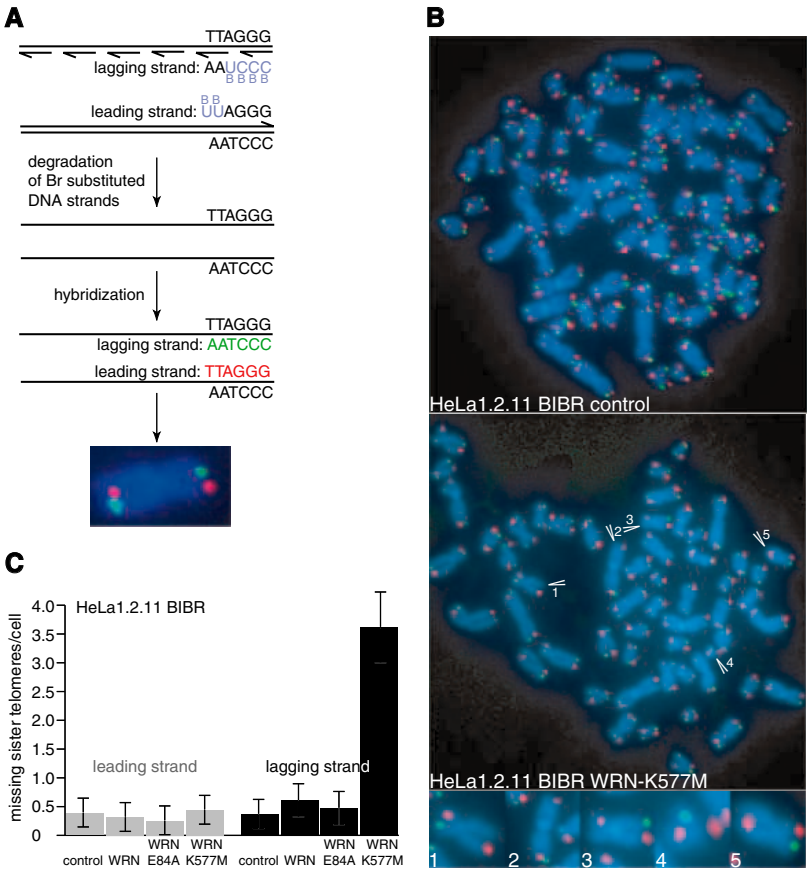

Fig. 3. Loss of lagging strand telomeres in WS cells. (**A**) Schematic of CO-FISH. Leading and lagging strand synthesis incorporates bromodeoxyuridine and bromodeoxycytidine (BrdC) into freshly synthesized DNA strands. Bromo-nucleotide–substituted DNA is degraded, and telomeres are hybridized with FITC-$[CCCATT]_4$ and TRITC-$[TTAGGG]_4$ probes (*8*). Currently, the CO-FISH technique can be used successfully only on cells with long telomeres (>15 kb), which excludes WS cells from the analysis. (**B**) CO-FISH of control HeLa 1.2.11 cells and HeLa 1.2.11 cells expressing WRN-K577M. Leading strand telomeres are shown in red and lagging strand telomeres in green. Cells were treated with the telomerase inhibitor BIBR1532 (Boehringer) 2 days before analysis. The arrows indicate missing sister telomeres. (**C**) Quantification of (B).

double staining with a fluorescein isothiocyanate (FITC)–coupled peptide nucleic acid probe specific for the G strand and a tetramethyl rhodamine isothiocyanate (TRITC)–coupled probe specific for the C strand (Fig. 3B). Inhibition of WRN by the dominant negative helicase-deficient allele led to the loss of single sister telomeres (Table 1), and this loss almost exclusively affected lagging strand telomeres (Fig. 3B, loss of green signal). The frequency of lagging strand sister telomere loss increased from 0.5 to 3.6 events per cell, after expression of the helicase-deficient WRN allele (Fig. 3C, $P < 0.0001$), whereas the frequency of leading strand telomere loss was unaffected.

Collectively, these data argue that WRN is required for efficient and complete lagging strand replication of the G-rich telomeric strand. G-quadruplexes, likely to form in this region (*22*, *23*), are potentially resolved by WRN, allowing the replication fork to progress through and replicate the telomeres completely. A possible interpretation is that lack of WRN helicase activity leads to stalling of telomere lagging strand synthesis, once the replication fork encounters structures it cannot bypass, explaining why Werner cells enter senescence with telomeres generally longer than control cells (*24*). As a result, the exposed single-stranded G-rich strand is degraded by an unspecified nuclease, leading to partial or complete loss of the few affected telomeres, a hypothesis that elucidates why analysis of individual telomeres using a G overhang–dependent technique failed to detect STL (*25*). Our model predicts that G-rich obstacles could occur not only at the base but also throughout the duplex TTAGGG region, leading to partial telomere loss. This is supported by the high frequency of unequal sister telomere staining intensity observed in aged WS cells (fig. S3). The existence of redundant activities that can resolve such structures is likely, and recently such a protein has been described in the mouse (*26*). By linking telomere loss with replication, the model presented here differs from previously suggested break repair– and recombination-dependent hypotheses for telomere loss in WRN-K577M–expressing cells (*6*).

Our model also explains why expression of telomerase rescues growth deficiency and STL. Telomerase, preferentially acting on short telomeres (*9*, *27*), could elongate affected chromosome ends, reducing the frequency of STL and reducing DNA damage signaling. This hypothesis is supported by the recent finding that a combined deletion of WRN and Terc in mice resembles WRN pathogenesis in humans (*28*). Our data provide a link between telomere dysfunction and the progeriatric disease WS and offer an explanation of why lack of WRN affects a wide number of cell types. It remains to be seen whether the genome instability observed in WS cells is due to telomere dysfunction.

References and Notes

1. P. L. Opresko, W. H. Cheng, C. von Kobbe, J. A. Harrigan, V. A. Bohr, *Carcinogenesis* **24**, 791 (2003).
2. F. S. Wyllie *et al.*, *Nature Genet.* **24**, 16 (2000).
3. P. L. Opresko *et al.*, *Mol. Cell* **14**, 763 (2004).
4. P. Mohaghegh, J. K. Karow, R. M. Brosh, V. A. Bohr, I. D. Hickson, *Nucleic Acids Res.* **29**, 2843 (2001).
5. L. Wang *et al.*, *Genetics* **154**, 357 (2000).
6. Y. Bai, J. P. Murnane, *Hum. Genet.* **113**, 337 (2003).
7. A. Smogorzewska, J. Karlseder, H. Holtgreve-Grez, A. Jauch, T. de Lange, *Curr. Biol.* **12**, 1635 (2002).
8. Materials and methods are available as supporting material on *Science* Online.
9. M. T. Hemann, M. A. Strong, L. Y. Hao, C. W. Greider, *Cell* **107**, 67 (2001).
10. M. Meyerson *et al.*, *Cell* **90**, 785 (1997).
11. T. M. Nakamura *et al.*, *Science* **277**, 955 (1997).
12. K. Damm *et al.*, *EMBO J.* **20**, 6958 (2001).
13. E. Pascolo *et al.*, *J. Biol. Chem.* **277**, 15566 (2002).
14. S. Huang *et al.*, *Nature Genet.* **20**, 114 (1998).
15. L. Chin *et al.*, *Cell* **97**, 527 (1999).
16. F. d'Adda di Fagagna *et al.*, *Nature* **426**, 194 (2003).
17. U. Herbig, W. A. Jobling, B. P. Chen, D. J. Chen, J. M. Sedivy, *Mol. Cell* **14**, 501 (2004).
18. C. J. Bakkenist, M. B. Kastan, *Nature* **421**, 499 (2003).
19. B. van Steensel, A. Smogorzewska, T. de Lange, *Cell* **92**, 401 (1998).
20. D. Loayza, T. de Lange, *Nature* **423**, 1013 (2003).
21. S. M. Bailey, M. N. Cornforth, A. Kurimasa, D. J. Chen, E. H. Goodwin, *Science* **293**, 2462 (2001).
22. D. Rhodes, R. Giraldo, *Curr. Opin. Struct. Biol.* **5**, 311 (1995).
23. C. C. Chang *et al.*, *Anal. Chem.* **76**, 4490 (2004).
24. V. P. Schulz *et al.*, *Hum. Genet.* **97**, 750 (1996).
25. D. M. Baird, T. Davis, J. Rowson, C. J. Jones, D. Kipling, *Hum. Mol. Genet.* **13**, 1515 (2004).
26. H. Ding *et al.*, *Cell* **117**, 873 (2004).
27. M. T. Teixeira, M. Arneric, P. Sperisen, J. Lingner, *Cell* **117**, 323 (2004).
28. S. Chang *et al.*, *Nature Genet.* **36**, 877 (2004).

29. We thank J. Campisi for WRN cDNAs; K. Damm for BIBR1532; H. Maruyama for antibody preparation; T. de Lange for discussion; members of the Karlseder lab and colleagues at The Salk, particularly V. Lundblad, for comments on the manuscript; B. Pau for co-directorship of a thesis committee (L.C.); R. Wang for CO-FISH suggestion and advice; and S. Chang for sharing unpublished data and material. Supported by the Mathers Foundation and NIH grant no. GM069525 (J.K.) and by a President's Fellowship and the Volontariat International program by the French Ministry of Foreign Affairs (L.C.).

Supporting Online Material

www.sciencemag.org/cgi/content/full/306/5703/1951/DC1
Materials and Methods
SOM Text
Figs. S1 to S3
Table S1
References and Notes

3 August 2004; accepted 21 October 2004
10.1126/science.1103619

COX-2–Derived Prostacyclin Confers Atheroprotection on Female Mice

Karine M. Egan,[1] John A. Lawson,[1] Susanne Fries,[1] Beverley Koller,[2] Daniel J. Rader,[1] Emer M. Smyth,[1] Garret A. FitzGerald[1]*

Female gender affords relative protection from cardiovascular disease until the menopause. We report that estrogen acts on estrogen receptor subtype alpha to up-regulate the production of atheroprotective prostacyclin, PGI_2, by activation of cyclooxygenase 2 (COX-2). This mechanism restrained both oxidant stress and platelet activation that contribute to atherogenesis in female mice. Deletion of the PGI_2 receptor removed the atheroprotective effect of estrogen in ovariectomized female mice. This suggests that chronic treatment of patients with selective inhibitors of COX-2 could undermine protection from cardiovascular disease in premenopausal females.

Age-dependent increases in cardiovascular disease are less pronounced in women than in men, but this difference narrows after the menopause (*1*). Estrogen (E_2) retards atherogenesis in models (*2*) and improves endothelial function in hyperlipidemic women (*3*). However, the mechanisms of atheroprotection are largely unknown.

The prostaglandin PGI_2 exhibits properties of relevance to atheroprotection, inhibiting platelet activation, vascular smooth muscle contraction and proliferation (*4*), leukocyte–endothelial cell interactions (*5*), and cholesteryl ester hydrolase (*6*). PGI_2 analogs retard atherogenesis (*7*), and atherosclerotic lesions exhibit a decreased capacity to produce PGI_2 ex vivo (*8*). Cyclooxygenase 2 (COX-2), expressed in vascular endothelial cells (*9*), catalyzes prostaglandin endoperoxide formation from arachidonic acid. This is subsequently transformed to PGI_2 by PGI_2 synthase (PGIS), a process that occurs in endothelial cells (*10*). Selective COX-2 inhibitors depress PGI_2 metabolite excretion (*11*). Inhibition of the COX-2–PGIS pathway may have particular relevance to atheroprotection in females because E_2 increases COX-2 expression in vascular tissues and augments PGI_2 production in vitro (*12*).

Mice lacking the low density lipoprotein (LDL) receptor (LDLR KO) were examined to address the role of PGI_2 in gender-dependent atheroprotection; males develop atherosclerosis more rapidly than females (*13*). No differences

[1]The Institute for Translational Medicine and Therapeutics, University of Pennsylvania, PA 19104, USA. [2]Department of Medicine, University of North Carolina, NC 27599, USA.

*To whom correspondence should be addressed. E-mail: garret@spirit.gcrc.upenn.edu

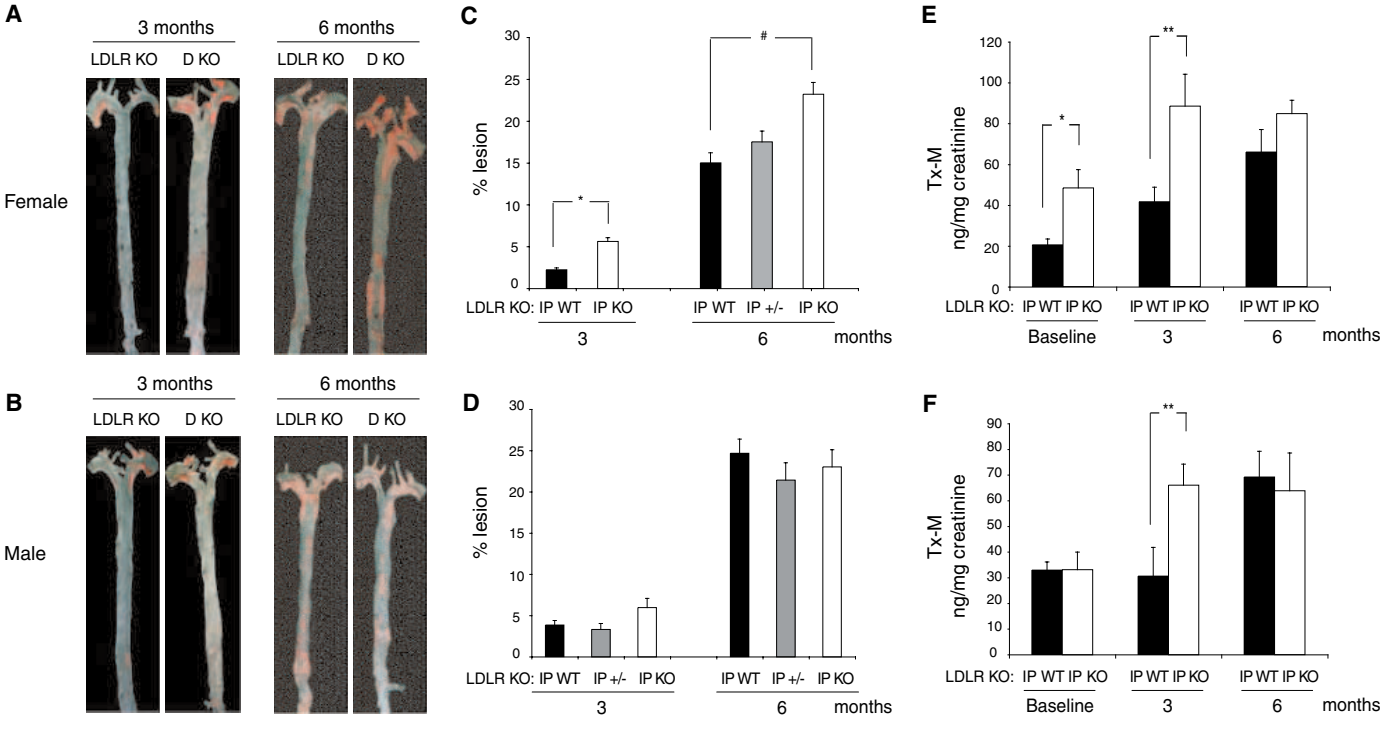

Fig. 1. Increased atherosclerosis and thromboxane (Tx) biosynthesis in IP/LDLR DKO female mice. (**A** and **B**) Representative en face aortae approximately equal to the mean % lesion area for each group are shown. (**C** and **D**) Percentage aortic lesion areas (stained red) in female and male LDLR KO and IP/LDLR DKO mice showed no significant difference between male IP/LDLR DKO and LDLR KO mice fed a high-fat diet for similar durations. IP deletion accelerated atherosclerosis at both time points in female mice only. IP/LDLR DKO females have a greater % lesion area ($^*P < 0.001$ versus LDLR KO at 3 months, $^{\#}P < 0.05$ at 6 months). Data are given as the mean ± SEM, $n = 10$ to 13 mice per group. (**E**) Excretion of urinary 2,3-dinor TxB_2 (Tx-M) in LDLR KO and IP/LDLR DKO mice at baseline and after being fed a high-fat diet for 3 and 6 months. Coincidental IP deletion increases Tx-M excretion in female mice ($F = 14.83$, $P < 0.001$). Pairwise comparisons reveal significant differences at baseline ($^*P < 0.05$) and at 3 months ($^{**}P < 0.01$). (**F**) Male IP/LDLR DKO mice do not have elevated Tx-M biosynthesis at baseline, but upon being fed a high-fat diet, show a significant increase (all males: $F = 6.14$, $P < 0.01$; all females: $F = 8.17$, $P < 0.01$). This is accounted for by a difference after 3 months ($^{**}P < 0.01$). Data are given as the mean ± SEM, $n = 10$ to 13 mice per group.

in plasma total cholesterol or high density lipoprotein (HDL) cholesterol were observed among groups (table S1). Body weight increased as the animals aged, but there were no differences with genotype. En face aortae analyses showed that the extent of atherosclerosis was greater at 3 and 6 months in males than in females (Fig. 1, A and B). Female mice lacking both the PGI_2 receptor (IP) and the LDLR (IP/LDLR DKO) developed greater aortic lesions than LDLR KO females after 3 months (5.6 ± 1.1% versus 2.2 ± 0.2%) and 6 months (23.2 ± 1.4% versus 15.0 ± 1.2%). This effect was gene dose dependent (Fig. 1C) and was not observed in male mice (Fig. 1D). There was a trend of greater lesion area in the IP/LDLR KO males than in LDLR KO males (5.95 ± 1.1%, n =12, versus 3.83 ± 0.5%, n =12) at 3 months, but this did not attain significance and was not evident at 6 months.

Platelet activation facilitates early atherogenesis and is reflected by the presence of the thromboxane metabolite 2,3-dinor TxB_2 (Tx-M) in urine. IP deletion increases urinary Tx-M in response to vascular injury (*4*) and increased urinary Tx-M in IP/LDLR DKO mice, compared to LDLR KO mice (Fig. 1, E and F). This effect was evident in both genders at 3 months. Although urinary Tx-M was higher in male than in female LDLR KO mice (32.8 ± 3.2 versus 20.5 ± 3.0 ng/mg creatinine), additional deletion of the IP elevated Tx-M excretion in females to exceed those in male IP/LDLR DKO mice at baseline. Thus, PGI_2 decreases the platelet activation that accompanies early atherogenesis in female mice.

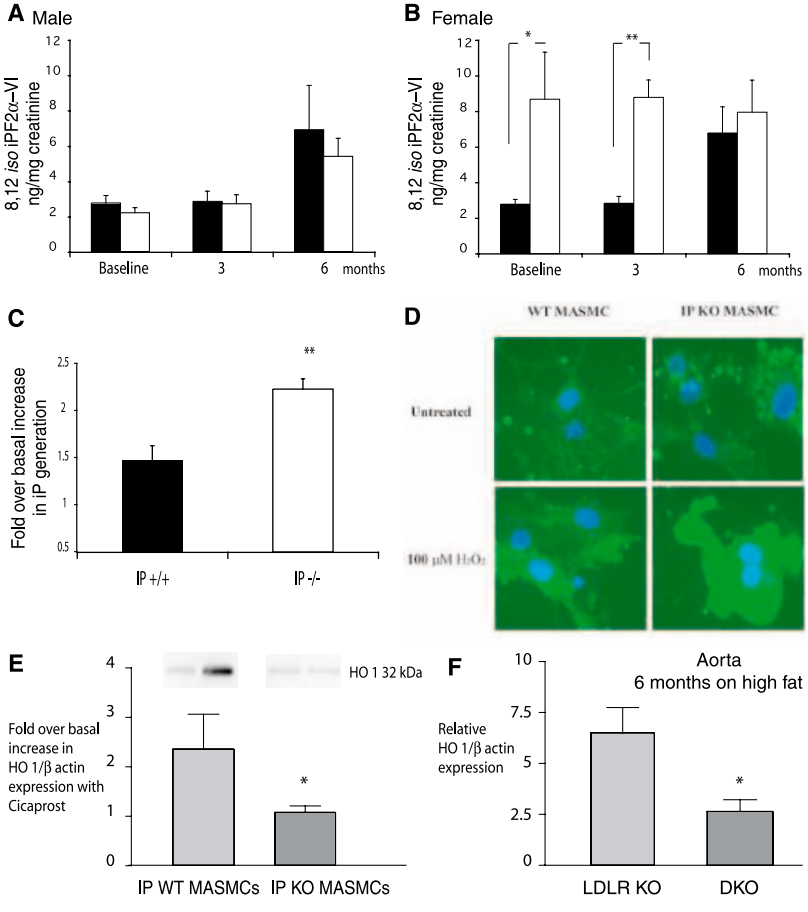

Fig. 2. Increased oxidant stress in female IP/LDLR DKO mice and an antioxidant effect of the IP in vitro. Urinary 8,12-*iso*-$iPF_{2\alpha}$-VI levels in (**A**) male and (**B**) female LDLR KO and IP/LDLR DKO mice. Urine collections were performed at 24-hour intervals before (baseline) and during (3 and 6 months) atherogenesis. Analysis of variance reveals a significant effect of IP deletion on lipid peroxidation in female (F = 15.82, P < 0.001) but not male LDLR KO mice (F = 2.70, P = 0.1082). Elevation in iP generation in female IP/LDLR DKO mice was evident at baseline (*P < 0.05) and at 3 months (**P < 0.01). Data are given as the mean ± SEM, n = 5 to 8 mice per group. (**C**) Increased oxidative stress in mouse aortic smooth muscle cells (MASMCs) lacking the IP. IP KO MASMCs show an exaggerated oxidative response to H_2O_2 exposure (30 min, 100 μM) [**P < 0.001 compared to wild-type (WT) MASMCs]. (**D**) As shown with the fluorescent probe, dichlorofluorescein, IP KO MASMCs were more fluorescent than WT MASMCs before and after stimulation with 100 μm H_2O_2. (**E**) Cicaprost (100 nm, 8 hours) treatment increases HO1 protein expression in WT MASMCS but not in IP KO MASMCs (*P < 0.05). (**F**) HO1 protein expression is attenuated in IP/LDLR DKO atherosclerotic aortas (*P < 0.05).

Oxidative stress increases lipid peroxidation, an effect reflected by the increased excretion of urinary isoprostanes (iPs) (*14*). One of the most abundant iPs in urine, 8,12-*iso*-$iPF_{2\alpha}$-VI, increased in LDLR KO mice during atherogenesis (Fig. 2). Although IP deletion had no effect in male IP/LDLR DKO mice (F = 1.77, P = 0.2) (Fig. 2A), its absence increased lipid peroxidation in female IP/LDLR DKO mice (F = 15.8, P < 0.0005). This was particularly evident at baseline (8.7 ± 2.6 versus 2.8 ± 0.3 ng/mg creatinine, P < 0.05) and at 3 months (8.8 ± 1.1 versus 2.8 ± 0.4 ng/mg creatinine, P < 0.001) (Fig. 2B), indicating that PGI_2 serves an antioxidant function in female LDLR KO mice prior to, and at initiation of, atherogenesis.

Given the importance of oxidant stress in atherogenesis (*14*), we examined the effect of PGI_2 in cultured mouse aortic smooth muscle cells (MASMCs) exposed to hydrogen peroxide (H_2O_2) (*15*). This treatment increased PGI_2 synthesis (*16*) and lipid peroxidation, and the latter was augmented by IP deletion (Fig. 2C). COX-2 expression was not affected (*16*). H_2O_2 treatment increased reactive oxygen species in MASMCs, as shown by the fluorescent probe dichlorofluorescein (*17*). Absence of IP expression increased this effect (Fig. 2D), suggesting that IP modulates oxidant stress under basal conditions. Cicaprost (100 nM), an IP agonist, limited the response of MASMCs to H_2O_2 with subsequent reduction of lipid peroxidation (fig. S1A) but did not affect unstimulated cells. Cicaprost also increased expression of the antioxidant heme oxygenase 1 (HO1) in an IP-dependent manner (Fig. 2E), whereas IP deletion decreased aortic HO1 expression in female IP/LDLR DKO mice (Fig. 2F).

MASMCs subjected to long-term E_2 exposure (10^{-8} M, 18 hours) were examined to determine whether E_2 alters the antioxidant effect of PGI_2 (*15*). E_2 stimulated COX-2 expression and PGI_2 formation as reflected by an increase in the PGI_2 hydrolysis product, 6-keto $PGF_{1\alpha}$ (from 2.4 ± 0.33 to 3.8 ± 0.38 ng/mg protein; *P < 0.05). Pretreatment of cells with E_2 (10^{-8} M, 18 hours) attenuated the response to H_2O_2, as reflected by diminished release of the iP (Fig. 3B), whereas direct coincubation of H_2O_2 with E_2 had no effect (*16*). E_2 administration (2 or 8 μg/day for 7 days) to ovariectomized LDLR KO mice increased PGI_2 biosynthesis, as reflected by increased excretion of the urinary PGI_2 metabolite 2,3-dinor 6-keto $PGF_{1\alpha}$ (PGI-M) (Fig. 3C) (** P < 0.01 and *P < 0.05, respectively, versus their own respective baseline controls) and depressed urinary iP (Fig. 3D) (*P < 0.05). Similarly, E_2

(3 μg/day for 7 days) administration to ovariectomized wild-type mice (C57Bl6) increased urinary PGI-M and depressed excretion of the iP (*16*). When MASMCs were treated with agonists selective for E_2 receptor α (ERα) (propyl pyrazole triol, PPT) (*18*) and ERβ (WAY-200070) (*19*), only the ERα-selective agonist increased 6-keto $PGF_{1\alpha}$ (Fig. 3E) (**$P < 0.05$). Furthermore, E_2 (0.5 μg/day for 7 days) increased urinary PGI-M in female ERβ KO mice but not in female ERα KO mice (Fig. 3F). Thus, estrogen increases PGI_2 biosynthesis by activating ERα. LDLR KO and IP/LDLR DKO mice were bilaterally ovariectomized to assess the atheroprotective effect of exogenous E_2 in the absence of PGI_2. One week after surgery, mice began feeding on a high-fat diet in the absence or presence of exogenous E_2 (8 μg/day) (*15*). After 3 months, aortic lesion area was significantly increased in the IP/LDLR DKO compared to the LDLR KO females (Fig. 4). E_2 significantly reduced lesion burden (by ~80%) in LDLR KO female mice (Fig. 4A). However, coincidental deletion of the IP reduced this effect significantly ($P < 0.0001$) to 32%.

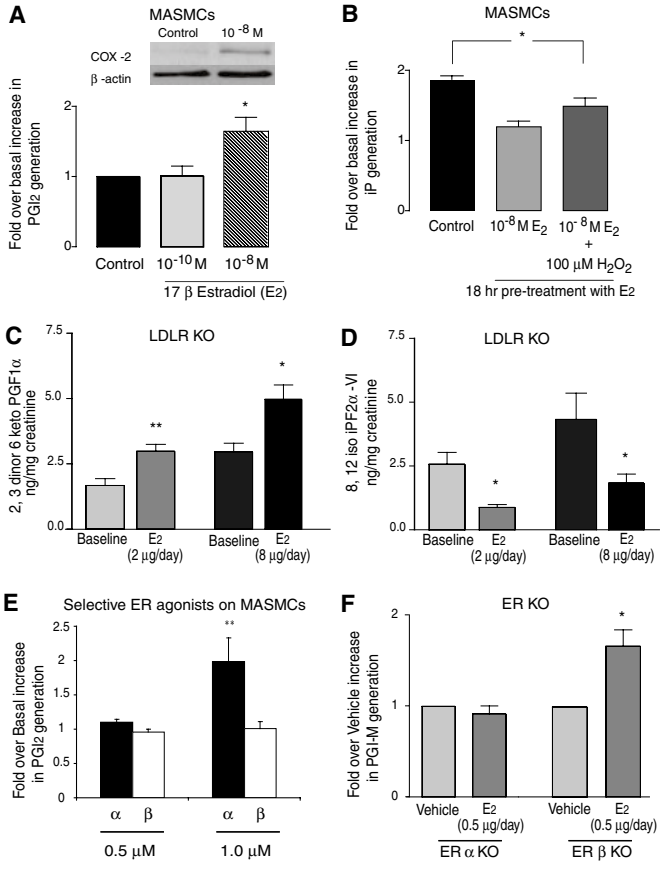

Fig. 3. E_2 increases PGI_2 biosynthesis in vitro and in vivo. (**A**) E_2 increased COX-2–mediated PGI_2 production from WT MASMCS exposed to E_2 (10^{-8} M, 18 hours). PGI_2 production was measured in the conditioned medium as 6-keto $PGF_{1\alpha}$. Values are expressed as fold over basal increase in 6-keto $PGF_{1\alpha}$ (pg/mg protein) (*$P < 0.05$). (**B**) Pretreatment with E_2 mediates an antioxidant effect on H_2O_2-induced oxidant injury. The increase in iP generation from WT MASMCs exposed to 100 μM H_2O_2 (30 min) was attenuated when cells were preincubated with 10^{-8} M E_2 for 18 hours (*$P < 0.05$). Treatment with 10^{-8} M E_2 alone does not significantly alter iP generation from MASMCs. (**C**) Subcutaneous E_2 administration increases urinary PGI_2 biosynthesis in ovariectomized LDLR KO mice (2 μg/day: **$P < 0.05$; 8 μg/day: *$P < 0.05$), coincident with (**D**) diminished urinary iP (2 μg/day: *$P < 0.05$; 8 μg/day: *$P < 0.05$). (**E**) An ERα-selective agonist (1.0 μM) elevates PGI_2 biosynthesis in MASMCs (**$P < 0.01$, fold over basal). (**F**) E_2 fails to increase PGI_2 biosynthesis in ovariectomized ERα KO mice. E_2 increases PGI_2 biosynthesis in ERβ KO mice (*$P < 0.05$). Data are given as the mean ± SEM, $n = 6$ to 10 mice per group.

Rofecoxib, a selective inhibitor of COX-2, was withdrawn from clinical use when a placebo-controlled trial revealed an increase in myocardial infarction and stroke (*20*). These patients were initially at low cardiovascular risk, and the hazard was detected after 18 months of treatment. Selective inhibitors of COX-2 depress PGI_2, but not platelet COX-1–derived TxA_2, which affords a mechanism whereby they might elevate blood pressure, accelerate atherogenesis, and augment the thrombotic response to plaque rupture (*5*, *21*, *22*). Depression of PGI_2 may accelerate atherogenesis by multiple mechanisms, including augmenting platelet and neutrophil interactions with the vasculature (*4*, *5*). PGI_2 also exerts an antioxidant effect, which may retard atherogenesis (*14*). IP deletion augments lipid peroxidation, whereas its overexpression in human embryonic kidney cells has the opposite effect (fig. S1B). An antioxidant role for PGI_2, which may reflect induction of HO1, is consistent with exacerbation of reperfusion injury by IP deletion (*23*).

Although extrapolation of results in mice to humans is performed with caution, the experience with rofecoxib has focused attention on the role of atherogenesis in transformation of cardiovascular risk during chronic treatment with selective inhibitors of COX-2 (*20*). We reveal a substantial contribution of ERα-mediated, COX-2–derived PGI_2 to atheroprotection in female LDLR KOs. This finding raises concern about the use of COX-2 inhibitors in juvenile arthritis, a disease that predominantly affects females. It may also have implications for the design and interpretation of trials of hormone-replacement therapy.

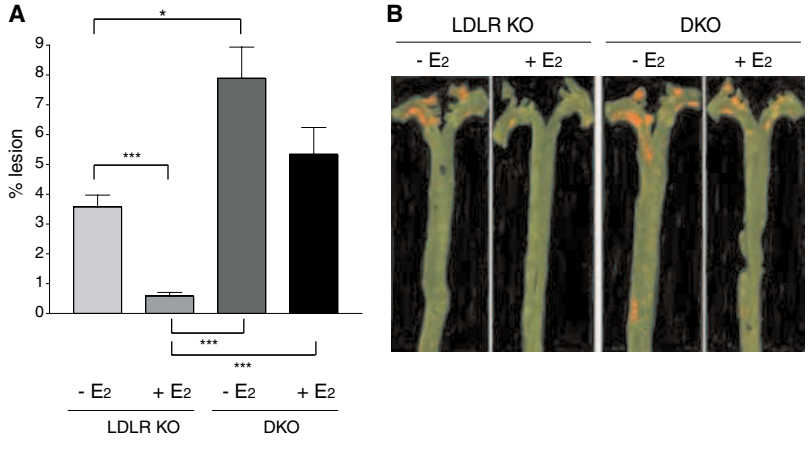

Fig. 4. The atheroprotective effect of estrogen is significantly reduced in the absence of the IP. (**A**) The atheroprotective effect of a subcutaneous regimen of E_2 (8 μg/day) in ovariectomized LDLR KO mice (***$P < 0.001$) is constrained in IP/LDLR DKO females. As expected, the % lesion area is greater in IP/LDLR DKO females than in LDLR KO females (*$P < 0.05$). (**B**) Representative en face aortas approximately equal to the mean % lesion area (stained red) are shown. Data are given as the mean ± SEM, $n = 11$ to 19 mice per group.

References and Notes

1. I. F. Godsland, V. Wynn, D. Crook, N. E. Miller, *Am. Heart J.* **114**, 1467 (1987).
2. P. A. Bourassa, P. M. Milos, B. J. Gaynor, J. L. Breslow, R. J. Aiello, *Proc. Natl. Acad. Sci. U.S.A.* **93**, 10022 (1996).
3. P. Collins *et al.*, *Circulation* **92**, 24 (1995).
4. Y. Cheng *et al.*, *Science* **296**, 539 (2002).
5. T. Kobayashi *et al.*, *J. Clin. Invest.* **114**, 6,784 (2004).

6. R. J. Gryglewski, S. Chlopicki, J. Swies, P. Niezabitowski, *Ann. N. Y. Acad. Sci.* **748**, 194; discussion 206–7 (1995).
7. M. C. Kowala *et al.*, *Arterioscler. Thromb.* **13**, 435 (1993).
8. H. Sinzinger *et al.*, *Thromb. Haemostasis* **42**, 803 (1979).
9. J. N. Topper, J. Cai, D. Falb, M. A. Gimbrone Jr., *Proc. Natl. Acad. Sci. U.S.A.* **93**, 10417 (1996).
10. S. Moncada, R. Gryglewski, S. Bunting, J. R. Vane, *Nature* **263**, 663 (1976).
11. B. F. McAdam *et al.*, *Proc. Natl. Acad. Sci. U.S.A.* **96**, 272 (1999).
12. P. Akarasereenont, K. Techatraisak, A. Thaworn, S. Chotewuttakorn, *Inflamm. Res.* **49**, 460 (2000).
13. R. K. Tangirala, E. M. Rubin, W. Palinski, *J. Lipid Res.* **36**, 2320 (1995).
14. D. Pratico, R. K. Tangirala, D. J. Rader, J. Rokach, G. A. FitzGerald, *Nat. Med.* **4**, 1189 (1998).
15. Materials and methods are available as supporting material on *Science* Online.
16. K. M. Egan *et al.*, data not shown.
17. T. Munzel, I. B. Afanas'ev, A. L. Kleschyov, D. G. Harrison, *Arterioscler. Thromb. Vasc. Biol.* **22**, 1761 (2002).
18. H. A. Harris, J. A. Katzenellenbogen, B. S. Katzenellenbogen, *Endocrinology* **143**, 4172 (2002).
19. E. M. Malamas *et al.*, *J. Med. Chem.* **47**, 5021 (2004).
20. G. A. FitzGerald, *N. Engl. J. Med.* **351**, 17, 1709 (2004).
21. T. Murata *et al.*, *Nature* **388**, 678 (1997).
22. Q. Zhonghua *et al.*, *J. Clin. Invest.* **110**, 1, 61 (2002).
23. C. Y. Xiao *et al.*, *Circulation* **104**, 2210 (2001).
24. We thank H. Ischiropoulos and D. Fries (Children's Hospital of Philadelphia) for assistance. G.A.F. is on the Arcoxia Advisory Board for Merck and has consulted for or received grant support from Bayer, Boehringer Ingelhelim, CV Therapeutics, GlaxoSmithKline, Johnson and Johnson, Merck, Nicox, Novartis, Portola Pharmaceuticals, Pfizer, and Pharmacia/Searle in the past 5 years. This work was supported by grants from the NIH (HL70128 and HL62250).

Supporting Online Material
www.sciencemag.org/cgi/content/full/1103333/DC1
Materials and Methods
Fig. S1
Table S1

28 July 2004; accepted 3 November 2004
Published online 18 November 2004;
10.1126/science.1103333
Include this information when citing this paper.

Host-Parasite Coevolutionary Conflict Between *Arabidopsis* and Downy Mildew

Rebecca L. Allen,[1] Peter D. Bittner-Eddy,[1] Laura J. Grenville-Briggs,[1]* Julia C. Meitz,[1] Anne P. Rehmany,[1] Laura E. Rose,[2] Jim L. Beynon[1]†

Plants are constantly exposed to attack by an array of diverse pathogens but lack a somatically adaptive immune system. In spite of this, natural plant populations do not often suffer destructive disease epidemics. Elucidating how allelic diversity within plant genes that function to detect pathogens (resistance genes) counteracts changing structures of pathogen genes required for host invasion (pathogenicity effectors) is critical to our understanding of the dynamics of natural plant populations. The *RPP13* resistance gene is the most polymorphic gene analyzed to date in the model plant *Arabidopsis thaliana*. Here we report the cloning of the avirulence gene, *ATR13*, that triggers *RPP13*-mediated resistance, and we show that it too exhibits extreme levels of amino acid polymorphism. Evidence of diversifying selection visible in both components suggests that the host and pathogen may be locked in a coevolutionary conflict at these loci, where attempts to evade host resistance by the pathogen are matched by the development of new detection capabilities by the host.

Disease resistance in plants is a complex process that provides many potential barriers to pathogen invasion. Among the plant's defense arsenal are the disease resistance (*R*) genes, whose products trigger defense responses, such as localized host cell death, when challenged with pathogen isolates carrying matching avirulence genes (*1*). The largest class of *R* genes encodes proteins containing intra- or extracellular leucine-rich repeat (LRR) domains. LRR domains have been implicated in protein:protein interactions (*2*). However, direct interaction between an avirulence protein and its cognate R protein has been demonstrated in only a few host/pathogen systems (*3*, *4*).

Avirulence genes have been cloned from the fungal plant pathogens *Cladosporium fulvum* (*5*–*7*), *Magnaporthe grisea* (*8*), and *Melampsora lini* (*9*), but apart from the chitin-binding capacity of the Avr4 protein from *C. fulvum* (*10*), their roles in pathogenicity are unknown. We have recently shown the *RPP13* (*Recognition of Peronospora parasitica 13*) resistance gene from *Arabidopsis thaliana* to be the most polymorphic gene so far analyzed in this species (*11*). *RPP13* encodes a CC:NB:LRR (coiled coil: nucleotide binding site:leucine rich repeat) protein, predicted to be cytoplasmically located, and the extreme variability of the protein was shown to reside within the LRR domain (*11*, *12*). This is consistent with the LRR domain experiencing diversifying selection. One selective agent could be a pathogen species exhibiting comparable levels of polymorphism in the avirulence protein detected via RPP13. From the plant's perspective, there are two basic outcomes of a coevolutionary conflict: either a selective sweep in which a single allele of a resistance gene reaches high frequency in the plant population or balancing selection, in which a diverse cohort of resistance gene alleles is stably maintained (*13*). The large number (19 among 24 *Arabidopsis* accessions) of diverse alleles present at the *RPP13* locus implies that it is subject to balancing selection (*11*). Haldane's theory (*14*) suggests that coevolution of host and pathogen could lead to the maintenance of variation in both organisms. The interaction between *Arabidopsis* and the biotrophic oomycete *Hyaloperonospora parasitica* (formally *Peronospora parasitica*) is an excellent system in which to study such coevolution because both organisms coexist in extensive naturally occurring populations (*15*). Therefore, concomitant with extreme *RPP13* gene diversity, we hypothesize that balancing selection on the pathogen gene products recognized by these *R* genes [*ATR13* (*Arabidopsis thaliana recognised 13*)] would also result in the maintenance of a highly polymorphic population of *ATR13* alleles. Here we report the cloning of *ATR13* and show that it is indeed under intense diversifying selection consistent with host/parasite conflict occurring between these two species. Both *ATR13* and *RPP13* are subject to balancing selection.

We previously isolated a range of *H. parasitica* genes [*Ppat* (*Peronospora parasitica in Arabidopsis thaliana*)] that were up-regulated on infection of *Arabidopsis* (*16*). Mapping of the *Ppat* sequences among 206 F_2 progeny of a cross between *H. parasitica* isolates Maks9 (predicted to contain *ATR13*) and Emoy2 (predicted to contain *atr13*) revealed cosegregation of a single-copy gene, *Ppat17*, and *ATR13* (*17*). Therefore, *Ppat17* was an *ATR13* candidate.

Because no mechanism of genetic transformation has been established for *H. parasitica*, we developed a functional assay for *ATR13* recognition based on a biolistic ap-

[1]Warwick, HRI University of Warwick, Wellesbourne, Warwick, CV35 9EF, UK. [2]Department of Evolutionary Biology, University of Munich, Großhadernerstrasse 2, 82152 Planegg-Martinsried, Germany.

*Present address: College of Life Sciences and Medicine, University of Aberdeen, IMS, Foresterhill, Aberdeen, AB25 2ZD, UK.
†To whom correspondence should be addressed. E-mail: jim.beynon@warwick.ac.uk

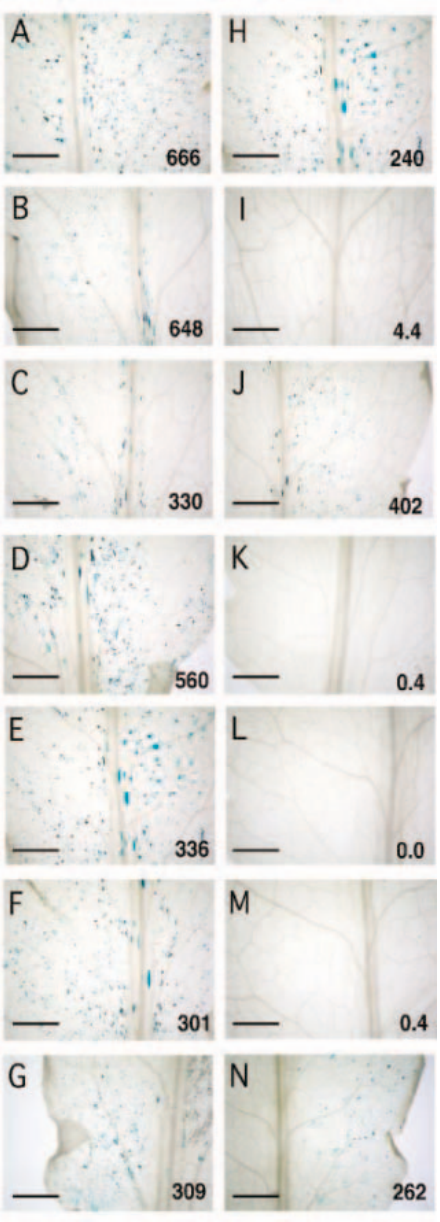

Fig. 1. Biolistic analysis of ATR13 alleles. (**A** to **G**) 8-week-old Col-5 leaves; (**H** to **N**) 8-week-old Col-5::*RPP13-Nd* leaves. (A) and (H) were bombarded with the control plasmid, pK2GW7, and the 35*S*::GUS plasmid; (B) and (I) were bombarded with the ATR13-Maks9 plasmid (without signal peptide) and the 35*S*::GUS plasmid; (C) and (J) were bombarded with the ATR13-Emoy2 plasmid (without signal peptide) and the 35*S*::GUS plasmid; (D) and (K) were bombarded with the ATR13-Aswa1 plasmid (with signal peptide) and the 35*S*::GUS plasmid; (E) and (L) were bombarded with the ATR13-Emco5 plasmid (with signal peptide) and the 35*S*::GUS plasmid; (F) and (M) were bombarded with the ATR13-Goco1 plasmid (with signal peptide) and the 35*S*::GUS plasmid; and (G) and (N) were bombarded with the ATR13-Hind4 plasmid (with signal peptide) and the 35*S*::GUS plasmid. Leaves were stained for β-glucuronidase activity and cleared with methanol. Numbers represent average numbers of blue-stained cells over five replicates. Scale bars, 2.5 mm.

proach. Three models could be proposed for the role of *ATR13* in the elicitation of plant cell death: (i) the presence of the ATR13 protein alone is sufficient; (ii) ATR13 acts in concert with monomorphic *H. parasitica* proteins; or (iii) ATR13 is an enzyme that produces a pathogen product, which triggers the hypersensitive reaction as in the case of *avrD* (*18*). Bombardment of *Arabidopsis* leaves with a plasmid carrying the bacterial *uidA* gene (*GUS*) fused to the 35*S* promoter results in blue-stained cells, in the presence of the substrate X-Gluc. (*17*). If model (i) is correct, then co-bombardment of *Arabidopsis* leaves expressing *RPP13* with the 35S::*GUS* plasmid and another carrying a 35*S*::*ATR13* fusion would result in cell death and consequently no *GUS* expression. Hence, we fused *Ppat17* to the 35*S* promoter and co-bombarded *Arabidopsis* accession Columbia, which contains an allele of *RPP13* that does not recognize Maks9 or Emoy2, and a Columbia transgenic line (Col5::*RPP13-Nd*) carrying the *RPP13* allele from the Niederzenz accession, which enables isolate-specific recognition of Maks9 but not Emoy2 (*12*, *19*). In an experiment using 35*S*::*GUS* and a control plasmid, large numbers of blue-stained cells were seen in both types of plant material (Fig. 1, A and H). However, when 35*S*::*GUS* and 35*S*::*Ppat17-Maks9* were co-bombarded, results similar to those with the control (648 blue-stained cells) were seen in Columbia, but this number was significantly reduced (4.4 blue-stained cells) in our Col5::*RPP13-Nd* line (Fig. 1, B and I). As a further test, we repeated the experiment using the Emoy2 allele of *Ppat17*, which would not be predicted to elicit a response from *RPP13-Nd*. In this experiment, the number of blue-stained cells was similar to the control in both plant lines (Fig. 1, C and J). We conclude that *Ppat17* is *ATR13*, and the protein it encodes is sufficient to trigger *RPP13*-dependent resistance.

To confirm the function of *ATR13* in vivo, we carried out in planta expression assays. We fused the *ATR13* Maks9 and Emoy2 alleles to a glucocorticoid-inducible plant promoter and generated transgenic Columbia plants and HRI3879, a selected recombinant inbred line containing *RPP13-Nd*, plants (*17*). In the presence of *RPP13-Nd*, the *ATR13-Maks9* gene caused wilting within 6 hours of dexamethasone application and death of the whole plant within 24 hours (Fig. 2, A and B). Induction of the Maks9 allele caused no phenotypic change in Columbia (Fig. 2, C and D). To confirm that ATR13-Maks9 protein was produced in these plants, they were crossed to Col5::*RPP13-Nd* and, as expected, all F_1 progeny tested died on induction of *ATR13-Maks9* (*20*). Induction of the Emoy2 *ATR13* allele in the presence or absence of *RPP13-Nd* resulted in no change in plant phenotype (*20*). These data imply that *RPP13* is expressed in a wide range of above-ground plant cell types and confirm the allele-specific nature of the interaction between *RPP13* and *ATR13-Maks9*.

ATR13-Maks9 encodes a 187–amino acid protein that shows no significant homology (BLASTP) (*21*) to other proteins but appears to have clear domain structures. ATR13-Maks9 has a heptad leucine/isoleucine repeat motif and, although reminiscent of coiled-coil domains that are involved in protein-protein interactions, this ATR13 domain is not predicted to lie within an α-

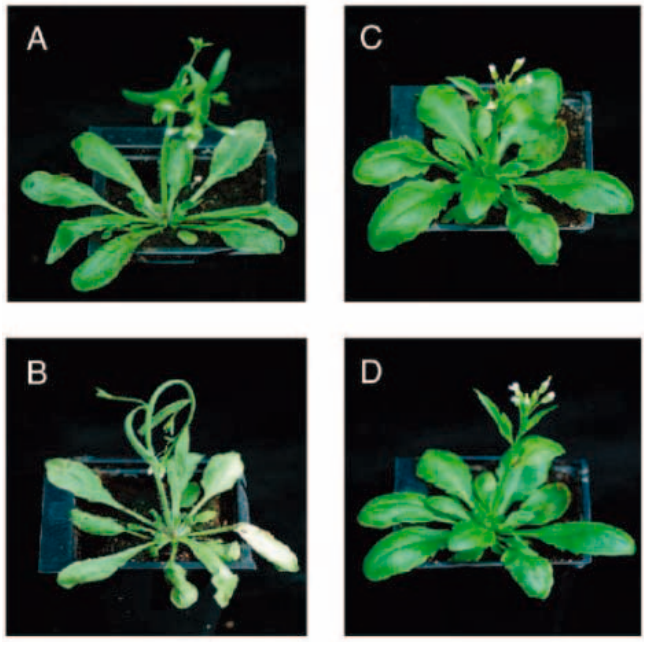

Fig. 2. Induced expression of *ATR13-Maks9* triggers a total cell death phenotype specific to *Arabidopsis* plants containing *RPP13-Nd*. *Arabidopsis* plant lines were transformed with *ATR13-Maks9* (minus signal peptide sequence) under the control of a dexamethasone-inducible promoter (*17*). Pictures were taken 6 hours (**A** and **C**) and 24 hours (**B** and **D**) after dexamethasone application. Representative T_3 homozygous transgenic HRI3879 plants (*RPP13-Nd*) (A) and (B) and Columbia (*RPP13-Col*) plants (C) and (D) are shown. Note the drooping inflorescence (A) and desiccated nature of the leaves in the transgenic HRI3879 plant (B). We observed similar responses when plants were transformed with full-length *ATR13-Maks9*.

helical structure (Fig. 3). An imperfect direct repeat of 4 × 11 amino acids lies between residues 93 and 136 and is followed by a C-terminal region within which no specific structures can be identified (Fig. 3). The program SignalP (*22*) reveals a high (P = 0.98) likelihood of a signal peptide being encoded at the N terminus with cleavage after the 19th amino acid (Fig. 3). This suggests that ATR13-Maks9 is secreted from *H. parasitica* during its growth in planta, which is consistent with it being exposed to and entering the plant cell where it could interact with RPP13-Nd.

The presence of an ATR13 signal peptide made no difference to the results obtained in the biolistic and in planta assays, and could be explained as a consequence of high levels of gene expression resulting in aberrant processing of ATR13 by the host's signal peptide recognition complex (*20*). Successful recognition of ATR13-Maks9 expressed without a signal peptide is consistent with its recognition by the intracellularly located RPP13-Nd, implying that ATR13-Maks9 is imported into the plant cell by an unidentified mechanism. Bacterial plant pathogens such as *Pseudomonas syringae* use the highly conserved type III secretion apparatus to transport their effector proteins across the plant plasma membrane (*23*), but an equivalent system has yet to be described in fungal or oomycete pathogens. The *AvrL567* gene family from *M. lini* encodes small potentially secreted proteins that have been shown to specifically trigger *R* gene–dependent cell death in flax lines carrying the cytoplasmically located L5, L6, and L7 resistance proteins (*9*). Both *H. parasitica* and *M. lini* possess specialized feeding structures called haustoria that form an intimate association with the plant plasma membrane (*24*), and potentially these are the sites at which these pathogens traffic their pathogenicity effectors.

RPP13-Nd initiates resistance reactions to the Aswa1, Emco5, and Goco1 isolates of *H. parasitica* in addition to Maks9, but not to Hind4 or Emoy2. To determine whether *ATR13* is central to this resistance, we cloned *ATR13* alleles from these additional isolates and tested their function using the biolistic assay. *ATR13-Aswa1*, *ATR13-Emco5*, and *ATR13-Goco1* all elicited an *RPP13-Nd*–dependent cell death response equivalent to that seen with *ATR13-Maks9* but *ATR13-Hind4* did not (Fig. 1, D to G and K to N). DNA sequence analysis revealed that all isolates carried a different *ATR13* allele than Maks9, but that of Emco5 and Goco1 were identical to each other (*25*). However, the overall structure of the predicted ATR13 proteins was retained (Fig. 3). Several amino acids varied within the heptad repeat region, but the heptad motif itself was conserved, suggesting a possible functional significance.

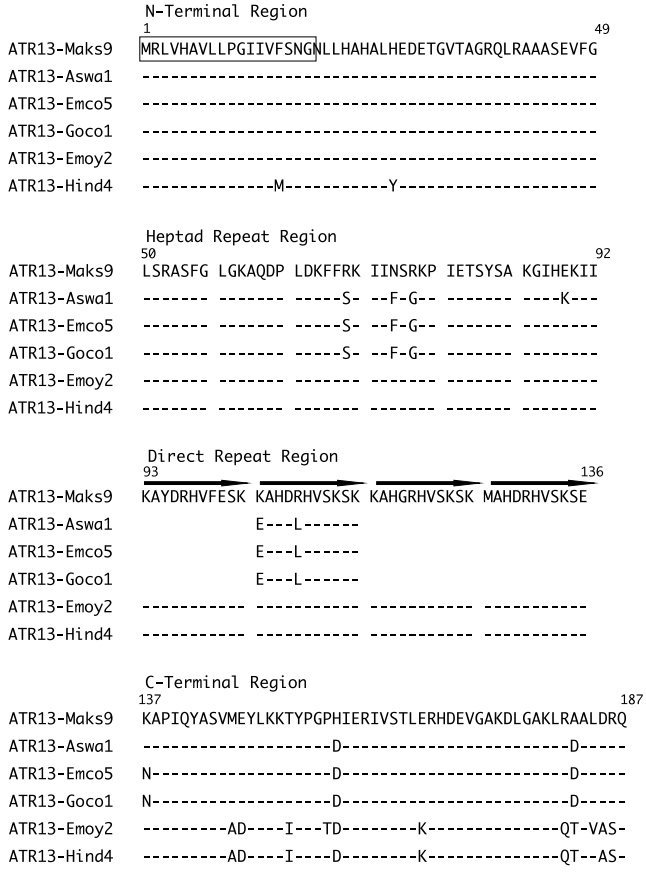

Fig. 3. Alignment of predicted proteins encoded by ATR13 alleles generated with Vector NTI. Dashes indicate amino acids identical to ATR13-Maks9. Amino acid residues differing from ATR13-Maks9 are shown. In the N-terminal region, the predicted signal peptide is boxed. In the direct repeat region, the repeats are shown by arrows. ATR13 from isolates Maks9, Aswa1, Emco5, and Goco1 triggers an *RPP13-Nd*–dependent resistance response, but ATR13 from isolates Emoy2 and Hind4 does not.

Surprisingly, ATR13 encoded by the alleles from Aswa1, Emco5, and Goco1 contained only one 11–amino acid repeat unit, indicating that repeats 1, 3, and 4 are dispensable for an *RPP13-Nd*–mediated resistance response. The *AvrBs3* avirulence gene family from *Xanthomonas campestris* pv. *vesicatoria* encodes proteins with a variable number of a 34–amino acid repeat motif, which was shown to determine specificity in its interaction with different plant *R* genes (*26*). In contrast, a repeated domain within ATR13 is not required for recognition by *RPP13-Nd*. However, we cannot preclude the possibility that the repeats have a role in determining recognition specificity via other *R* genes.

The Maks9 and Emoy2 alleles have identical DNA sequences throughout the N-terminal, heptad repeat, and direct repeat regions and only a single nucleotide polymorphism in 218 bases 5′ to translation initiation (*25*). This stretch of shared sequence identity between these two alleles over the first three-quarters of the protein, followed by a region of dissimilarity, uncovers two biologically relevant features. First, it reveals that the C-terminal portion of these two proteins is the region causing differential recognition by the *RPP13-Nd* allele. Second, it suggests that recombination has played a role in the evolutionary history of the *ATR13* gene. The inference of recombination is supported by permutation analysis, which detected a significantly long stretch of sequence identity between these two alleles (P = 0.008) (*27*).

RPP13 has evolved under intense diversifying selection (*11*) and as such offers a stark contrast to the related *Arabidopsis RPM1* gene where, presumably, invariant *Pseudomonas* effector proteins AvrRPM1 and AvrB do not appear to have driven the evolution of alternative *RPM1* alleles (*28*, *29*). If the evolution of *RPP13* were driven by its interaction with *H. parasitica*, then one would expect to see a similar evolutionary pattern in the matching avirulence gene. Among the five *ATR13* alleles, there are 26 nonsynonymous, two synonymous, and two indel polymorphisms. Based on a total of 351.5 nonsynonymous and 113.5 synonymous sites at *ATR13* (*30*), this represents a significant excess of nonsynonymous polymorphism relative to the neutral expectation (X^2 = 4.48, P = 0.034) and indicates selective maintenance of amino acid polymorphism at this locus. Amino acid polymorphism at ATR13 is not limited to differences between alleles that are recognized by RPP13-Nd and those that are not. Only eight amino acid differences are fixed between the two phenotypically distinct classes of alleles. There are nine amino acid and two indel polymorphisms among the three alleles recognized by RPP13-Nd, and four amino acid differences between the two alleles not recognized by RPP13-Nd. This is reminiscent of

the situation in *M. lini*, where two paralogs of the *AvrL567* gene, exhibiting significant amino acid variation, show differential recognition and response by the *L5*, *L6*, and *L7* flax resistance genes (*9*). However, *ATR13* alleles, showing not only extensive amino acid variation but also deletions of repeated domains, were equally effective in triggering resistance via *RPP13-Nd*. The high level of amino acid variation among alleles that are recognized by RPP13-Nd may indicate that these variants are selectively favored in *H. parasitica* parasitizing host populations not expressing *RPP13-Nd*. To confirm that not all *H. parasitica* genes are undergoing an equivalent extreme rate of change, we sequenced *Ppat5* from the same *H. parasitica* isolates. *Ppat5* encodes a dnaK-type molecular chaperone (*16*) and hence is likely to be under different selective pressures as compared to *ATR13*. DNA sequence analysis of *Ppat5* revealed only nine segregating polymorphisms across the 1983–base pair ORF and, in contrast to ATR13, only one of these is a nonsynonymous polymorphism (*25*).

Our study reveals the *RPP13/ATR13* plant/pathogen interaction to be an excellent model for studying the coevolution of resistance and avirulence genes within host and pathogen populations. The high levels of amino acid polymorphism relative to silent polymorphism in both plant and pathogen genes is consistent with a history of balancing selection operating at both loci. Within RPP13, it is the LRR domain that shows diversifying selection, whereas the rest of the gene shows selection for conservation of protein sequence (*11*, *12*). This study shows that the C-terminal domain of ATR13 plays a role in determining the specificity of interaction with RPP13, suggesting a direct interaction with the LRR domain. However, our initial yeast two-hybrid studies have not revealed a direct interaction between RPP13 and ATR13 (*31*). It is possible that different alleles of RPP13 recognize other pathogen proteins, and variation at this locus could be influenced by additional pathogen interactions, not necessarily limited to *H. parasitica*. Additionally, ATR13 may be detected by more than one host resistance gene, leading to increased selection for diversity in this protein. ATR13 must have a role in enabling *H. parasitica* to grow as an obligate biotrophic pathogen on *Arabidopsis*, and the elucidation of the roles of the observed motifs in planta will add substantially to our understanding of the mechanisms of biotrophic pathogenicity as well as those of host defense.

References and Notes

1. J. L. Dangl, J. D. Jones, *Nature* **411**, 826 (2001).
2. D. A. Jones, J. D. Jones, *Adv. Bot. Res.* **24**, 90 (1997).
3. Y. Jia, S. A. McAdams, G. T. Bryan, H. P. Hershey, B. Valent, *EMBO J.* **19**, 4004 (2000).
4. L. Deslandes *et al.*, *Proc. Natl. Acad. Sci. U.S.A.* **100**, 8024 (2003).
5. M. H. Joosten, T. J. Cozijnsen, P. J. De Wit, *Nature* **367**, 384 (1994).
6. J. A. van Kan, G. F. van den Ackerveken, P. J. de Wit, *Mol. Plant Microbe Interact.* **4**, 52 (1991).
7. R. Luderer, F. L. Takken, P. J. de Wit, M. H. Joosten, *Mol. Microbiol.* **45**, 875 (2002).
8. M. J. Orbach, L. Farrall, J. A. Sweigard, F. G. Chumley, B. Valent, *Plant Cell* **12**, 2019 (2000).
9. P. N. Dodds, G. J. Lawrence, A.-M. Catanzariti, M. A. Ayliffe, J. G. Ellis, *Plant Cell* **16**, 755 (2004).
10. N. Westerink, R. Roth, H. A. Van den Burg, P. J. De Wit, M. H. Joosten, *Mol. Plant Microbe Interact.* **15**, 1219 (2002).
11. L. E. Rose *et al.*, *Genetics* **166**, 1517 (2004).
12. P. D. Bittner-Eddy, I. R. Crute, E. B. Holub, J. L. Beynon, *Plant J.* **21**, 177 (2000).
13. R. M. May, R. M. Anderson, in *Coevolution*, D. J. Futuyma, M. Slatkin, Eds. (Sinauer, Sunderland, MA, 1983), pp. 189–206.
14. J. B. S. Haldane, *Ricerca Sci.* **19** (suppl. 1), 68 (1949).
15. E. B. Holub, J. L. Beynon, I. R. Crute, *Mol. Plant Microbe Interact.* **7**, 223 (1994).
16. P. D. Bittner-Eddy, R. L. Allen, A. P. Rehmany, P. Birch, J. L. Beynon, *Mol. Plant Pathol.* **4**, 501 (2003).
17. Materials and methods are available as supporting material on *Science* Online.
18. N. T. Keen *et al.*, *Mol. Plant Microbe Interact.* **3**, 112 (1990).
19. Fusions of *Ppat17* were made with and without the predicted signal peptide sequence and were tested in the biolistic and in planta assays. Similar results were obtained with both forms of the gene.
20. R. L. Allen *et al.*, data not shown.
21. S. F. Altschul *et al.*, *Nucleic Acids Res.* **25**, 3389 (1997).
22. J. D. H. Bendtsen, Nielsen, G. von Heijne, S. Brunak, *J. Mol. Biol.* **340**, 783 (2004).
23. Q. Jin, R. Thilmony, J. Zwiesler-Vollick, S. Y. He, *Microbes Infect.* **5**, 301 (2003).
24. M. Hahn, K. Mendgen, *Curr. Opin. Plant Biol.* **4**, 322 (2001).
25. See supplementary figures on *Science* Online.
26. G. Van den Ackerveken, E. Marois, U. Bonas, *Cell* **87**, 1307 (1996).
27. GENECONV: A computer package for the statistical detection of gene conversion, S. A. Sawyer (1999). Distributed by the author, Department of Mathematics, Washington University, St. Louis, MO, and available at www.math.wustl.edu/~sawyer. The Geneconv method was used to determine whether some regions of a pair of sequences had more consecutive identical polymorphic sites than would be expected by chance. This test assumes that mutations are neutral and independently distributed and that there has been no history of recombination between sequences. Permutation of the sequences was used to assign *P* values to the observed shared fragments and to evaluate their statistical significance.
28. M. R. Grant *et al.*, *Science* **269**, 843 (1995).
29. E. A. Stahl, G. Dwyer, R. Mauricio, M. Kreitman, J. Bergelson, *Nature* **400**, 667 (1999).
30. J. Rozas, J. C. Sánchez-DelBarrio, X. Messeguer, R. Rozas, *Bioinformatics* **19**, 2496 (2003).
31. R. L. Allen, S. Hall, J. L. Beynon, unpublished results.

32. We thank H. Kaminaka and J. Dangl for allowing us to use pBDex; S. Bright, V. Buchanan-Wollaston, S. Hall, and B. Thomas for critical review of the manuscript; and E. Holub for provision of pathogen isolates. Supported by the Biotechnology and Biological Sciences Research Council and the Department of Environment, Food and Rural Affairs (under license PHL275/4864).

Supporting Online Material

www.sciencemag.org/cgi/content/full/306/5703/1957/DC1
Materials and Methods
Figs. S1 and S2
References

13 August 2004; accepted 22 October 2004
10.1126/science.1104022

Leading-Edge Vortex Lifts Swifts

J. J. Videler,[1,2]* E. J. Stamhuis,[1] G. D. E. Povel[2]

The current understanding of how birds fly must be revised, because birds use their hand-wings in an unconventional way to generate lift and drag. Physical models of a common swift wing in gliding posture with a 60° sweep of the sharp hand-wing leading edge were tested in a water tunnel. Interactions with the flow were measured quantitatively with digital particle image velocimetry at Reynolds numbers realistic for the gliding flight of a swift between 3750 and 37,500. The results show that gliding swifts can generate stable leading-edge vortices at small (5° to 10°) angles of attack. We suggest that the flow around the arm-wings of most birds can remain conventionally attached, whereas the swept-back hand-wings generate lift with leading-edge vortices.

The discovery of leading-edge vortices (LEVs) on the wings of insects in flight greatly advanced the knowledge of their dominant lift-generating mechanisms (*1, 2, 3*). Sharp leading edges induce high lift production through flow separation with vortical flow attached to the upper surface of insect wings during flapping and gliding.

[1]Department of Marine Biology (Experimental Marine Zoology Group), Groningen University, Post Office Box 14, 9750 AA, Haren, Netherlands. [2]Evolutionary Mechanics, Institute of Biology, Leiden University, Post Office Box 9516, 2300 RA Leiden, Netherlands.

*To whom correspondence should be addressed. E-mail: j.j.videler@biol.rug.nl

Avian wings, unlike insect and aircraft wings, consist of two distinct parts: an arm-wing and a hand-wing. Cross sections through arm-wings show conventional aerodynamic profiles with a rounded leading edge. In contrast, the leading edge of hand-wings is sharp, because it is the edge of the narrow vane of the outermost primary feather. Birds often use the hand-wings in a swept-back position forming a V-shaped wing configuration. Here, we apply digital particle image velocimetry (DPIV) (*4*, *5*) using models of the wing of the common swift (*Apus apus*), tested in a water tunnel, to investigate the lift generated by swept-back hand-wings of gliding birds (Fig. 1).

The common swift is an extremely aerial bird species (*6*) with short arm-wings and very long hand-wings. An adult swift has a streamlined body: a short, forked tail and long, curved scythe-like wings (Fig. 1). The average wing chord (the length of the cross section in the flight direction) along the hand-wing is approximately 5 cm.

Quantitative measurements of the flow patterns near a wing in flight are required to discover the lift-generating mechanisms. Such measurements on a real wing of a bird in flight are difficult and have not yet been done. Experiments quantifying the flow at some distance behind a flying bird have been carried out in a wind tunnel (*7*), but the resulting pictures of the disturbances in the air do not indicate exactly what happens at the wings.

Flow patterns in air and in water are the same as long as the flow is studied at the same Reynolds number (*Re*). *Re* expresses the relative importance of inertial over viscous forces in a dimensionless way: $Re = vl\,\nu^{-1}$, where v is the velocity in m s^{-1}, l is a relevant measure of length in m, and ν is the kinematic viscosity (the ratio of viscosity over density) in m^2 s^{-1}.

The *Re* number of a swift wing with an average chord length of 5 cm, gliding at an average speed of 11 m s^{-1} [the mean measured value for free-gliding swifts under conditions without wind (*8*)] in air of 20°C, at sea level, is 37,500.

We used a 1.5-times-enlarged and a real-size physical model of a swift wing in fast gliding posture (60° sweep of the hand-wing leading edge, based on direct observations and series of pictures of gliding swifts) to study the interactions with water in our recirculating water tunnel using DPIV (*4–6*).

Runs with the large model revealed the presence of a prominent LEV on top of the hand-wing. An angle of attack relative to the arm-wing chord as small as 5° with respect to the oncoming flow readily provided a stable LEV on top of the hand-wing. The wing was illuminated with a 3-cm-thick laser sheet perpendicular to the flow, in four planes successively. The results of the DPIV analysis of the pictures taken from behind are shown in Fig. 2. The LEV can be easily recognized in each vector field. The LEV core diameter increases from the wrist (Fig. 2A) toward the wing tip (Fig. 2C), indicating that the LEV has a conical shape. The vortex center is located above the wing and follows the wing inward of the leading edge toward the tip. Two cm behind the wing (Fig. 2D), the center is in a position inward from the wing tip, and the core diameter is still increasing. The maximum downwash flow velocity increases along the wing (with the LEV strength) and is twice as high at the wing tip (Fig. 2, C and D) compared with the position just behind the arm-wing (Fig. 2A), which indicates lift increase along the wing. The maximum downward velocity component at the wing tip is about 10% of the free-flow velocity.

The real-size cast of the swift wing showed the same flow patterns with stable LEVs at three speeds when tested at an angle of attack of about 10° relative to the proximal arm-wing chord. Figure 3A shows the increase of the LEV radius. The rotational velocities increase with the flow speed, but that does not substantially affect the radius of the vortex. Figure 3B shows how the distance between the leading edge of the wing and the vortex center increases to reach values of about 4 cm near the tip. This effect is also virtually independent of the flow velocity. These data are combined in the artist's impression of the total flow on the wings of a gliding swift in Fig. 4.

LEVs are robust, lift-producing aerodynamic flow systems allowing high angles of attack (*9*). At high angles of attack, the drag component of the aerodynamic force is large. We assume that swifts take advantage of the high lift as well as the high drag component of the LEVs to increase their agility in flight. They can, for example, use the high angle-of-attack LEVs to brake in midair without losing height immediately, as they do while catching insects in flight.

Conventional aerodynamic profiles provide high lift and low drag at high velocities under small angles of attack. The attached flow pattern is vulnerable because high angles of attack easily cause separation and uncontrolled stall.

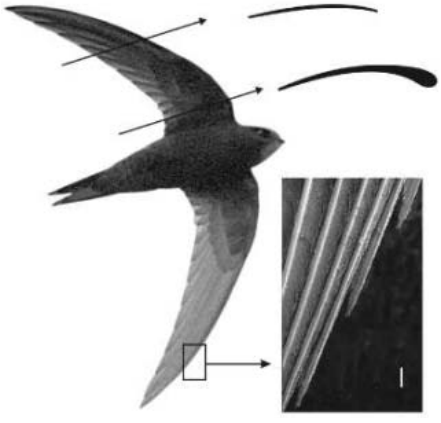

Fig. 1. Adult common swift (*Apus apus*) in gliding flight showing the torpedo-shaped body and the scythe-shaped wings with relatively short arm-wings and long slender hand-wings [picture: J. F. Cornuet]. Cross-sectional profiles through the arm-wing and the hand-wing taken from the indicated positions are shown. The inset is a scanning electron microscope picture of the sharp leading edge of the hand-wing (the white scale bar is 100 μm). The pointed barbs of the narrow anterior vane of the outermost primary feather form a serrated sharp cutting edge.

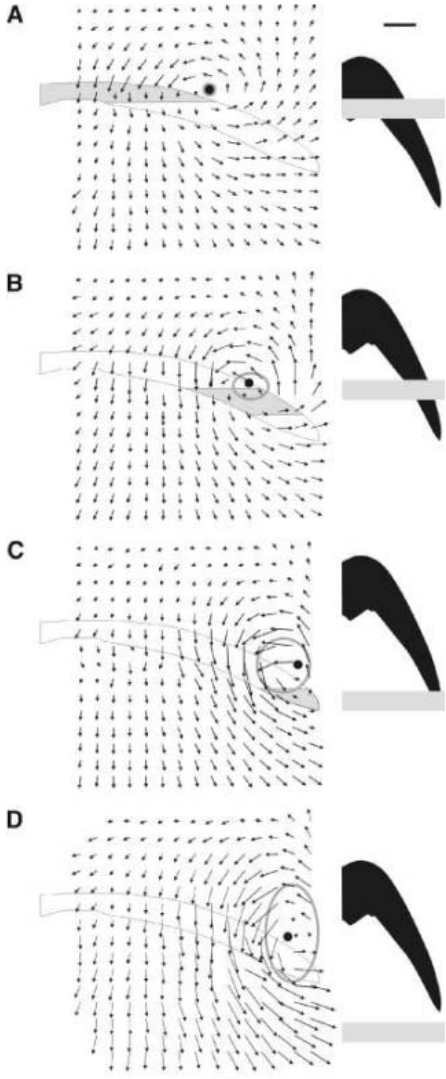

Fig. 2. Results of flow visualization from DPIV near a 1.5-times-enlarged model of a swift wing in a water tunnel. The *Re* number based on an average chord length of 7.5 cm is 37,500. Equally distributed flow vector maps are calculated from vertical particle displacements in four planes perpendicular to the flow, filmed from the rear at three positions on the hand-wing (**A**, **B**, and **C**) and at one position just behind the wing (**D**). The outline of the wing model is indicated in each case. A 3-cm-thick laser sheet was used for illumination of the particles. A gray area on the wing outlines in (A), (B), and (C) indicates the position of the laser sheet. The gray bar in each of the small pictures of the wing model in top view on the right gives an indication of the position and width of the laser sheet in top view. The scale bar (top right in A) is 5 cm and relates to all wing model drawings in top view. The flow in (D) shows the resulting rotation and the position of the vortex behind the wing (Movie S1); the position of the core is above the wing and slightly inward from the wing tip. The vectors are drawn at the same scale in all four panels. The LEV center is indicated with a black dot; the gray loops represent the core diameter at the level of maximum vorticity in each velocity diagram. Each loop approximates the solid-body rotation core radius.

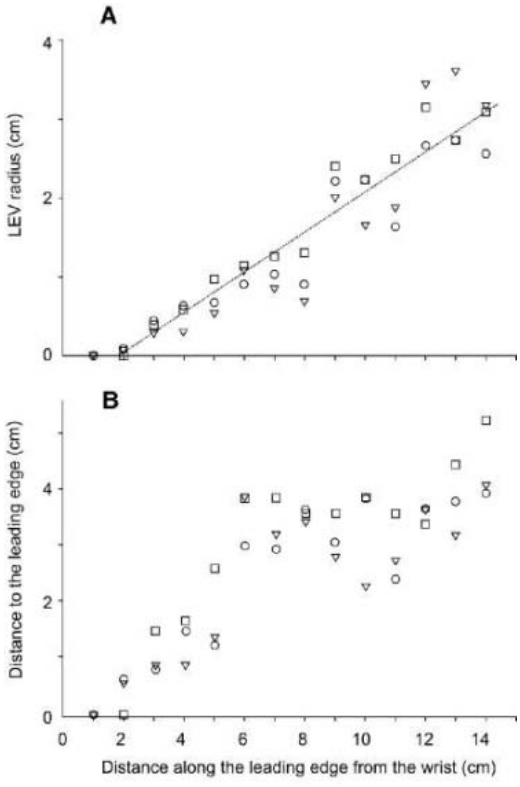

Fig. 3. Results of measurements in a water tunnel of LEV characteristics on a real-sized swift wing model at three speeds (*Re* numbers 3750, 7500, and 22,500) indicated by symbols: square, 0.05 m s^{-1}; circle, 0.1 m s^{-1}; triangle, 0.3 m s^{-1}. (**A**) The LEV radius from the wrist to the tip of the wing with the linear regression line through all data points (r^2 = 0.89). (**B**) The increase of the distance between the leading edge and the center of the vortex, measured perpendicular to the leading edge.

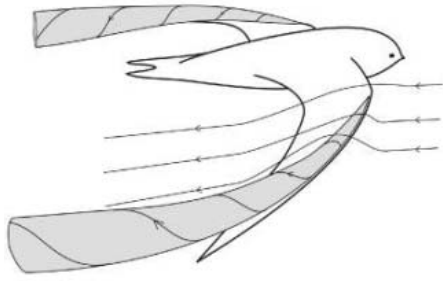

Fig. 4. Artist's impression of the conical LEVs on the wings of a swift in gliding flight. The oncoming flow is deflected downward by the attached LEV system, showing the lift-generating downwash. LEV separation starts at the wrists. From there the LEVs are attached over most of the wing length but start to go upward and inward approaching the wing tip and behind it.

Many birds use swept-back hand-wings during gliding. The sweep-back angle of pigeons, for example, varies in relation to gliding speed (*10*). Landing in most birds requires high lift and high drag at low speeds; LEVs on swept-back hand-wings kept at high angles of attack provide these forces and make landing on a branch possible. Birds use the high lift to keep the right altitude and use the high drag to brake during the approach glide.

Here, we have shown that LEVs do not require large angles of attack and can be generated at *Re* numbers as low as 3750. We speculate that LEVs are also present during flapping flight in the swift and in other birds. We propose, furthermore, that the arm-wing and hand-wing in birds play different roles. The arm-wing is typically built to use the conventional aerodynamic principle with attached flow, whereas the hand-wing can induce airflow separation, resulting in a LEV to generate lift. This changes the general view of how birds fly, and we think that the consistent difference in the anatomy between arm-wing and hand-wing in birds can now be better understood.

References and Notes

1. C. P. Ellington, C. van den Berg, A. P. Willmott, A. L. R. Thomas, *Nature* **384**, 626 (1996).
2. M. H. Dickinson, F. O. Lehmann, S. P. Sane, *Science* **284**, 1954 (1999).
3. R. B. Srygley, A. L. R. Thomas, *Nature* **420**, 660 (2002).
4. E. J. Stamhuis, J. J. Videler, *J. Exp. Biol.* **198**, 283 (1995).
5. E. J. Stamhuis, J. J. Videler, L. A. van Duren, U. K. Müller, *Exp. Fluids* **33**, 801 (2002).
6. Materials and methods are available as supporting material on *Science* Online.
7. G. R. Spedding, M. Rosén, A. Hedenström, *J. Exp. Biol.* **206**, 2313 (2003).
8. B. Bruderer, A. Boldt, *Ibis* **143**, 178 (2001).
9. M. V. Lowson, A. J. Riley, *J. Aircraft* **32**, 832 (1995).
10. C. J. Pennycuick, *J. Exp. Biol.* **49**, 509 (1968).
11. We thank J. F. Cornuet for permission to use the photograph of the gliding swift, J. Batsleer for collecting the data in Fig. 3, and N. Verloop (Dental Laboratory Vanderburg) for making the accurate cast of the swift wing. J. H. H. Videler, H. Videler, R. Gesser, and W. Wolff are acknowledged for critically reading the manuscript.

Supporting Online Material
www.sciencemag.org/cgi/content/full/306/5703/1960/DC1
Materials and Methods
References
Movie S1

31 August 2004; accepted 25 October 2004
10.1126/science.1104682

Phosphopeptide Enrichment Spin Columns

BD Phosphopeptide Enrichment Spin Columns allow the user to enhance detection of phosphorylated peptides that might otherwise be undetectable. The kits provide optimized buffers and a simple purification protocol for peptide phosphorylation studies. The disposable spin columns have the capacity to bind up to 250 μg of phosphopeptide and a range of sample concentration and volumes (up to 850 μl) can be loaded. The disposable spin columns are convenient and fit into most microcentrifuges. The enriched peptide fractions are ready for analysis by mass spectroscopy or high performance liquid chromatography.

BD Biosciences For more information 877-232-8995 www.bdbiosciences.com/clontech

Increased Recombinants from any Vector

Incorporating a unique transformation-boosting technology, the UltraClone DNA Ligation and Transformation Kit increases plasmid, cosmid, and bacterial artificial chromosome recombinant yields up to tenfold using any *E. coli*-type cloning vector. Simply use the kit reagents to ligate your insert into your vector and transform. The kit's includes CloneSmart engineered DNA ligase, buffers, and a choice of E. cloni high-efficiency chemically competent or electrocompetent cells.

Lucigen For information 608-831-9011 www.lucigen.com

Genomic DNA Preparation in Minutes

GenScript Tissue Direct and BloodReady PCR (polymerase chain reaction) Systems enable scientists to prepare genomic DNA in less than 12 minutes from any tissue, including blood, animal tails, paraffin tissue, fresh or frozen tissue microdissection, hair shaft, buccal cells, saliva, sperm, and cells. The genomic DNA can then be used to amplify a single or multiple sequences. Highly specific amplification of genomic DNA is achieved by using HotStart Script DNA polymerase. The system is highly automation-compatible.

GenScript For information 732-885-9188 www.genscript.com

Anti-PolyHistidine Antibody

A Biotinylated Anti-PolyHistidine antibody is available for use in protein immunoblot detection of fusion proteins tagged with 6xHistidine. The antibody is raised in goat against a synthetic 6xHis peptide, affinity-purified, and optimally labeled with biotin. Binding of this antibody is equivalent whether the polyhistidine tag is on the N- or C-terminus of the recombinant protein.

Vector Laboratories For information 650-697-3600 www.vectorlabs.com

Gentle Protein Purification

The novel Softag purification system is an epitope tag immunoaffinity product that allows for single-step, high-purity, gentle isolation of recombinant proteins. Resins are available that are suitable for purification of recombinant proteins in eukaryotic or prokaryotic expression hosts. The elution method does not denature the target protein or disrupt the associated protein complex. Researchers will find uses in the isolation of multi-subunit enzymes, difficult-to-purify proteins, protein–protein interaction studies, immunoprecipitation, and isolation of labile, enzymatically active proteins. It requires no expensive protein purification equipment nor expensive reagents for elution. The gentle nature of the isolation method also means the resin can be re-used multiple times.

NeoCline Biotechnology For information 608-260-8190 www.neoclone.com

Compound Stability Measurements

A new method is available for using the CoulArray electrochemical (EC) system as a tool to perform compound oxidative stability measurements in the drug discovery process. The EC system, used as an oxidative method, closely mimics the oxidative degradation of compounds. The CoulArray performs a wide variety of single electron oxidation reactions for predicting the oxidative stability of a compound under one or more conditions. These assays can be conducted very rapidly, in a few seconds per sample, allowing for the quick testing of large numbers of samples. The CoulArray allows researchers to gather important information about a compound's inherent stability and make earlier and better decisions about a compound's suitability for development, which can have a major impact on both synthetic and medicinal chemistry efforts.

ESA For information 978-250-7000 www.esainc.com

Filtered Balance Systems

XPert Filtered Balance Systems provide user protection during weighing procedures by keeping powders and particulates frequently found in pharmaceutical, dry chemical, mold, and asbestos weighing operations contained and away from the operator. The interior depth of 23 inches accommodates large micro and analytical balances. Containment-enhancing features include the patented Clean-Sweep air foil that allows air to sweep the work surface, the upper containment sash foil to bleed air into the enclosure to direct concentrations of contaminants away from the users' breathing zone, and a zone-perforated rear baffle that creates horizontal laminar airflow. A true bag-in/bag-out filter disposal system allows the high efficiency particulate air filter to be safely removed and replaced by a certified technician.

Labconco For information 800-821-5525 www.labconco.com

Newly offered instrumentation, apparatus, and laboratory materials of interest to researchers in all disciplines in academic, industrial, and government organizations are featured in this space. Emphasis is given to purpose, chief characteristics, and availability of products and materials. Endorsement by *Science* or AAAS of any products or materials mentioned is not implied. Additional information may be obtained from the manufacturer or supplier by visiting www.science.labvelocity.com on the Web, where you can request that the information be sent to you by e-mail, fax, mail, or telephone.

ScienceCareers.org

Classified Advertising

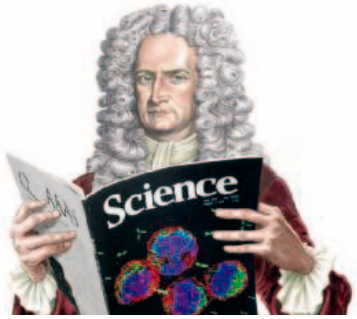

For full details on advertising rates, deadlines, mechanical requirements, and editorial calendar go to **www.sciencecareers.org** and click on **How to Advertise** or call one of our representatives.

United States & Canada

E-mail: advertise@sciencecareers.org
Fax: 202-289-6742

JILL DOWNING
(CT, DE, DC, FL, GA, MD, ME, MA, NH, NJ, NY, NC, PA, RI, SC, VT, VA)
Phone: 631-580-2445

KRISTINE VON ZEDLITZ
(AK, AR, CA, CO, HI, ID, IL, IA, KS, LA, MN, MO, MT, NE, NV, NM, ND, OK, OR, SD, TX, UT, WA, WI, WY)
Phone: 415-956-2531

BETH DWYER
(AL, IN, KY, MI, MS, OH, TN, WV and Internet Sales)
Phone: 202-326-6534

EMNET TESFAYE
(Line Advertising)
Phone: 202-326-6740

DARYL ANDERSON
(Canada and Meetings and Announcements)
Phone: 202-326-6543

Europe & International

E-mail: ads@science-int.co.uk
Fax: +44 (0) 1223-326-532

TRACY HOLMES
Phone: +44 (0) 1223-326-525

EMILIE STOTT
Phone: +44 (0) 1223-326-527

CLAIRE GRIFFITHS
Phone: +44 (0) 1223-326-528

CHRISTINA HARRISON
Phone: +44 (0) 1223-326-510

JASON HANNAFORD
Phone: +81 (0) 52-777-9777

To subscribe to *Science*:
In U.S./Canada call 202-326-6417 or 1-800-731-4939
In the rest of the world call +44 (0) 1223-326-515

Science makes every effort to screen its ads for offensive and/or discriminatory language in accordance with U.S. and non-U.S. law. Since we are an international journal, you may see ads from non-U.S. countries that request applications from specific demographic groups. Since U.S. law does not apply to other countries we try to accommodate recruiting practices of other countries. However, we encourage our readers to alert us to any ads that they feel are discriminatory or offensive.

POSITIONS OPEN

ASSISTANT PROFESSOR [NO. 212725S] SCIENCE EDUCATION

Applications are invited to fill a tenure-track position in post-secondary science education at the **ASSISTANT PROFESSOR** level. Applicants must have a doctoral degree in a natural science. The successful candidate will be expected to establish and maintain a vigorous, externally funded research program in post-secondary science education, teach effectively at the graduate and undergraduate levels, supervise graduate students, and perform appropriate Departmental and University service. Tenure for this position will reside in a traditional science department in the College of Arts and Sciences. Candidates from traditional research degree programs should provide evidence of expanded professional development specifically designed to integrate disciplinary and pedagogical knowledge. Preferred scholarly interests are in the development and application of new approaches to post-secondary science education supporting multidisciplinary teaching efforts in the life sciences. The successful candidate would have a primary appointment in one of the natural science departments. The application should include: (i) a cover letter; (ii) curriculum vitae; (iii) a summary of research experience and plans for future research; and (iv) a statement of teaching experience, philosophy, and interests. Applicants should arrange for at least three letters of recommendation to be sent. Names and addresses of references should be included in the cover letter. Applicants may send application materials and arrange for letters of recommendation to be sent electronically, preferably in PDF or Word format, to **e-mail: asdeans@kent.edu,** or by mail to: **Office of the Dean, College of Arts and Sciences, Kent State University, P.O. Box 5190, Kent, OH 44242-0001.** Review of applications will begin on November 29, 2004, and will continue until position is filled. For a complete description of this position, visit our job site at **website: http://jobs.kent.edu.** All documents submitted to Kent State University for employment opportunities are public records and subject to disclosure under the Ohio Public Records Law. *Equal Opportunity/Affirmative Action Employer.*

ANIMAL PHYSIOLOGIST

Towson University invites applications for a tenure-track, **ASSISTANT PROFESSOR** beginning August 2005. Teaching responsibilities include undergraduate and graduate courses in anatomy and physiology. Candidate is expected to establish an extramurally funded research program involving undergraduates and M.S. candidates. Ph.D. in relevant field and commitment to excellence in both teaching and research required. Send letter of interest, one page descriptions of teaching philosophy and research plans, curriculum vitae, photocopies of all transcripts, and direct three confidential reference letters to be sent to: **Jay A. Nelson, Department of Biological Sciences, Towson University, Towson, MD 21252-0001.** Application review begins January 17, 2005. Additional information available at **website: http://www.towson.edu/biology.** *Towson University is an Equal Opportunity/Affirmative Action Employer and has a strong institutional commitment to diversity. Women, minorities, persons with disabilities, and veterans are encouraged to apply.*

The Plant and Soil Science Department at Texas Tech University is seeking applicants for a tenure-track position at the **ASSOCIATE PROFESSOR/PROFESSOR** level in plant genomics of abiotic stress. Please send a letter of intent, curriculum vitae, statement of research and teaching goals, and three letters of reference to: **Dr. Dick Auld, Chair, Department of Plant and Soil Science, Texas Tech University, Lubbock, TX 79409-2122 (e-mail: dick.auld@ttu.edu).** Consideration of applications will begin on January 1, 2005, and continue until a suitable candidate is identified. Position # 2006TLF043. *Women and members of other underrepresented groups are encouraged to apply.*

POSITIONS OPEN

ASSISTANT/ASSOCIATE PROFESSOR Medicinal Chemistry University of Washington

The Department of Medicinal Chemistry at the University of Washington invites applications for a vacant tenure-track position from individuals with major interests in areas that complement current research efforts of the Department. Major areas of interest include chemical genomics, metabolomics, proteomics, drug metabolism and toxicity, pharmacogenetics, and protein misfolding diseases. The Department has excellent core resources including a large mass spectrometry facility, nuclear magnetic resonance, and facilities for protein expression. In addition, ample opportunities for collaborative research exist in the Department, School, and University. (See **website: http://depts.washington.edu/medchem/** for further details.) Responsibilities of the position include graduate and undergraduate teaching, mentoring of graduate students, and the development of an independent extramurally funded research program.

Applicants should forward a cover letter, curriculum vitae, a statement that describes current and future research interests, and arrange for three letters of reference to be forwarded to: **Dr. Kent L. Kunze, Search Committee Chair, Medicinal Chemistry Box 357610, University of Washington, Seattle, WA 98195-7610. E-mail: medchem@u.washington.edu.** Applications must be submitted prior to March 31, 2005.

The University of Washington is building a culturally diverse faculty and strongly encourages applications from female and minority candidates. The University of Washington is an Affirmative Action/Equal Opportunity Employer.

AKITA UNIVERSITY

We invite applications for a **PROFESSOR** of Venture Business Laboratory (VBL). The successful candidate will be expected to develop either (1) a research on advanced technology for resource recycling and environment, or (2) a study on international and domestic policy for natural resource, and a coordination of industry-university cooperation and technology transfer. Visit our **website: http://www.akita-u.ac.jp/vbl/** for additional information about VBL of Akita University.

Candidates must have a Ph.D. and are expected to be aged 55 or above. The Professor position is available in the next five years from April of 2005. Please send curriculum vitae, summary of research experience, list of achievements including papers and/or patents, copy of less than five publications, plan of research in VBL, other necessary documents indicative of research activity, and contact information for two references, to: **Academic Cooperation Division, Akita University, 010-8502 Japan.** Deadline of application is December 20, 2004. For further information please contact: **Professor S. Ishio, the director of VBL,** at **e-mail: ishio@ipc.akita-u.ac.jp.**

ASSISTANT PROFESSOR, Biology. Montana State University-Billings is seeking to fill a full-time, tenure-track faculty position in biology starting August 2005. Ph.D. in an area of biomedical science and postdoctoral research experience required. Evidence of college teaching experience and potential for productive research in an undergraduate, liberal arts setting desired. A commitment to undergraduate science education is essential. Teaching duties may include biology, genetics, molecular biology, and courses in area of expertise. Position is 50 percent teaching, 50 percent research. Establishment of a research program involving undergraduates is required. Startup package is available. Review of applications will begin December 31, 2004, and continue until position is filled. For a complete description, qualifications, and application process, please visit our **website: http://www.msubillings.edu** or contact the Human Resources Office at **telephone: 406-657-2278.** *Equal Employment Opportunity/Affirmative Action/ADA.*

UNIVERSITY OF COLORADO HEALTH SCIENCES CENTER AT FITZSIMONS

ASSOCIATE PROFESSOR
Cancer Biology
Department of Craniofacial Biology
University of Colorado Comprehensive Cancer Center

The University of Colorado Comprehensive Cancer Center and the Department of Craniofacial Biology at the University of Colorado School of Dentistry invite applications for a full-time tenure-eligible position in Cancer Biology at the Associate Professor level. Applicants should have a Ph.D., M.D. or equivalent degree with postdoctoral research experience in Cancer Biology or a related field, and an exceptional record of research accomplishments and extramural funding. Individuals with experience in the area of cancer biology including malignant transformation, cell proliferation, signal transduction, cell motility and migration, metastasis, and apoptosis are especially encouraged to apply. The successful applicant will have a joint appointment within a suitable Department within the School of Medicine or the School of Pharmacy, and will be expected to take a leadership role within the Cancer Center. He or she will also be expected to develop a vigorous externally funded research program and contribute to the teaching mission at the School of Dentistry and the Graduate School. Applicants should submit a curriculum vitae, brief description of research interests, and arrange to have three letters of reference forwarded by mail or email to the address listed below, **ATTENTION: CBR Project Coordinator**. For full consideration, completed applications should be received by **February 15, 2005**.

ASSISTANT PROFESSOR
Biomaterials/Bioengineering
Department of Craniofacial Biology

The Department of Craniofacial Biology at the University of Colorado School of Dentistry invites applications for a full-time tenure-track position in Biomaterials/Bioengineering at the Assistant Professor level. In addition to a Ph.D. related to the fields of biomedical engineering, chemical and biological engineering, or materials science with postgraduate experience, an exceptional record of research accomplishments are required. Individuals with research interests that encompass all aspects of tissue engineering, biomaterials, cellular biology and controlled release are especially encouraged to apply. The successful applicant will stimulate collaborations within the School of Medicine and/or the School of Engineering at the University of Colorado-Boulder with the possibility for a joint appointment. The successful candidate will be expected to develop and maintain a vigorous, innovative externally funded research program, and to contribute to the teaching mission at the School of Dentistry and the Graduate School (The assistant professor will have his/her first year free of any teaching or service obligations). Applicants should submit a curriculum vitae, brief description of research interests, and arrange to have three letters of reference forwarded to the address listed below, **ATTENTION: BMR Project Coordinator**. For full consideration, completed applications should be received by **February 1, 2005**.

ASSISTANT PROFESSOR
Craniofacial Molecular Genetics/Developmental Biology
Department of Craniofacial Biology

The Department of Craniofacial Biology at the University of Colorado School of Dentistry invites applications for a tenure-track position at the Assistant Professor level. Applicants should have a Ph.D. or equivalent degree with post-doctoral research experience in the fields of molecular genetics and/or developmental biology, and an excellent record of research accomplishments. Individuals with research interests that encompass any aspect of craniofacial research in vertebrate model systems, including neurulation, neural crest development, as well as formation and patterning of the head skeleton and dentition, are especially encouraged to apply. The School of Dentistry is an integral component of the Health Sciences Center and the successful applicant will obtain a joint appointment with a suitable Department within the School of Medicine. He or she will also be expected to develop an externally funded research program and contribute to teaching at the graduate and undergraduate levels. Applicants should submit a curriculum vitae, brief description of research interests, and arrange to have three letters of reference forwarded to the address listed below, **ATTENTION: CDBR Project Coordinator**. For full consideration, completed applications should be received by **February 1, 2005**.

Completed materials for all positions should be sent to: **Dr. Barbara Zimmerman, Department of Craniofacial Biology, University of Colorado Denver Health Sciences Center, Mailstop 8120, P.O. Box 6511, Aurora, CO 80045. (FEDEX address: 12801 E.17th Ave, Rm. L18-11109, Aurora, CO 80010). barbara.zimmerman@uchsc.edu**. For more information see: **http://www.uchsc.edu/sod/units/research/researchHome.html** and **http://www.uccc.info**.

The University of Colorado is committed to diversity and equality in education and employment.

University at Buffalo
The State University of New York

Faculty Positions in Exercise and Nutrition Sciences

The University at Buffalo, State University of New York, invites applications for three faculty positions in the Department of Exercise and Nutrition Sciences, School of Public Health and Health Professions. One position is for a tenure-track Associate Professor; the second is for a tenure-track Assistant Professor; and the third is for a Research Assistant Professor. The preferred start date is August 1, 2005. Screening of applicants will begin February 7, 2005 and continue until the positions are filled. Candidates should have an earned doctorate in a discipline relevant to exercise and/or nutrition, which should complement the Department's current research strengths in applied physiology, biomechanics, and basic and clinical nutrition. Postdoctoral experience for the Assistant Professor positions is preferred. A record of outstanding achievement in research with publications in high quality journals is desired, commensurate with the rank.

Successful candidates will be expected to develop an independent research program, seek external funding, and contribute to teaching and service. Candidates should submit 1) a letter of application, 2) a curriculum vitae, 3) a brief statement of future research plans, and 4) the names and contact information for three references to: **Ms. M. Lannen, Assistant to the Chair, Department of Exercise and Nutrition Sciences, Kimball Tower, Room 405, University at Buffalo, Buffalo, NY 14214-3079** ***OR*** **E-mail: lannen@buffalo.edu**

The University at Buffalo is an Equal Opportunity/Affirmative Action Employer. The Department of Exercise and Nutrition Sciences is interested in identifying prospective minority and women candidates and professionals with disabilities. Qualified individuals with a disability may request needed reasonable accommodation to participate in the application process. No person in whatever relationship with The State University of New York shall be subject to discrimination on the basis of age, creed, color, disability, national origin, race, religion, ethnicity, sex, sexual orientation, marital or veteran status.

The Department of Exercise and Nutrition Sciences is one of the academic units in the School of Public Health and Health Professions. There are well-established research programs and excellent facilities available within the School and Department. The Department employs 18 full-time faculty and offers a BS in Exercise Science, a BS/MS in Exercise Nutrition, a BS/MS in Athletic Training, a Dietetic Internship with Advanced (Graduate) certificate program, MS degrees in Exercise Science and Nutrition and a Ph.D. degree in Exercise Science. Approximately 12 graduate students on a thesis/dissertation track, and 120 undergraduate juniors, are accepted annually. The University at Buffalo is a Research I institution. With 24,000 students, it is New York's largest and most comprehensive university. The Western New York area provides a highly livable environment rich in music, theater, and professional sports in addition to the advantages of its location on the international border with Canada.

POSTDOCTORAL RESEARCH IN MARINE MOLECULAR MICROBIAL ECOLOGY

Stony Brook University's Marine Sciences Research Center invites applications to join lab investigating environmental factors controlling decay of viruses in coastal environments. Researcher is also expected to apply modern techniques to investigate anaerobic prokaryotic communities. Includes laboratory and ocean-going field components.

Required: Candidates must possess Ph.D. (or equivalent) in Microbiological Oceanography, Microbiology, or related field. Must be proficient at Quantitative Real-Time PCR, cultivation of viruses, bacteria, and mammalian cell lines, and mammalian viral and bacteriophage plaque assays. Outstanding analytical, quantitative, and scientific writing skills are essential. Experience with T-RFLP, gel electrophoresis, genotyping preparation, radioassays, FISH, CARD-FISH, and anaerobic cell culture are highly desirable.

Position starts February 1, 2005, or when filled and lasts 2-3 years. Salary range: $36,000-$43,000.

To apply send application letter, CV, publications, brief description of research experience, and name and contact information of three references to: Professor Gordon Taylor, MSRC, Stony Brook University, Stony Brook, NY 11794-5000

E-mail: *Gordon.Taylor@stonybrook.edu*

AA/EOE. Visit *www.stonybrook.edu/cjo* for further job information or *www.msrc.sunysb.edu/people/taylor.htm*

STONY BROOK

Assistant Professor Developmental Genetics

NYU School of Medicine Skirball Institute of Biomolecular Medicine

The Developmental Genetics Program at the Skirball Institute and NYU School of Medicine invites applications for a tenure track position at the Assistant Professor level. We are searching for a candidate who will carry out strong independent research in the field of developmental genetics. We are particularly interested in research that uses model organisms to study the developmental and molecular basis of disease.

Our program covers faculty studying a wide range of topics in Developmental Genetics using a variety of model organisms. Details about individual research programs can be found at: http://saturn.med.nyu.edu/programs/dg/. NYU School of Medicine offers excellent resources to support new faculty, including generous start-up packages and core facilities for cell sorting, imaging, proteomics, mouse transgenics and genomics. The new faculty member will also be part of our Developmental Genetics Graduate Training Program.

Applicants should submit a C.V., a statement of research interests and three letters of reference by January 15th, 2005 to: **mckeown@saturn.med.nyu.edu. Or mail to: Nan McKeown, HR Coordinator, Skirball Institute, 3rd floor, NYU School of Medicine, 540 First Avenue, New York, NY 10016.** We are an equal opportunity employer and provide a drug-free workplace.

SCHOOL OF MEDICINE

NEW YORK UNIVERSITY

Vascular Biology Center

The Vascular Biology Center at the Medical College of Georgia is accepting applications from outstanding candidates to fill a tenure-track, faculty position at the **Associate** or **Full Professor** level. The successful candidate will have earned PhD or MD/PhD degrees in a biomedical science and a nationally recognized extramurally funded program in vascular biology. Preference will be given to applicants with expertise in pulmonary vascular biology. He/she will be expected to interact closely with other members of the Center and the MCG scientific community and devote approximately 15% effort to the teaching and service missions of the institution. The Vascular Biology Center employs 12 highly successful, tenured or tenure-track faculty and a total of 85 scientists (fellows, students, research assistants) with expertise in the biology of nitric oxide, endothelin, eicosanoid and the rennin-angiotensin system, who raise in excess of $6.5 million extramural research funds per year. The Center directs the PhD program in Vascular Biology, as well as pre-doctoral and post-doctoral T32 training programs in Integrative Cardiovascular Biology. Competitive salary, newly renovated laboratory space and generous start-up funds are available. Interested individuals should forward a letter of intent, detailed CV and three reference letters to: **Dr. John D. Catravas, Director, Vascular Biology Center, Medical College of Georgia, Augusta, Georgia 30912-2500 (tel: 706 721-6338; jcatrava@mcg.edu)** by **February 1, 2005**.

The Medical College of Georgia is an EO/AA Employer and applications from women and under-represented minorities are particularly encouraged.

Michael G. DeGroote
SCHOOL OF MEDICINE
McMaster University

Endowed Chair in Cancer Research, Michael G. DeGroote School of Medicine, McMaster University

The Michael G. DeGroote School of Medicine, Faculty of Health Sciences, McMaster University invites applications for the position of Scientific Director, Basic Cancer Research, for the new Michael G. DeGroote Institute for Cancer Research. The Scientific Director will help lead an ambitious renewal and expansion of basic and translational cancer research made possible through a landmark gift from Mr. DeGroote. This undertaking will be done in conjunction with our affiliated partner, the Juravinski Cancer Center at Hamilton Health Sciences.

We seek an internationally recognized leader in cancer biology to champion and develop basic cancer research in the Faculty. This individual will assist in the recruitment of faculty members in basic cancer research, building on a $10 million endowment provided by Mr. DeGroote. In addition, the Faculty has committed additional resources in this area, including Canada Research Chairs for exceptional candidates.

The candidate must hold a PhD and /or MD degree and have an outstanding record of research accomplishments and demonstrated leadership in cancer research. His/her interests should complement and extend existing and/or emergent priority areas in the Faculty. These research areas include but are not limited to molecular profiling, model organisms, cancer stem cell biology, drug discovery and therapeutics, molecular imaging, cancer immunology, functional oncogenomics/proteomics, and related fields. The candidate must have superb leadership skills and will be expected to maintain a vigorous, externally funded research program, and participate in teaching and other academic activities.

The successful candidate will have qualifications commensurate with appointment to the academic rank of Professor in an appropriate basic science and/or clinical Department and will hold the Michael G. DeGroote Chair in Cancer Research. Reporting to the Dean and Vice-President (or delegate), the Scientific Director will be responsible for strategic planning around cancer research with a vision for advancing translational programs that complement our strengths in basic, clinical and population health research within the broader McMaster academic health sciences network.

McMaster University is one of Canada's premier research intensive universities and, along with our affiliated teaching hospitals and research institutes, we provide an exceptional environment for interdisciplinary research within a fully integrated academic health network. The Scientific Director and new faculty will be provided with modern laboratory space, and will have access to state of the art core facilities for molecular profiling, advanced microscopy, chemical biology, high-throughput small molecule screening and high content analysis, molecular imaging, and structural biology.

Please send curriculum vitae, a short statement of research interests, and names and addresses of 3 referees prior to January 31, 2005 to:

Dr. John P. Capone, Chair, Cancer Research Search Committee
Associate Dean, Research, Faculty of Health Sciences
McMaster University, Room HSC 2E5, 1200 Main St. W. Hamilton, Ontario Canada, L8N 3Z5
email: caponej@mcmaster.ca

McMaster University

For more information about the Faculty, visit our web-site at **www.fhs.mcmaster.ca**

Dr. Peter George
President and Vice-Chancellor
McMaster University

Dr. John Kelton
Dean and Vice-President
Faculty of Health Sciences

An equal opportunity employer
McMaster University is committed to Employment Equity and encourages applications from all qualified candidates, including women, aboriginal people, people with disabilities, sexual minorities, and visible minorities. In accordance with Canadian immigration requirements, Canadian citizens and permanent residents of Canada will be considered first.

TOGETHER, ADVANCING HEALTH THROUGH LEARNING AND DISCOVERY

Faculty Position
Biological Imaging
Center for Brain Science and Division of Engineering and Applied Sciences
Harvard University

Applications and nominations are invited for a tenure-track faculty position in imaging at the assistant, associate, or full professor level. We seek individuals with outstanding records of innovation in the development of new imaging or image processing techniques with potential applications to cell biology or neuroscience. We strongly encourage applications from, or information about, qualified women and minority candidates. All areas of biological imaging research are of interest, particularly: (1) innovative optical imaging techniques at the molecular, cellular, and systems level; (2) medical image processing; (3) MRI physics and novel MRI imaging techniques; and (4) other innovative imaging methods. Responsibilities include participation in Harvard's undergraduate degree programs in engineering and applied sciences, as well as in research and teaching at the graduate level. A Ph.D. is required.

Appointees will hold an academic appointment in the Division of Engineering and Applied Sciences (DEAS), which is home to Harvard's programs in applied physics, engineering, computer science, and applied mathematics. A significant enlargement of DEAS is now underway, including expansion of the faculty, new laboratory buildings, increased graduate admissions, and closer links between DEAS and Harvard's basic science departments and medical school. Further information is available at **http://www.deas.harvard.edu**.

The successful candidate will also hold an appointment in Harvard University's new Center for Brain Science, which will bring together scientists involved in research on neurons, neural networks, and behavior. The aims are to build the tools (mechanical, molecular, computational and theoretical) required to map neural circuits that underlie experimentally accessible behaviors in diverse species. Ten or more new faculty will be appointed over the next few years. The Center will foster interactions across disciplinary boundaries: faculty from several academic departments will be housed in common research space and connections will reach out across the University.

Because of the opportunity for synergistic appointments, we encourage applicants to inform us of other exceptional candidates including present or potential collaborators. For full consideration, applications should be received by **January 15, 2005**.

Please send a cover letter, curriculum vitae, copies of 1-3 publications, and the names and contact information (including email addresses) of at least 3 references to: **Imaging Search Committee , Kate Zirpolo, Division of Engineering and Applied Sciences, Harvard University, Cambridge, MA 02138.** Inquiries and applications (using pdf files please) may be directed to **imaging@deas.harvard.edu**.

Harvard is an Affirmative Action/Equal Opportunity Employer.

Division of Vaccine Research
Institute of Human Virology
University of Maryland
Biotechnology Institute
725 West Lombard Street
Baltimore, Maryland 21201

An opening is available for a full-time, tenured or tenure track Associate Professor in the Division of Vaccine Research at the Institute of Human Virology, University of Maryland Biotechnology Institute, in Baltimore. The candidate should be an established Ph.D. or M.D. investigator with a demonstrated track record establishing an independently funded and highly regarded research program in cell biology or biophysics of viral membrane fusion and the development of methods to study this interaction. The successful candidate will be poised to rapidly reestablish their research program at the Institute as part of an active research group focusing on the development of a vaccine against HIV-1, and to participate in the training of graduate students and postdoctoral trainees. Salary is commensurate with experience.

Interested candidates should send a letter of application that includes their current curriculum vitae and names and contact information for three referees to the following address: **George K. Lewis, Ph.D., Professor and Director, Division of Vaccine Research, Institute of Human Virology, 725 W. Lombard Street, Baltimore, Maryland 21201**. Please refer to **Position #300550** in your letter. Review of applications will continue until a suitable candidate is selected.

The University of Maryland Biotechnology Institute is an Equal Opportunity/Affirmative Action Employer. Women, minorities, veterans, and candidates with disabilities are encouraged to apply.

KU Medical Center

TENURE TRACK FACULTY POSITION
MOLECULAR BIOTECHNOLOGY
UNIVERSITY OF KANSAS MEDICAL CENTER

The Department of Clinical Laboratory Sciences in the School of Allied Health at the University of Kansas Medical Center (KUMC) invites applications for a full-time tenure-track 12 month appointment (rank commensurate with experience). Candidates must have a Ph.D. (or equivalent degree) in a molecular life science and postdoctoral experience. Qualified candidates must have demonstrated excellence in research and be committed to quality undergraduate and graduate education. The successful applicant will have the opportunity to collaborate with faculty in the many interdisciplinary programs at KUMC (**www.kumc.edu**), and will be expected to maintain an externally-funded research program that utilizes molecular biological/biotechnology approaches. The area of research specialty is open, but individuals with interests relevant to human health and/or disease states are encouraged to apply. Teaching responsibilities will include molecular biology/biotechnology, and academic teaching experience is preferred. The position description can be viewed at **http://jobs.kumc.edu**, Position # J0201345.

If interested please submit a letter of application, curriculum vitae, statement of research interests, statement of teaching interests and philosophy, and up to three reprints. Application materials and three letters of reference should be sent to **Dr. Eric Elsinghorst, Univ. of Kansas Medical Center, 3901 Rainbow Blvd., Mail Stop 4049, Kansas City, KS 66160**. Review of applications begins February 1, 2005 and will continue until the position is filled. EO/AA Employer.

KU Medical Center is proud to be an Equal Opportunity Affirmative Action Employer.

Georgia Institute of Technology

Georgia Tech & Emory
Joint Biomedical Engineering Department

The Wallace H. Coulter Department of Biomedical Engineering at Georgia Tech and Emory University, a joint department between Georgia Tech's College of Engineering and Emory University's School of Medicine, invites nominations and applications for tenure track faculty positions at all levels: assistant, associate, and full professor. We seek innovative, collegial individuals to enhance and contribute to ongoing research initiatives in the following research focus areas: cellular/molecular imaging, bio–nanotechnology, cardiovascular mechanics and biology, systems biology and neuroengineering. For information on our research focus areas, please see Research Overviews at our Web site: www.bme.gatech.edu.

Candidate must hold a Doctoral Degree in Biomedical Engineering/ Science or a related discipline. Candidates should also have demonstrated ability to develop a funded research program and to participate in teaching and advising in our undergraduate and graduate programs. Candidates meeting these minimum requirements are encouraged to submit a: 1.) letter of application, 2.) curriculum vitae, 3.) research statement, 4.) teaching statement and 5.) list of three references, complete with name, address (including e-mail), and telephone number to:

Larry V. McIntire, Ph.D.
Wallace H. Coulter Chair and Professor
The Wallace H. Coulter Department of Biomedical Engineering
at Georgia Tech and Emory University
Atlanta, GA 30332-0535
E-mail: bme@bme.gatech.edu

An Equal Education/Employment Opportunity Institution

The Jackson Laboratory

Faculty Recruiting

The Jackson Laboratory, an independent, mammalian genetics research institution, and an NCI-designated Basic Cancer Center has just launched a major research expansion. New faculty will be recruited in the following areas:

- **Neurobiology**
- **Cancer Biology**
- **Reproductive/Developmental Biology**
- **Immunology/Hematology**
- **Metabolic Disease Research**
- **Computational Biology/Bioinformatics**

We are recruiting scientists at all levels who hold a Ph.D., M.D. or D.V.M., completed postdoctoral training, have a record of research excellence and have the ability to develop a competitive, independently funded research program, taking full advantage of the mouse as a research tool.

The Jackson Laboratory offers a unique scientific research opportunity, including excellent collaborative opportunities with our staff of 35 Principal Investigators, unparalleled mouse and genetic resources, outstanding scientific support services, highly successful Postdoctoral and Predoctoral training programs, and a major meeting center, featuring courses and conferences centered around the mouse as a model for human development and disease.

For more information, please visit our web site: www.jax.org.

Applicants for faculty positions should send a curriculum vitae, 2-3 page statement of research interests and plans, and the names of at least three references to: Director's Office, The Jackson Laboratory, 600 Main Street, Bar Harbor, Maine 04609, or email: facultyjobs@jax.org (preferred method of application).

The Jackson Laboratory is an EOE/AA Employer

www.jax.org

Tenure-Track Faculty Position In Immunobiology

The Division of Rheumatology in conjunction with the newly created Center for Immunobiology at the Indiana University School of Medicine, is seeking two outstanding investigators with expertise in the immunopathogenesis of rheumatic diseases. Under the direction of David S. Wilkes, M.D., the 12,000 square foot Center for Immunobiology, represents a new venture within the School of Medicine to bring together basic, clinical and translation research focused on the immunological basis of disease. Areas of research include organ transplantation, autoimmunity, innate immunity, infectious diseases, and cancer. Candidates for the current positions must have a doctoral degree and an outstanding publication record. This is a tenure-track position in the Department of Medicine with appropriate secondary appointments in basic science departments; rank and salary will be commensurate with experience.

Send a curriculum vitae, a 2 – 3 page statement of research interests and future plans, and the names and contact information of three professional references by e-mail to: **Rafael Grau, MD, Director, Division of Rheumatology, Department of Medicine, Indiana University School of Medicine, e-mail: rgrau@iupui.edu**

Indiana University is an Affirmative Action/Equal Opportunity Educator and Contractor. M/F/D are encouraged to apply.

Director of Urban Coast Institute

Monmouth University is establishing a new research and education center in the area of marine and environmental biology and policy focused on urban coastal management. It is intended that the UCI will integrate the efforts of faculty and undergraduate and graduate students in a variety of fields including biology, social work, business and real estate, mathematics and more. The UCI will be a science-based framework for the development of leading edge approaches to the solution of problems facing local communities and decision-makers at all levels of government.

The Director will support the research of principal investigators and their students in the development and operations of the Urban Coast Institute. Coordinates outreach activities and involves external communities in assessment and feedback regarding public policies. Will be responsible for representing the Institute to the public and for the administrative management of the budget, progress reports, staff and other critical functions of the UCI. The Director will be an active research participant, and occasionally may be called on to teach as appropriate. Other duties as assigned.

The successful candidate must have a Ph.D. or other terminal degree in a discipline represented in the UCI with significant active research experience in a related area. The candidate should have a record of successful proposal writing, government relations, project management and budget overview. Experience working in an academic environment is desirable.

The University offers excellent fringe benefits including tuition remission for employee, spouse and IRS dependent children. Applicants should send two current resumes and cover letters indicating Reference #1769 to: Office of Human Resources, Monmouth University, West Long Branch, NJ 07764 or email: mujobs@monmouth.edu. Applications will be accepted until position is filled. Review of applications will begin December 17, 2004. For further information or additional vacancies, visit our website: **www.monmouth.edu** or call our job opportunity hotline at (732)571-3513.

The Intellectual Center of the Jersey Shore

MONMOUTH UNIVERSITY

West Long Branch, New Jersey 07764-1898

Monmouth University is an Affirmative Action/Equal Employment Opportunity Employer.

CHAIR, DEPARTMENT OF LABORATORY MEDICINE UNIVERSITY OF CALIFORNIA, SAN FRANCISCO

The School of Medicine of the University of California at San Francisco is seeking applications for the position of Professor and Chair of the Department of Laboratory Medicine. We seek an individual of vision who is committed to the Department's goal of becoming a leading force in the development and application of new technologies for the diagnosis and management of human disease.

Applicants should have an MD, PhD or MD and PhD degree(s) and have a nationally recognized research program in basic or translational research. The successful applicant will play a leading role in building cross-cutting translational research programs at UCSF; will become a member of the Biomedical Sciences Graduate Program at UCSF; and will participate actively in the mentoring of fellows and residents in Laboratory Medicine, Pathology and other translational research disciplines.

Applicants should submit a CV and brief statement of research interests and plans by **15 January 2005**. Submit a hard copy and an electronic copy to:

Don Ganem, MD
Laboratory Medicine Search Committee Director
c/o Michael Armanini
G.W. Hooper Foundation, Box 0552
University of California
513 Parnassus Ave
San Francisco, CA 94143
e-copies to : Armanin@itsa.ucsf.edu

UCSF is an Affirmative Action/Equal Opportunity Employer. The University undertakes affirmative action to assure equal employment opportunity for underrepresented minorities and women, for persons with disabilities, and for Vietnam-era veterans and special disabled veterans.

Max Planck Institute for Demographic Research

Directors: Prof. James W. Vaupel - Prof. Jan M. Hoem

The Max Planck Institute for Demographic Research

is seeking to recruit a

Post-Doc or Research Scientist

to play a leading role in setting up and overseeing a

Laboratory for *Hydra* and *Pristina*

and running a range of projects aimed at understanding fundamental

life history processes and the evolution of senescence

The successful candidate will complement an existing biodemographic research team of 14 staff, working alongside a total of some 80 employees from diverse backgrounds engaged in a range of issues in demography. The team aims to gain a fundamental understanding of how demographic processes are shaped by evolution. There are ongoing projects on age-specific schedules of mortality, reproduction and growth, on the evolution of senescence, on reproductive effort, parental investment and intergenerational transfers, and on the costs of reproduction and the delayed effects of stress. See www.demogr.mpg.de for information about the Institute.

We are seeking a scientist with a keen interest in **evolutionary biodemography,** and the ability to play a leading role in setting up the laboratory and supervising technical and research staff. The successful candidate will be supported within the team and have the expert guidance of an external collaborator in California. Candidates with experience in postdoctoral research and team leadership (requirements for appointment at the Research Scientist level) are preferred, though promising applications with only postgraduate experience will be considered.

Applications should be addressed to Executive Director, Prof. James W. Vaupel and should include a CV with a statement of academic interests and relevant experience, a list of publications and the contact details of 3 referees. All material should be e-mailed to: Evodemo.positions@demogr.mpg.de

The Max Planck Society wishes to increase the share of women in areas where they are underrepresented and strongly encourages women to apply.

The Max Planck Society is committed to employing more handicapped individuals and especially encourages them to apply.

Evo-Demo Positions, Attn. Prof. James W. Vaupel
Max Planck Institute for Demographic Research
Konrad-Zuse-Strasse 1, D-18057 Rostock, Germany
E-mail: Evodemo.positions@demogr.mpg.de

MAX PLANCK SOCIETY

Postdoctoral Research Positions Microbial Ecology and Community Genomics

Postdoctoral positions are available in the Environmental Sciences Division, Oak Ridge National Laboratory (ORNL) **http://www.ornl.gov**, for individuals with training in molecular biology, genetics, biochemistry, and microbiology. Opportunities exist for successful applicants to participate in a wide range of microbial ecology and genomics projects focusing on (1) developing and using microarray-based genomic technologies for analyzing microbial communities related to bioremediation, global changes, carbon and nitrogen dynamics in both terrestrial and marine environments, and carbon sequestration in terrestrial ecosystems, and (2) sequencing and analyzing the entire microbial community at the NABIR Field Research Center using metagenomics approaches. The candidates will also have opportunities to work on functional analysis *Shewanella oneidensis* MR-1 and *Desulfovibrio vulgaris* using both microarray-based genomic and/or phage display-based proteomic approaches.

Candidates must have a Ph.D with demonstrated experience in molecular techniques such as gene cloning, gene expression, microbial ecology or environmental engineering. Additional experience is desired but not required in bioinformatics, physiology, microarray technology. Individuals will work cooperatively with scientists at ORNL, Michigan State University, Stanford University, Pacific Northwest National Laboratory, and Lawrence Berkeley National Laboratory.

Send a curriculum vitae, a description of research accomplishments and interests, and the names and telephone numbers of three references to: **Dr. Jizhong Zhou, Oak Ridge National Laboratory, P.O. Box 2008, Oak Ridge, TN 37831-6038; Phone 865-576-7544; Fax: 865-576-8646; e-mail: zhouj@ornl.gov; web site http://www.esd.ornl.gov/facilities/genomics/index.html**. Please reference the position title and number (**ORNL05-07-ESD**), when corresponding about this position.

This appointment will be offered through the ORNL Postdoctoral/Postmasters Research Associates Program (**http://www.orau.gov/orise/edu/ornl/ornl-pd/ornlpdoc.htm**). Salaries will be competitive.

The program is open to all qualified U.S. and non-U.S. citizens without regard to race, color, age, religion, sex, national origin, physical or mental disability, or status as a Vietnam-era veteran or disabled veteran.

UNIVERSITÄT KONSTANZ

The TR SFB 11 (Konstanz-Zürich) »Structure and Function of Membrane Proteins« (Code number 2004/155) invites applications for the position of an

Independent Junior Group Leader

at the University of Konstanz. Candidates (no more than 6 years after PhD) should have an excellent research record and interest in topics relevant to the TR SFB 11, with the following subsections

A, Structure and function of transport proteins and ion pumps

B, Structural analysis and protein folding

C, Membrane proteins involved in cellular interaction and transmembrane signalling

The applicant will be expected to have accumulated relevant postdoctoral research experience and be capable of independently leading a research group.

The Independent Junior Research Group will be incorporated in the general research programme of the Collaborative Research Centre »TR SFB 11« (further information at www.uni-konstanz.de/FuF/TR-SFB11/trafo/) and located at the University of Konstanz.

The Independent Junior Research Group will be funded for up to 5 years and will enable independent research to be carried out within a research network.

The grant given by the DFG may include the group leader's position (BAT I a), one postdoc, up to two PhD-positions, and technical assistance as well as consumables and equipment.

The selection process includes an oral presentation by the applicant, which will be evaluated by a review panel.

The University of Konstanz is an equal opportunity employer and tries to increase the number of women in research and teaching.

The University encourages disabled persons, who will be given preference if appropriately qualified, to apply (Contact 0049-7531/88-3725).

For applications – **deadline January 21th, 2005** – (including project outline, CV, a list of publications and copies of the most important publications) and informal inquiries please contact Prof. Dr. Claudia Stürmer, Dept. of Biology, University of Konstanz, Phone: 0049-7531/88-2236, Fax: 0049-7531/88-3894, e-mail: Claudia.Stuermer@uni-konstanz.de

Systems Neuroscientist

The Department of Psychology, University of California, Riverside, invites applications for a tenure-track Assistant Professor position, beginning July 1, 2005. The Ph.D. degree is required. Applicants should have demonstrated compelling promise of research and publication using modern approaches in neuroscience to address fundamental problems in brain mechanisms relevant to mammalian behavior. Those with research interests in mechanisms of plasticity or cortical function are especially encouraged to apply, as are individuals interested in interacting with a broad-based psychology department. Applicants should also be committed to excellence in undergraduate and graduate education. The deadline for review of completed applications begins January 15, 2005 and continues until the position is filled. Interested candidates should send their curriculum vitae, reprints if available, a cover letter describing research and teaching interests, and arrange to have three letters of recommendation sent to:

Dr. Glenn Stanley
Chair, Systems Neuroscience Search Committee
Department of Psychology Box B
University of California – Riverside
Riverside, CA 92521

The Riverside campus of the University of California is growing rapidly and has an excellent psychology department with a strong record of success in research, teaching and extramural funding. For information on the Department of Psychology, see our web site at: **www.psych.ucr.edu**. For the Neuroscience Graduate Program, see our web site at: **http://neurograd.ucr.edu**. The campus is centrally located in Southern California, about 50 miles east of Los Angeles and less than an hour's drive from the area's mountains, deserts and beaches.

The University of California, Riverside is an Equal Opportunity/ Affirmative Action Employer.

Faculty Positions in Marine Science

The University of Southern Mississippi's Department of Marine Science (DMS) is undergoing an expansion of its faculty and anticipates openings for four nine-month, tenure-track faculty positions at the Assistant Professor level. DMS is a vibrant, rapidly developing, multidisciplinary academic unit with research and teaching programs in biological, geological, and physical oceanography, marine chemistry, numerical ocean modeling, and hydrographic science. The department is located at the John C. Stennis Space Center on the Mississippi Gulf Coast near the Louisiana border. The Stennis Space Center is home to more oceanographers and hydrographers than any other location in the world. In addition to NASA research activities, the Stennis Space Center is also the home of the Naval Research Laboratory (NRL-SSC), the U.S. Naval Oceanographic Office, NOAA's National Data Buoy Center, the NOAA Coastal Data Development Center, and the Maury Oceanographic Library, one of the country's premier oceanographic libraries. Detailed information about the department is available on the Internet at **http://www.usm.edu/marine**.

New faculty are sought in the areas listed below. Candidates must hold a Ph.D. and post-doctoral experience is preferred. We are particularly interested in receiving applications from scholars whose research interfaces with multiple disciplines and who have capabilities to augment departmental initiatives in ocean observing, global change, numerical ocean modeling, hydrographic science, and multidisciplinary problems in neritic ocean environments.

Biological Oceanographer: Applications are sought for a faculty position in biological oceanography that will complement current studies in phytoplankton ecology and microbiology. Areas of interest include, but are not restricted to, zooplankton ecology, fisheries oceanography, and benthic ecology. Individuals with expertise in application of molecular methods and biosensor technology to ecological problems are also encouraged to apply.

Coastal Geologist: Applicants are sought with demonstrated expertise in sedimentology, preferably depositional processes and sediment transport in shelf and coastal environments. Applicants must have a strong background in geology. The successful candidate is expected to conduct an active research program and teach graduate courses in sedimentology. Expertise in field observation and modeling is desirable, and collaboration in studies of neritic processes is encouraged with a multidisciplinary group, including hydrographers.

Marine Chemistry: A faculty member is needed to complement current departmental expertise in trace element analysis. Areas of interest include, but are not limited to, organic geochemistry, carbon cycle biogeochemistry, and sedimentary geochemistry. Geochemical facilities currently available include Element 2 sector-field ICP-MS, clean lab, nutrient analyzer, and CHN analyzer.

Remote Sensing/Ecosystem Modeling: The search will target applicants involved in oceanography, marine science, or a closely related field with a strong research interest in using airborne or satellite remote sensing in the characterization and modeling of coastal and oceanic biogeochemical processes. Applicants with interests in ocean color imagery (SeaWiFS, MODIS, airborne hyperspectral sensors, LIDAR) and its application in the study and modeling of coastal and ocean ecosystems are particularly encouraged to apply.

Applicants must submit, preferably by electronic mail, a curriculum vitae with a research plan; a statement of teaching philosophy; and names, mailing addresses, and e-mail addresses of four referees to: **Marine Science Faculty Search, Department of Marine Science, The University of Southern Mississippi, 1020 Balch Boulevard, Stennis Space Center, MS 39529 USA** (FAX: **228-688-1121**; electronic mail: **marine.science@usm.edu**). Please specify the position for which you are applying. Review of applications will begin **January 10, 2005** and will continue until positions are filled.

AA/EOE/ADAI

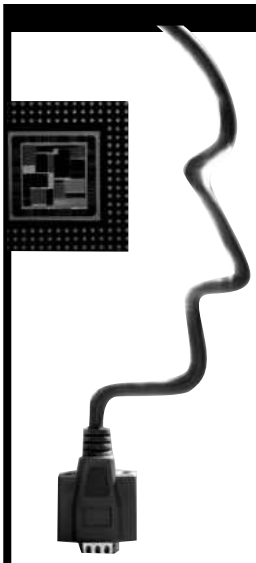

Chemistry Division Leader

Summary: We are seeking a world-class leader for the Chemistry Division at Los Alamos National Laboratory. The Chemistry Division provides scientific and technical leadership to a substantial array of fundamental and applied national security and civilian programs, often in collaboration with industry, universities and other national laboratories. The mission of the division is to serve the nation by providing chemical research for nuclear weapons, non-proliferation, homeland security and energy independence by applying world-class capabilities in synthesis, characterization, diagnostics and predictive modeling. The division maintains state-of-the-art capabilities in actinide and fission product chemistry, inorganic and organometallic chemistry, catalysis, radioisotope production and distribution, chemical and electrical engineering, detection technologies, nanoscience and nanotechnology, analytical chemistry, environmental chemistry, nuclear and radiochemistry, physical chemistry, chemical and nuclear physics, and optical and vibrational spectroscopy. The division leader will provide external visibility for LANL Chemistry, leadership for internal collaborations and promotion of operational and scientific excellence. The successful candidate will provide scientific, technical and operational leadership to a workforce of approximately 450 in eight groups located across nine technical areas with a total budget of approximately $110M. The C Division leader will effectively address recruiting, diversity, affirmative action, Integrated Safety Management (ISM), Integrated Safeguards and Security Management (ISSM) and maintain positive, effective working relationships with other managers, external customers, sponsors, and stakeholders.

Required Skills: Applicants must have a strong record of significant and distinguished leadership, scientific and managerial accomplishments demonstrating the ability to effectively lead change, develop future teams and leaders and build and sustain sponsor relationships; demonstrated drive for excellence, delivery, and results. The candidate must have a well-established track record, deep technical knowledge and experience in one or more of C Division's core competencies, experience in managing high-hazard laboratory operations and a demonstrated commitment to high-quality operations and goals in defense and basic research activities. A record of effective communication skills in briefings, presentations, reports, publications, and meetings is required. Have the ability to obtain a Q Clearance, which normally requires U.S. citizenship.

Desired Skills: Knowledge of DoE, NNSA, DoD, and Department of Homeland Security; significant Washington, D.C. experience in program interactions and development; in-depth background in management of nuclear materials and nuclear/radiological facilities; ability to maintain scientific and intellectual excellence in a culture dedicated to safety, security and environmental responsibility.

Education: A Ph.D. degree in any chemical or physical science or equivalent combination of related education and experience.

For a full job description visit **www.lanl.gov/jobs** and search for Job# 209160. To Apply: Send a comprehensive CV/resume and cover letter addressing all required and desired skills of the position to **jobs@lanl.gov referencing Job# 209160-ACS in the subject line.**

Los Alamos National Laboratory is operated by the University of California for the National Nuclear Security Administration of the Department of Energy. AA/EOE

Put your brain to good use.

Los Alamos
NATIONAL LABORATORY
www.lanl.gov/jobs

POSITIONS OPEN

FACULTY POSITION
BIOCHEMISTRY
University of Central Florida

The Chemistry Department invites applications for a tenure-track faculty to begin in fall 2005 at the **ASSISTANT PROFESSOR** level. Candidates with research interests in all areas of structural biology, biophotonics, or biosensors are especially encouraged to apply. Appointment requires a Ph.D. degree in chemistry or closely related field with postdoctoral research experience preferred. Exceptional candidates at higher ranks with a demonstrated record of accomplishment in extramural funding, publication, and teaching may be considered for Provost's Research Excellence Professorships. In addition to contributing to teaching at both the graduate and undergraduate levels, applicants are expected to develop an externally funded, nationally recognized research program, and participate in the Ph.D. Chemistry and Biomolecular Science programs. Successful candidates are expected to develop interactions with University of Central Florida (UCF)'s world-renown CREOL, Biomolecular Science Center, Nanoscience Center, and other departments within the university. The University of Central Florida is located in Orlando, Florida, and has become one of the nation's largest universities with 43,000 students and is continuing to build nationally recognized research programs. Applicants should submit curriculum vitae, description of their research plans, graduate/undergraduate course teaching interests, and teaching philosophy and should arrange to have three letters of recommendation sent on their behalf to: **Biochemistry Search Committee, Department of Chemistry, University of Central Florida, Orlando, FL 32816-2366** or send via **e-mail: cmorales@mail.ucf.edu.** Indicate at which rank you wish to be considered. The Committee will begin its review on December 15, 2004, but will continue to accept applications until the position is filled. As an agency of the State of Florida, UCF makes all application materials (including transcripts) available for public review upon request. *The University of Central Florida is an Equal Opportunity Employer and welcomes nominations and applications from women and minority group candidates.*

PROFESSOR AND HEAD. Auburn University's (**website: http://www.auburn.edu**) Department of Fisheries and Allied Aquacultures is accepting applications and nominations for the position of Professor and Head. The Department Head serves as senior faculty member and administrator of departmental teaching, research, and extension programs. A position announcement that contains requirements, application instructions, and other information can be found at **website: http://www.ag.auburn.edu/faculty-staff/jobs/** or obtained by contacting: **Don Conner, Chairman, Search Committee, Department of Poultry Science, 236 Funchess Hall, Auburn University, AL 36849. Telephone: 334-844-2639; fax: 334-844-2641; e-mail: connede@auburn.edu.** *Auburn University is an Affirmative Action Employer. Ethnic Minorities and Women are encouraged to apply.*

PROFESSOR AND HEAD. Auburn University's (**website: http://www.auburn.edu**) Department of Horticulture is accepting applications and nominations for the position of Professor and Head. The Department Head serves as senior faculty member and administrator of departmental teaching, research, and extension programs. A position announcement that contains requirements, application instructions, and other information can be found at **website: http://www.ag.auburn.edu/faculty-staff/jobs/** or obtained by contacting: **Dr. Steven Taylor, Chairman, Search Committee, Department of Biosystems Engineering, 209 Tom Corley Building, Auburn University, AL 36849. Telephone: 334-844-4180; fax: 334-844-3530; e-mail: taylost@auburn.edu.** *Auburn University is an Affirmative Action Employer. Ethnic Minorities and Women are encouraged to apply.*

POSITIONS OPEN

MICROBIAL FUEL CELLS

POSTDOCTORAL POSITIONS available for research and development of microbial fuel cells converting waste organic matter to electricity. Studies will include investigations into the mechanisms for microbe-electrode interactions and electron transfer mechanisms as well as evaluation of novel electrode materials and development of improved fuel cell design. These studies will take advantage of a full array of genome-based experimental and in silico metabolic modeling tools. Minimum qualifications are a Ph.D. in microbiology, environmental and civil engineering, or a related field and experience in microbial physiology, genetics, biochemistry, or environmental engineering. Salary is commensurate with experience. Positions are available for three years with the possibility of continuation. Please e-mail curriculum vitae and names of references to: **Dr. Derek Lovley, Department of Microbiology, University of Massachusetts, Amherst, MA; e-mail: dlovley@microbio.umass.edu.** Or send information to: **Search Committee Chair R23294 Microbiology, 203N Morrill IVN, University of Massachusetts, Amherst, MA 01003**. Review of applications will begin December 13, 2004, and continue until the positions are filled. *University of Massachusetts is an Equal Opportunity/Affirmative Action Employer. Women and members of minority groups are encouraged to apply.*

TENURE-TRACK POSITION AND RESEARCH DIRECTOR
School of Podiatric Medicine
Temple University

Temple University School of Podiatric Medicine (TUSPM) is seeking an established, independent investigator for a tenure-track **FACULTY POSITION** to provide scientific leadership in the areas of diabetes and wound care. Qualified applicants must have a Ph.D. or equivalent degree and an outstanding research record. The successful applicant will be expected to establish an independent research program as well as direct the overall research efforts at TUSPM. Candidates should provide curriculum vitae, statement of current research, and a brief description of their long-range goals to **e-mail: jburke@tuspm.temple.edu** or to:

James P. Burke, Ph.D.
Associate Dean for Academic Affairs
Temple University
School of Podiatric Medicine
8th Street at Race Street
Philadelphia, PA 19107

Applications will be reviewed upon receipt and accepted until the position is filled. *Temple University is an Affirmative Action/Equal Opportunity Employer. Women and Minorities are encouraged to apply.*

POSTDOCTORAL RESEARCHER

A Postdoctoral position is available immediately to analyze the expression and function of a new growth factor in prostate cancer. The study involves cell molecular biology methodologies to determine the effect of the growth factor on human prostate cancer cells' proliferation, cell death protection, migration, and invasion and on signal transduction pathways. Ph.D. in cell/molecular biology or biochemistry or equivalent degree with major course work in molecular biology is required. Candidates must possess an extensive laboratory experience and solid background in molecular/cellular biology techniques (e.g., Northern analysis, Western analysis, immunoprecipitation, cell adhesion, polymerase chain reaction, cloning, mutagenesis, among others). Salary midpoint is $40,083. Depending on qualifications, publications, and experience, salary may be higher. Send resume, a brief summary of research experience, and three references (names, telephone numbers, and e-mail addresses) to: **Assistant Business Manager, Stanley S. Scott Cancer Center, Louisiana State University Health Sciences Center, 2025 Gravier Street, New Orleans, LA 70112. E-mail: emares@lsuhsc.edu.**

Louisiana State University Health Sciences Center is an Equal Opportunity Employer/Affirmative Action.

POSITIONS OPEN

ASSOCIATE DIRECTOR
Pharmaceutical Research Institute
at Albany College of Pharmacy

The Pharmaceutical Research Institute (PRI) at Albany College of Pharmacy is seeking qualified candidates for the position of Associate Director. The successful candidate will head a team of scientists involved in pharmaceutical preformulation/formulation studies. A Ph.D. in pharmaceutics is required, along with five years industrial and/or academic experience in preformulation/formulation/drug delivery as well as hands-on laboratory experience using analytical instrumentation such as high performance liquid chromatography, gas chromatography, Affirmative Action (atomic absorption), XRD (X-ray diffraction), UV, Fourier Transform Infrared, KF (Karl Fischer), differential scanning calorimeter, and thermogravimetric analysis. This key position involves business development networking, negotiating and securing contracts, and supervising and working with Ph.D. scientists and research associates on various pharmaceutical, biotechnology, and government projects.

Please send a letter of application, curriculum vitae, and names and addresses of three references to:

Dr. Shaker Mousa
Director
Pharmaceutical Research Institute at Albany College of Pharmacy
106 New Scotland Avenue
Albany, NY 12208
E-mail: mousas@acp.edu
Website: http://www.pri-albany.org

Albany College of Pharmacy is an Affirmative Action/Equal Opportunity Employer.

ASSOCIATE OR ASSISTANT PROFESSOR MOLECULAR PARASITOLOGY

The Department of Medicine at the University of Alabama at Birmingham invites applications for a tenure-track faculty position at the Associate Professor level, although outstanding applications at the Assistant Professor level will also be considered. The successful applicant is expected to develop a strong, independently funded research program that focuses on malaria or other apicomplexan parasites to dovetail with the existing strengths and programmatic focus of the Division of Geographic Medicine. The position requires a Doctorate degree in molecular biology, immunology, medicine, or a related discipline.

Interested candidates should submit curriculum vitae, the names of three references, and a one-page statement of research interests and plans by February 1, 2005, to **e-mail: tunnasch@uab.edu** or to:

Thomas R. Unnasch, Ph.D.
Chair, Search Committee
Division of Geographic Medicine
University of Alabama at Birmingham
845 19th Street South
Birmingham, AL 35294-2170

UAB is an Equal Employment Opportunity Employer.

ASSISTANT PROFESSOR. Auburn University (AU, **website: http://www.auburn.edu**), Department of Poultry Science (**website: http://www.ag.auburn.edu/dept/ph**), is accepting applications and nominations for Assistant Professor. The Assistant Professor serves as a faculty member in the AU Poultry Products Safety and Quality Program and develops instructional, research, and outreach programs in poultry processing and further processing of value-added products with an emphasis in food microbiology. A position announcement that contains requirements, application instructions, and other information can be found at **website: http://www.ag.auburn.edu/faculty-staff/jobs/** or obtained by contacting: **Shelly McKee, Chairman, Search Committee, Department of Poultry Science, 234 Upchurch Hall, Auburn University, AL 36849. Telephone: 334-844-2765; fax: 334-844-2649; e-mail: mckeesr@auburn.edu.** *Auburn University is an Affirmative Action Employer. Ethnic Minorities and Women are encouraged to apply.*

POSITIONS OPEN

FACULTY POSITIONS: ONE IN MEDICINAL CHEMISTRY, ONE IN PHARMACOGNOSY

The Department of Medicinal Chemistry and Pharmacognosy, University of Illinois at Chicago, invites applications for full-time, tenured or tenure-track Faculty Positions. A Doctorate and postdoctoral experience are required, and a background in pharmacy is desirable. The successful candidates must develop a strong, extramurally funded, independent research program that complements existing programs in the Department and fosters collaborative interactions with others. Teaching in the professional and graduate programs of the College of Pharmacy is required. Candidates should send curriculum vitae, a one- to two-page research plan, and three letters of reference to:

Dr. Steven M. Swanson
Chair, Search Committee
Department of Medicinal Chemistry and Pharmacognosy, M/C 781
University of Illinois at Chicago
833 S. Wood Street,
Chicago, IL 60612-7231
E-mail: mcp@uic.edu

Further information can be found at **website: http://www.uic.edu/pharmacy/depts/pmch/.** For fullest consideration, submit all application materials by March 1, 2005.

The University of Illinois is an Equal Opportunity/Affirmative Action Employer.

STRUCTURAL BIOLOGY

The Program of Biomolecular Structure at the University of Colorado Health Sciences Center (UCHSC) invites applications for a full-time, tenure-track **FACULTY POSITION** at any level. Candidates will actively pursue an independent, externally funded research program in solution NMR spectroscopy of biomolecules. UCHSC has excellent research instrumentation facilities in NMR (500, 600, 800, and 900 MHz NMR spectrometers). The successful candidate will have some medical school and graduate teaching responsibilities. The candidate should have a Ph.D. in biochemistry, pharmacology, biophysics, chemistry, or a related field; a strong background in NMR spectroscopy; and at least two years of postdoctoral or equivalent experience in the field of structural biology.

Applicants should send a letter of application, curriculum vitae, and a summary of research interests, and should have three letters of reference sent, to: **Dr. Robert Hodges, University of Colorado Health Sciences Center, P.O. Box 6511, Mail Stop 8101, Aurora, CO 80045 (or FedEx to 12801 E. 17th Avenue, Room L18-10101, Aurora, CO 80010).** Applications received by February 1, 2005, will be assured of consideration. Additional departmental information can be obtained via **website: http://biomol.uchsc.edu.**

The University of Colorado is committed to diversity and equality in education and employment.

The Denver Museum of Nature & Science (DMNS) seeks a **CURATOR OF HUMAN HEALTH** who will curate our health science collection, establish an active community-based research program, deliver and support innovative science education and exhibitions, build strong local partnerships, and supervise students and adult volunteers. Applicants should have an advanced degree, a strong background in medical science, public health, or health education, and a strong interest in museum-based science and community health. The position is for three years and is subject to renewal. Send letter of interest, curriculum vitae, contact information for three references, and sample publications by January 17, 2005, to: **Kirk Johnson, Chief Curator, Denver Museum of Nature & Science, 2001 Colorado Boulevard, Denver, Colorado 80205.** *DMNS is an Equal Opportunity Employer.*

POSITIONS OPEN

PHYSIOLOGICAL ECOLOGIST (WILDLIFE)

The Division of Biological Sciences (DBS) at The University of Montana invites applications for a tenure-track position in physiological ecology at the **ASSISTANT PROFESSOR** level, to begin August 2005. The position involves responsibilities in the Wildlife Biology Program (WBIO) and DBS. The successful candidate is expected to develop a vigorous externally funded research program in organismal-level physiological ecology of vertebrates that is relevant to wildlife issues, teach courses in physiological ecology and related areas, mentor M.S. and Ph.D. students, and interact with conservation agencies and organizations. Requirements include a doctoral degree focused in animal physiological ecology, a strong record of research achievement and teaching excellence, and formal training in animal physiology. Preference will be given to applicants whose research complements existing research programs within DBS and WBIO. We hope to obtain a strong, diverse applicant pool. Send curriculum vitae, statements of research and teaching goals, and contact information for three references to: **Physiological Ecologist (Wildlife) Search Committee, DBS, The University of Montana, Missoula, MT 59812, U.S.A. Telephone: 406-243-6009; fax: 406-243-4184.** A detailed position description is available on the DBS **website: http://biology.dbs.umt.edu/dbs.** Review of applications begins 21 January 2005. *Affirmative Action/Equal Opportunity Employer.*

VISITING MOLECULAR BIOLOGIST AND VISITING VERTEBRATE BIOLOGIST

The Mount Holyoke College Department of Biological Sciences invites applications for two Visiting Assistant Professorships during the 2005-2006 academic year. Ph.D. required, teaching experience preferred. Molecular Biologist: responsibilities include teaching the molecular biology half of a sophomore-level genetics/molecular biology course and teaching an upper-level molecular genetics course with laboratory. Vertebrate Biologist: responsibilities include co-teaching an introductory biology course and teaching a vertebrate anatomy course with laboratory. Both positions also involve supervising undergraduate research. Send curriculum vitae, statements of teaching interests/philosophy and research interests (including potential research projects for undergraduates), transcripts, and reprints of recent publications, and arrange for three letters of recommendation to be sent to: **Frank DeToma, Chair, Department of Biological Sciences, S. Hadley, MA 01075. E-mail: biology@mtholyoke.edu.** Application review will begin on January 5, 2005. *Mount Holyoke is committed to fostering multicultural diversity and awareness in its faculty, staff, and student body and is an Affirmative Action/Equal Opportunity Employer. Women and persons of color are especially encouraged to apply.*

CELL BIOLOGIST POSITION INFLAMMATORY BOWEL DISEASE

The Cleveland Clinic Foundation Department of Pathobiology is recruiting for an **ASSISTANT PROFESSOR** level scientist in the Inflammatory Bowel Disease (IBD) research group. Applicants for this position should have a demonstrated interest in IBD and a focus on leukocyte recruitment and the consequences of cell-cell interactions in IBD. Applicants must have a Ph.D. and/or M.D. and show promise of developing active, independent research in IBD. Applicants should send curriculum vitae, research statement, and three letters of reference (mailed directly by the referees) to: **Roseanne Baldrey, The Cleveland Clinic Foundation, Department of Pathobiology, NB4-40, 9500 Euclid Avenue, Cleveland, Ohio 44195.**

The Cleveland Clinic Foundation is an Equal Opportunity/Affirmative Action Employer.

POSITIONS OPEN

The U.S. Department of Agriculture (USDA), Agricultural Research Service (ARS), Mosquito and Fly Research Unit, Gainesville, Florida, is seeking a permanent full-time **SUPERVISORY RESEARCH ENTOMOLOGIST/CHEMIST/PHYSIOLOGIST (INSECTS)/MOLECULAR BIOLOGIST.** In addition to research duties the incumbent, as Research Leader, is responsible for exercising leadership, including the management of human, fiscal, and physical resources. Specific research objectives include one or more of the following: development of an interactive mosquito surveillance system on species selective trapping and geographic information system technology; development of new classes of compact, robust, inexpensive, and low maintenance mosquito traps to be used to gather and remotely communicate data; identification, characterization, and synthesis of mosquito and fly attractants/repellents to be used in traps and/or control systems; discovery, development, and testing of biocontrol agents for integrated pest management tactics; identification and development of control agents and dispersal tactics to efficiently and efficaciously control mosquitoes, flies, and their related diseases abroad; and basic investigation of the epidemiology of invasive vectors and pathogens in support of producers and national homeland defense missions. Salary range of $82,438 to $126,064. For details and application directions, see **website: http://www.afm.ars.usda.gov/divisions/hrd/.** To have a printed copy mailed, call **Jackie Sullivan** at **telephone: 352-374-5861.** *U.S. citizenship is required.* Announcement closes February 18, 2005. *USDA/ARS is an Equal Opportunity Employer and Provider.*

BIOCHEMISTRY Oakland University

The Department of Chemistry invites applications for a tenure-track position at the **ASSISTANT PROFESSOR** rank in biochemistry beginning fall 2005.

We seek an individual who will enthusiastically participate in teaching at both the undergraduate and graduate (M.S. and Ph.D.) levels and establish a vigorous, nationally competitive biomedical research program. A Ph.D. degree in chemistry, biochemistry, or a related field is required; postdoctoral experience is strongly preferred. Please submit curriculum vitae, a three to five page description of future research interests, and a statement of teaching interest; also arrange for delivery of three letters of recommendation.

Application materials may be sent in PDF format to **e-mail: search@ouchem.chem.oakland.edu,** or by mail to: **Biochemistry Search Committee, Department of Chemistry, Oakland University, Rochester, MI 48309.** Applications will be reviewed beginning January 31, 2005, and will be considered until the position is filled.

Oakland University has 16,000 students enrolled in 114 bachelor and 72 graduate and certificate programs. Located 25 miles north of Detroit, the University also offers extensive cultural and social programs. *Oakland University is an Equal Opportunity Employer and encourages applications from women and minorities.*

DOCTORAL FELLOWSHIPS CONSERVATION SCIENCE

The Department of Environmental Science and Policy of George Mason University and the Smithsonian Institution's National Zoological Park (NZP) are pleased to announce the availability of Doctoral Fellowships in Conservation Science. Two fellowships are available starting in the fall of 2005 for students with an M.S. in conservation biology or a related field whose research interests coincide with those of scientists in the NZP Departments of Conservation Biology and/or Reproductive Sciences. Prospective candidates must qualify for admission to the Ph.D. program in environmental science and policy at George Mason University. For more information and to apply for these fellowships, please see our **website: http://mason.gmu.edu/~espp/ConservationFellowships.** Deadline for submitting all application materials is January 31, 2005.

PHYSIOLOGIST
Section of Neurobiology, Physiology and Behavior
University of California, Davis

The Section of Neurobiology, Physiology and Behavior, University of California, Davis, invites applications for a Physiologist at the associate or full professor level. Applicants specializing in any area of animal physiology consistent with the broad goals of the Section will be considered. Candidates using genomic approaches and genetic models of organ system development and function are encouraged to apply. We are also interested in candidates whose research can interact with programs in gender-based biology and/or metabolic control in the Division of Biological Sciences and the School of Medicine, and who have demonstrated ability as academic leaders. UC Davis has made a tremendous investment in the genome sciences that will complement existing strengths in physiology. For more information, please visit the following web site: **www.npb.ucdavis.edu/facultyposition/**. Successful applicants will be expected to maintain a vigorous research program and contribute to the Section's teaching mission. Candidates must possess a Ph.D. or M.D. degree with significant experience as an established independent investigator. Applicants should send a letter describing their research and teaching interests, a curriculum vitae, copies of representative publications, and the names of five persons from whom references can be obtained to: **Chair, Physiology Search Committee, Section of NPB, One Shields Avenue, University of California, Davis, CA, 95616-8519**. Application review will commence **February 1, 2005**, and the search will continue until the position is filled. *The University of California is an Affirmative Action/Equal Opportunity Employer.*

Western

The UNIVERSITY of WESTERN ONTARIO
Faculty of Medicine and Dentistry
CHAIR
DEPARTMENT OF ANATOMY AND CELL BIOLOGY
Request for Applications

The Faculty of Medicine and Dentistry, at The University of Western Ontario, is inviting applications for the position of Chair in the Department of Anatomy and Cell Biology.

The Department of Anatomy and Cell Biology is a research-intensive department with a strong record of excellence in teaching. Current primary research areas include the study of gap junctions in intercellular communication and disease, molecular signaling in cell and developmental biology, neurobiology and imaging. Renovations scheduled for completion in 2005-06, combined with existing facilities, will provide16,000 sq. ft of new laboratory space and complement recently acquired core facilities for confocal microscopy, live cell imaging, cell micromanipulation and FACS analysis totaling over $ 4 million. The successful applicant will have several recruitment opportunities to build and enhance research programs through upcoming retirements. The Department has a strong graduate program in Anatomy and Cell Biology and provides teaching to medical, dental, science and health science students through undergraduate programs in the Faculties of Medicine and Dentistry, Science, and Health Sciences. The successful candidate should have a reputation for effective interpersonal, administrative and leadership skills and a strong commitment to excellence in teaching of the anatomical sciences. Candidates with a background in the anatomical sciences and a research program complementing existing research strengths, or candidates with outstanding accomplishments in any relevant research area, are encouraged to apply.

Details concerning the Department of Anatomy and Cell Biology, the Faculty of Medicine and Dentistry, and The University of Western Ontario, London, Ontario, may be found through the University's home page at **www.uwo.ca**.

Interested candidates should submit a CV outlining their research, teaching, and administrative experience and interests, including future directions, together with the name and addresses of three referees to: **Dr. Carol Herbert, Dean, Faculty of Medicine and Dentistry, Health Sciences Addition, The University of Western Ontario, London, Ontario N6A 5C1; FAX: (519) 850-2357.** The competition will remain open until the position is filled. Positions are subject to budget approval. Applicants should have fluent written and oral communication skills in English. All qualified candidates are encouraged to apply; however, Canadians and permanent residents will be given priority.

The University of Western Ontario is committed to employment equity and welcomes applications from all qualified women and men, including visible minorities, aboriginal people and persons with disabilities.

MUSC
HOLLINGS CANCER CENTER

Tobacco Related Malignancies including Lung, Head and Neck, and Bladder Tenure-Track Faculty Positions
The Hollings Cancer Center
Medical University of South Carolina
Charleston, SC

The Hollings Cancer Center at the Medical University of South Carolina is seeking outstanding applicants who are engaged in disease focused research in tobacco related malignancies including *lung, head and neck, and bladder* for tenure-track positions. New faculty will have primary appointments in Basic Science Departments and will have space in the new Hollings Cancer Research Building. All faculty are expected to participate in professional and graduate education as well as to maintain/develop an active and nationally recognized research program.

The Medical University of South Carolina is a rapidly growing research environment. Extramural research support has consistently increased over the past 10 years, topping $170 million last fiscal year. State-of-the-art research facilities include x-ray crystallography, mass spectrometry, proteomics, microarrays, flow cytometry, bioinformatics, animal imaging, lipidomics, and confocal microscopy.

The Charleston area provides an outstanding quality of life in a historic coastal city offering excellent opportunities to enjoy the beach, arts, sports, and excellent cuisine.

Please respond to posting **BSA525** by sending your curriculum vitae, statement of research interests, and the names of three references to: **Hollings Cancer Center, Medical University of South Carolina, Recruiting BSA525, PO Box 250955, 86 Jonathan Lucas Street, Charleston, SC 29425**. Or fax: to **843-792-9456** or e-mail **hccjobs@musc.edu**.

The Medical University of South Carolina is an Affirmative Action/ Equal Opportunity Employer.

NIMH National Institute of Mental Health

Department of Health and Human Services
National Institutes of Health
National Institute of Mental Health

With nation-wide responsibility for improving the health and well being of all Americans, the Department of Health and Human Services (DHHS) oversees the biomedical research programs of the National Institutes of Health (NIH) and those of NIH s research Institutes.

The National Institute of Mental Health (NIMH), a major research component of the NIH, and the DHHS, is recruiting for a tenure-track appointment in the new Genes, Cognition and Psychosis Program under the direction of Daniel R. Weinberger, M.D. This program includes investigators from many disciplines including molecular genetics, cell biology, clinical genetics, and behavioral neuroscience. With a complementary budget and staff, the individual selected for this position will be expected to establish an independent research program focused on translational genetics related to schizophrenia and related cognitive dysfunction. This will include discovery of specific genetic variants that increase risk for schizophrenia, understanding mechanisms by which these variants act, developing intermediate phenotypic measures, acquiring new subject data sets, and developing new therapeutic approaches based on these discoveries. The opportunity exists for this position to be a joint appointment with NIMH and with the National Human Genome Research Institute (NHGRI).

The successful individual must possess an M.D. and/or Ph.D. degree, and experience in a relevant area of clinical and translational genetics as well as neuroscience. At least five years of relevant research experience is required.

Salary is commensurate with experience and accomplishments, and a full Civil Service package of benefits (including retirement, health, life, and long term care insurance, Thrift Savings Plan participation, etc.) is available.

The strong scientific environment and outstanding equipment resources at NIH makes this a unique opportunity for an outstanding scientist. Interested candidates should send curriculum vitae, statement of research interests, accomplishments and future goals, and six letters of recommendation to the **Chair, Search Committee for a Tenure Track Investigator in the area of Translational Genetics, National Institute of Mental Health, Building 10, Room 4N-222, 9000 Rockville Pike, Bethesda, MD 20892**, or by email to: **steyerm@mail.nih.gov** by **January 24, 2005**.

DHHS and NIH are Equal Opportunity Employers

POSITIONS OPEN

ECOLOGIST
Earlham College

Earlham College seeks an Ecologist for a two-year, full-time position including a team-taught introductory ecology course, an upper-level population and community ecology course, and other courses in the candidate's field of interest. Earlham is among the top institutions nationally in the proportion of its biological sciences graduates completing the Ph.D. The College is a Quaker liberal arts undergraduate institution where excellence in teaching is emphasized. The College continues to build a community that reflects the gender and racial diversity of society. Ph.D. or A.B.D. is required. More information at **website: http://www.earlham.edu/~biol.** Please send curriculum vitae, transcripts, statement of teaching philosophy, and three letters of recommendation to: **Dr. William H. Buskirk, Department of Biology, Earlham College, Richmond, IN 47374.** Reading of applications will begin 15 January 2005. *Earlham College is an Affirmative Action/Equal Opportunity Employer.*

CELL/MOLECULAR/ DEVELOPMENTAL BIOLOGIST

The Department of Biological Sciences at Marquette University has a tenure-track **ASSISTANT PROFESSOR** position available August 16, 2005, for a developmental biologist to join a faculty with broad research interests (**website: http://biology.marquette.edu**). Applicants must have a Ph.D. with postdoctoral experience. The successful candidate is expected to develop an extramurally funded research program. Teaching responsibilities include an annual undergraduate lecture course in animal development in one semester and a graduate lecture or seminar course in the candidate's area of expertise in the other semester. Send curriculum vitae, statement of research interests, and three letters of reference by January 3, 2005, to: **Dr. Robert Fitts, Chairman, Marquette University, Department of Biological Sciences, WLS 112, P.O. Box 1881, Milwaukee, WI 53201-1881.**

FACULTY POSITION
Department of Biology

Temple University's Department of Biology is anticipating openings for full-time, nontenure-track faculty position starting August 2005. Primary teaching assignments will include courses in developmental biology/embryology and immunology, some at a suburban campus. Additional assignments may include interdisciplinary and other courses, development of new courses, and other activities determined by programmatic needs. Requires a Ph.D. in biological sciences. Candidates may send resume, letter of interest, three letters of recommendation, and transcript of highest academic degree to: **Dr. Shohreh Amini, Chair, Biology Department, Attn: Faculty Search, Temple University, 1900 N. 12th Street, Biology Life Sciences Building, Room 255, Philadelphia, PA 19122.** *Temple University is an Equal Opportunity/Equal Access/Affirmative Action Employer committed to achieving a diverse community.*

BIOLOGY–ASSISTANT PROFESSOR: University of New England (UNE) invites applications for a tenure-track Assistant Professorship in the Department of Biological Sciences to teach anatomy and physiology and possible advanced courses in biological specialties. Requirements include a doctoral degree in a biological field, a demonstrated commitment to teaching, and an ability to maintain a research program that includes undergraduates. Review of applications will begin in January 2004 and will continue until the position is filled. Send curriculum vitae, statements of teaching philosophy and research interests, and three letters of recommendation, all electronically, to: **Chair, Biology Search Committee** at **e-mail: iyokana@une.edu.** Refer to the Human Resources **website: http://www.une.edu/hr/.** *UNE is an Equal Opportunity/Affirmative Action Employer and strongly encourages candidates of diverse backgrounds.*

POSITIONS OPEN

The Department of Medicine Section of Hematology/Oncology at The University of Chicago has a **POSTDOCTORAL SCHOLAR** position available for training in research focused on the pharmacogenetics of anticancer agents. Possible projects will include the characterization of genetic variation of proteins playing a vital role in the pharmacokinetics and mechanism of action of anticancer agents. The information arising from these projects will be used to design more powerful studies aimed at elucidating the clinical impact of common and rare variants on response of patients. The Postdoctoral Scholar will be part of a multi-institutional research group (**website: http://www.pharmacogenetics.org**) which involves frequent interactions with a broad range of scientists with expertise in human genetics, bioinformatics, clinical pharmacology, and molecular pharmacology. Duties involve performing gene sequencing, RNA and DNA extractions, polymerase chain reaction, reverse transcription polymerase chain reaction, and functional promoter assays. Candidates must have a Doctorate in biological sciences, medicine, or related field and should have experience in human genome bioinformatics, molecular biology techniques, and statistics. Excellent communication and organizational skills preferred. Applicants should send a letter describing their prior research experience, current interests and goals, contact information for three references, and curriculum vitae to: **Federico Innocenti, M.D., Ph.D., Department of Medicine, MC 2115, The University of Chicago, 5841 South Maryland Avenue, Chicago, IL 60637** or via **e-mail: finnocen@medicine.bsd.uchicago.edu.** *The University of Chicago is an Affirmative Action/Equal Opportunity Employer.*

FACULTY POSITIONS
BIOINFORMATICS

The Department of Biomedical Informatics of the Ohio State University College of Medicine and Public Health (**website: http://bmi.osu.edu/**) seeks applications for tenure-track Faculty Positions at all levels.

We seek broadly trained scientists with computational research programs with biomedical relevance and collaborative potential. Programs complementing current research efforts are of particular interest. Current research programs in the Biomedical Informatics and affiliated departments include: promoter and chromatin analysis, protein structure, biomedical image processing and quantification, comparative genomics and phylogenetics, pharmacogenomics, cancer research, high performance and data intensive computing.

Applicants must have a proven record of publications in leading peer-reviewed journals and demonstrated potential to obtain extramural funding. Senior level applicants (Associate Professor and above) should have extramural funding. Teaching duties will include a course in the applicant's area of specialty. Applicants should send curriculum vitae, brief statements of research and teaching interests, and copies of two to four representative publications, and should have four letters of reference sent directly to: **Bioinformatics Search Committee, Biomedical Informatics, The Ohio State University, 3184 Graves Hall, 333 W. 10th Avenue, Columbus, OH 43210.**

Recruitment is open immediately and will be ongoing until positions are filled.

A **POSTDOCTORAL POSITION** is available in the area of molecular biology of hepatitis B and C viruses. Research interests of the laboratory are in the area viral RNA replication, signal transduction, endoplasmic reticulum/oxidative stress, steatosis, and mechanism of liver oncogenesis associated with both viruses. Laboratory will be relocating to the University of California, San Diego, California in late spring 2005. Interested students with Ph.D. or M.D. in the related fields are encouraged to apply. Send inquiries to: **Aleem Siddiqui, Department of Microbiology, Program in Molecular Biology, Campus Box B172, University of Colorado Health Sciences Center, Denver, CO 80262 (e-mail: aleem.siddiqui@uchsc.edu). Telephone: 303-315-7106; fax: 303-315-8330.**

POSITIONS OPEN

FACULTY POSITION, IMMUNOLOGY

A tenure-track faculty position in immunology is open at the **ASSISTANT** or **ASSOCIATE PROFESSOR** level in the Department of Microbiology and Immunology, Virginia Commonwealth University, Richmond, Virginia. Applicants should have a Ph.D. or equivalent, a record of research accomplishments, and an interest in graduate and medical education. Expertise in molecular or cellular immunology is sought. This is an exceptional opportunity to join a strong, research-oriented Department in a very desirable geographic location. See **website: http://www.vcu.edu/micro/** for additional information. Please submit curriculum vitae with a statement of research interests and have three letters of reference sent to: **Dr. Daniel Conrad, Search Chairman, Immunology Search Committee, c/o M. Crewey, Department of Microbiology and Immunology, Medical College of Virginia Campus, Virginia Commonwealth University, P.O. Box 980678, Richmond, VA 23298-0678. E-mail: micacct@vcu.edu.** Applications will be reviewed upon receipt and considered until February 15, 2005, or until a suitable candidate is identified. *VCU is a culturally diverse, Equal Opportunity Employer. Women, Minorities, and Persons with Disabilities are encouraged to apply.*

The interdepartmental Computational Biology Program of the University of Colorado School of Medicine is soliciting applications for computational biology and bioinformatics **FACULTY** at the junior and senior levels. The recruitment spans all departments, and is open to scientists doing outstanding computational research relevant to any aspect of human health. Topics of interest include (but are not limited to): whole genome comparison, polymorphism analysis, informatics related to Type I Diabetes or autoimmune diseases, cancer informatics, neuroinformatics, and mass spectrometry informatics. Recruitment packages include substantial startup resources and extensive space at the new Fitzsimons campus. To apply, please send your curriculum vitae, names of at least three references, and a statement of teaching and research interests to: **Bioinformatics Search Committee, c/o Kathy Thomas, University of Colorado Health Sciences Center at Fitzsimons, Mail stop 8303, P.O. Box 6511, Aurora, CO 80045-0511,** or by **e-mail: kathy.r.thomas@uchsc.edu.** Review of applications will begin immediately and continue until the position is filled. *The University of Colorado is committed to Diversity and Equality in education and employment.*

Illinois Wesleyan University seeks a **VISITING ASSISTANT PROFESSOR** for a one-year, nontenure-track appointment to start fall 2005. The successful candidate will teach introductory genetics, portions of introductory biology, introductory biology laboratories, and a course for nonscience majors. A Ph.D. in genetics is preferred. Review of applications will begin immediately and continue until the position is filled. Send curriculum vitae, undergraduate and graduate transcripts, statement of teaching philosophy, and three letters of recommendation to: **R. Given Harper, Chair, Department of Biology, Illinois Wesleyan University, P.O. Box 2900, Bloomington, IL 61702. E-mail: gharper@iwu.edu.** For further information, see our jobs **website: http://www.iwu.edu/~iwujobs.**

NEUROSCIENCE. Three-year renewable **ASSISTANT PROFESSOR** starting August 2005. Teach biological psychology, introductory biology, upper-level psychology laboratory class, and mentor student research. Prefer Ph.D.; all but dissertation considered. See **website: http://psych.hanover.edu/search/neuroscientist/.** Send letter, teaching and research statement, curriculum vitae, transcripts, and three reference letters to: **Neuroscience Search, c/o Chris Wilcox, P.O. Box 108, Hanover College, Hanover, IN 47243.** Reviews begin January 10, 2005. *Women and members of underrepresented ethnic groups are encouraged to apply; Equal Opportunity Employer.*

POSITIONS OPEN

VERTEBRATE MORPHOLOGIST

The College of the Holy Cross invites applications for a tenure-track **ASSISTANT PROFESSORSHIP** in Biology. A Vertebrate Biologist will be hired to teach a laboratory course in chordate morphology, a second upper-division course in an area compatible with current offerings, and an organismal biology course for premedical students. Supplementary areas of departmental interest include paleontology, functional morphology and the biology of any vertebrate class. Development of a research program involving undergraduates is expected. The successful candidate will hold a Ph.D. at the time of appointment. Further information can be found at the departmental **website: http://www.holycross.edu/departments/biology/ website.** Holy Cross is a highly selective, exclusively undergraduate, Jesuit, liberal arts college (enrollment 2,700) that values excellence in both teaching and research. Applications, consisting of curriculum vitae, transcripts, copies of publications, research and teaching statements, and letters from three referees, should be submitted no later than 18 January 2005 to: **Dr. Ken Prestwich, Chair, Vertebrate Search Committee, Department of Biology, College of the Holy Cross, Worcester, MA 01610.** *The College is an Equal Opportunity Employer and complies with all federal and Massachusetts laws concerning Equal Opportunity and Affirmative Action in the workplace.*

POSTDOCTORAL FELLOW

The Department of Pathology at the University of Cincinnati is seeking a highly motivated Postdoctoral Fellow to study a role of Niemann-Pick type C proteins in the regulation of cellular cholesterol homeostasis. Major duties include the planning, carrying out, and analysis of experiments on sterol regulation in cell and animal models. Applicants should have a Ph.D. in cell/molecular biology, biochemistry, or related fields; and research experience in regulation of gene transcription, signal transduction, or protein/lipid chemistry.

Position open until filled. Please send curriculum vitae (including position control #24UC3335) to: **Andrey Frolov, Ph.D., Department of Pathology and Laboratory Medicine, Genome Research Institute, University of Cincinnati, 2120 E Galbraith Road, Cincinnati, OH 45237** or **e-mail: andrey.frolov@uc.edu.** *The University of Cincinnati is an Affirmative Action/Equal Opportunity Employer.*

Two **POSTDOCTORAL FELLOW POSITIONS** are available immediately in a well-funded laboratory at Mount Sinai School of Medicine in New York City. The major research interest of this laboratory is to develop novel gene therapy technologies for treatment of cancer and genetic diseases. The minimum requirements for the positions include a Doctorate degree in life science or related fields, skills in recombinant DNA technology and cellular biology, small-animal work experience. Experience and training in hematology, virology, and/or immunology are highly desired.

Application should be submitted to: **Hengjun Chao, M.D., Division of Hematology/Oncology, Box 1079, Department of Medicine, Mount Sinai School of Medicine, One Gustave L. Levy Place, New York, NY 10029. Fax: 212-824-7016; e-mail: hengjun.chao@mssm.edu**.

POSTDOCTORAL POSITION available immediately to understand the mechanism and dynamics of adenosine triphosphate-driven DNA packaging in viruses using bacteriophage T4 model. Novel combinatorial mutagenesis, biochemical, and structural approaches will be used. Strong background in protein biochemistry desired. Send curriculum vitae and names of three references to: **Dr. Venigalla Rao, Department of Biology, Catholic University, 620 Michigan Avenue, N.E., Washington, DC 20064. E-mail: rao@cua.edu.**

POSTDOCTORAL FELLOW/ RESEARCH ASSOCIATE POSITIONS IN BIOCHEMICAL FLUORESCENCE

The Center for Fluorescence Spectroscopy has positions available at both the Postdoctoral and Research Associate level for individuals with a Ph.D. and suitable experience in biochemical surface interactions and experience in surface preparations such as vapor deposition and lithography. All applications should have an interest at applying state-of-the-art fluorescence based methods to biomedical research, with a particular emphasis on fluorophore-surface interactions. A good working knowledge of biochemistry, DNA, RNA, and fluorescence sensing is also desirable. Appointments are to be at the Postdoctoral or Research Associate level as soon as a suitable candidate is found, salary commensurate with experience. Applicants should forward curriculum vitae, a publication list, and at least three letters of recommendation to: **Search Committee, c/o Dr. Chris D. Geddes, Assistant Director, The Center for Fluorescence Spectroscopy, Medical Biotechnology Center, 725 West Lombard Street, Baltimore, MD 21201, U.S.A.** Informal inquiries may be made to **e-mail: cfs@cfs.umbi.umd.edu.**

POSTDOCTORAL POSITION available in the Behavioral Neuropsychopharmacology Laboratory at the University of Nebraska-Lincoln. Ongoing NIH-funded research includes assessment of pharmacological and behavioral factors affecting associative learning processes with abused drugs and preclinical evaluation of immunotherapy techniques for nicotine addiction. We are interested in someone that will contribute to the progress of these projects as well as bring an infusion of new ideas. If interested, the successful candidate will have the opportunity to teach one undergraduate class a year in their specialty. This is a unique opportunity to receive closely mentored teaching experience. Candidates must have a Ph.D. and salary will be competitive. Send curriculum vitae and the names of three references to: **Rick Bevins, Psychology Department, 238 Burnett Hall, University of Nebraska-Lincoln, Lincoln, NE 68588-0308** or **e-mail: rbevins1@unl.edu.** Contact: **Claudia Price-Decker** at **telephone: 402-472-3721** for assistance. *The University of Nebraska is committed to a pluralistic campus community through Affirmative Action/ Equal Opportunity. We assure reasonable accommodation under the Americans with Disabilities Act.*

POSTDOCTORAL POSITIONS
Neuropharmacology and Neuroscience

The Center for Neuropharmacology and Neuroscience of Albany Medical College has two Postdoctoral positions available in the neurobiology of drug addiction. These positions are part of a National Institute of Drug Abuse-supported training program focusing on the behavioral, neurochemical, and molecular bases of drug addiction and dependence. Fellows will be mentored by one or more of 12 NIH-funded training faculty in fully equipped state-of-the-art laboratories. Candidates, *who must be U.S. citizens or permanent residents,* should submit curriculum vitae and three letters of reference to: **Dr. Stanley D. Glick, Center for Neuropharmacology and Neuroscience, Albany Medical College, MC-136, 47 New Scotland Avenue, Albany, NY 12208-3479. Fax: 518-262-5799; e-mail: glicks@mail.amc.edu.**

Affirmative Action/Equal Opportunity Employer.

A **POSTDOCTORAL POSITION** is available to study molecular mechanism of cardiac disease including cardiomyopathy and congenital heart disease. Interested individuals should send curriculum vitae and contact information of three references to: **Dr. Ju Chen** at **e-mail: juchen@ucsd.edu.** *University of California San Diego is an Equal Opportunity Employer.*

POSTDOCTORAL RESEARCH FELLOW, NANOTOXICOLOGY

Interdisciplinary research training in the toxicology and biocompatibility of nanomaterials. This is a collaborative project between **Dr. Robert Hurt** in the Division of Engineering and **Dr. Agnes Kane** in the Department of Pathology and Laboratory Medicine at Brown University. Research space will be provided in newly renovated laboratories with modern core facilities for synthesis and characterization of carbon nanomaterials, genomics, cell imaging, flow cytometry, and molecular pathology. Trainees are expected to have a Ph.D. degree in biology, chemistry, or toxicology and *must be a U.S. citizen or permanent resident* to qualify for support by the National Institute of Environmental Health Sciences-funded Training Program in Environmental Pathology. Experience in cell culture, immunofluorescence, and confocal microscopy is desirable. Send curriculum vitae, recent publications, a description of career objectives, and three letters of recommendation to: **Agnes B. Kane, M.D., Ph.D., Professor and Chair, Department of Pathology and Laboratory Medicine, Brown University, Box G-E534, Providence, RI 02912. Fax: 401-863-9008. E-mail: agnes_kane@brown.edu.** *Brown University is an Equal Employment Opportunity/ Affirmative Action Employer.*

POSTDOCTORAL FELLOW in Molecular Biology, The City College of New York–Primary responsibilities include experimental research in RNA metabolism, cellular senescence, carcinogenesis, and apoptosis. Additional responsibilities would include assisting in mentoring graduate and undergraduate researchers, contributing to proposal development, and preparing research reports and publications. Qualifications: an earned Ph.D. in biology, biochemistry, or molecular biology, acceptable writing skills, a strong mathematical background, and excellent computing skills. Good communication skills in English are a must. Salary: $30,000 to $40,000 commensurate with experience. Please send a statement of relevant research experience/interests and curriculum vitae including three references to: **Dr. Karen Hubbard, PVN # REA-169, The City College/City University of New York, Department of Biology, Room J526, 160 Convent Avenue, New York, NY 10031** or **e-mail: khubbard@sci.ccny.cuny.edu.** Open until filled. *The Research Foundation of the City University of New York is an Equal Employment Opportunity/Affirmative Action/ADA/IRCA Employer.*

POSTDOCTORAL POSITION: GENOMICS/PROTEOMICS
Boston University

The position is for a laboratory scientist to work on the development, testing, and application of new array based methods, and as part of a team testing new computational methods. Applications include combined in vitro/in silico approaches to cis regulatory site identification; diagnosis and prognosis of complex disorders. Experience with mass spectrometry desirable. Appointment begins no later than April 1, 2005. Reply to: **Professor Charles DeLisi, Metcalf Professor of Science and Engineering, Bioinformatics Program, Boston University, 44 Cummington Street, Boston, MA 02215.**

Two **POSTDOCTORAL POSITIONS** are available in the Division of Nephrology at University of Utah in Salt Lake City. The research concerns mechanisms of chronic renal diseases and hypertension with focus on COX-2. The research program is supported by three NIH grants and University funds. Strong background in renal physiology and molecular biology is desirable. Interested individuals should send curriculum vitae along with contact information of three references and a statement of research interest to: **Dr. Tianxin Yang, Associate Professor** at **e-mail: tianxin.yang@hsc.utah.edu; telephone: 801-582-1565, extension 4334; fax: 801-583-9624.**

Control of Gene Function Has Never Been Easier!

HuSH™ shRNA Expression Plasmids For Long-Term Gene Silencing

Now Available
Pre-made shRNA Plasmids for 200 Kinases

HuSH™ shRNA Expression Plasmids

- Ready-made sequence-verified plasmids for human genes
- Multiple (3-8) constructs for each target to ensure optimized inhibition
- U6 promoter for efficient shRNA expression
- Puromycin-resistance marker for stable transfection and long-term knock-down

TrueClone™ Full-Length Human cDNA

- Vast collection of over 22,000 non-redundant transcripts
- Authentic clones obtained directly from cDNA libraries without PCR-introduced mutations
- Ready to express in mammalian cells and cell-free systems
- Collection includes **over 560 protein kinases**

ORIGENE
TECHNOLOGIES, INC.

1-888-267-4436 www.origene.com